UNIVERSITY OF KWAZULU-NATAL

INYUVESI YAKWAZULU-NATALI

Quantitative comparison of the aerosol optical properties over Durban using ground and satellite based instrumentation

By

Priyanka Singh

210514851

Submitted in fulfilment of the requirements for the degree of Bachelor of Science (Masters) in Environmental Science, in the School of Environmental Science, Department of Geography, College of Agriculture, Engineering and Science

Supervisor: Prof. Sivakumar Venkataraman

Co-Supervisor: Dr. Michael Gebreslasie

2017

DECLARATION

This research has not been previously accepted for any degree and is not being currently considered for any other degree at any other university. I declare that this Dissertation contains my own work except where specifically acknowledged

Name Priyanka Singh (210514851)

Signed………………………………………..

Date…30 March 2017……………………..

ACKNOWLEDGEMENTS

ABSTRACT

Aerosols are ubiquitous constituents in the atmosphere and are important for atmospheric processes. This is due to their ability to scatter and absorb solar radiation and influence cloud microphysics. This study will focus on discerning trends in aerosol optical properties in Durban (29.8587° S, 31.0218° E), a coastal city on the east coast of South Africa, using the preliminary results from the sun-photometer located at the University of KwaZulu-Natal. These results will also be compared to the well-established Skukuza sun-photometer. Skukuza is a rural agricultural area in the north eastern parts of South Africa. The Aerosol Optical Depth (AOD), Angstrom Exponent ($\alpha_{440-870}$), Columnar Water Vapour (CWV), Volume Size Distribution (VSD), Single Scattering Albedo (SSA), Asymmetry parameter (ASP), Real and Imaginary parts of the complex refractive index were studied for Durban and Skukuza. Analysis of the aerosol optical properties suggested that various sources of aerosols were identified for Durban, such as biomass burning, urban industrial aerosols and marine aerosols. Biomass burning aerosols impacted Skukuza during spring. There was a high extent of fine mode aerosols present throughout the year for Skukuza, indicating that urban industrial emissions from the South African Highveld region can also contribute to aerosol loads in the region.

Preliminary results from the ground-based Durban sun-photometer was used to compare aerosol optical depth at 550 nm (AOD) to the satellite Moderate Resolution Imaging Spectroradiometer (MODIS) for the Aqua, Terra and Aqua and Terra combined (average of both) datasets for the dark target (DT) and deep blue (DB) retrieval algorithms to validate satellite retrievals. The results gave way to moderate correlations between MODIS Terra and the Durban sun-photometer for both DB ($R^2 = 0.70$) and DT ($R^2 = 0.60$), and between MODIS Aqua and the Durban sun-photometer for DB (0.68). Good correlations were observed for MODIS Terra and Aqua merged for both DB (0.79) and DT (0.74). The ability of MODIS to predict AOD was noted as dependent on the season and location.

HYSPLIT 720 hour–backward trajectory analysis, AOD and $\alpha_{440-870}$ from the Durban sun-photometer, a Lidar profile and satellite imagery were used to determine if air mass from the Calbuco volcanic eruption in Chile in April 2015 reached Durban. Trajectory analysis found that only during May 2015, was air masses arriving from South America, within the 20 km altitude. This led to the assumption that stratospheric aerosols from the Calbuco volcano, travelled to Durban. Analysis of the AOD found that only during 2015 was a constant phenomenon driving AOD in Durban and this was attributed to the eruption. Lidar observations

coupled with the backward trajectory analysis allowed for the identification of air masses in Durban arriving from the Calbuco volcano in Chile.

TABLE OF CONTENTS

LIST OF TABLES

LIST OF FIGURES

ACRONYMS AND ABBREVIATIONS

Aerosol Asymmetry Parameter	ASP g
Aerosol Optical Depth	AOD
Aerosol Optical Thickness	AOT
Aerosol Radiative Forcing	ARF
Aerosol radiative forcing / atmospheric forcing	ARF
Aerosol Robotic Network	AERONET
Air pollution potential	APP
Air Quality Act of 2005	AQA
Air Resources Laboratory	ARL
Ammonia	NH_3
Ammonium	NH_4
Ammonium nitrate	NH_4NO_3-
Angstrom Exponent	$\alpha_{440-870}$
Biogenic Volatile Organic Carbon	BVOC
Black carbon	BC
Bottom of the Atmosphere	BOA
Carbon disulphide	CS_2
Carbon monoxide	CO
Carbon-dioxide	CO_2
Cloud Aerosol Lidar and Infrared Pathfinder Satellite Observation	CALIPSO
Cloud condensation nuclei	CCN
Collection 6	C6
Council for Scientific and Industrial Research	CSIR
Dark target	DT
Deep Blue	DB
Digital number	DN
Fine mode fraction	FMF
Forcing efficiency	FE
Global Data Assimilation System	GDAS
Greenhouse gases	GHG
Gross Domestic Product	GDP
Hybrid Single-Particle Lagrangian Integrated Trajectory	HYSPLIT
Imaginary	Im
Intergovernmental Panel on Climate Change	IPCC
KwaZulu – Natal	KZN

Light Detection and Ranging	LIDAR
Micrometres	μm
Moderate resolution Imaging Spectroradiometer	MODIS
Multiangle Imaging Spectroradiometer	MISR
Nanometres	nm
National Aeronautics and Space Administration	NASA
National Ocean and Atmosphere Administration	NOAA
Nitrate	NO_3^-
Nitric acid	HNO_3
Nitrogen oxides	NO_x
Optical Thickness	τ
Organic carbon	OC
Ozone	O_3
Particulate Matter	PM
Precipitable water content	PWC
Radiative forcing	RF
Radon	^{220}Rn
Real	Re
Root mean square error	RMSE
Single Scattering Albedo	SSA
Small wavelength infrared	SWIR
South African Weather Services	SAWS
South Durban Industrial Basin	SDIB
Southern African Fire Atmosphere Research Initiative	SAFARI
Stratospheric Aerosol and Gas Experiment II	SAGE II
Sulphate	SO_4^{2-}
Sulphur-dioxide	SO_2
Sulphuric acid	H_2SO_4
Top of the Atmosphere	TOA
Ultra Violet - B	UV-B
Visible	VIS
Volatile Organic Compounds	VOCs
Volume size distribution	VSD
World Health Organization	WHO
World Meteorological Organisation	WMO

<div align="center">**CHAPTER ONE**</div>

<div align="center">**1. INTRODUCTION**</div>

1.1 Background

1.1.1 Overview and importance aerosols

Human activities, including rapid urbanization are steadfastly impacting the atmospheric environment. According to the World Meteorological Organisation (WMO) the high magnitude and rapidity of widespread urbanization has resulted in an increase in aerosol pollution, on a global scale (Zhu, et al., 2012). An aerosol can be fundamentally described as a solid or liquid particle suspended within a gas. Therefore, aerosols are a combination of particulate matter (PM) and its gaseous suspending medium (Hinds, 2012). Atmospheric aerosols are released from both natural and anthropogenic sources and originate from emissions of primary PM or of secondary PM from gaseous agents. The foremost constituents of atmospheric aerosols are from inorganic species such as sulphate and nitrates as well as organic species such as black carbon, mineral and biological aerosol particles (Boucher, 2015). Atmospheric aerosols are particles which range in size from a few nanometres (nm) to tens of micrometres (μm) in diameter. Aerosols can be transported from areas of high emissions to areas that are cleaner, isolated regions. Aerosols are able to alter life on earth, through their part in heterogeneous chemistry in the stratosphere and troposphere. Moreover, aerosols have radiative effects due to their impact on climate by scattering sunlight back to space and inducing condensation nuclei for cloud droplet formation (Boucher, 2015).

Stratospheric aerosols are aerosol particles which exist in the stratosphere region of the Earth's atmosphere. Volcanic eruptions such as that of Mt. Pinatubo are a major source of stratospheric aerosols and significantly influence earth's climate. Sulphur dioxide (SO_2) gas is released from these eruptions causing a build–up of sulphuric acid in the stratosphere. Stratospheric winds transport aerosols throughout the stratosphere and they can stay in the stratosphere for about two years. Aerosols in the stratosphere that are smaller than 0.1 μm are of tropospheric origin, those between 0.1 and 1.0 μm are formed within the stratosphere from oxidation of SO_2 and hydrogen sulphide (H_2S) gas (Junge, et al., 1961). Regardless of this, the effects of aerosols occur mainly within the planetary boundary layer (PBL) within the troposphere. The PBL is the region where the most amount of atmospheric aerosol mass is located. The amount of

<div align="center">1</div>

aerosols decrease according to distance from the source. As such, due to the variable height–dependent distribution of aerosols, predicting aerosol radiative effects is uncertain (Sakaeda, et al., 2011). Most aerosols of tropospheric origin comes from human activities, from fossil fuel and biomass burning. This study will focus on tropospheric aerosols.

Tropospheric aerosols arise from both natural and anthropogenic sources. The main natural sources of aerosols are the release of sea–salt into the atmosphere, windblown mineral dust, and precursor gases from volcanic eruptions, natural wildfires and vegetation. Anthropogenic sources consist of emissions from fossil fuel and bio fuel combustion, industrial processes, agricultural activities, human induced biomass burning and photochemical smog caused by emissions from vehicles (Tesfaye, et al., 2011). Particles can be directly emitted into the atmosphere or formed by the oxidation of precursor gases, such as sulphur dioxide, nitrogen oxides and volatile organic compounds (VOCs), where the resulting oxidation products nucleate to form new particles or condense on pre–existing ones (Hinds, 2012).

Tropospheric aerosols have short residence times in the atmosphere, with disparate spatial distributions that has primarily to do with the sources that the aerosols originate from. Due to the various sizes and properties of aerosols, aerosols may change shape when they interact with the atmosphere (Kanike & Sivakumar, 2015). Aerosols may travel considerable distances even though they have short life times and can be transported from areas of high aerosol emissions to relatively clean regions. Furthermore, there are large variances in the magnitude and spatial distribution of atmospheric aerosols due to changes in the burning of fossil fuels and other industrial activities (Cook & Highwood, 2004).

Tropospheric aerosols make up an important part of the climate system because aerosols play a vital role in the Earth's radiation budget (Cook & Highwood, 2004). This is done both directly, by scattering and absorbing solar radiation and, indirectly through the affect aerosols have on cloud microphysics, causing a reduction in solar radiation reaching the earth's surface (Haywood & Boucher, 2000). Aerosols impact air quality and human health therefore their climatic and environmental effects are of extreme importance to researchers. However, despite their importance, current knowledge of their properties and their interactions with climate are still lacking especially in southern Africa (Cook & Highwood, 2004). This is due the complex nature of tropospheric aerosols, as aerosols do not occur as individual species but as a mixture of different particles. The impingement of tropospheric aerosols on the atmosphere has largely to do with their optical, physical, radiative and chemical properties, the source of the aerosol

and advection due to local synoptic meteorological conditions (Kaufman, et al., 1997). The warming influence of aerosols in the lower troposphere can increase low–level cloud evaporation, consequently causing a decrease in cloudiness as well as the slowing of the hydrological cycle and convection processes (Tesfaye, et al., 2013). Furthermore, the heating effects of absorbing aerosols changes atmospheric circulation.

Tropospheric aerosols of different types create radiative forcings of various magnitudes (Ramaswamy, et al., 2001). Radiative forcing (RF) is a measure of the change occurring in earth's energy balance due to alterations in the composition of the atmosphere or in the properties of the earth's surface. It is measured in terms of watts per square meter and is known as aerosols direct radiative forcing (ARF). The measurement of RF at the bottom and top of the atmosphere are significant parameters in the calculation of the impact of aerosols on climate (Ramaswamy, et al., 2001).

The ARF is one of the major sources of uncertainty with regard to estimating climate change, due to the large spatial variability in aerosol radiative properties. According to the Intergovernmental Panel on Climate Change (IPCC), climate change can be described as a change in the Earth's climate that is greater than what would be expected to occur from natural climate variability (Stocker, et al., 2013). Unprecedented climate change is caused by unmediated anthropogenic activity, resulting in an increased rate of global warming (Stocker, et al., 2013). Given the cooling effects that aerosols have by scattering and absorption of solar radiation, radiative forcing by aerosols is of extreme importance and essential to predict climate change.

Quantitative understanding of the complex biological, physical and chemical reactions that influence current climate phenomena is a prerequisite for developing confident projections of the way in which Earth's climate system will change and evolve across timescales (Solomon, 2007). The climate community thus far has relied heavily on quite comprehensive ground–based measurements, space–borne measurements and mathematical models of Earth's climate, that serve to integrate the different components of the earth, namely land, ocean and the atmosphere (Palmer, 2008). The above measurements have resulted in vast conclusions drawn regarding the nature of earth's climate, however, there is still a great deal that is not yet understood (Palmer, 2008). Aerosols are ubiquitous in the atmosphere and have important implications for understanding earth's climate. For that reason it is useful to integrate ground

based and satellite based sensing techniques to give a robust methodological retrieval of aerosol optical characteristics on a global and local scale.

Long–term, detailed measurements from satellites, ground–based instruments and weather quality data are required to adequately measure aerosols for a given area. Field measurements (ground based) offer detailed observation of aerosol chemical and physical properties (Chin, et al., 2016). However, they have limited spatial and temporal coverage. Satellite instrumentation provides the widespread temporal and spatial coverage required however, they cannot give robust information regarding the properties of aerosols in specific localities. Satellite and ground measurements alone are unable to offer detailed information regarding aerosol distributions, physical, chemical and optical properties (Chin, et al., 2016). Therefore, in order to gain a better understanding of aerosol impacts, studies need to combine satellite, ground – based measurements and established climate models. There is a need to study aerosol radiative forcing and optical properties, using a combination of instruments for locations within South Africa.

Urban areas are significantly impacted by poor air quality due to a coupling of high anthropogenic emissions and high population density. The lowest–income tier of the population tend to be exposed to the worst air quality due to their homes located in informal settlements. Informal settlements are usually situated near highways, power generation facilities and industry which are some of the main sources of air pollution (Hersey, et al., 2015). South Africa is a developing country and undergoing economic expansion. The highest concentration of PM in South Africa, have been measured in townships and informal settlements during the winter months, when domestic burning is utilized for heating and cooking (Hersey, et al., 2015). In developing countries, low income households are predisposed to using non–electricity energy sources such as coal, wood and paraffin which cause the increased emissions of PM thus deteriorating air quality (Hersey, et al., 2015). There is the potential for significant increase in the emissions of anthropogenic aerosols in South Africa (Roberts, 2008).

The highest authority that regulates air quality in the country is the South African Constitution, which specifically states that everyone has the right to an environment (including an atmospheric environment) that is not harmful to their health and well–being (South Africa , 2009). The National Environmental Management Act 107 of 1998 (NEMA), provided the platform for the Air Quality Act of 2005 (AQA), which serves to manage air quality in the

country. As part of this Act the government provides guides regarding their air quality decisions such as ambient air quality standards, emissions and the management of air quality principles (South Africa, 2009). According to the summarised State of Air in South Africa Report of 2013, PM is regarded as the greatest national cause for concern in terms of air quality. The report also indicated that it was important to take action at the local level, to alleviate high particulate emissions (DEA, 2013). It is for this reason, that investigating air pollution at the local level, i.e., Durban, is important. Similarly, a number of air pollution "hot spots" exist around South Africa, hindering air quality. An example of a community degraded by air pollution is located in Durban, within the South Durban Industrial Basin (SDIB) (Guastella & Knusden, 2007). Since aerosols are important particulate pollutants, information about their properties provides useful knowledge to air quality decision makers. Therefore, the sun-photometer's ability to measure aerosol properties at the local level is beneficial to air quality studies in the region of Durban.

Durban is located at an optimum position to receive aerosols from South American regions, such as Chile. The Calbuco volcano, in Chile, erupted on 22 April 2015 at 18:04h LT. This was a major 90 minute eruption of a greyish column of ash that rose up approximately 15km above the crater (Figure 1.2). It drifted towards the north and north east (Reckziegel, et al., 2016). It and was followed by smaller eruptions on 23 April 2015 at 01:00h LT and 30 April 2015 at 13:10h LT. Due to the position of Durban, it is possible that aerosol plumes from the Calbuco volcanic eruption reached Durban (Figure 1.1). It is useful to determine if aerosols from the eruption reached Durban, by using trajectory analysis as well as aerosol optical properties.

Figure 1.1 Depicts the relation of Chile from Durban, obtained from Google Earth.
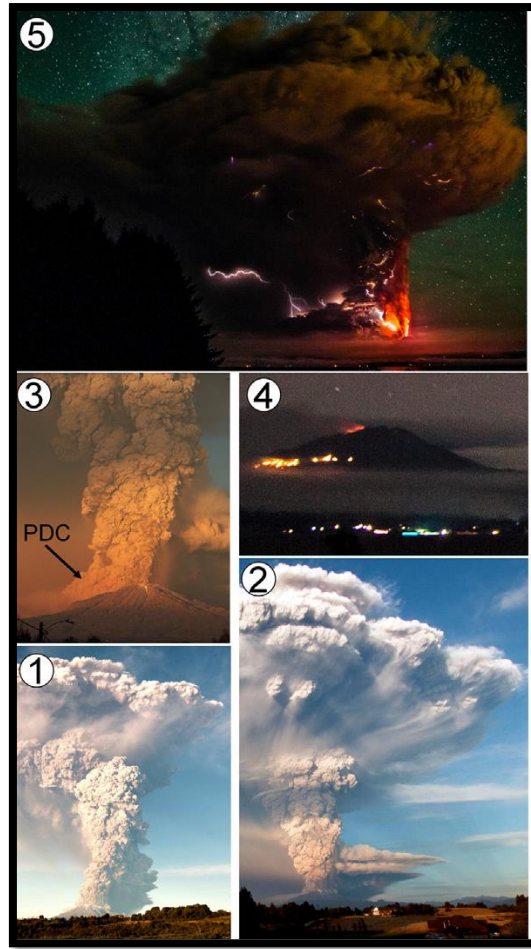
Figure 1.2 Calbuco Eruptive column during the 22 – 23 April 2015 obtained from Romero, et al., 2016.

1.2. Aim and Objectives

1.2.1 Aim

The main aim of this study to examine aerosol microphysics and optical properties over Durban using ground based and satellite based data.

1.2.2 Objectives

1. To study the aerosol optical properties over Durban
2. To compare the differences in aerosol properties over Durban and Skukuza
3. To compare aerosol properties measured from Ground Based sun-photometer and MODIS satellite data over Durban.
4. To identify the source regions and transport pathways of aerosol loading over Durban using HYSPLIT trajectory model.

6

5. An exploratory study to determine if air mass from the Calbuco Volcano eruption in Chile impacts over Durban.

1.3 Study Area

South Africa is extended between 22°S – 36°S latitude and 16°E – 34°E longitude. South Africa's atmosphere is impacted by most aerosol types formed by both natural and anthropogenic activities (Kumar, et al., 2014a). This study will focus on Durban, a coastal city on the east coast of Southern Africa. Durban is the third largest urban area in South Africa and the largest city in the province of KwaZulu – Natal (KZN). Durban is the largest city in KwaZulu-Natal. It has a total municipal area of 2292 km^2 and forms part of the eThekwini Municipality. The municipality and has a population of approximately 3.5 million people (Lehola, 2012). Durban has become one of the most important contributors to economic development in South Africa, the industries in this region contributes to approximately 22% of the cities Gross Domestic Product (GDP) (Thambiran & Diab, 2010). The local government responsible for managing the city is the eThekwini Municipality. The management of climate change and air quality are controlled by the eThekwini Municipality. There are very few studies informing the municipality regarding aerosol optical properties over Durban.

Durban lies at an altitude of 46m above sea level therefore the synoptic meteorology is important in understanding aerosol characteristics and transport mechanisms. Durban has many sources of air pollutants; however the combustion of fossil fuels and road transport are responsible for the most air pollutants (Thambiran & Diab, 2011). Durban is home to the SDIB which extends to cover ~60km of land on the eastern seaboard of South Africa (Scott & Diab, 2000). It contains small chemical, food, beverage and textile industries and is dominated by two oil refineries (Engen and SAPREF), the Mondi paper mill, a sugar refinery, chemical industries and the busiest port in Africa (Guastella & Knusdon, 2007). The land is used for several purposes such as residential, commercial and industrial activities and the low–lying location of the SDIB (situated between two ridges) causes increase in air pollution potential (Scott & Diab, 2000). Therefore, due to the high aerosol potential in the SDIB, the study of aerosol radiative forcing and optical properties in Durban is quite important. The approach to air quality studies has been discontinuous and unsystematic in South Africa as a whole and although a number of studies have been completed, results are not integrated and easily accessible (South Africa, 2009). The use of different instrumentation will provide the necessary information for the study of aerosol properties in Durban. Aerosol pollutants that have

originated from the interior of the city travels towards the coast at night in the regional mountain plain winds only to be brought back to the ocean during the day by the sea breeze system (Scott & Diab, 2000). This study will focus on comparing and evaluating the measurements of tropospheric aerosols from satellite and ground based observations, for Durban, South Africa. As well as comparing measurements from the Durban sun-photometer with the Skukuza sun-photometer.

Skukuza is a rural, agricultural area located within the Kruger National Park in the north–eastern parts of South Africa (latitude: 24° 59′ S; longitude: 31° 35′ E; elevation: 150 m above sea level) (Kumar, et al., 2013). Skukuza is home to the first AERONET site operating on the Southern African sub–continent and has provided routine monitoring of aerosol optical properties since 1998 (Kumar, et al., 2013). Aerosols come from various different sources in Skukuza, such as being released from biomass burning or smoke aerosols during the dry season and natural sources such as sea salt and dust. Major cities in South Africa produce copious amounts of aerosols and trace gases due to industrial activities and automobile emissions (Kumar, et al., 2013). Therefore, the characterisation of aerosol optical properties in South Africa is important, hence aerosol properties from Durban and Skukuza will be compared. Skukuza is the first AERONET site in southern Africa hence there is a variety of literature on the aerosol optical properties in Skukuza (Eck, et al., 2003; Freiman & Piketh, 2002; Kumar, et al., 2013; Kumar, et al., 2014a; Kumar, et al., 2015a; Ogunjobi, et al., 2008), therefore the preliminary results from the Durban sun-photometer will be compared to Skukuza for validation purposes. Skukuza lies on the same latitudinal gradient as Durban (Kumar, et al., 2014). Skukuza is more inland and is representative of the regional area of north–eastern South Africa, whereas Durban lies on the east coast of South Africa, therefore, it is useful to compare the contrasting aerosol optical properties and sources in both regions. Also, due to the lack of data for Durban, seasonal variations are not possible, therefore, a long term dataset from Skukuza from July 1998 to July 2011 will be used to determine the seasonal aerosol trends.
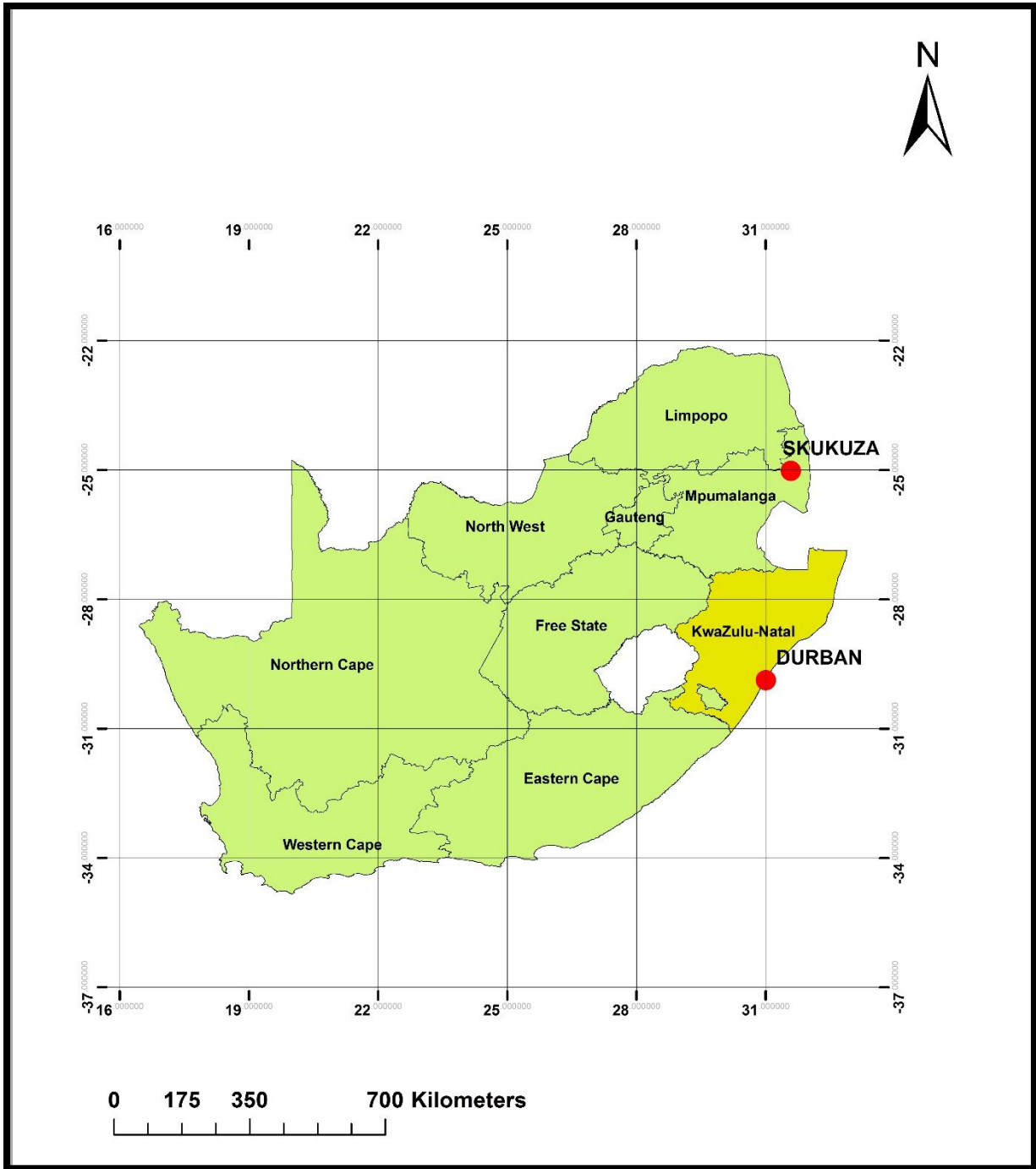
Figure 1.3 Map of study area, including location of AERONET sites (red dot)

1.4 Thesis structure

The next chapter will detail the aerosol optical properties and characteristics, as well as aerosol studies carried out in South Africa with a greater focus on Durban. Chapter three will serve to outline the methods and instrumentation used in this study as well as the processed used to analyse the data. Chapter 4, will present the results of the analysis of aerosol optical properties over Durban from January to September 2014. Chapter 5, will depict the comparisons between

aerosol optical properties in Durban, with that of Skukuza. Chapter 6 will detail the comparison between AOD obtained from the Durban sun-photometer with AOD obtained from MODIS satellite data. It will also outline the source, path and trajectory of aerosol plumes reaching Durban, by using the HYSPLIT model to ascertain trajectories. Chapter 6, will depict if the volcanic plumes from the Calbuco volcanic eruption in late April 2015 reached Durban. Chapter 7 will outline the major conclusions reached in this study.

CHAPTER TWO

2. A REVIEW OF AEROSOL PROPERTIES AND CHARACTERISTICS

2.1 Introduction

The first assessment carried out by the Intergovernmental Panel on Climate Change (IPCC) during 1990 identified the presence of numerous gaseous agents that can impact climate change. These agents were greenhouse gases, tropospheric aerosols, land–use change, solar irradiance and stratospheric aerosols injected into the stratosphere from large scale volcanic eruptions. These agents serve to provide key quantitative estimations as to the extent of gas forcing climate change since the pre–industrial times (Watson , et al., 1990). These gases play crucial roles in the current understanding of climate change and influence weather conditions. In order to underpin the facets of climate change, it is vital to study these particles and the impact that they have on meteorological conditions.

Subsequent IPCC assessments have recognised various other agents that have the ability to alter climate. There is a significant body of knowledge on the characteristics of these gaseous agents such as their atmospheric lifetimes, sizes and their impact on other meteorological features. This is because these particles change the amount of heat energy reaching the surface of the earth thereby acting as radiative forcing agents (Houghton, et al., 2001; Solomon, 2007; Stocker, et al., 2013; Watson , et al., 1990). The concept of radiative forcing has been extensively viewed as important for climate prediction and the necessity of studying it at the local level, on seasonal timescales is highly recognised. The IPCC (1992) highlighted the importance of climate forcing due to anthropogenic aerosols and calculated this effect quantitatively for the first time (Watson, et al., 1990). Aerosols are short lived (contrary to greenhouse gases), therefore, observations of their concentration over large spatial and temporal distributions are required to study their radiative effect (Stocker, et al., 2013).

The study of aerosols has been on the rise since its commencement by John Tyndall (1870) who performed experimental studies on light scattering from aerosols and the first theoretical work of Rayleigh in 1871 and 1881. Light scattering of particles has been utilised to investigate many physical characteristics and phenomena (Berne & Pecora, 2000). The development and advancement of aerosol science improved at a steadfast pace with the acknowledgment of industrial pollutants being detrimental to human health and the environment. Industrial hygienists grouped themselves into scientific and professional fields that connected researchers, consultants and governments in order to reduce workplace toxicology (Sellers,

1994). The advent of quantitative monitoring aimed at safe concentration levels of harmful gases heightened the interest in aerosol studies. During the 1950s, the development of specific advancements in cloud microphysics also allowed for the development of aerosol science (Lee, et al., 2009).

In the 1960s greater attention was placed on aerosol loads due to a number of air pollution events which led the United States Congress to pass the Air Pollution Control Act of 1955 which established the federal government as having preeminent control over air pollution matters. Further consideration was imposed on automotive and industrial emission control during the 1970s. The huge regard placed on air pollutants resulted in the development of many technologies to monitor and evaluate aerosols and greenhouse gases. In recent years, aerosol properties have been studied using ground based and satellite instrumentation. It has been greater than three decades since the launch of the first satellite instrument utilised for atmospheric aerosol detection (Lee, et al., 2009). This has followed the advent of many powerful remote sensing and ground based technologies for aerosol detection.

The use of these new technologies has led to a generation of various aerosol constituents such as aerosol spatial distribution, temporal variation, fraction of fine and coarse modes, vertical distribution, light absorption, and some spectral characteristics. These parameters can be employed to understand aerosol trajectories and sources; interactions between aerosols and natural cycles; and the involvement of aerosols in the climate system (Lee, et al., 2009). This literature review discusses the properties and characteristics of aerosols, such as aerosol particle size distribution, aerosol shape and aerosol optical depth. Additional focus of this review will be on aerosol pollutants in Durban, South Africa and the influence that aerosols have on local and synoptic meteorology in Durban.

2.2 Aerosols definition

Atmospheric aerosols can loosely be defined as small particles that are suspended in the atmosphere. Therefore atmospheric aerosols are a suspension of liquid and solid particles in air which includes both the particles and the gas that it is suspended in (Kanike & Sivakumar, 2015). However there is currently no universal, accepted definition of the term aerosol. Nevertheless, there exist certain definitive characteristics that allows for the differentiation between aerosols and other objects suspended in gas (Lushnikov, 2010). The first distinguishable trait is that aerosol particles can exist beyond the aerosol for a sustained period of time. The additional trait is that an aerosol can be described in terms of the concentration of

aerosol particles, also known as a concentration field (Lushnikov, 2010). Aerosols are produced in the atmosphere through several natural and anthropogenic processes, and they are entrained both horizontally and vertically throughout the atmosphere (Ramachandran & Kedia, 2013). Aerosols are extremely diverse in terms of their spatial and temporal distributions. They have various local source mechanisms, swift aging and chemical transformation processes and a short lifespan. Therefore, their climatic roles are quite complex and not easily quantifiable (Tesfaye, et al., 2013).

Aerosols can be separated into two categories, namely, primary aerosols and secondary aerosols according to the processes involved in their origination. Primary aerosols are formed from various either fragmentation or combustion processes and occurs in the carrier gas as definitively shaped objects (Figure 2.1). Therefore primary refers to those emitted in particle form (Després, et al., 2012). Secondary aerosols on the other hand appears in the carrier gas as a consequence of gas to particle conversion and is essentially formed from "nothing" (Lushnikov, 2010). Differentiating between natural and anthropogenic particles in the atmosphere remains to be quite difficult especially due to global environmental changes caused by human activities which affect all aerosol source processes (Heintzenberg, 2003). Mineral dust, sea salt, black carbon and biological aerosol particles enter the atmosphere as primary particles, whereas non–sea–salt sulphate, nitrate and ammonium mainly materialize from secondary aerosol formation processes. Figure 2.1, displays primary aerosols emitted into the atmosphere from sea–spray, volcanic ash, biogenic emissions and anthropogenic activity. Some of the direct emissions undergo oxidation and convert into secondary aerosol particles.
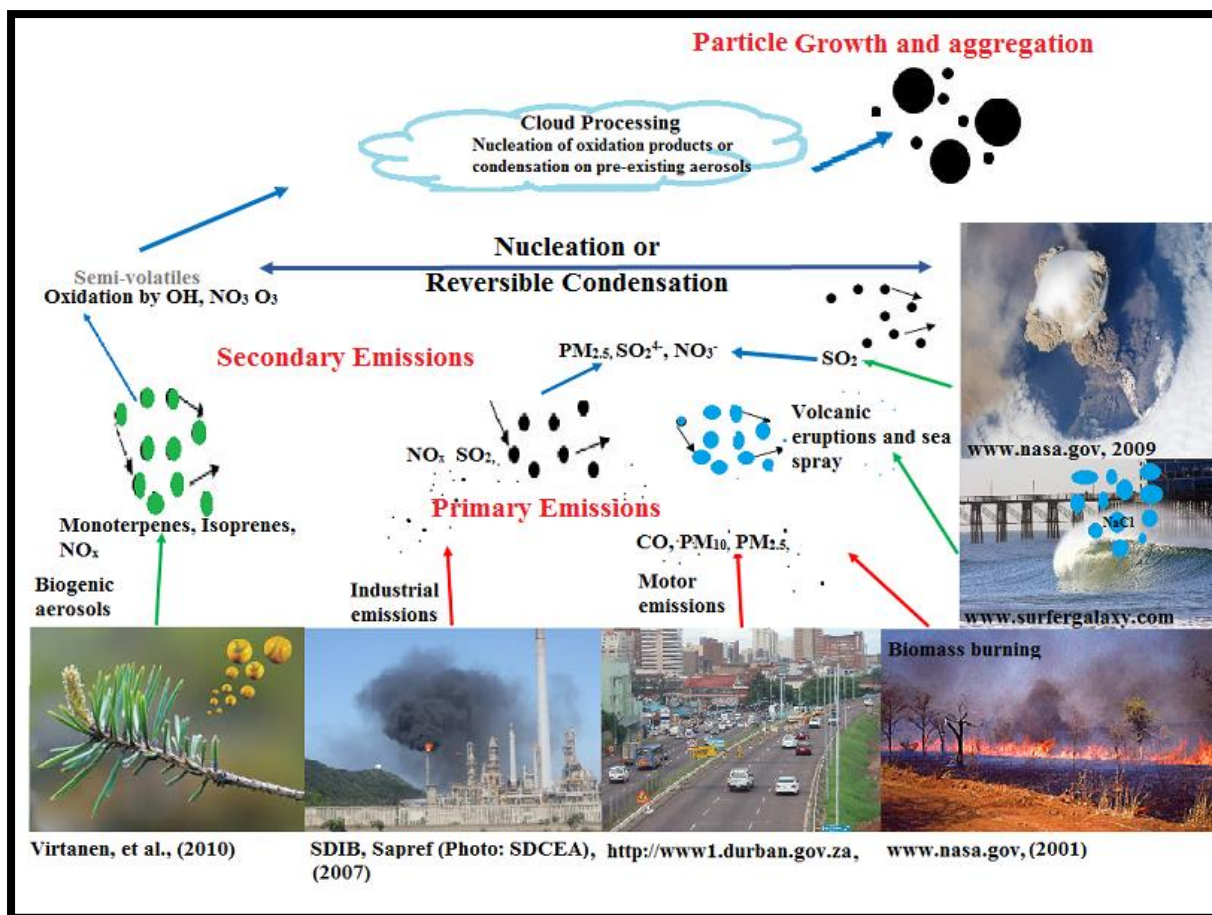
Figure 2.1 Schematic diagram showing the formation of primary and secondary aerosols (adopted from the web resources – see in the picture)

Both primary and secondary aerosol particles are characterized, recognized and identified by their size, shape and chemical content. The shapes of aerosols are of importance because they affect the physical characteristic of the particle by influencing its scattering abilities (Shao, et al., 2012). The assumption that aerosol particles are true spheres are rarely made since most aerosol particles are to a certain degree non–spherical (Shao, et al., 2012). The shape and size of aerosols can provide information as to their origin. Furthermore, the formation and development processes of atmospheric aerosols are essential for understanding and quantifying the dynamics of atmospheric aerosols, such as their climatic effects (Kulmala, et al., 2001).

2.3 Aerosol and climate: Direct and Indirect effects

The climatic effects of aerosols only gained attention in the mid– 1970s, however research into aerosols climatic effects was neglected in the 1980s due to the increase in carbon dioxide (CO_2) and other GHGs (Andreae & Crutzen, 1997). In the last decade there existed a shift in scientific interest in aerosols due to the proposed relationship between aerosols and global climate

change. This relationship has resulted in a plethora of information regarding the role of anthropogenic aerosols in climate change and it was suggested that aerosols may exert a climate forcing similar in magnitude but opposite in sign to that of GHGs (Andreae & Crutzen, 1997).

The climate of the earth has the capacity to be altered due to shortwave radiation from the sun, being scattered and absorbed, and thermal infrared radiation being absorbed and emitted by the earth atmosphere system. If the climate system is in equilibrium then the absorbed solar energy is exactly balanced by radiation emitted to space by the Earth and atmosphere. As such, any factor that disturbs this balance is regarded as a radiative forcing agent (Ramaswamy, et al., 2001). Radiative forcing as defined by Ramaswamy, et al., (2001) is the variation in net (down minus up) irradiance (solar plus longwave; in Wm^{-2}) at the tropopause after taking into account stratospheric temperatures, to readjust to radiative equilibrium, but with surface and tropospheric temperatures and state held fixed at the unchanged values. Radiative forcing is changes in the energy fluxes of solar radiation (shortwave) and terrestrial radiation (long wave) in the atmosphere caused by anthropogenic activities resulting in changing atmospheric composition. Therefore radiative forcing is used to ascertain and compare the anthropogenic and natural drivers of climate change. Though, it is quite challenging to calculate the extent of this forcing. Additionally, we lack the ability to better quantify non–greenhouse gas radiative forcing, especially those that arise from aerosols – cloud interactions (Boucher, et al., 2007).

Figure 2.2 below depicts how clouds and aerosols influence climate change. Forcings associated with agents such as GHGs and aerosols affect the global mean surface temperature by their impact on the global radiative budget. Rapid adjustments occur when forcing agents change the flows of energy internal to the climate system, affect cloud cover or other parts of the climate system and indirectly change the global radiation budget. These adjustments are usually rapid and occur within a few weeks and are not mediated by mean surface temperature. Feedbacks deal with changes in climate variables that are mediated by a change in global mean surface temperature. Therefore feedbacks, serve to heighten or hinder global temperature changes due to their impact on the radiative budget (Boucher, et al., 2007). The radiative forcing of clouds and aerosols can be divided into direct and indirect effects.
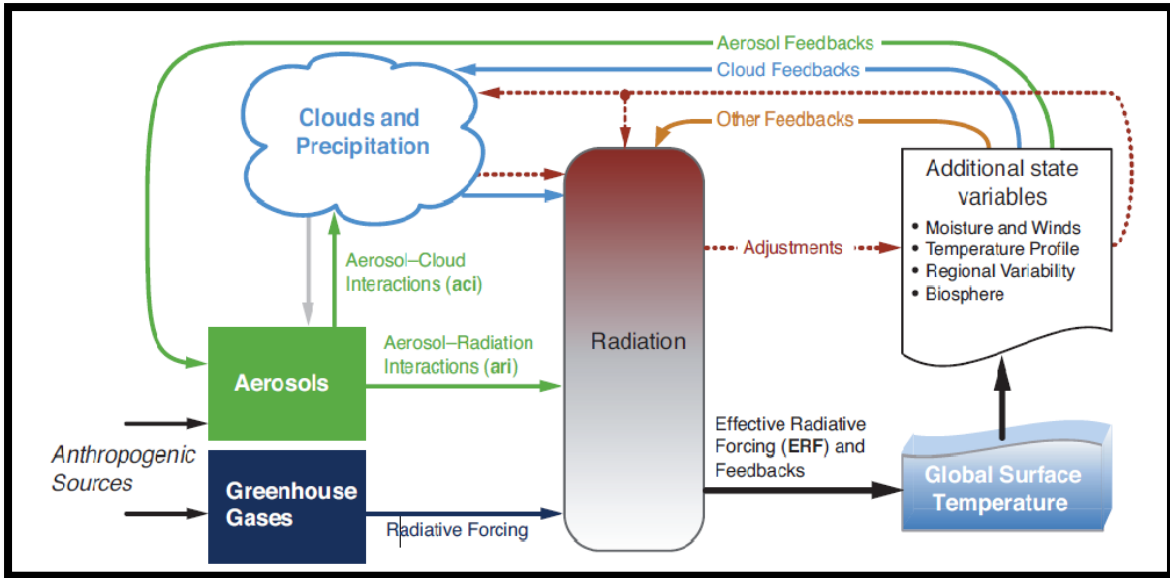
Figure 2.2 Overview of forcing and feedback pathways involving greenhouse gases, aerosols and clouds (Obtained from, Boucher, et al., 2007).

Forcing agents are given in the green and dark blue boxes, with forcing mechanisms indicated by the straight green and dark blue arrows. Feedback loops, caused by changes in the surface temperature, are signified by curving arrows (blue represents cloud feedbacks; green represents aerosol feedbacks; and orange represents other feedback loops such as those involving the lapse rate, water vapour and surface albedo). The final temperature response depends on the effective radiative forcing (ERF) that is felt by the system after accounting for rapid adjustments and feedbacks (Boucher, et al., 2007).

2.3.1 Aerosols direct effect on radiative forcing

The incident solar radiation initiates the climate system, atmospheric chemistry as well as life on Earth. Approximately 30% of the incoming solar radiation is reflected back to space whereas the other 70% is absorbed by the surface (the atmosphere system) (Ramanathan & Feng, 2009). It is this energy that heats the planet and the atmosphere (Ramanathan & Feng, 2009). The warming of the atmosphere and surface causes the emittance of energy as infrared radiation (long wave radiation). Greenhouse gases (GHGs) absorb and emit solar radiation whereas aerosols absorb and scatter solar radiation (Ramanathan & Feng, 2009). The scattering of incoming solar radiation back to space cools the earth and certain areas of the troposphere. This is due to their perturbation of sunlight from the Earth's surface. Aerosols can also absorb and emit long wave radiation which prompts heating effects; however, depending on the underlying surface and the atmospheric conditions it might also result in cooling (Tesfaye, et al., 2013).

16

2.3.2 Aerosols indirect effect on radiative forcing

Indirect radiative forcing refers to changes caused by aerosols on other participants in the climate system such as clouds. Cloud brightness is influenced by the availability of aerosol particles which act as cloud condensation nuclei. The indirect effect is therefore divided into two categories relating to radiative forcing, the first category is caused by the altering of the radiative properties of clouds (cloud albedo effect) and second category is the effect of anthropogenic aerosols on the lifetime of clouds (cloud lifetime effect) (Boucher, et al., 2007). It deals with the aerosols in the lower atmosphere changing the size of cloud particles by acting as cloud condensation nuclei and ice nuclei. This affects rainfall by altering the size and number of rain droplets. As such, the indirect effect changes how clouds reflect and absorb solar radiation and affects rain drop formation. This causes changes to earth's radiation budget and rainfall patterns (Ramachandran & Kedia, 2013). Figure 2.3, displays aerosols direct affect by scattering incoming solar radiation and aerosols indirect affect, depicting the process of aerosols acting as cloud condensation nuclei.
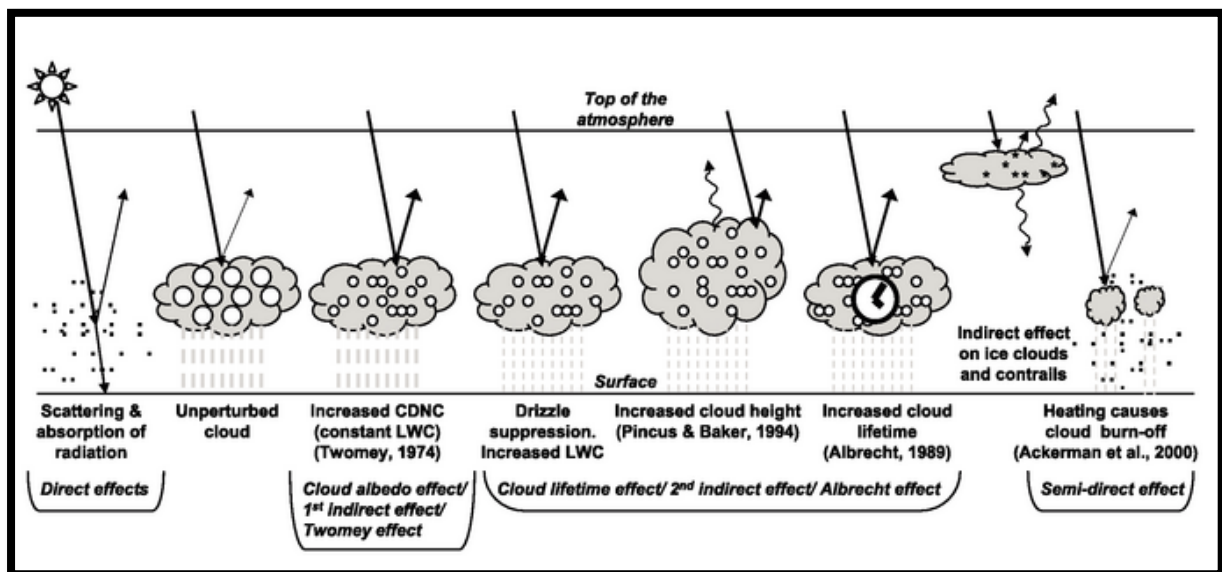
Figure 2.3 Schematic diagram showing the various radiative mechanisms connected with aerosols' direct and indirect effects (obtained from Haywood & Boucher, 2000).

2.4 Optical properties of aerosols

The optical properties of aerosols that cause both the direct and indirect effects are determined by aerosol size distribution, morphology and chemical composition. It is important to understand these factors because they determine radiative forcing at a particular region (Boucher, 2015). Aerosol optical properties are essential to understand the impact that aerosols

17

have on climate. The major spatial and temporal variability of aerosol particles are due to their optical properties, which are in turn influenced by their chemical composition, size, shape, concentration and mixing state (Montilla, et al., 2011). The optical properties of anthropogenic aerosols are usually characterized by three parameters: a) the extinction coefficient which determines the amount of interaction of radiation and the aerosol particles; b) the single scattering albedo which determines the degree of absorption and c) the scattering phase function which determines the angular distribution (Haywood & Boucher, 2000). These parameters and aerosol characteristics is strongly influenced by atmospheric processes such as coagulation, condensation, sedimentation, chemical transformation and cloud processing.

2.4.1 Aerosol optical depth

Aerosol optical depth (AOD) is an important parameter to determine the climate forcing of aerosols. AOD is a measure of the degree to which airborne aerosols inhibit the transmission of light by absorption or scattering of light. Therefore it describes the attenuation of solar radiation by a column of aerosol and thus acts as a measure of aerosol column concentration (Hinds, 2012). It is the integrated extinction coefficient over a vertical column of a cross section of air and is useful for gaining information regarding aerosol source regions and aerosol evolution (Adesina, et al., 2014).

2.4.2 The Angstrom Exponent ($\alpha_{440-870}$)

Another, useful aerosol property is the Angstrom Exponent ($\alpha_{440-870}$) which is often used as a qualitative indicator of aerosol particle size, values that are greater than two represent small particles associated with combustion by–products and values less than one represent large particles such as sea salt and dust (Schuster, et al., 2006). The $\alpha_{440-870}$ is dependent upon the aerosol size distribution and is a measure of the ratio of course–to–fine–mode aerosols (Ångström, 1964). The $\alpha_{440-870}$ is governed by the following equation (Ångström, 1964):

$$\tau(\lambda) = \tau_1 \lambda^{-\alpha}$$

$\tau(\lambda)$ is the AOD at the wavelength λ, τ_1 is the estimated AOD at a wavelength of 1 mm (sometimes called the turbidity coefficient, and α is the Angstrom exponent (Ångström, 1964). The $\alpha_{440-870}$ is measured using sun photometry and can also be accessed from satellite retrievals. Kumar, et al., (2015), used the $\alpha_{440-870}$ obtained from MODIS satellite data, to study aerosol optical properties over Durban. It was found that there was a prevalence of fine–mode aerosols during spring and summer and an increase of coarse–mode aerosols in winter.

2.4.3 Single Scattering Albedo

The Single Scattering Albedo (SSA) is the ratio of scattering efficiency to the total extinction efficiency. SSA depends on aerosol composition and size distribution. It is zero for pure absorbing aerosols (e.g. soot) and one for pure scattering aerosols (e.g. sulphates). SSA is influenced by wavelength due to the impact of dust and anthropogenic activities during the summer and winter seasons (Adesina, et al., 2014). According to Takemura, et al., (2002), the inherent parameters for controlling the atmospheric shortwave radiation absorption are the AOD, SSA for an optically thin atmosphere and surface albedo. The values of SSA are quite inconsistent because of the differing chemical and physical characteristics associated with aerosols (Takemura, et al., 2002). SSA of column integrated aerosols can be obtained from optical observations provided by AERONET and is an important parameter to consider when estimating aerosol radiative forcing. According to Montilla, et al., (2011), the aerosol SSA, "ω" is the portion of aerosol light scattering over the extinction and is given by:

$$\omega_0 = \frac{\sigma_s}{\sigma_s + \sigma_a}$$

where σ_s and σ_a are the aerosol scattering and absorption coefficients, respectively. The SSA ω_0 is an especially important aerosol optical property because it influences the radiative effect of aerosols (Montilla, et al., 2011). For South Africa SSA values tend to be lower in winter and spring and higher in summer. The lower SSA values in winter are the result of pollutants being released from the onset of biomass burning or forest fires (Adesina, et al., 2014). Eck, et al., (2013), studied SSA during the biomass burning season from July to November, using AERONET sites at Mongu and Zambia in southern Africa. It was found that the monthly mean SSA at 440 nm in Mongu increased significantly from ±0.84 in July to ±0.93 in November, indicative of biomass burning during spring (Eck, et al., 2013).

2.4.4 The Aerosol Asymmetry Parameter

The Aerosol Asymmetry Parameter ASP (g) is a measure of the preferred scattering direction (forward or backward) for the light that reaches the aerosol. In terms of radiative forcing the ASP factor (g) is of extreme importance because it characterises the angular scattering (Adesina, et al., 2014). Angular scattering influences the variability of radiative forcing efficiency (Ogren, et al., 2006). The ASP factor (g) is defined as the cosine–weighted average of the phase function, where the phase function is the probability of radiation being scattered in a given

direction. Angular scattering is represented by a single value such as backscatter fraction, up scatter fraction or asymmetry parameter and is represented as (Ogren, et al., 2006):

$$g = \frac{1}{2} \int_0^\pi \cos\theta P(\theta) \sin\theta d\theta$$

Where θ is the angle between the transmitted and the scattered radiation and $P(\theta)$ is the phase function which is the angular distribution of scattering light. The phase function is the energy scattered per unit solid angle in a given direction to the average energy in all directions. The value of g ranges from -1 for light that is completely back scattered to $+1$ for completely forward scattered light. The ASP and SSA are spectrally dependent variables (Adesina, et al., 2014). ASP values tend to decrease with an increase in wavelength. For South Africa, the seasonal concentration decreases in spring (September to November) due to a greater abundance of anthropogenic (absorbing) pollutants (Adesina, et al., 2014).

2.4.5 The refractive index

The next important aerosol property to consider is the complex refractive index (index of refraction). The complex index of refraction consists of real (Re) and imaginary (Im) parts of the refractive index. The real part is a measure of how much the speed of light is decreased inside the medium relative to the speed of light within a vacuum (Patterson, et al., 1977).

The Re part of the refractive index is given by:

$$n = \frac{c}{v_p}$$

Where n is the refractive index, c is the phase velocity of a wave of light, v_p is the velocity of light in the medium itself (the aerosol). The higher the index the more light is slowed down within the medium. It is challenging to determine the refractive index of ambient aerosol particles because of their complex chemical compositions (Redmond & Thompson, 2011).

The imaginary part of the refractive index is a measure of the level of absorption when electromagnetic waves propagate through the medium. The real and imaginary parts of the complex refractive index are representative of the potential of scattering and absorption of incoming solar radiation (Adesina, et al., 2014). The higher the real part values suggests a greater concentration of scattering aerosol types and the higher imaginary values suggests absorbing aerosol types (Adesina, et al., 2014). Therefore, the complex index of refraction is given by:

$$n = n_{RE} - n_{IM}$$

Where n_{RE} is the real part, which is ratio of the speed of light in a vacuum to the speed of light in the material and n_{IM} is the imaginary part which is an absorption parameter representative of the material (Patterson, et al., 1977).

2.5 Aerosol size

Atmospheric aerosols are polydisperse which means that they display a multitude of size ranges (Boucher, 2015). Hence an aerosol population is first characterised by its size distribution. The size of atmospheric aerosols can span several orders of magnitude from a few nanometers (nm; 1 nm = 10^{-9} m) for new particles formed due to nucleation to approximately 100 micrometres (μm; 1μm; 1μm = 10^{-6} m) for the largest particles. This is an extremely wide size range since the mass of a 10 μm diameter particle is equivalent to the mass of one billion 10 nm particles. It is probable to identify different classes of aerosols based on their size range. It is possible to identify up to five different size modes, namely nucleation mode also called ultrafine mode, the Aitken mode, the accumulation mode (it is duly named because mass accumulates in this size range by the processes of condensation and coagulation), the coarse mode and the super coarse mode (Boucher, 2015). Figure 2.4 depicts the different aerosol size modes and their sources. Therefore, aerosol size distribution is characterised by various relative maxima and modes and represents different populations of particles generally classified in three or more modes (Boucher, 2015). The nucleation, accumulation and coarse mode particles are generally grouped within the following size ranges defined by using the particle aerodynamic diameter (D_a[1]). The aerodynamic diameter is the diameter that a particle with ideal unitary density $1000kg/m^3$ should have to sediment the same speed of a particle with its real density and diameter. Nucleation and Aitken mode ($D_a < 0.1$ μm), accumulation mode ($0.1 < D_a < 1$ μm) and coarse mode ($D_a > 1$μm) (Boucher, 2015).

Fine aerosols are made up of particles grouped within the first two modes ($D_a < 0.1$ μm) and coarse aerosols are of a larger size ($D_a < 10$ μm). If particles are smaller than the molecular mean path, they are referred to as fine particles (Lushnikov, 2010). Fine particles are formed chiefly by secondary processes such as gas–to–particle conversion mechanisms and by primary sources such as the various types of combustion (Seinfeld & Pandis, 2012). The nucleation mode occurs due to the nucleation of new particles from rapid gas condensation.

Aerosol particles less than 0.1 µm in diameter are usually the most abundant among all particles in the air (Kang, et al., 2013). Their concentrations can be determined with the Aitken counter which is a measurement of particle number density. Due to their small size, Aitken particles contribute very little to the total mass concentration of all aerosol particles. The Aitken mode results from the condensation of vapours into nucleation mode particles and from their resultant coagulation as well as from primary combustion emissions (Dall'Osto, et al., 2012). The nucleation mode occurs from prolonged condensation of vapours on Aitken particles and from the production of particle mass by chemical reactions in non–precipitating cloud droplets. The aerosol condensation sink controls how fast molecules condense onto pre–existing aerosols and this is heavily influenced by the shape of the size distribution (Kulmala, et al., 2001). Therefore, nucleation is the formation of ultrafine particles distinguished at a few nm and the consequent growth of these particles to approximately 100 nm in 1 to 2 days (Kulmala, et al., 2001). This is noticed frequently in the particle boundary layer (Kulmala, et al., 2001).

Accumulation mode refers to the "aged" mode of aerosol development. Aerosol particles within this mode grow from smaller sizes due to coagulation from transient nuclei or condensation and usually stay within this size range throughout its lifetime (Kanike & Sivakumar, 2015). Therefore, accumulation mode occurs in the atmosphere and is responsible for most of the surface area of the aerosol. As a consequence of their long residence times accumulation mode particles contribute to air pollution and causes variation of atmospheric transparency along expansive geographical borders.

Coarse particles are formed primarily via mechanical processes like dust suspension or re–suspension and sea spray (Srimuruganandam & Nagendra, 2011). Coarse particles have quite large sedimentation velocities allowing them to settle by dry deposition within a few hours of transport in the lower troposphere. Due to their high velocities, course particles settle rapidly therefore their mass, shape and maximum size tends to be quite variable (Srimuruganandam & Nagendra, 2011). When particles are accumulated in the coarse mode, they can be removed more rapidly by dry or wet deposition because of the larger particle size (Seinfeld & Pandis, 2012). Coarse particles do not account for more than a few percent of the particles by number concentration however they do account for a large portion of particulate mass.

The difference between fine and coarse mode particles is of significance to studies dealing with physical and chemical aerosol properties and studies dealing with the adverse health effects of aerosols. There are many studies that measure aerosol size distributions in urban, rural, and

remote sites around the globe and most measurements of size include some measurements of aerosol size distribution (Kanike & Sivakumar, 2015).
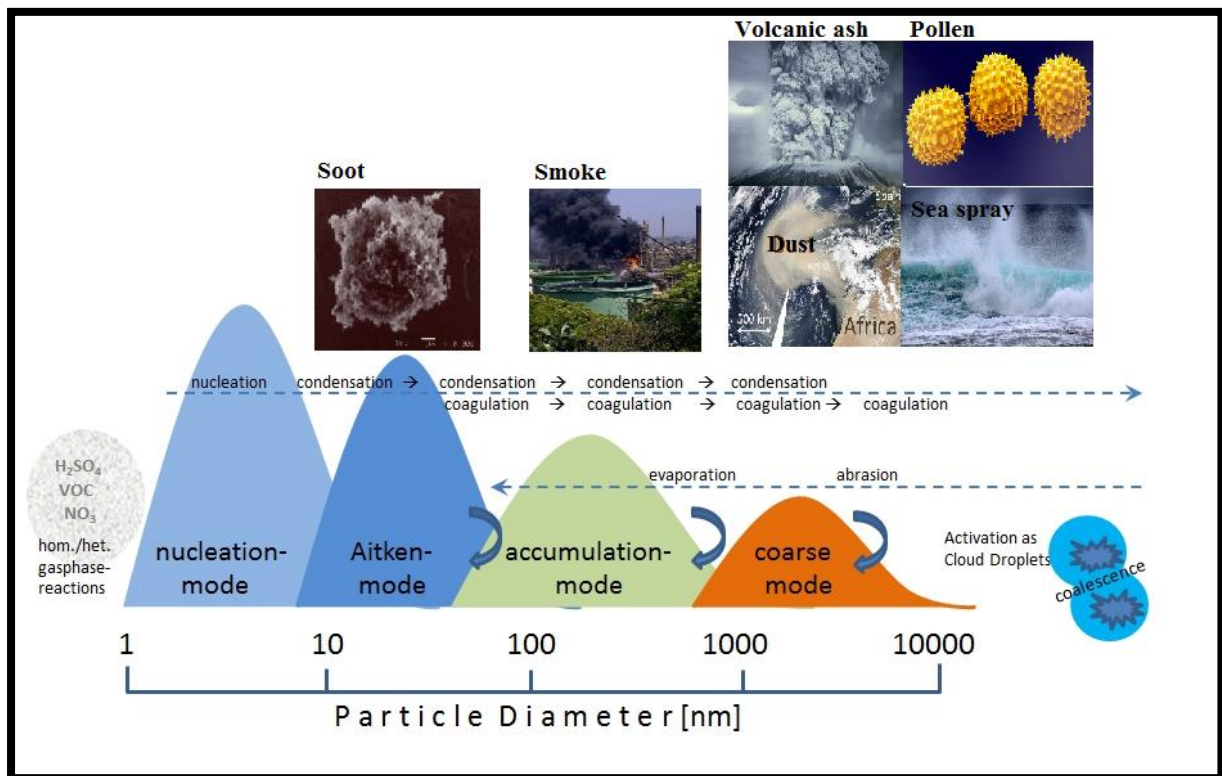
Figure 2.4 Classification of different aerosols and their modes adapted from (Deutscher Wetterdienst , 2010; IRIN, 2014; NASA, 2015; Specialists, New Jersey Allergy and Asthma, 2016).

2.5.1 Particle size distributions

In both urban and rural areas the atmosphere contains a considerable amount of aerosol particles. Due to the aforementioned wide size distribution of aerosol particles it is important to develop mathematical methods to characterize aerosol particles. An aerosol particle is understood to have an integer number '*k*'of molecules or monomers (Seinfeld & Pandis, 2012). The smallest aerosol particle could be characterized as containing two molecules. The aerosol size distribution could then consist of the number concentration of each cluster (N_k), which is the concentration (per cm^3 of air) of particles containing '*k*' molecules. However, this discrete method of characterizing aerosols cannot be used in practice due to the large number of molecules that comprise even the smallest aerosol particles (Seinfeld & Pandis, 2012).

It is important to determine how much the individual particle sizes in an aerosol contribute to total concentration rather than determining just the total number concentration. The size distribution is achieved by plotting the particle number concentration per size bin ΔN_i against

23

the average diameter D_i of the respective size bin. The size bins tend to increase with increasing diameter therefore the measured number concentrations of different size bins cannot be compared directly. It is for this reason that a given size distribution is formulated in a differential way, meaning the measured number concentrations are divided by the respective size bin, $\Delta N_i / \Delta D_i$, which becomes dN/dD in the limit where the widths of the size bins go to zero N = $\sum_{i=1}^{N} \Delta N$ (Seinfeld & Pandis, 2012).

The average size and width of an aerosol size distribution is to a large extent dependent on the chemical composition, physical properties and age of the aerosol. There exist various distribution functions to represent atmospheric aerosols, however, the most common is the lognormal distribution function (Kanike & Sivakumar, 2015). This is because measurements of natural variables are generally characterised by probability distributions which has a close likelihood to the lognormal distribution. Each of the different size modes of aerosols is defined by an individual lognormal distribution. The log–normal distribution for the number concentration is given as follows, where σ_i is the width of the distribution:

$$n_N\left(D_p\right) = \frac{dN_a}{dD_p} = \sum_{i=1}^{n} \frac{N_i}{\sqrt{2\pi}\, D_p \ln \sigma_i} \exp\left[\frac{-\left(\ln D_p - \ln D_{pi}\right)^2}{2\ln^2 \sigma_i}\right] \quad (1)$$

Aerosol populations can be distinguished in terms of their number concentration, surface distribution or volume distribution. Number distributions are used when the ability of the aerosol particles to act as cloud condensation nuclei or ice nuclei is studied (Kanike & Sivakumar, 2015). Surface distributions are significant when the radiative properties of the aerosols are of interest because the surface area of the aerosol determines the amount of solar radiation it scatters. Volume or mass distributions are important when acquiring information about the total mass of the aerosol in the atmosphere or the mass that is deposited (Kanike & Sivakumar, 2015). The following equations display the number, surface area and volume distributions respectively (Kanike & Sivakumar, 2015):

Number distribution:

$$n_n(\log D_p) = \frac{dN}{d}(\log D_p) \qquad (2)$$

Surface area distribution:

$$n_s(\log D_p) = \frac{dS}{d}(\log D_p) \qquad (3)$$

Volume distribution:

$$n_v(\log D_p) = \frac{dV}{d}(\log D_p) \qquad (4)$$

2.6 Radiative Forcing of aerosols

Aerosol radiative forcing (RF) at the top of the atmosphere (TOA) and at the bottom of the atmosphere (BOA) is defined as the net change in radiative flux (down minus up) in W/m^2 with (F_N) and without (F°_N) aerosol brought about by instantaneous change in aerosol content in the atmosphere. The radiative forcing at the BOA is given by the following equation:

$$RF_{BOA} = F_{N,BOA} - F^0_{N,BOA} \qquad (5)$$

The radiative forcing for the atmosphere (RF_{ATM}) can be acquired from the radiative forcings at the TOA and BOA (Adesina, et al., 2014):

$$RF_{ATM} = RF_{TOA} - RF_{BOA} \qquad (6)$$

The radiative properties of a particle is determined by the particle composition and the accompanying, refractive indices, particle size and shape. It works according to the Mie theory, that, to a first order, aerosol extinction per unit aerosol mass is largest when the aerosol radius is comparable to the wavelength of the radiation. Consequently, this has major considerations for natural and anthropogenic aerosol radiative effects (Stier, et al., 2007). RF_{BOA} characterizes the combined effects of scattering and absorption of solar radiation by air suspended particles on the net flux at the surface. RF_{TOA} includes the reflection of solar radiation to space by aerosols and RF_{ATM} deals with the absorption of solar radiation within the atmosphere due to the absorbing particles (Adesina, et al., 2014). Therefore, negative RF values correspond to an aerosol cooling effect, whereas positive values correspond to a warming effect.

The aerosol radiative forcing efficiency (FE), is the rate at which the atmosphere is forced per unit of aerosol optical depth, at a specific wavelength. The influence of the aerosol load is ruled out of radiative forcing efficiency calculations (Garcia , et al., 2012). FE deals with the actual or total radiative effects of atmospheric aerosol.

The FE is thus calculated as follows:

$$FE_{BOA} = RF_{BOA}/AOD_\lambda \qquad (7)$$

2.7   Chemical composition

The concentration, chemical composition, and size distribution of atmospheric aerosols are characterised by immense spatial and temporal variability (Redmond & Thompson, 2011). This

variability reflects the different sources of the aerosols, transformation of aerosols and removal processes. The chemical composition of individual aerosol particles can be uniform (internally mixed aerosols) or different from their precursor species (externally mixed aerosols). As such, the particle sources and aging processes such as coagulation, gas particle partitioning and chemical reactions determine the chemical composition of aerosol particles (Pöschl, 2005). Aerosol particles are made up of complex mixtures of both organic and inorganic carbonaceous products, sulphates, nitrates, ammonium salts, sea salts, soluble and insoluble carbonaceous material, and insoluble inorganic compounds (Pöschl, 2005).
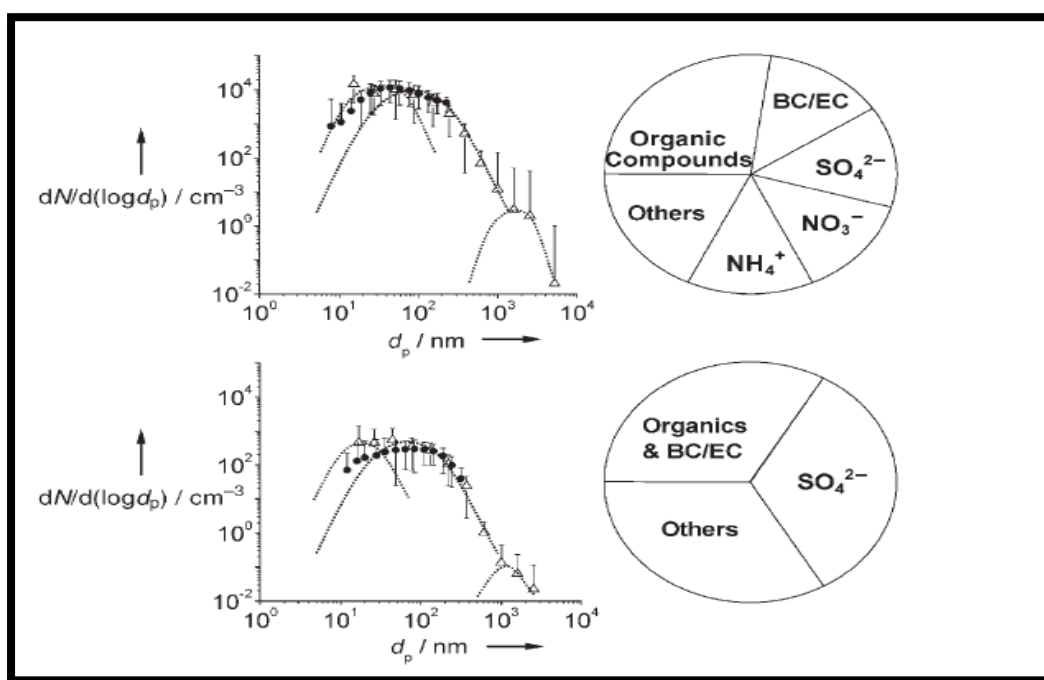
Figure 2.5 Characteristic examples of aerosol particle–size distribution and chemical composition in urban (top) and high alpine air (bottom). Graphs (left): number size distribution function dN/d (log dp). Pie charts (right): typical mass proportions of main components (obtained from Pöschl, 2005).

2.8 Sources of aerosols

Atmospheric aerosols originate from many natural and anthropogenic processes. Natural sources include windblown mineral dust, precursor gases from volcanic eruptions, natural wild fires, vegetation and oceans (Tesfaye, et al., 2011). Anthropogenic aerosol sources include emissions from fossil fuel and biofuel combustion, industrial processes, agricultural activities, human induced biomass burning and smog caused by photochemical reactions, that are essentially, the result of vehicle emissions (Tesfaye, et al., 2011). The primary sources of

biogenic aerosols are from the emission of dimethyl sulphide (DMS) from the oceans and of non–methane hydrocarbons (NMHCs) from terrestrial vegetation, as well as by their oxidation in the troposphere (Andreae & Crutzen, 1997).

2.8.1 Windblown dust

The impact of dust transport on aerosol composition and deposition are known to extend globally from major dessert regions. Dusts are notable atmospheric aerosols due to their effect on scattering and absorption of solar radiation and there is additional evidence as to the effect of dust aerosols on clouds. The effect of Saharan dust can decrease precipitation in shallow convective clouds near the source (Kok, et al., 2012). There have been various studies that have depicted that sand–dust aerosols, present in the troposphere originate from desert regions of the northern hemisphere and are transported in the atmosphere due to atmospheric circulation (Zhang & XingMing, 2012). It is the world's arid and semi-arid regions that contribute the most towards the concentration of sand–dust aerosols in the atmosphere. Research suggests that mineral dust plays an integral role in climate forcing by changing the radiation balance in the atmosphere, affecting cloud nucleation and optical properties (Ginoux, et al., 2001). Furthermore, dust can serve as a catalyst for reactive gas species in the atmosphere resulting in photochemical reactions (Ginoux, et al., 2001).

The transport of aerosol particles by wind occurs in several particle modes depending on size and wind speed. As wind speed increases, sand particles of $\sim$100 μm diameter are the first to be entrained by fluid drag. After these particles become dislodged they travel along the surface in a process known as saltation. This process can result in the mobilization of particles from a wide range of sizes. Dust particles are not easily lifted by wind, they are mainly ejected from the soil due to the impacts of saltation. Once the dust particles are suspended, they can remain in the atmosphere for a short term (usually particles $\sim$ 20 – 70 μm diameter) or are suspended for a long term (usually particles < $\sim$20 μm diameter). The transport of soil particles by wind can therefore be loosely divided into several physical regimes based on their duration in the atmosphere, namely, long–term suspension (< $\sim$20 μm diameter), short–term suspension ($\sim$20 – 70 μm), saltation ($\sim$70 – 500 μm), and reptation and creep (> $\sim$500 μm) (Kok, et al., 2012).

Dust deflation from the surface of the earth is one of the greatest sources of atmospheric dust. The size distribution, residence time and transport of dust aerosols in the troposphere is controlled by the theory of dust production delineated by Gillette and Goodwin (1974) which states that fine particles which have radii between 20 – 50 μm tend to become dislodged as the

wind speed increases over a threshold of erosion (Gillette & Goodwin , 1974). Thereafter, these fine particles dislodge and collide with other particles, entraining and disaggregating smaller particles into the atmosphere. Particles that are greater than 20 μm will return to the surface quickly when wind velocities begin to decrease. However, smaller particles can remain for days and sometimes even weeks in the atmosphere.

The texture of the soil determines the particle size classes and the chemical characteristics of these aerosol particles in the atmosphere (Gillette & Goodwin , 1974). African dusts originates mainly from uninhabited regions 15° N. Dust emissions from Africa are impacted by large–scale air circulation, which influences flow from the continent and drought conditions. Figure 2.6 displays how African dust influences the monsoon season in India, by strengthening of the pressure gradient over the Arabian Sea. This leads to increased monsoon winds, moisture convergence and precipitation over the Indian region (Vinoj, et al., 2014).The sources of Aeolian dust in South Africa are both local and regional. The local dust aerosol occurs primarily in the coarse fraction. Regional dust is produced throughout the western desert and semi–desert and the wetter parts of southern Africa (Piketh, et al., 1999).
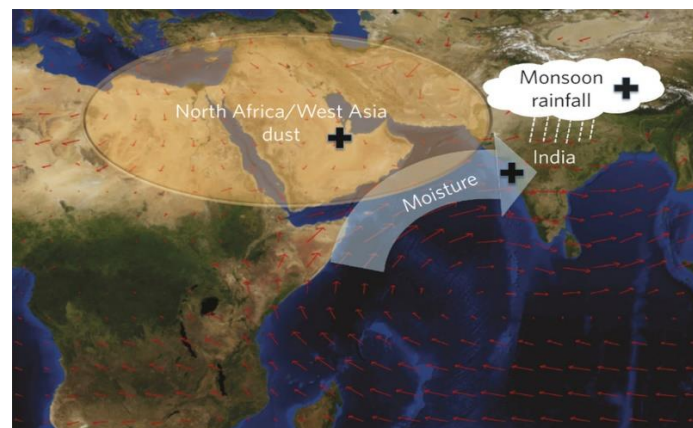
Figure 2.6 Depicts the true–colour image of the Earth, with wind vectors representing the climatological winds at 850 millibars between June and August The highlighted area (African dust region) indicates the areas of increased warming from high dust concentrations. This leads changes in pressure gradients which causes increased monsoon winds, moisture convergence and precipitation over the Indian region (obtained from Vinoj, et al., 2014).

2.8.2 Oceanic sources of aerosols

Oceans are key sources of atmospheric aerosols due to the release of sea salt into the atmosphere. These types of aerosols reside directly above the marine boundary layer. There are two components to aerosols in the marine boundary layer namely continental (background) and

locally produced sea–spray droplets. Sea–spray droplets are generated primarily by the bursting of bubbles at the sea surface (Prather, et al., 2013). These bubbles are produced by biological activity, chemical reactions and breaking waves (white cap formation) resulting in a strong dependence on wind speeds. At wind speeds greater than 3 meters per second, white caps are the main precursor to the bursting of bubbles. It is for this reason that the sea surface is regarded as a continuous source of sea–salt aerosols in the marine boundary layer. Furthermore, this aerosol may be the primary contributor to both light scattering and cloud nuclei in those areas of the marine atmosphere where wind speeds are high and aerosol sources are weak (Kanike & Sivakumar, 2015). Sea salt particles are good cloud condensation nuclei therefore knowledge of their production processes is of importance when determining the indirect impacts of aerosols. Due to the diverse size range (about 0.05 to 10 μm diameter) of these oceanic aerosols they display wide–ranging atmospheric lifetimes (Prather, et al., 2013). According to Piketh, et al., (1999), with the exception of coastal areas marine aerosol concentrations over South Africa are usually low. It was only recorded to be significant when inland advection of marine aerosols reached the South African Lowveld.

2.8.3 Volcanoes

Volcanoes are one of the major natural sources of pollutants in the atmosphere both during and between eruptions. Large scale volcanic eruptions considerably affect climate and cause ozone (O_3) depletion due to the release of particles and gases into the stratosphere where they have fairly long residence times (Anderson, et al., 2013). Figure 2.7 shows the process of volcanic gas interaction in the atmosphere, whereby, volcanic eruptions result in the conversion of sulphur dioxide (SO_2) to sulfuric acid (H_2SO_4). This results in the formation of fine sulphate aerosols in the stratosphere. Although the source strength of volcanic emissions is weaker than that of anthropogenic aerosol sources; sulphur particles released from volcanoes may have a greater effect on earth's radiation budget than anthropogenic aerosol emissions. The reason for this is the difference in height of the sources. There are many volcanoes that de–gas into the free troposphere, however, anthropogenic emissions are usually entrained in the planetary boundary layer where species lifetimes are significantly reduced (Vernier, et al., 2011). Volcanically influenced aerosols are characterised by primarily ash, sulphate and also includes a carbonaceous component (Anderson, et al., 2013).
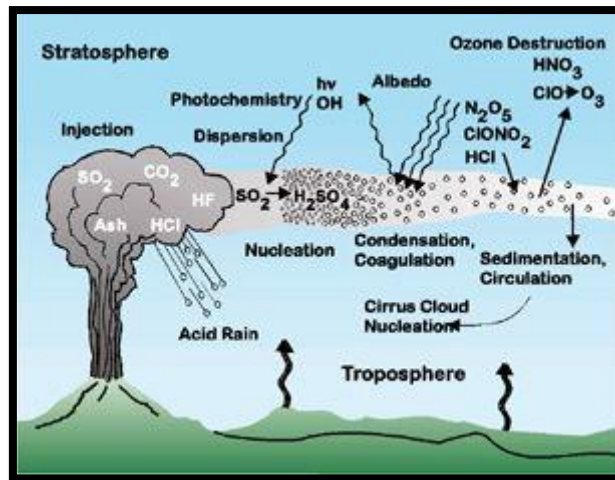
Figure 2.7 Schematic diagram displaying the physical and chemical processes of volcanic gas interactions in the atmosphere (obtained from USGS, 2016).

2.8.4 Anthropogenic and Industrial sources

It is widely concluded that anthropogenic aerosols exert a cooling radiative effect on earth's climate. The primary sources contributing vast amounts of aerosols to the atmosphere are electrical power stations, oil refineries, industrial factories, mine dumps, biomass burning and motor vehicles (Tesfaye, et al., 2011). Individual aerosol particles may encompass distinct species such as sulphates, organics, black carbon and dust (Ramanathan, et al., 2001). However, it is most common that aerosols are a composite mixture of core refractory material (black carbon, dust, sea salt) with a coating of organics, sulphates and nitrates (Ramanathan, et al., 2001).

2.8.5 Biomass burning

Biomass burning is a significant contributor to aerosol loads in the atmosphere. Biomass burning is both a natural and anthropogenic phenomenon. Natural fires are usually started by lightning however a small portion is started by spontaneous combustion of dry fuel such as saw–dust and leaves (Adler, et al., 2011). Human–induced fires occurred mainly to clear the land for agricultural purposes, weed and pest control as well as energy for the cooking of food (Goudie & Viles, 2013). Biomass burning emissions create both solid and liquid particles of several different shapes, sizes and chemical structures. These particles influence the heat balance of the earth. The sources of biomass burning aerosols are usually determined from satellite retrieval of burned areas and or forest fires (Petrenko, et al., 2012).

For southern Africa biomass burning was only thoroughly investigated and recognised as a significant contributor to aerosol loads during the SAFARI 92 field campaign. The intensity of fire and its coverage is primarily influenced by biomass availability. It is for this reason, that biomass burning is dependent upon rainfall. In Africa, most of the continent's population relies on fuel wood as a main source of energy and biofuels are considered the largest source of carbon emissions in the region (Swap, et al., 2003). Although the SAFARI programmes concluded that biomass burning was a major contributor to aerosol loading, further, studies by Piketh et al., (2002), suggested that the significance of biomass burning has been over estimated as a source of aerosols. It was outlined that south of 20°S, aeolian dust and industrial emissions is the main contributor to total aerosol loading (Piketh, et al., 2002). It is important to consider that Piketh, et al., (2002), study period was not confined to the biomass burning season, thus explaining the contrary results to SAFARI. For example, Eck, et al., (2003) used several AERONET sun–sky scanning radiometers established around southern Africa for the SAFARI 2000 dry season experimental campaign. These instruments were used to study the spatial, temporal, and spectral variance of total column–integrated radiative effective aerosol optical properties in the region (Eck, et al., 2003). Aerosol characteristics at many of the sites were primarily biomass burning in origin. This indicates that AOD from biomass burning most likely peaks on a seasonal basis in southern Africa only during the biomass burning season and throughout the rest of the year other constituents are responsible for aerosol loads in the region. According to Hersey, et al., (2015), the biomass burning emissions that significantly impacts South Africa are produced in neighbouring countries, mainly Zimbabwe and Mozambique. These emissions are transported in stratified layers and influence aerosol optical properties but do not affect particulate conditions on the ground.

2.8.6 Biogenic aerosol

The primary sources of biogenic aerosols are from the emission of DMS from the oceans and of NMHCs from terrestrial vegetation, as well as by their oxidation in the troposphere (Sahu, 2012). The marine production of DMS is dependent on plankton dynamics which is affected by climate and oceanic circulation. Biogenic aerosols such as carbonyl sulphide (COS) has various natural and anthropogenic sources. Natural sources include its release from oceans, volcanoes and deep sea vents. The photo – production of COS is a function of the intensity of ultraviolet – B (UV – B) radiation. Key anthropogenic sources include its use as a chemical intermediate and as a by–product of carbon disulphide (CS_2) production and its emittance from vehicles (especially vehicle tyre wear) and coal–fired power plants. The largest sink of COS in

the troposphere is absorption by vegetation, next is the consumption in toxic soils and also oxidation by the hydroxyl (OH) radical (Whelan, et al., 2013). Globally, COS is the most abundant sulphur gas in the atmosphere (Bruhl, et al., 2012). Bruhl, et al., (2012) depicted that upward transport of COS from the troposphere largely influences the sulphur budget and the aerosol loading of the background stratosphere. Therefore COS is an important source for stratospheric sulphate (SO_4^{2-}) aerosol and therefore indirectly plays a pivotal role in stratospheric O_3 chemistry. Biogenic Volatile Organic Carbon (BVOC) emissions depend on the amount and type of vegetation, temperature, radiation, the ambient COS concentration and soil humidity (Boucher, et al., 2007). The total global BVOC emissions is uncertain, regardless of the seeming convergence in different model–based estimates (Sahu, 2012).

One of the areas of interest to the SAFARI 2000 experimental campaign was the characterization of biogenic, nutrient and energy fluxes at the land–atmosphere boundary layer. Leaf level measurements of BVOCs were made for Mopane, a tree species dominant in southern Africa. Emissions of terpenes (belonging to a large group of volatile unsaturated hydrocarbons) was found to be heavily dependent upon light. Further measurement depicted that measurements of terpene fluxes with CO_2 fluxes depicted that terpene flux contributes to 25% of net carbon exchange (Greenberg, et al., 2003).

2.8.7 Carbonaceous compounds

Carbonaceous aerosols make up a substantial fraction of total aerosol loads. It is estimated that this fraction is between 20 and 50 % of $PM_{2.5}$ and approximately 70 % of PM_{10} mass (Calvo, et al., 2013). Although, carbonaceous compounds contribute significantly to the formation of atmospheric aerosols, their quantities in the total aerosol load is highly inconsistent. One of the major contributors to the carbon cycle is the combustion of fossil fuel and biomass, with carbonaceous PM being one of the most important combustion by–products. Carbonaceous aerosols released from biomass burning consists of both absorbing and non–absorbing aerosols (Petzold, et al., 2013). Carbonaceous particles are generally divided into two groups black carbon (BC) and organic carbon (OC).

BC is generated from fossil fuel and biomass combustion and it is the most obstinate and polymerized part of the aerosol. BC contributes minimally to aerosol mass however, it influences radiative forcing in the atmosphere due to its ability to absorb visible and near–IR radiation (Calvo, et al., 2013). Soot, elemental carbon and graphitic carbon are terms that are used synonymously with black carbon (Long, et al., 2013).

Conversely, OC is the non–absorptive part of carbonaceous aerosol species and can form from either primary or secondary sources. Primary sources include the direct emission into the atmosphere from the burning of fossil fuels. Secondary sources are formed in the atmosphere as a result of oxidation products of certain VOCs which condense on pre–existing aerosols. However, sources of OC, especially secondary sources are not entirely known. It is possible for Secondary OC to make up approximately 90% of OC. A substantial portion of OC is sourced from bywater soluble compounds, found in the atmospheric aqueous phase (Calvo, et al., 2013). OC are an aggregate of hundreds of individual compounds with a wide range of chemical and thermodynamic properties making concentration measurements quite challenging using any single analytical technique. OC aerosol content is usually determined from the difference between total carbon and BC contents (Fernández, et al., 2015). The characterisation of organic aerosols is quite difficult due to the vastly different properties that have to be considered, such as oxidation state, volatility and hygroscopicity, and the exceptionally diverse sources and atmospheric reactions that typify organic aerosols. Oxidation state is indicative of the degree of oxidation (loss of electrons) of an atom in a chemical compound, volatility is the tendency of a material to vaporize and hygroscopicity deals with the property of absorbing moisture from the air.

Particulate organic compounds are abundant in the atmosphere and characterise quite a substantial portion of atmospheric fine particles, responsible for 20 to 90% of aerosol mass in the lower troposphere (Lee-Tayler, et al., 2015). The manifestation of polar functional groups especially carboxylic and dicarboxylic acids allow many of the organic compounds in aerosols to become soluble in water and they can also participate in cloud droplet formation processes. There exists no uniform technique for analysing organic aerosol and often a combination of analytical techniques are required such as the use of filters and impactors (Hallquist, et al., 2009).

2.8.8 Nitrates

Nitrogen compounds occur mainly from secondary formation processes from the reaction of natural and anthropogenic precursor agents. Nitrate (NO_3^-) and ammonium (NH_4) are the main nitrogen compounds found in the atmosphere. The emission of nitrogen oxides (NO_x) from motor vehicles and large electric power stations are the most significant precursor for the nitrate aerosol (NO_3^-). Other natural sources of NO_x are soils, biomass burning and lightening (Calvo, et al., 2013). A large proportion of nitrogen oxides are transformed to gaseous nitrous and

nitric acids in the atmosphere. NO_3^- is chemically produced in the atmosphere and the foremost gases responsible for production are ammonia (NH_3) and nitric acid (HNO_3). Atmospheric ammonium nitrate (NH_4NO_3) are produced when sulphate (SO_4^{2-}) is completely neutralised and there is a surplus of NH_3. Therefore, radiative forcing due to NO_3^- aerosol is closely related to atmospheric concentrations of NH_3, as well as NO_x emissions. The diminishing of the radiative forcing of the SO_4^{2-} aerosol in many regions is caused by a decrease in sulphur emissions and can be potentially balanced by increases in the NO_3^- aerosol (Bauer, et al., 2007). The condensation of HNO_3 on aerosol particles could strengthen aerosol formation on cloud droplets by contributing to the particle surface and increasing the water intake and development of aerosol species (Bauer, et al., 2007).

The mean direct radiative forcing for nitrate is calculated to be -0.10 Wm^{-2} at the top of the atmosphere however there exists large uncertainty surrounding this estimate because the number of studies undertaken is inadequate to precisely quantify the magnitude and uncertainty of radiative forcing (Boucher, 2015). The quantification of aerosol composition including the calculation of NO_3^- and NH_3 compositions is important for the determining of aerosol radiative forcing. If there is more NH_3 available than required to neutralise sulphuric acid (H_2SO_4), nitrate can still form tiny aerosols capable of absorbing and reflecting radiation.

NO_3^- and NH_3 aerosols contribute additional particle surfaces for scattering incoming ultraviolet solar radiation thus having an impact on tropospheric chemistry (Bauer, et al., 2007). This will lead to disturbances in photochemical oxidant production by changing photolysis frequencies. Additionally, nitrate aerosol is formed through heterogeneous reactions of nitrogen radicals on aerosol surfaces (Bauer, et al.,2007). Trans–boundary pollution contribute towards sulphate and nitrate background concentrations in the United States. Trans– boundary transport of human induced emissions from Canada and Mexico is the most significant contributor to nitrate loads in the United States (Lloret & Valiela, 2016).

The formation of $NH_4NO_3^-$ is reliant on the thermodynamic state of its precursor gases and environmental conditions. Gaseous NH_3 and HNO_3 react in the atmosphere to produce $NH_4NO_3^-$:

$$NH_3\,(g) + HNO_3\,(g) \rightleftharpoons NH_4^+ + NO_3^- \qquad (1)$$
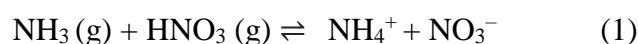
2.8.9 Sulphates aerosol

Sulphate aerosols are formed mainly via secondary formation processes due to the oxidation of gaseous precursors with SO_2 and DMS and particle formation through nucleation and condensation. Sulphur dioxide (SO_2) is a precursor of atmospheric sulphuric acid (H_2SO_4) and SO_4^{2-}. Sources of SO_2 are the burning of fossil fuels for industrial activities, biomass burning, volcanic eruptions and the oxidation of dimethyl sulphide (DMS) from oceans. The primary source of the anthropogenic emission sources of SO_2 are from the burning of sulphur–containing fossil fuels, smelting sulphide ores, as well as petroleum refining. The main sinks of SO_2 are the oxidation by hydroxyl (OH) and deposition on wet surfaces (Calvo, et al., 2013).

SO_4^{2-} is produced by aqueous phase reactions with cloud droplets, the oxidation of SO_2 through gaseous phase reactions with OH and by condensational growth onto pre–existing particles. SO_4^{2-} is fundamentally a completely scattering aerosol which scatters across the solar spectrum and to a certain extent also absorbs radiation in the near–infrared spectrum. The SO_4^{2-} aerosol contributes significantly to submicron aerosol mass, to tropospheric aerosol loads and to radiative forcing (Boucher, 2015). Furthermore, SO_4^{2-} aerosol is externally and internally mixed with other compounds such as BC, nitrates and mineral dust resulting in a complex aerosol amalgamation which varies with respect to radiative indices, size distributions, physical and chemical morphology and optical properties. The IPCC (2013) reported radiative forcing due to SO_4^{2-} aerosol to be approximately – 0.40 Wm^{-2} (Boucher, 2015). An increase in SO_4^{2-} has caused localized as well as on a planetary scale descent in air quality which is determined by local meteorology and topographical occurrences.

SO_2 concentrations in Durban increased from the years 1954 to 1962 and raised further during the 1960s and early 1970s, this was due to the increase of industrial activities as a result of refineries and the operation of Mondi paper mill (Diab & Motha, 2007). South Durban is Durban's largest industrial zone and contains paper, petroleum and chemical industries which directly contribute to SO_2 concentrations and PM (Ramsay & Naidoo, 2012).

2.9 Impact of aerosols on air quality

Urban environments are made up of multifaceted structures which include social, economic and physical systems that are intrinsically related. The world's urban population is on the rise therefore it is essential to ascertain and understand the dynamic interactions between human activities and the environment (Hersey, et al., 2015). Rapidly increasing urbanisation is a primary environmental driving force in the 21st century and majorly impacts air quality on local,

regional and global scales. As of 2015 there are approximately 35 megacities (cities with more than 10 million inhabitants) in the world, this has risen from 19 in 2005 (Safarik, et al., 2016). One of the major consequences of population increase, is an increase in aerosol pollution. This results in widespread consequences for human health, cultivated and natural ecosystems, visibility, weather, radiative forcing and tropospheric oxidation capacity. Aerosols also changed the formation and precipitation capacity of liquid water, ice and mixed–phase clouds.

Atmospheric aerosols are key constituents of the atmosphere and influence Earth's energy balance, climate, human health and the environment. According to the World Health Organisation (WHO), O_3, PM, heavy metals and some hydrocarbons make up the main pollutants in the troposphere (WHO, 2016). Determining the environmental impacts of aerosols is quite challenging and is based on the aerosols physical and chemical characteristics. Therefore the characterisation of the environmental impacts of aerosols involves determining aerosols size, size distribution, shape, optical features, elemental and isotope structure. The size of an aerosol particle determines its aerodynamics, lifetime and removal from the atmosphere. The toxicology of an aerosol is strongly dependent on its shape (Calvo, et al., 2013).

One of the major examples of aerosol pollution in Africa, is the Asian Brown Cloud (ABC) and the semi–permanent African tropospheric haze layer which results in a decrease in the visibility in an area. Haze is the disappearance of light through a process of scattering and absorption which is related to the ambient concentration of fine and coarse PM, secondary SO_4^{2-}, NO_3, O_3 and OC (Zunckel, et al., 2004). Aerosol pollutants are quick to disperse and have the greatest impact near their sources, therefore, their impact on air pollution needs to be studied from local to global scales (Hersey, et al., 2015).

2.10 Health effects of aerosols

There exist various epidemiological studies that depict a strong linkage between particulate air pollution and an increase in respiratory diseases. Additional studies pertain to particulates causing a heightened number of deaths from cardiovascular disease and respiratory diseases especially amongst the elderly (WHO, 2016). Ultrafine particles stimulate alveolar inflammation causing lung disease and increases in coagulation of the blood. Coarse particles (2.5 to 10 µm) are chiefly associated with the perturbation of the respiratory system and with diseases such as asthma in humans. Air pollution is destructive on cardiovascular health and can likely cause arrhythmogenesis, myocardial infarction and cardiac hypertrophy. There are two possible ways in which air pollution could be linked to heart disease. The first is the

classical pathway which deals with indirect effects facilitated by pollutants causing pulmonary oxidative stress and inflammatory responses. The other pathway is direct and deals with the process of pollutants directly impacting the cardiovascular system, blood and lung receptors (Shrey, et al., 2011).

The fine and ultrafine particles have the capacity to infiltrate much deeper into the lung tissue and eventually deposit in the alveoli. As such, fine particles (<2.5 μm) are severely hazardous to human health causing an increase in heart, lung and respiratory disease resulting in asthma, decreased lung function and premature death. These fine particles are especially dangerous to human and animal health because they are small enough to penetrate the membranes of the respiratory tract and enter the blood circulation and thus be transported along the olfactory nerves to the brain (WHO, 2016).

2.11 Atmospheric aerosols and meteorological parameters

Seasonal meteorological conditions determine the movement of aerosols (how far aerosols have travelled from their source regions), their vertical distribution in the atmosphere and concentration in a particular region. The deposition and dispersion of aerosols are affected by meteorological conditions such as temperature, precipitation, wind direction and wind speed. Aerosols in turn, affect these meteorological variables. Therefore it is of importance to understand the effect of meteorological parameters on aerosol levels in a specific locality (Kumar, et al., 2015b).

2.11.1 Wind direction and wind speed

Typically, high wind speeds are associated with low pollutant and aerosol concentrations in a region as a result of advection and deposition (Thambiran & Diab, 2010). This is because aerosol layers can be entrained by strong winds and transported over large distances, such as air mass transport from Africa or Asia to America and from America to Europe (Creamean, et al., 2013). There are numerous significant factors that influence the transport of aerosols, namely wind speed, wind direction and turbulence. These factors are important for air circulation and influence the distribution of aerosols. According to Eichelberger, et al., (2008) long–term changes in large–scale atmospheric circulation will include a poleward shift and the enhancement of westerly winds. These effects are expected to continue (Eichelberger, et al., 2008). Long–range transport of materials from continents to the ocean surface has indelibly impacted the marine atmosphere. Historically, the transport of aerosols of crustal origin has gained more attention than the transport of sulphur and nitrogen containing compounds.

However, these compounds have a major impact on tropospheric chemistry and circulation. The emission, transportation and deposition of sand and dust by wind are termed Aeolian processes (Kok, et al., 2012).

In Durban, daily temperature profiles were investigated using a Light Detection and Ranging (Lidar) device. In winter stratospheric temperatures were impacted by the activity of atmospheric waves, more especially, gravity waves and planetary waves (Bencherif, et al., 2000). Gravity waves are generated in a fluid medium or at the boundary between two different media, when the force of gravity tries to restore equilibrium (e.g., the boundary between the atmosphere and the ocean) which produces wind waves. Planetary waves are a natural phenomenon in the atmosphere and oceans of planets and are influenced by rotation. Atmospheric planetary waves are giant meanders in high altitude winds that significantly impact weather. These waves are generated in the troposphere and in Durban are propagated via westerly winds in winter in the middle atmosphere (Bencherif, et al., 2000). A study conducted by Bencherif, et al., (2003), linked Lidar observations of lower stratospheric aerosols over Durban to large scale transport across the southern subtropical barrier. The study recorded aerosol extinction profiles in April 1999 and observed a high variability in stratospheric aerosols. This variability was attributed to the transition of the stratospheric zonal–mean winds to the westerly regime (Bencherif, et al., 2003). Therefore winds play a major role in aerosol movement, distribution and concentration in a region.

In Durban, marine aerosols contribute to both fine mode and coarse mode particles, with large fractions of inorganic sea–salt and organic particles in the super–micron and submicron modes, respectively. The monthly mean variation of AOD and wind speed depict minimum values in winter. The threshold value of surface wind speed for generating emissions of maritime aerosols is 4.1 ± 0.1m/s. Therefore when wind speeds exceeds this threshold value, the coarse mode marine AOD is linearly correlated to the surface wind speed. Thus knowledge on wind speed and direction is important for estimating the average background wind – induced marine aerosol loading in Durban. During summer it is estimated that marine aerosols contribute to 51% of total aerosol loading (Tesfaye, et al., 2011).

2.11.2 Atmospheric aerosols and precipitation

Aerosols have significant impacts on precipitation. Due to aerosols scattering and absorbing solar radiation, the formation of clouds becomes energised. Furthermore aerosols impact the size distribution of cloud droplets because all cloud droplets require pre–existing aerosol

particles to act as cloud condensation nuclei (CCN) (Boucher, 2015). Approximately 37% of the energy input to the atmosphere is due to the escape of latent heat from vapour that condenses into cloud droplets and ice crystals. The re–evaporation of clouds takes back the escaped heat. Therefore, when water falls to the surface as rain, the heat is left in the atmosphere and is able to energise convection and larger scale atmospheric circulation systems. The extensive nature of aerosols influences cloud composition, precipitation, the hydrological cycle and atmospheric circulation systems (Rosenfield, et al., 2008). A greater number of aerosols produces a smaller number of droplets thereby impeding warm rain–forming processes. However, delaying precipitation initiation to above the freezing level converts rain into ice hydrometeors. The escape of extra latent heat could stimulate the vertical development of clouds thus increasing precipitation. Increased melting and evaporative cooling (the cooling of air due to the evaporation of water) at lower levels can stimulate convection which causes precipitation. Therefore, the effects of aerosols on clouds is a complex field of study (Li, et al., 2011). Li., et al., (2011) conducted a study to investigate the long–term impact of aerosols on the vertical development of clouds and rainfall frequencies, using a 10–year dataset of aerosol, cloud and meteorological variables collected in the Southern Great Plains in the United States. This study found that that precipitation frequency and rain rate are modified by aerosols. Rain increases with aerosol concentration in deep clouds that have a high liquid–water content, but decreases in clouds that have a low liquid–water content. Therefore, the frequency of precipitation increases with an increasing concentration of condensation nuclei for clouds with high water content but decreases for clouds with low water contents. It can be induced that pollution of aerosols would result in a net decrease in rainfall from clouds that form in dry environments therefore enhancing and compounding the effects of drought. On the contrary, high aerosol levels in moist climates will probably stimulate convective clouds and increase flooding during summer time (Li, et al., 2011). The impact of aerosols on clouds are two–fold, depending on the climate of the region. As such, precipitation is of immense importance when dealing with the climatological effects that aerosols pose.

The Aerosol Recirculation and Rainfall Experiment (ARREX) was initiated in 1998 to investigate the distribution of aerosols and trace gases over southern Africa and the probable effects aerosols have on rainfall production efficiency (Terblanche, et al., 2000). It dealt with cloud–aerosol links, with attention being placed on the observed cloud property differences between the continental Highveld and the maritime region along the Indian Ocean coast. The study showed that industrial pollution (more especially SO_2), over the Highveld area of South

Africa, changes CCN characteristics and cloud properties in such a way that could affect precipitation processes. Furthermore, the links between industrial pollution and rainfall production in South Africa are quite complex, displays a high degree of spatial and temporal variability, is impacted by synoptic variability and influenced by the physical and chemical characteristics of the aerosols present (Terblanche, et al., 2000). For the SAFARI 2000 experiment campaign, Cyclone Eline caused a heightened growing season for the southern African region, thus contributing to additional biomass (grass) that was utilized as fire fuel in the dry season (Swap, et al., 2003). Due to the wet season that occurred in 2000 the ''river of smoke'' was observed. It is an aerosol and trace gas transport pathway that exits off the south–eastern coast of southern Africa. This transport was postulated to occur during wet climatic conditions (Swap, et al., 2003). Laakso, et al., (2012) identified precipitation as the most important annual cycle affecting aerosol particles in the South African Highveld. Due to the minimum rain in winter, widespread wild and man–made fires occur in the regions during winter. During the rainy seasons, rain prevents fires during summer and decreases aerosols originating from windblown dust (Laakso, et al., 2012).

There are two processes that define wet deposition of aerosols; these processes are washout and rainout. Washout is the removal of aerosols that occurs within clouds. Rainout is the removal by falling precipitation. The washout effect depends upon various factors such as emission, solubility, advection, and precipitation; however most washout models focus on more simple variables such as precipitation rate and solubility. With dry deposition, emphases is placed on the direct aggregation of gaseous and particulate agents on land or aqueous surfaces (Yoo, et al., 2014).

2.11.3 Atmospheric aerosols and temperature

Sunlight enters earth's climate and is responsible for heating the earth and absorbing moisture content (Ramanathan & Feng, 2009). The reflection and absorption of solar radiation due to aerosol particles causes a reduction in surface temperatures (Ramanathan & Feng, 2009). Different aerosols influence earth's temperature differently. Pure sulphates and nitrates result in atmospheric cooling because they reflect solar radiation almost entirely (Adesina, et al., 2014). On the other hand, BC absorbs solar radiation thereby causing a warming effect on the atmosphere but cooling the surface (Koch & Del Genio, 2010). Dust aerosols influence radiation on different scales depending on the composition of the dust minerals that make up the dust grains. Salt particles reflect all the sunlight they encounter (Koch & Del Genio, 2010).

Most aerosol particles however are highly reflective and raise the planet's albedo thus cooling the surface and counteracting the warming caused by greenhouse gases, by anything between 25 to 50% (Kaufman, et al., 2002). Aerosols containing BC, are dark and thus absorb incoming solar radiation. These types of aerosols warm the atmosphere but cool the surface before a redistribution of the energy occurs in the column (Kaufman, et al., 2002). In terms of Durban, daily maximum temperatures currently range from 20 to 26°C and temperatures are likely to increase by 2 to 3°C in 2070 to 2100. The concentration of atmospheric aerosols is likely to impact temperature levels in Durban. However, the radiative forcing by aerosols is expected to increase through the 21st century which might offset warming temperatures in Durban (Naidu, et al., 2006).

2.11.4 Synoptic climatology and aerosol concentrations

In coastal regions such as Durban, the movement of pollutants is controlled by sea breezes and local circulations, which are heavily impacted by small–scale thermodynamic processes. Therefore, regional air quality over an area is determined by many complex elements, the most important of which being the emissions of pollutants and largescale meteorological conditions. Existing weather conditions, influence air quality and climate because these factors influence the spatiotemporal distribution of aerosols (Zheng, et al., 2015). Therefore, atmospheric circulation in a region is considered to play a significant part in the state of air quality in that region. This is because, the relationship between the concentration of aerosols and the current circulation, both synoptic and local scale is important for predicting expected aerosol concentrations and the impact of aerosols on climate change.

Various meteorological factors such as wind, pressure, temperature, humidity and precipitation can influence the levels of pollutants in the atmosphere by resulting in the buildup or dispersion of aerosols (Zheng, et al., 2015). It is quite complex to study each meteorological variable in isolation because air pollutant levels and air mass trajectories respond to all meteorological variables (Oanh, 2012). For example, Krintz, et al., (2014), studied lower tropospheric and column–averaged AOD parameters in the South East United States. It was found that various synoptic factors influenced AOD. Aerosol loads increased with increasing temperature and pressure. Moist, tropical weather plumes caused increases in AOD, causing larger particle sizes due to the hygroscopic growth of aerosols (Krintz, et al., 2014). In South Africa aerosols and trace gases are removed from the Highveld region by atmospheric circulation patterns and transported to remote regions of southern Africa. This alludes to the major influence that

prevailing synoptic situations have on aerosol concentrations in a locality (Freiman & Piketh, 2002). Synoptic meteorology is therefore, the study of large–scale atmospheric processes and weather prediction using synoptic weather information. Synoptic weather characterization has become an important method for assessing the impacts that meteorological conditions have on air pollution (Cheng, et al., 2007).

2.11.5 Influence of synoptic factors and local meteorology in South Africa with particular attention placed on Durban

Aerosols are influenced by local to synoptic meteorological processes. It is therefore important to measure and understand the changes in aerosol loading over time, on a regional scale in order to predict climate in a specific area. The South African climate is impacted by four important factors, namely, the latitudinal position, distance from the sea and ocean currents, the presence of the escarpment and atmospheric circulation. South Africa is situated at the center of a sub–tropical high pressure belt. Due to South Africa's width, it is influenced by weather systems predominant in the tropics and temperate regions (Preston-Whyte & Tyson, 1988). South Africa is also effected by sub–tropical high pressure cells. The topography, weather and climate of an area determines the aerosol loads in that region. Certain meteorological conditions support the removal of aerosols from the atmosphere while other conditions such as, during the presence of inversions, stable conditions, or light winds hinder the removal of aerosols causing a rise in local pollutant levels (Freiman & Piketh, 2002).

Atmospheric circulations and weather patterns over Durban are mainly influenced by sub–tropical anticyclones. Durban is a coastal city, coastal winds will also impact aerosol levels. Scott and Diab (2000) used the synoptic climatology approach to predict air pollution potential (APP) in South Durban. There are three main synoptic regimes that influence air pollution and aerosol dispersion in Durban, namely, the established high pressure system, the prefrontal situation and the postfrontal situation (Scott & Diab, 2000). These three synoptic regimes give rise to three different air pollution episodes in Durban.

The first synoptic regime is the high pressure system which is described by fine weather, light north easterly winds and low to moderate mixing depths caused by the presence of upper air subsidence inversions (Scott & Diab, 2000). In the course of a high pressure system due to quick surface radiative losses caused by clear sky and light wind conditions nocturnal surface inversions develop. This supports meso–scale circulations such as the development of land and sea breezes and topographical winds. During such conditions the ability of the atmosphere to

scatter pollutants is reduced (Scott & Diab, 2000). The prefrontal situation usually occurs after a dominant high–pressure system and before a coastal low or cold front system. A coastal low or cold front system lowers the subsidence inversion causing it to reach its lowest level directly before the wind changes from north easterly to southwesterly. As such, the APP increases as the subsidence inversion lowers just before a low pressure system (Scott & Diab, 2000). The post–frontal situation occurs after the low pressure system has passed and the subsidence has lifted. This causes moderate to strong southwesterly winds and rainfall increasing the dispersion of pollutants.

2.12 Global distribution of aerosols

Aerosols have various effects on earth's climate as discussed in previous sections. The intensity of these effects depends on the vertical distribution of the aerosol (Winker, et al., 2013). Aerosols do not spread across the globe as uniformly as gases. Higher concentrations of aerosols tend to be found close to their sources. The warming capabilities of absorbing aerosols are heightened when they are located above bright clouds and the atmospheric lifetime of aerosols are much greater when they are located in the free troposphere than in the planetary boundary layer (Winker, et al., 2013). Aerosols with longer lifetimes can be transported further from their sources thus affecting the geographical pattern of aerosol impacts.

Recent studies have depicted a great diversity in the global distribution of aerosols based on global aerosol models. This diverse range is the result of uncertainties in the simulation of aerosol processes such as transport and removal processes. A study by Winker, et al. (2013) on the vertical distribution of aerosols was undertaken using the Cloud–Aerosol Lidar and Infrared Pathfinder Satellite Observation (CALIOP) Lidar carried on the CALIOP satellite. It was an investigation of global AOD and it was an investigation of global AOD and a sample measurement is shown in Figure – 2.8 and 2.9. It is based on 5 year mean global distributions of CALIOP 532 nm AOD computed from four different types of profiles: all–sky daytime, all sky night time, cloud free daytime and cloud free night time.
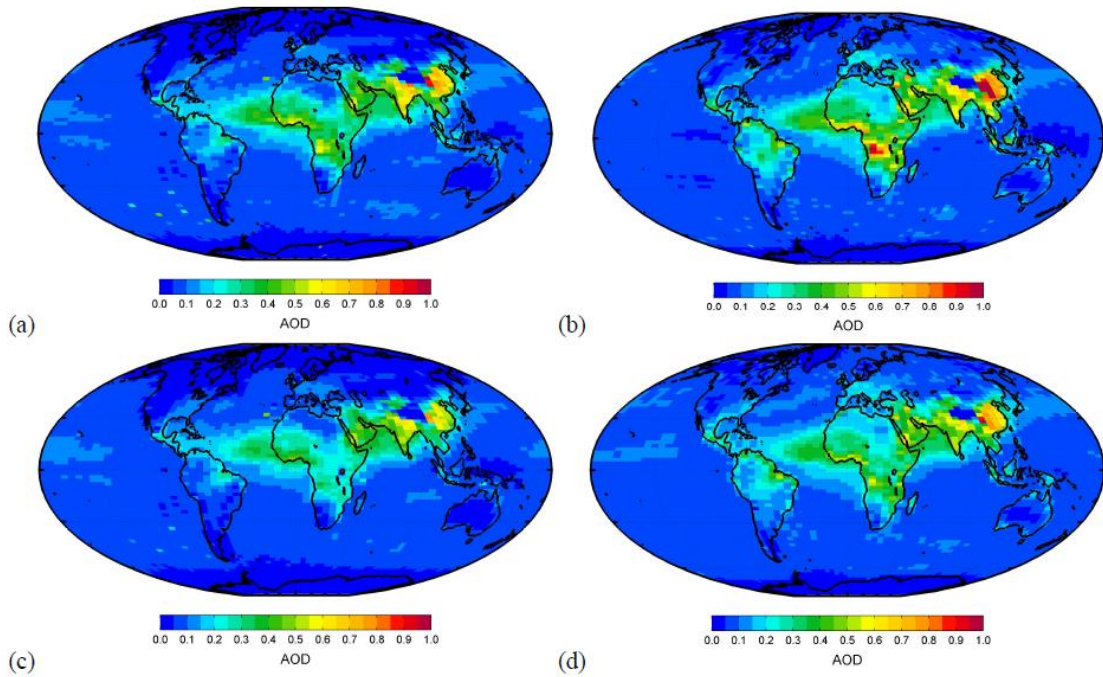
Figure 2.8 Mean 532 nm AOD, January 2007toDecember 2011: (a) cloud–free, daytime; (b) cloud–free, night time; (c) all–sky, daytime; (d) all–sky, night time (obtained from Winker, et al., 2013).
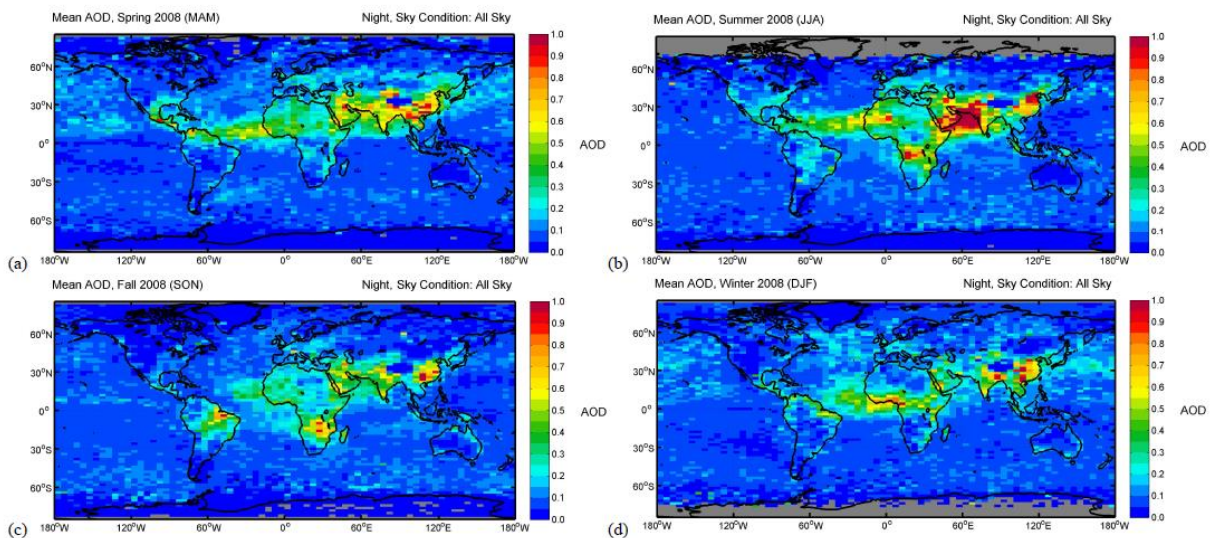
Figure 2.9 Seasonal mean AOD for 2008, night time, all–sky: (a) March, April, May; (b) June, July, August; (c) September October November; (d) December, January, February (obtained from Winker, et al., 2013).

The results depicted that patterns of AOD were similar for all maps, especially all–sky and cloud–free column AOD. All four global distributions are quite similar, and depicted major source regions in Africa, India, and eastern China. Africa transports air mass plumes to the

44

Atlantic Ocean and Asia transports to the north Pacific Ocean. A clear seasonal variation is evident, with a larger magnitude of variation over land than over ocean. Dust transport was apparent moving from the Sahara eastward across Arabia and southwest Asia and into central China. Transport of dust from the Sahara westward across the Atlantic Ocean into the Caribbean occurs throughout the year. The transport of dust from Asia to the northern Pacific occurs most prominently during spring. Southern Argentina is a ubiquitous source of dust, except during autumn with a peak during spring. Dust transport in the Southern Hemisphere comes mainly from South America. Over the oceans most aerosols remain in the marine boundary layer. There is a prominent westward transport during all seasons. Dust occurs at low altitudes during summer and at high altitudes during winter (Winker, et al., 2013).

Van Donkelaar, et al., (2015), mapped global ground–level PM$_{2.5}$ concentrations using total column AOD from the MODIS and MISR (Multiangle Imaging Spectroradiometer) satellite instruments and aerosol vertical profiles from the Geostationary Operational Environmental Satellite (GOES) global chemical transport model. It was found that PM$_{2.5}$ concentrations exceeded WHO standards over central Asia for 38% of the population and over eastern Asia for 50% of the population (van Donkelaar, et al., 2015).

Meskhidze, et al., (2011), studied global distribution of marine organic aerosol emissions using the National Center of Atmospheric Research's Community Atmosphere Model with the Pacific Northwest National Laboratory's 7–mode Modal Aerosol Module. Global emissions of submicron marine primary organic aerosol is approximately, 7.9 to 9.4 Tg yr^{-1}. The Northern Atlantic, Northern Pacific, and the Southern Ocean show marine–source submicron organic aerosol surface concentrations of 100 ng m^{-3}, with values up to 400 ng m^{-3} over biologically productive areas (Meskhidze, et al., 2011).

2.13 Aerosol Distribution over Southern Africa

Historically, the northern hemisphere has been highlighted as being the biggest and most significant contributor of industrial emissions and there has been very little attention placed on the emissions released from the southern hemisphere because it was considered to be negligible in comparison (Piketh, et al., 2002). However, southern Africa is a major regional source of aerosol and trace gases from Aeolian dust, industrial processes and biomass burning (Piketh, et al., 2002).

The first leading international experimental campaign to study tropospheric aerosols in southern Africa was the Southern African Fire Atmosphere Research Initiative (SAFARI 92)

performed in 1992. The aim of this experiment was to study fire emissions in southern Africa. In collaboration with Transport and Atmospheric Chemistry Near the Equator–Atlantic (TRACE–A), SAFARI 92's main objective was to delineate fire processes and its impacts on regional atmospheric chemistry. The primary outcomes of SAFARI 92 was that southern Africa has various ecological and environmental systems that are intrinsically linked by the semi–permanent anti–cyclonic regional atmospheric circulation system. This system was able to transport aerosols for thousands of kilometres. Aerosols are the reason for the extensive haze layer noted over southern Africa. The layer reaches a depth of ~5 km and is covered by a persistent, stable layer created by subsidence within the subtropical anticyclonic circulation. It is within this haze layer that aerosols are recirculated (Diab, et al., 2003). The SAFARI 92 experiment also emphasized other sources of different aerosol types and trace gases apart from biomass burning. Additionally, it is found that the smoke and haze displayed over South Africa during the southern Hemisphere spring comes from countries further north (Koppmann, et al., 1996; Swap, et al., 2003).

SAFARI 92 was preceded by SAFARI 94 and investigated the concentration and physical constituents of tropospheric aerosols and trace gases over southern Africa outside the burn season. The major findings from SAFARI 94 indicated a thick layer with many trace elements within the upper part of the mixed layer over majority of southern Africa, even outside of the biomass burning season (Koppmann, et al., 1996). The Southern African Regional Science Initiative 2000 (SAFARI 2000) followed SAFARI 92 and 94 and was a major surface, airborne and space–borne field campaign undertaken in southern Africa in 2000 and 2001 that encompassed widespread coverage of phenomena that deals with land atmosphere interactions and the biogeochemical functioning of the southern African climate system (Swap, et al., 2003). SAFARI 2000 was conducted during climatologically different conditions than those that existed during SAFARI 1992. The SAFARI 2000 measurement campaign occurred during the extreme wet end of southern African climatic conditions (relating to La Nina phase of the El Nino Southern Oscillation) and the measurement campaign in 1992 occurred during extreme dry climatic conditions relating to an El Nino event. Thus providing results within a climatological framework that includes extensive environmental and ecological phenomena (Swap, et al., 2003).

Initially SAFARI 2000's main purpose was not a fire–specific field campaign. However, the major dry season observational campaign was followed by a period of high precipitation and consequent vegetation growth hence, biomass burning emissions became the foremost

influence on the southern African atmosphere during the next dry season. Therefore, SAFARI 2000 is outlined by certain key issues such as fuel, biomass burning and fire emissions and their impacts (Swap, et al., 2003). The primary atmospheric characteristics observed during the dry season campaign was "massive thick aerosol layers covering much of southern Africa" and more distinct smoke and haze escaping of the south eastern part of southern Africa known as the "river of smoke" which crossed the subcontinent during early September 2000 (Swap, et al., 2003).

According to Diab, et al., (2003) aerosols are the reason for the development of the widespread haze layer over the African subcontinent. It is a stable layer generated by subsidence within the subtropical anticyclonic circulation. Inside the haze layer, aerosols are recirculated until they escape the subcontinent and move east as a giant haze plume, estimated to be 1000 km wide. The plume extends more than 5000 km to the southeast, as far as Amsterdam Island and has the capability to reach Australia. Greater than 75 % of the plume transported off southern Africa lies between the surface and 500 hPa. It is directed towards the east and it is approximated that 45 Mt yr^{-1} of aerosols is transported of the east coast of southern Africa in this plume (Diab, et al., 2003).

Within southern Africa, there are major cities that produce large loads of aerosols due to industrial activities and vehicle emissions in addition to natural biomass burning. In the Saharan desert and northern Africa, volcanic eruptions and desert dust make up significant portions of aerosol load concentrations (Sivakumar, et al., 2010). After SAFARI 2000 aerosol measurements have been continually taken at Mongu in Zambia and Skukuza in South Africa. Recently, continuous measurements of aerosol properties haven been taken at Durban. These sites form part of the AERONET program (Queface, et al., 2011).

2.14 The use of the HYSPLIT model to determine aerosol transport pathways in southern Africa.

Adesina, et al., (2015) studied air mass transport in Gorongosa in Mozambique, using the HYSPLIT model to compute 7 day back trajectories. This was done to study the sources of aerosols arriving in Gorongosa on one day per month during the study period July to December, 2012.The back trajectories were computed for 500 m, 1500 m and 3000 m above sea level. The HYSPLIT air mass trajectories were in agreement with the measured high and low AOD during the study period. The trajectories depict the transport of air parcels from the source region to Gorongosa. It was observed that during September and October, the dry months of the study

region, the air parcels at all levels originated from Madagascar and the mainland of Africa. It transported smoke aerosols from forest fires and or biomass burning activities. In November and December, the air parcels arrived from the oceanic environment, showing long range transport of sea–salt aerosols. These aerosols have shorter residence times, and drop out before reaching the measurement sites, resulting in decreased AOD at the site.

Sivakumar, et al., (2009), used back trajectory analysis for a time period of approximately 24 hours of Lidar measurement undertaken at the University of Pretoria in South Africa. The height levels used for the back trajectory analysis was 2000 m, 2500 m and 3000 m. It was found that there was air–mass transport from Botswana over the height region from 2000m to 3000m and from Zimbabwe from less than 2000 m. There also existed internal recirculation of air within South Africa. The above 3000 m height region depicted air mass transport from Namibia and Botswana. Also, from the analysis of the back trajectory, it was found that air mass transport originated from various source regions from 2000 m to 3000 m, however, the most prominent region was Mozambique. The height regions between 3500 m and 4500 m shows transport from Namibia to Pretoria passing through Botswana (Sivakumar, et al., 2009).

Adesina, et al., (2014), used HYSPLIT trajectory analysis to determine the airmass parcels entering the Pretoria from January to December 2012. The meteorological input was GDAS and the trajectories were computed for 500 m, 1500 m and 3000 m above sea level. Back trajectory analysis was done for 168 hours on four days, during the four different seasons. It was found that, on days with high AOD, airmass parcels came from the mainland of South Africa and surrounding arid/semi–arid regions traveling a short distance before reaching the location. Aerosols travel from biomass burning regions in Mozambique and Madagascar. On days where AOD was low, the air mass trajectory travelled longer distances, originating from fairly pristine marine environments. These trajectories carry sea–salt particles that undergo deposition before reaching the site due to their short residence times.

Ben Ami, et al., (2010), studied long–range transport of dust from North African desert regions using the HYSPLIT trajectory model. The North Africa desert regions are responsible for providing important minerals to the Amazon rain forest. The main dust source is from the Bodélé depression in the southwest of Chad, therefore, it was expected that there would be a close linkage between Bodélé emissions and the volumes and mineral supply to the Amazon. This study made use of space–borne and ground data with reanalysis model data and surface measurements to investigate the validity and type of the proposed link between the Bodélé

depression and the Amazon forest. This study analysed dust events from 11 to 16 and 18 to 27 February 2008 from emissions in the Bodélé depression. Forward trajectories were calculated using the HYSPLIT trajectory model focusing on the Bodélé depression at 0, 500 m and 1000 m, above ground level. It was found that there was an increase in crustal elements between 22 and 26 February due to dust emitted from Bodélé between 14 and 15 February. The model depicted that dust arrived to the Amazon Basin in height between 1700 and 5000 m above ground level, and the transport time from the Bodélé to the Amazon Basin took approximately 10 to 17 days (Ben-Ami, et al., 2010).

Vakkari, et al., (2011), conducted a study in Botsalano game reserve, northwest of South Africa, based on data from 20 July 2006 to 5 February 2008. Measurements of aerosol particle size distributions, air ion size distributions, trace gas concentrations and basic meteorology in the savannah of South Africa. The air mass trajectory was analysed using HYSPLIT back–trajectories and the model was run with GDAS meteorological parameters. The HYSPLIT model was run for 96–hour back–trajectories at every hour throughout the complete measurement period. The trajectories showed that the source of high SO_2 emissions was released from the Highveld (Vakkari, et al., 2011).

Tiitta, et al., (2014), studied non–refractive submicron aerosols and BC over a one year period in an atmospheric measurement station in Welgegund, South Africa. Measurements were done using a mobile atmospheric monitoring trailer that was fixed at Welgegund in May 2010. Air mass trajectory history was investigated using back trajectories from HYSPLIT to determine the source of the aerosols. The model was run using GDAS meteorological archive data and 96 hour back trajectories were attained for every hour throughout the measurement period at a height of 100m. The air mass trajectory classified Welgegund into four source regions based on air mass history. The first is an anticyclonic recirculation path made up of pollutants emitted in the primary source regions. This allows for the chemical transformation and aging of various source pollutants. However, within the error of back trajectory calculations, the anticyclonic region of Welgegund considerably interconnects with the western and eastern Bushveld Igneous Complexes (BIC). As such, the first source region is made up both the anticyclonic region and the eastern BIC (ACBIC). The next source region identified was the industrialised and densely populated Vaal Triangle (VT), which contains many large point sources including petrochemical and metallurgical production plants. The next source region was the industrial Highveld (iHV), which encompasses the eastern parts of the Gauteng Province to Middleburg in Mpumalanga. iHV is actually a grouping of two large source regions, the Mpumalanga

Highveld which contains 11 coal manufacturing plants and a petrochemical industry and the Johannesburg–Pretoria megacity. The next source region acknowledged was the regional background (BG), which had no large point sources and is located west of Welgegund. This source region extends from parts of North–West and the Free State provinces to the entire Northern Cape province of South Africa. This region is inclusive of the Kalahari Desert (Tiitta, et al., 2014).

Due to African cities not having emission reduction laws, African cities add to global atmospheric pollution. The West African troposphere is affected by Saharan dust events which transport mineral dust particles over long distances which may reach Europe. Deboudt, et al., (2010) studied the scavenging of carbonaceous compounds by African dust during the African Monsoon Multidisciplinary Analysis project (AMMA) using single particle analysis. The study was performed on the Atlantic coast due to it being located on the path of Saharan dust parcels transported westward over the northern tropical Atlantic, being impacted by biomass burning and anthropogenic pollutants from African cities. The HYSPLIT model was performed and 120 hour back trajectories were computerised for the 2, 8, 9, 12, 13 and 15 of February 2006. Meteorological data from the National Weather Service's National Centre for Environmental Prediction (NCEP) FNL data were used. Backward trajectories were made at an ending point of 500m. From the trajectories of sampled air masses, it was ascertained that most of the dust came from selected events from north–west Sahara. The trajectory analysis also highlighted that from the 13 to the 15 February 2006, more than 60% of time trajectories deal with relative humidity higher than 70%. From the trajectory analysis it was noted that transport of airmasses from 9 to 12 February 2006 was due to marine airmasses, and was significantly impacted by local emissions from the West African coast and the city of M'Bour (Deboudt, et al., 2010).

Escudero, et al., (2006), undertook a study using the HYSPLIT model to compute the proportions of mineral dust that came from specific regions in northern Africa. The model was used to study the daily PM_{10} levels transported over the Iberian Peninsula from North Africa by using measurements recorded at three Spanish EMEP (Cooperative Programme for Monitoring and Evaluation of the Long–Range Transmission of Air pollutants in Europe) air quality network stations. The study was performed from the 12 to 15 March 2003. It was found that 20 to 30% of the PM_{10} in dust in central Iberia originated in Mauritania and the western Sahara, 15 to 20% from Mali, Mauritania and the western banks of the Ahaggar Mountains, and 55 to 60% from other north western African sources. From the trajectory analysis it was found that a dust outbreak occurred from the 12 to 15 March 2003 over the Iberian Peninsula,

and in the days prior to this outbreak, an anticyclone was noted over the Iberian Peninsula. The air mass transport started with a depression over the Atlantic Ocean in front of the Moroccan coast which caused the shift of the anticyclone toward northern Algeria. This event lasted until 5 March 2003, when an anticyclone over Europe caused an easterly flow which dislodged the dust to the west affecting Iberia (Escudero, et al., 2006).

Hand, et al., (2010), studied the interaction between naturally occurring dust aerosols and biomass burning aerosols due to radiative forcing of biomass burning aerosols being altered by dust aerosols. Aerosols were sampled from regions impacted mainly by dust aerosol, impacted mainly by biomass burning aerosol, and a sample containing a mixture of both dust and biomass burning aerosol across Africa. Samples were collected from 28 January to 22 August 2006. HYSPLIT back trajectory simulations were computed for each sample site, seven days before the sample data, in order to determine the source of the aerosols. From the back trajectory analysis, it was found that samples that were impacted mainly by dust aerosols, were from Libya and transported in a westerly fashion to Algeria, North Malie, Mauritania and northern Senegal. Back trajectory analysis for samples containing both dust and biomass burning aerosol, showed air masses originating from Nigerian fires, from northern Benin and from Algeria. The back trajectory analysis for samples that were impacted mainly by biomass burning aerosol showed airmasses originating from fires in Mali and Nigeria and biomass burning in Ghana and the Cote d'Ivoire (Hand, et al., 2010).

2.15 Aerosol studies in South Africa

South Africa is located at the southernmost tip of the African continent and shares borders with Namibia, Botswana, Zimbabwe, and Mozambique. Despite the importance of biomass burning on aerosol loads in South Africa, it is not the foremost source of aerosols for the country. According to Piketh, et al., (2002) South Africa is accountable for the demand of most of subequatorial Africa's electrical energy due to its coal power generators. Piketh, et al., (2002), studied aerosol loading in the troposphere over Ben Macdui Mountain in the Eastern Cape, South Africa. The study determined the different source contributions of aerosols as a percentage of the total detected elemental mass being transported in the atmosphere for the various size modes. For the coarse mode, soil dust comprises the largest component (75%) of the aerosol mass, industrial sulphur comprises 20.5% and sea–salt aerosols 4.5% of the aerosol mass. In terms of fine mode, aerosols from industrial sources dominate the detectable aerosol

loading (52%), aerosol loading from soil dust varies between 13% and 87%. Soil dust contributes less than industry in the fine mode (Piketh, et al., 2002).

Tesfaye, et al., (2011) undertook an intensive investigation on seasonal trends in various aerosol characteristics for South Africa. This study observed maximum aerosol extinction optical depth during spring which correlates with biomass burning activities in southern Africa. The lower parts of South Africa (encompasses Durban) showed low levels of AOD as compared to the central and upper parts which displayed medium and high aerosol loads respectively. The lower part of South Africa contains primarily coarse mode aerosols during summer and the concentration of coarse mode aerosols decrease as we move further away from summer. There is approximately 35% increase in aerosol loads during summer in comparison to the other seasons. Therefore, South Africa is a region typified by aerosols that display distinct seasonality and mixing of air masses (Diab, et al., 2003; Tesfaye, et al., 2011).

2.16 Aerosol loading: Durban

Durban has become one of the most important contributors to economic development in South Africa (Roberts, 2008), its industries contributes to approximately 22% of the cities Gross Domestic Product (GDP) (Thambiran & Diab, 2011). Durban's population is currently growing at a rate of 150 000 people per year, thus increasing the energy demands in the city. In addition to Durban's population demand, Durban is also situated at an ideal position, on the east coast of South Africa, at the approximate centre of the "River of Smoke". This makes Durban a region of interest to investigate aerosol properties (Diab, et al., 2003). Durban is a coastal region thus it has the potential to be a major source of natural marine aerosols (Tesfaye, et al., 2011). Furthermore, aerosol loads in Durban are also affected by the influx of industry in the SDIB (Diab & Motha, 2007).

2.17 Summary

Over the past three decades aerosol science has certainly garnered a great deal of attention and research, however, it can be observed that much of this research is isolated to regions in the northern hemisphere. The academic progress of research in science and technology in Africa, in particular has been quite a fluctuating process, influenced by colonialist movements, politics and various other complex institutionalised issues (Zeleza, 2002). Therefore, research in African countries have been slower than elsewhere and aerosol research in specific lacks in southern Africa. For this reason, aerosol optical properties are better understood in countries such as the United States of America, Europe and China, however, Southern African countries

have the highest global emissions of biomass burning aerosols making Africa a place of interest in aerosol studies.

The purpose of this review, was to gain insight into the properties and effects of aerosols, as well as the state of aerosol pollution research in South Africa and in Durban particularly. The study of the optical properties of aerosols in a specific location is important, because the properties determines the climatic effect and sources of aerosols in that region. Knowledge of the different sources and transport mechanisms of aerosols in a specific locality is important for policy reaction measures. The background synoptic and meteorological factors govern the transport of aerosols in a region and thus is also important when describing aerosol optical properties.

The use of data from different satellite sensors, models and from ground based remote sensors, allows for a holistic understanding of the effects and trends of aerosols in a certain area. Aerosol studies in Durban have been discontinuous with a lack of ground based monitoring stations, to compare to satellite sensors of aerosols. Additionally, the lack of ground based monitoring of aerosol trends extends to aerosol climatic effects and properties. More research and testing is required to gain a better understanding of what are the main sources of aerosols in Durban and on the optical properties of aerosols in order to make policy decisions. Due to the lack of ground based aerosol monitoring stations in Durban, it is important to conduct research which compares satellite results with ground–based results for the purposes of validating satellite measurements.

CHAPTER 3

3.   METHODS AND INSTRUMENTATION

3.1 Introduction

This chapter outlines the research methods, tools and techniques that were used to conduct this study. Aerosol characteristics and properties were measured by using different instrumentation and the data were analysed to determine trends of aerosol pollutants in Durban and to compare satellite data with ground based instrumentation. There are various measurement factors that have to be considered before deciding what instrumentation to use to measure aerosol properties. These factors relate to the specific measurement challenges that are inherent to each aerosol property and therefore careful consideration is required when choosing an instrument to measure aerosol loads. The measurement capabilities of satellites are always improving in terms of their resolution, coverage and analysis algorithms. This allows satellites to provide the necessary means to validate climate models. These advances have been accompanied by complex validation programs that compare in–situ ground based measurements with satellite products. These validation studies provide the information needed to support high powered airborne instruments on platforms that can cover wide spatial range over many pixels of satellite resolution (Baumgardner, et al., 2011). Due to the inconsistent nature of aerosol loads, different instrumentations are required to measure their impacts. This chapter will include information pertaining to the sensors and instrumentation that were used to measure aerosol properties in this study. It will also include how the data were analysed and the research design that was appropriated.

3.2 Instruments used in this study to collect aerosol optical data

There exist several factors that influence the detection of aerosol constituents in the atmosphere, namely, the amount of colour of light emitted by the object (initial radiance), the transmittance of the light from the object to the observer and the scattering of ambient light into the sight path by the atmosphere (McMurry, 1999).   The light scattering and absorption coefficients are the optical properties from which extinction, optical depth and single scattering albedo are derived.

Aerosols differ from region to region, therefore, multiple instrumentation are required to measure their impacts. Long–term, detailed measurements from satellites, ground–based instruments and weather quality data are required to adequately measure aerosols for a given

area. Field measurements (ground based) offer detailed observation of aerosol chemical and physical properties. However, they have limited spatial and temporal coverage. Satellite instrumentation provide the widespread temporal and spatial coverage required to perform robust studies. Therefore, this study made use of both satellite and field measurements. A common variable used to link measurements from different instruments is the aerosol optical thickness (AOT) (AOT and aerosol optical depth (AOD) which will be used interchangeably) (Chin, et al., 2002). The next few sections, will detail the networks and instruments (both satellite and ground based) used in this study.

3.2.1 Meteorological Instrumentation Measurements

There are six weather stations that constantly measure a variety of meteorological parameters. A RM Young Model 27005 gill UVW anemometer at Southern Works measures three orthogonal vectors of wind. The remaining five stations use the RM Young Model 05103 to monitor horizontal wind speed and direction. These monitors measure in the 0 to 30m/s range of wind speeds. Ambient temperature is measured continuously at five stations equipped with the RM Young Model 41372VC/VF using relative humidity/temperature probes. The measuring ranges are –10 ℃ to 60℃ for temperature, and 0 to 100 % for relative humidity (eThekwini Municipality, 2006). The hourly average data was requested from the South African Weather Services (SAWS) and obtained for the period from January 2004 to December 2014.

3.2.2 Aerosol Robotic Network (AERONET)

Investigations regarding aerosol characteristics are of importance because they deal with critical issues such as radiative forcing by aerosols, the long term impacts of aerosols on climate change, effects of aerosols on human health and impacts on ecological systems. However, the resources that are used to measure the aforementioned characteristics are heavily isolated to particular locations. Therefore, there is a need to have a reliant, coordinated database that can provide the measurements necessary to perform continuous, valid, vigorous assessments of aerosol loads across various regions and timescales (Holben, et al., 2001). Such information is provided by large scale ground based observatories and satellite measurements. The AERONET federated network is the most globally distributed ground–based group resulting in a database of extensive environmental conditions (Smirnov, et al., 2000). This study made use of aerosol data from the Durban sun-photometer, a registered AERONET site, located at the University of KwaZulu – Natal to collect ground based aerosol measurements.

According to the AERONET website, the AERONET program is a collaboration of ground–based remote sensing aerosol monitoring networks established by the United States of America's National Aeronautics and Space Administration (NASA) and France's PHOtométrie pour le Traitement Opérationnel de Normalisation Satellitaire (PHOTONS) and also includes other networks and collaborators from national agencies, institutes, universities, scientists and partners. The network ensures standardization of instruments, calibration, processing and distribution. Herein, lies the strength of such measurements, allowing for widespread comparison of measurements. AERONET provides globally distributed measurements of spectral AOD, inversion products, and precipitable water vapour in diverse aerosol regimes (AERONET, 2015). AERONET uses automatic sun/sky CIMEL radiometer CE – 318 that acquires data irrespective of sky conditions. The radiometer takes two measurements, either direct sun or diffuse sky radiances within several programmed sequences (Smirnov, et al., 2000). The network provides high resolution data available from over 700 stations world–wide. The stations are chosen based on their physical location to gain the most widespread coverage of the earth.

The understanding of the instrumentation used in the AERONET program is important when using measurements from AERONET. The following sections will provide information regarding the instrumentation used. The various inversion algorithms used by AERONET are specifically formulated to meet aerosol parameter retrieval accuracy required for satellite data validation and better comprehension of the radiative effects of aerosols (Dubovik & King, 2000). The data supplied by AERONET in their data archive are external data and will have passed all the relevant quality checks. The main area of consequence is the presence of clouds, as it may interfere with the data (Rainwater & Gregory, 2005). Therefore, it is important to remove cloud affected data, which is done by removing data with an $\alpha_{440-870}$ of less than 0.5 (Rainwater & Gregory, 2005). AOD is calculated for three data quality levels, level 1 (unscreened), level 1.5 (cloud–screened) and level 2 (cloud screened and quality assured) (AERONET, 2015). According to AERONET, the accuracy of the AOD is approximately, 0.01 to 0.02 for field operated Cimel sun-photometers and ~5% for sky radiance measurements (AERONET, 2015).

3.2.2.1 Cimel sun-photometer

The Cimel sun-photometer is a multi–channel, automatic sun and sky scanning radiometer that measures the direct solar irradiance and sky radiance at the Earth's surface. It is produced by

Cimel Electronic in France and is part of the AERONET program. Measurements are recorded at discrete wavelengths in the visible and near–infrared parts of the electromagnetic spectrum to determine atmospheric scattering and transmission properties (Holben, et al., 2001). The sun-photometer is a passive remote sensing instrument that makes use of sunlight to take measurements of aerosol optical properties and can therefore only be operated in the daytime. The sun-photometer measures these aerosol optical properties and the data is sent to AERONET to undergo cloud screening procedures (Holben, et al., 2001).

The AERONET program provides aerosol information from two different categories of ground–based observations, namely, spectral data of direct sun radiation extinction and angular distribution of sky radiance (Dubovik & King, 2000). AERONET thereafter provides observations of the spectral AOD, precipitable water content (PWC), inversion aerosol products such as the spectral deconvolution algorithm, aerosol volume size distribution (VSD), SSA, ASP, complex refractive index (Real and Imaginary), aerosol scattering phase functions, fine and coarse mode AODs are also available for larger solar zenith angles (>50°) and high aerosol loading conditions (AOD_{440} >0.4). An inversion algorithm is needed for the retrieval of these properties. The algorithm is required to ensure that the available data can be easily integrated with satellite data (Dubovik, et al., 2000).

The CE 318 – 2 sunphotometer, is the polarised model and contains filters at 340 nm, 380 nm, 440 nm, 500 nm, 675 nm, 870 nm and 1020 nm for the measurement of aerosol optical depth and it contains a filter at 939 nm for measuring atmospheric water vapour and a bandwidth of 10 nm at full width at half maximum. It contains an optical head with two collimators. It tracks along the zenith and azimuthal planes. Therefore, the instrument is able to automatically deduce the positon of the sun and track its movements with great accuracy. It requires internal batteries for the optical head and has external batteries for the robot that recharges from the solar panels (Rainwater & Gregory, 2005).
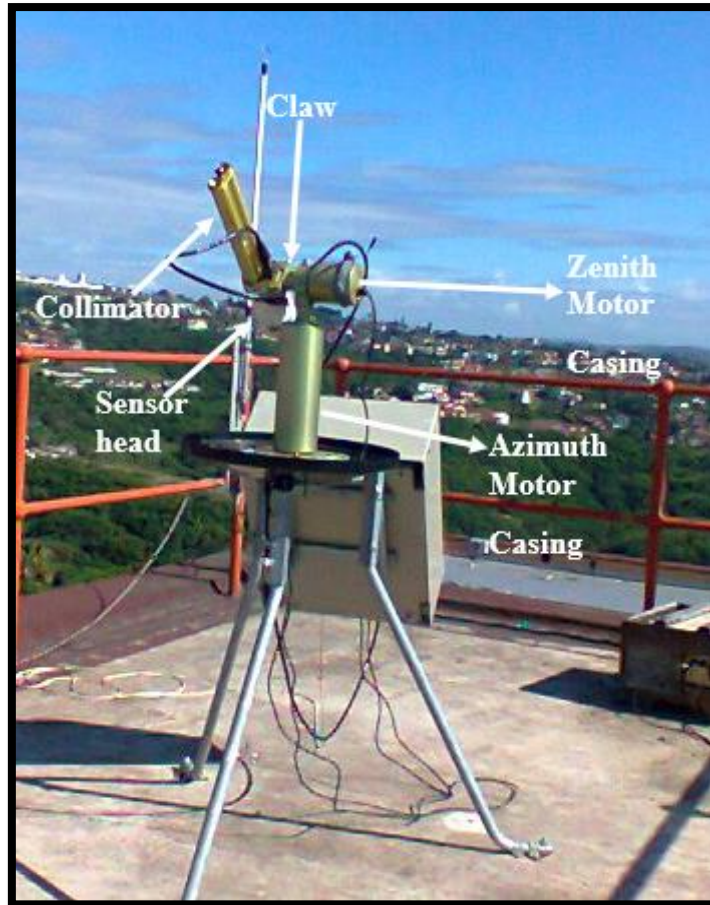
Figure 3.1 Cimel sun-photometeron the roof top of the physics building at the University of KwaZulu– Natal, Westville (obtained from Atmospheric Science Research Group at UKZN).

The Cimel sun-photometeris made up of essentially three distinct components. First of which is the instrument, which encompasses the sensor head, scanning motors and robot arm. Second, is the control box which offers the software required for controlling the timed scanning and sampling regimes for recording the data. The third component is a computer for data collection and transmission purposes. The instrument is made up of the primary stem which encompasses the azimuth motor. On the top of the motor is an attached robot arm consisting of the zenith motor on the one side and the sensor head on the other side. The collimators are joined to the sensor head (Figure 3.1). The sensor head contains two silicon detectors, one for each of the collimators. The two collimators have the same field of view (1.2°) however, they differ in the size of their apertures. The larger collimator is known as the aperture collimator and is able to view the sky. The smaller collimator is known as the sun–viewing collimator and is able to view the sun. The collimators are attached to the sensor head by a long screw (Rainwater & Gregory, 2005).

A filter wheel is positioned in between the collimator windows and the detectors, located inside the sensor head. The filter wheel is made up of eight narrowband interference filters (at 340, 380, 440, 500, 675, 870, 1020, and 1640 nm) all standing along the circumference of the wheel. There exists three cables, a large cable required to attach the sensor head to the control box and two battery powered cables that are plugged in to each of the motors. The primary stem is connected to a base plate consisting of mounting holes to enable the instrument to be fixed to a surface (Rainwater & Gregory, 2005).

The control box, is a rectangular box that controls the scan and measurement sequence of the sun-photometer. It contains an internal battery that serves merely the software portion of the instrument. The box also stores a battery pack to supply power to the control box. A battery charger supplies power to the input mains. The instrument should be positioned at a height of approximately 1.5m above the ground to reduce accidental obstruction of the field of view of the collimators. The instrument should be placed in an area that permits a clear view of the sky, during sunrise and sunset at above 5° of elevation (Rainwater & Gregory, 2005).

3.2.2.2 Measurement technique

The sun-photometer operates automatically, by pointing the collimator towards the estimated position of the sun based on a program that considers the time of year and the coordinates of the location that the sun-photometer is positioned at. The sun-photometer contains a four quadrant detector that locates the sun at the middle of the field of view of the collimators by utilizing a control feedback loop. Rotation of the filter wheel occurs in front of the detector in order to gain a measurement sequence. Each sequence takes about ten seconds and three measurements are taken in order to account for the presence of thin cirrus clouds which may obscure results, thus lasting approximately thirty–five seconds (Rainwater & Gregory, 2005).

The measured voltages are compared to eliminate non–uniform scenes. Almucantar sky radiances are gained by scanning the sky at the solar zenith angle but different azimuth angles to gain the angular variation of skylight in four filters. Solar principal plane sky measurements are determined by scanning the sky in a plane that encompasses the sun and the instrument and is normal to the surface. Observations are usually undertaken near the sun as the intensity varies rapidly in the solar aureole. The sky brightness observations are inverted by radiative transfer algorithms to derive the aerosol distribution and phase function (Rainwater & Gregory, 2005).

Direct solar irradiance data are measured in all filters every 0.5 airmasses above an airmass of 2 and every fifteen minutes apart. Solar almucantar data (sky radiance at constant solar zenith

angle) are obtained twice daily, at a solar zenith angle of approximately 60 degrees in four wavelengths — 440, 670, 870, and 1020 nm. Solar principal plane sky radiance is obtained four times daily in the same wavelengths as for the almucantar. Cloud mode zenith radiance observations are obtained at constant intervals. The data are stored in the memory of the Cimel control box, the computer collects the observations and transmits it via the internet to AERONET for processing (Rainwater & Gregory, 2005).

3.2.2.3 Equations to gain aerosol components

There exist various equations that are specifically formulated to gain the aerosol properties required to determine the concentration of aerosols in a particular region and their climatic effects. Bouguer's Law provides an equation for the Direct Normal Solar Irradiance (E (W/m^2)) at the surface at a certain wavelength. The equation is as follows:

$$E = \frac{E_0}{R^2} \exp(-m \times \tau)$$

where E_0 is the extra–terrestrial solar irradiance at a distance of one Astronomical Unit (AU), R is the distance between the sun and the earth, given in AU at the time of measurement, m is the airmass, and the total vertical optical thickness is τ. If the instrument voltage is V for irradiance E, the above equation can be written as:

$$V = \left(\frac{V_0}{R^2}\right) \exp(-m \times \tau)$$

The calibration coefficient is represented as V_0 in the above equation. It is calculated by measuring voltage (*v*) as a function of airmass (m) and inducing the resulting curve to zero airmass. The total optical depth (τ) incorporates molecular (Rayleigh) scattering, trace gas absorption and aerosol extinction. Therefore by adequately estimating the molecular contributions, AOT can be calculated. The correctness of the estimation is dependent on the uncertainty in *V* and V_0. The 940 nm channel measures the precipitable water content and Bouger's Law is not applicable in this wavelength due to the exponential attenuation law being valid for monochromatic radiation.

For the application of a band attenuation filter, attenuation occurs preferentially at the line centres thus causing saturation and continued passage through the atmosphere. This results in the exponential attenuation law being adequate, only in the pressure broadened line wings where the attenuation is weaker. Transmission can be modelled as a two parameter expression:

$$T = \exp(-a \times w^b)$$

Transmission in the band is represented as T, a and b, which are constants that are determined by modelling with a radiative transfer equation and convolving the result with the shape of the 940 nm band, for a given atmosphere. By selecting a narrow 940 nm band width, sensitivity to atmosphere can be removed from the equation for any atmosphere (Halthore, et al., 1997)

$$V = \left(\frac{V_0}{R^2}\right) \exp(-m \times \tau) \exp(-a \times w^b)$$

The optical thickness (τ), incorporates Rayleigh and aerosol components that are estimated independently (by interpolation in the case of aerosol), w, the water column abundance, m*PW, where PW, the precipitable water, is obtained once the calibration constant is known. Calibration for the 940 nm channel is accomplished in a manner similar to the previous case and is described below (Rainwater & Gregory, 2005).

3.2.2.4 Calibration

Calibration deals with the identification of the calibration coefficients required to convert the instrument output digital number (DN) into a desired output. The desired output is a reference to AOD, PWC, and radiance (W/m^2/μm). The field instruments are usually returned to the Goddard Space Flight Centre (GSFC) for inter–comparison with reference instruments every 6 to 12 months in order to ensure accurate calibration. The reference instruments are calibrated by using the Langley technique at Mauna Loa Observatory (MLO) in Hawaii. The Langley technique, involves a Langley plot which is a logarithm of the digital numbers taken during these times plotted against the optical air mass between a range of 5 and 2 for 340 nm. The intercept is the calibration coefficient (zero air mass) and the slope is the optical depth. AERONET reference instruments are calibrated at the MLO every 2 to 3 months using the aforementioned Langley plot technique. For the sky radiance measurements, calibration is performed at the NASA GSFC, using a calibrated integrating sphere to an accuracy of +/– 5% (Rainwater & Gregory, 2005). The sun–sky radiometers at sites other than GSFC are intercalibrated against a MLO AERONET reference instrument both before use in the field and after use (Rainwater & Gregory, 2005).

3.2.3 Satellite Instrumentation

Space borne satellite instrumentation is becoming increasingly important because it enables the observation of the planet from space thus aiding pertinent climate change research. The advent

of the global Earth observation era has led to the storage of vast amount of data records related to geophysical attributes. Satellite derived geophysical attributes are combined into statistical portions that are used to recognize environmental conditions and trends (Kahn, et al., 2009). Many studies require an in depth understanding of the strengths and weaknesses of the derived attributes. This is quite challenging because the retrieval algorithms for several derived attributes are extremely complex and are still being improved upon. Algorithms improve due to results obtained during field campaigns as well as comparison studies. Therefore, studies regarding the validation and comparison of satellite retrieval algorithms are extremely important for assessing the quality and accuracy of satellite observations (Kahn, et al., 2009).

Satellite instruments allows us to take accurate aerosol retrieval measurements on a nearly daily basis across a broader geographic area and across a longer time frame than other ground based instruments. There are numerous space agencies that have launched satellite instrumentation to be used in aerosol measurement. It has been greater than thirty years since the launch of the first satellite used for atmospheric detection. The advent of satellite technology to measure aerosol properties has led to the derivation of various important aerosol products such as aerosol spatial and temporal distributions, fraction of fine to coarse mode particles, vertical distribution, light absorption and spectral characteristics. Therefore, satellite remote sensing has greatly improved aerosol studies and the number of products available has significantly expanded (Lee, et al., 2009).

Satellite data can be classified into three broad groups. The first group deals with representing the spatial and temporal dynamics of aerosols. The second group deals with columnar aerosol property retrievals such as aerosol columnar mass retrievals. The third group gives information on the vertical profile of aerosols from the surface into the stratosphere. Depending, on the requirements of the study or the information needed, a single satellite or a combination of satellites can be used (Lee, et al., 2009). Satellite instruments can be divided into two categories depending whether they take either vertical or horizontal measurements. Most instruments are vertical (nadir viewing) and the instruments face the nadir or near nadir and senses radiation coming from the Earth. The majority of instruments use this method to provide column integrated products. Observations that occur in the horizontal direction include limb–viewing and occultation sounding, probing the Earth's limb at different depths in the atmosphere. This observation is categorized by the altitude and the geolocation of the tangent point. Any method employed requires accurate calibration of instruments (Lee, et al., 2009).

The USA's NASA and the National Ocean and Atmosphere Administration (NOAA), the European Space Agency (ESA), le Centre National d'Etudes Spatiales (CNES) in France, the Japanese Aerospace Exploration Agency (JAXA), the China Meteorological Administration, the Royal Netherlands Meteorological Institute (KNMI) and the German Aerospace Centre (DLR), have all contributed to the satellites available for aerosol research (Lee, et al., 2009). This section will review the satellites used in this study to measure aerosol properties.

The basic premise of satellite observation deals with electromagnetic radiation (incident light) being scattered and or absorbed by aerosol particles and the products of this interaction reflecting to satellite sensors. There are two basic types of sensors, namely, passive and active. Passive sensors record the radiation emitted by the sun and reflected back to the sensor. Active sensors, on the other hand, receive energy emitted by the sensor itself (Du, et al., 2000).

The main goal of aerosol remote sensing is to decompose mixed signals emanating from atmospheric gases, aerosols and the surface after clouds are filtered out. The ratio of radiances received by a sensor over that reaching the top of the atmosphere (TOA) in a particular direction is given by the following equation:

$$p_{POA}(\theta_0, \theta_s, \varphi) = p_{atm}(\theta_0, \theta_s, \varphi) + \frac{T_0(\theta_0).T_s(\theta_s).A_g}{1 - s.A_g}$$

where $\rho_{atm}(\theta_0, \theta_S, \varphi)$ is the reflectance by the atmosphere, and $T_0(\theta_0)$ and $T_S(\theta_S)$ are downward and upward total transmission (diffuse plus direct); θ_S is the satellite zenith angle, θ_0 is the solar viewing angle, and φ is the relative azimuth angle. The spherical albedo is given by s and A_g is the surface reflectance. Reflection from clouds is quite damaging for satellite measurements. Cloud screening provides the largest degree of uncertainty when measuring aerosol loads (Jeong, et al., 2005). Reflection from clouds can be quite distracting therefore, it is important to identify the presence of clouds because aerosol remote sensing is only valid under clear sky conditions. The presence of clouds may result in confusion between the dim signal of prevalent aerosols, and too much of cloud screening may actually remove pixels that contain aerosols.

Next, the instrument has to account for molecular scattering caused by atmospheric molecules and gas absorption. The Rayleigh path radiance can be determined using the spectral dependence of known Rayleigh optical depth and the Rayleigh phase function. The third step of satellite retrievals is to remove the reflection from the satellite received signal and determine aerosol loadings (Lee, et al., 2009).

3.2.3.1 Moderate resolution Imaging Spectroradiometer (MODIS)

The Moderate Resolution Imaging Spectroradiometer (MODIS) is a relatively new sensor with the ability to characterize the spatial and temporal characteristics of the global aerosol field. The MODIS sensors measures various environmental parameters such as ocean and land surface temperatures, fire products, snow and ice cover, vegetation characteristics and processes, surface reflectance and emissivity, cloud and aerosol characteristics, atmospheric temperature, water vapour, ocean biological and colour pigments. It was launched aboard NASA's Terra and Aqua satellites in December 1999 and May 2002, MODIS has 36 channels which span the spectral range from 0.41 to 15m representing three spatial resolutions: 250m (2 channels), 500 m (5 channels), and 1km (29 channels). The aerosol retrieval makes use of seven of these channels (0.47 to 2.13 m) to retrieve aerosol properties and uses further wavelengths in other parts of the spectrum to identify clouds and river sediments. The MODIS satellite sensor has a unique strength in that it is able to retrieve aerosol optical thickness with greater accuracy and it is able to retrieve parameters that can characterize aerosol size (Remer, et al., 2005).

The first MODIS sensor was launched aboard Terra at the end of 1999 and began transmitting data at the end of February 2000. The MODIS satellite sensor has a unique strength in that it is able to retrieve aerosol optical thickness with greater accuracy and it is able to retrieve parameters that can characterize aerosol size (Remer, et al., 2005). Algorithms were specifically formulated to observe radiances to derive many important aerosol products. MODIS data have been used to gauge comprehensive aerosol products including AOT, fine mode fraction (FMF), effective radius of aerosol particles (equal to the ratio of the third to the second moment of the aerosol size distribution), and mass concentration (Lee, et al., 2009). The comparison of the retrieved aerosol parameters from MODIS have been compared with ground based validation and agreement was noted between both measurement techniques and it also showed areas in which algorithms needed to be further evaluated and improved. The modified MODIS algorithms generate the Collection 6(C6) product which has considerably improved accuracy when compared with other earlier versions of MODIS algorithms. MODIS aerosol products in C6 are retrieved using two quite distinct algorithms, namely, the dark target (DT) approach and the deep blue (DB) approach (Hsu, et al., 2004).

In the MODIS DT algorithm, the 500m spatial resolution reflectance at three bands (470, 650, and 2130 nm) are organized into nominal 10 x 10 km^2 boxes corresponding to 20 x 20 pixels

per a box. This was carried out after correction for water, O_3 and CO_2. The remaining pixels are subjected to further processing in order to retrieve AOD. The processing is done in four steps to attain AOD. The first step involves identifying dark pixels whose reflectance at 2130 nm falls in the typical value range of 0.01 to 0.25 and are within 20% to 50% of the corresponding reflectance at 650 nm (red band). Step two involves parameterizing the surface reflectance at visible (VIS) bands (470 nm and 650 nm) in terms of the small wavelength infrared (SWIR, 2130nm) surface. The third step deals with selecting the proper aerosol mode and type from a look up table (LUT), which is the function of geography and season. The last step details the derivation of optical thickness and mass concentration of the accumulation and course mode from the detected radiance (Xie, et al., 2011). The MODIS DT AOD retrieval is founded on the relationship between the surface reflectance at VIS and SWIR, and works for most vegetated land surfaces but is generally not applicable for arid, semi–arid, urban and desert areas (Hsu, et al., 2004).

The MODIS DB approach is used to retrieve aerosol properties over brightly, reflecting surfaces by employing blue bands in which the surface reflectance are low enough to make such retrievals possible. The first key step in the DB algorithm is to apply Rayleigh correction for terrain evaluation in order to measure reflectance. This accounts for variations in the surface pressure. Cloud screening is performed by investigating both the spatial homogeneity within a 3 x 3 pixel window and absorbing aerosol index values. The second step involves delineating the surface reflectance of a given pixel from a clear–scene database based upon its geolocation. The third step is to compare the surface reflectance at 412, 470, and 650 nm bands with the values recorded in a look up table (LUT) in dimensions containing the solar zenith, satellite zenith, and relative azimuth angles, surface reflectance, AOT, and SSA (Xie, et al., 2011). The most appropriate match is determined by using the maximum likelihood method and iterative method. The fourth step involves recording the AOD and $\alpha_{440–870}$ after the aerosol models and the mixing ratio are determined (Xie, et al., 2011). The chief means of validation of MODIS measurements is comparison with equivalent measurements from AERONET ground–based sun/sky radiometers (Remer, et al., 2005). This study made use of area averaged, C6, level 3 MODIS gridded atmospheric daily product which contained daily 1x1 degree grid average values of atmospheric parameters.

3.3 HYSPLIT Model

It is useful to study back–trajectory transportation of air masses, in order to determine, the source, path and direction of air masses during the study period. Back–trajectory and forward–trajectory analysis were done in this study using NOAA's, Air Resources Laboratory (ARL), online version which run interactively on the web via the READY system (http://www.arl.noaa.gov/ready). The Hybrid Single–Particle Lagrangian Integrated Trajectory (HYSPLIT) model was run from the NOAA ARL READY website (http://www.arl.noaa.gov/ready/hysplit4 .html) (Draxler & Hess, 1998). The HYSPLIT model is a beneficial tool for projecting and computing both simple air parcel trajectories and complex dispersion and deposition simulations (Draxler & Rolph, 2003). It is used to identify synoptic–scale, atmospheric transport and pollution sources for a particular site. Gridded meteorological data are calculated at regular time periods and were used in the analysis to generate air mass trajectories. For the back–trajectories, in specific, data and information were gained from archives. The inputs were entered into the HYSPLIT model using the NOAA, Global Data Assimilation System (GDAS) meteorological database. The back–trajectory and forward–trajectory analysis was computed within HYSPLIT by a Langrangian three dimensional air mass velocity algorithm that has been utilized for air trajectory analysis for many decades (Draxler & Rolph, 2003).

A Langrangian modelling technique involves the dispersion being computed by adding the contribution of each pollutant "puff" that is advected through the grid cell by its trajectory (Draxler & Hess, 1998). HYSPLIT calculates a pollutant distribution starting with a single particle or puff, or by following the dispersive movement of a large number of particles. It is assumed that a particle's trajectory is dependent on wind flow and is thus the integration of the particle position vector in space and time (t). The final position is calculated from the average velocity (V) at the initial position (P) and first–guess position (P_0). It is given by the following equations:

$$P(t + \Delta t) = P(t) + 0.5[V(P, t) + V(P', t + \Delta t)]\Delta t$$

$$P'(t + \Delta t) = P(t) + V(P, t)\Delta t$$

A puff that follows a single trajectory cannot adequately describe the growth of a pollutant plume when the wind dimension changes both horizontally and vertically. As such, the single puff needs to be dispersed into multiple puffs or the simulation needs to be conducted using many pollutant "particles" (Escudero, et al., 2006). HYSPLIT uses three main methods to represent how dispersive pollutants are. The first method, is the "puff" mode and is a 3–D cylindrical puff, which has a set concentration distribution in the vertical and horizontal. The puffs will grow vertically and horizontally based on rules of dispersion and split if they become too outsized. The next mode is the "particle" mode, an extremely small particle is known as a point mass of contaminant, releasing a fixed number of particles. In the particle mode, the particles are moved by wind and do not split. The last method, the "hybrid" mode deals with a circular 2–D object such as a mass, having zero vertical depth. The horizontal contaminant has a ''puff'' distribution. The vertical contaminant is limited due to airmasses functioning as particles in that dimension. In the horizontal dimension, air masses grow, following the dispersion rules for puffs and split of they become too large (Draxler & Hess, 1998).

In order to calculate air concentrations, it is important to establish the particle distribution about the mean of the trajectory path. Following the particle mode, this is done by adding a random component to the mean advection velocity to ascertain the dispersion of the pollutant cloud. The particle distribution can be depicted by the following equations for the horizontal component (Draxler & Hess, 1998):

$$X(t + \Delta t) = X_{mean}(t + \Delta t) + U'(t + \Delta t)\Delta t$$

$$U'(t + \Delta t) = R(\Delta t)U'(t) + U''(1 - R(\Delta t)^2)^{\frac{1}{2}}$$

$$R(\Delta t) = \exp(-\Delta t/T_{Lx})$$

$$U'' = \sigma_u \lambda$$

U' is the random velocity component, X_{mean} is the original position caused by advection by the mean winds, R is the turbulent velocity autocorrelation, σ_u is the standard deviation of the

turbulent velocity, T_{Lx} is a constant Langrangian timescale and λ is a computer generated value with 0 mean and a standard deviation of 1.

Air concentrations are calculated by summing each particle's mass as it moves over the concentration grid. In a homogenous, uniform environment, the size of the puff at a single point in time should relate to the second moment of the particles position (Draxler & Hess, 1998).

3.4 Data analysis

Quantitative research methods were used in this study, which deals with maximizing objectivity and ensuring the results are replicable (Harwell, 2011). Quantitative methods are usually characterised as assuming there is a universal truth that exists uninfluenced by human perception and ideas. Definitions of quantitative research design focuses on the development of an experimental design based on a dependent and independent variable (Harwell, 2011). Quantitative methods assisted in this study because it allowed for the generation of trend analysis graphs for aerosol and meteorological data. It allowed for a visual representation of the seasonal trends in air pollution and climate. Additionally, it permitted statistical comparisons between satellite and ground based instrumentation.

3.4.1 Meteorological data analysis

Meteorological data were obtained from SAWS. The parameters used were wind speed and direction, relative humidity and temperature from hourly average measurements from January 2004 to December 2014. The data was checked for quality, days with greater than three zero values were deleted and days which did not include data were also deleted. The data used in the study, amounted to 70581 observations for wind speed and direction, 62220 observations for relative humidity and 62398 observations for temperature. The meteorological station used in this analysis was the Cato Ridge station in KwaZulu–Natal. Cato Ridge was used because it provided all the meteorological parameters of interest in this study.

Matlab (2015) version b, was used to complete the analysis. Wind rosettes were created by using the wind speed and wind direction. Wind rosettes were created in order to aptly show the frequency of winds and which direction the winds blow in. The wind speed and direction was also averaged for each month and the standard deviation was calculated. This was done to show which months have high wind speeds and in which direction the wind was travelling. Monthly average relative humidity and temperature were presented in a line graph, with error bars

depicting the standard deviation. This was done in order to gauge monthly temperature variability for Durban.

3.4.2 Sun-photometer data collection and processing

Level two data from the Durban sun-photometer from January 2014 to September 2014, was downloaded from AERONET and used to study aerosol properties in Durban. The sun-photometer is located at the University of KwaZulu–Natal's Westville campus. AERONET checked the data from the Durban sun-photometer for abnormalities and screened the data for clouds. The data is available for download from the AERONET website (aeronet.gsfc.nasa.gov). The AOD, the $\alpha_{440-870}$, columnar water vapour (CWV), particle VSD, SSA, and ASP, together with the Re and Im parts of the complex refractive index were downloaded. All points were downloaded, amounting to 7591 observations in order to perform seasonal trend analysis of aerosol characteristics in Durban. Point measurements are taken daily by the sun-photometer at approximately 5 minute intervals. Additionally daily average observations were also downloaded amounting to 110 days, in order to compare the daily observations from satellite data with that from the sun-photometer. These observations were for the year January to September 2014. The data were quite limited for the Durban sun-photometer, therefore, analysis is from January to September of 2014 only. Due to the lack of seasonal data for Durban, data were also downloaded for the Skukuza sun-photometer from 1998 July to 2011 July, totalling approximately 68 000 point observations. Skukuza lies along the same longitudinal plane as Durban and is the first AERONET site in southern Africa hence there are numerous studies undertaken addressing aerosol optical properties in Skukuza (Freiman and Piketh, 2003; Kumar, et al., 2013, Kumar, et al., 2014). Therefore the preliminary results from the Durban sun-photometer were compared to Skukuza for validation purposes.

Monthly average AOD, $\alpha_{440-870}$ and CWV, were averaged for Durban from January to September 2014 and for Skukuza from July 1998 to July 2011. Matlab 2015 (version b) was used to create bar graphs, with error bars representing the standard deviation. The parameters of the VSD in the coarse mode and fine mode were averaged and the standard deviation was depicted in tables for each month. The VSD derived from sky radiance as a function of particle radiance was averaged for the different seasons with the accompanying standard deviations. This was presented in a log–graph because the best–fit for the data was a log normal distribution. Measurements of the SSA, ASP and Re and Im part of the complex refractive index were seasonally averaged with and presented with the standard deviations in line graphs,

with error bars representing the standard deviation. Radiative forcing and forcing efficiency at the TOA and BOA were presented in tabular format with the standard deviation. The means and standard deviations of the different aerosol parameters were illustrated in order to determine a monthly trend of aerosol properties in Durban and Skukuza. As well as to compare the trends noted for Skukuza with that of Durban.

The sun-photometer, was also used to study aerosols over Durban from 1 April to 3 June, for 2014, 2015 and 2016. The daily average AOD and α were analysed and depicted in line graphs. This was done in order to determine if there were any differences in aerosol optical properties observed over Durban as a result of the Calbuco volcanic eruption in Chile. A Lidar profile was also obtained from the portable 2D scanning Lidar, located at the University of KwaZulu – Natal to study the vertical distribution of airmass arriving in Durban on 14 May 2015. The Lidar profile coupled with trajectory analysis, was used to determine if air mass arriving in Durban came from the Calbuco volcano in Chile.

3.4.3 Sun-photometer and MODIS data

This study made use of area averaged, C6, level 3 MODIS gridded atmospheric daily product which contained daily 1 x 1 degree grid average values of atmospheric parameters. AOD was derived for Durban for 2014 in order to compare with AERONET daily averaged values. MODIS observations at the L3 nominal 10 km spatial scale was used and it was derived from DT and DB algorithms. MODIS AOD properties were downloaded from http://giovanni.gsfc.nasa.gov/giovanni/.

Statistics were generated for MODIS derived AOD and AERONET derived AOD for Durban. The means and the standard deviations of MODIS and AERONET parameters were compared. It is not possible to compare single MODIS pixel values to AERONET point measurements because the value derived from MODIS is the spatial average over the pixel surface whereas the value from AERONET is a point in space. Additionally, the likelihood of overlap of the centre of a pixel and the point observed by the sun-photometer is quite diminutive and there exists a temporal difference between the acquisitions of data by the two instruments. Due to the dynamic state of air masses, an air mass sensed by MODIS across a horizontal width of the sun-photometer location is sometimes sampled by the sun-photometer at a different time interval (Tripathi, et al., 2005). Area averaged MODIS values were extracted for Durban for 2014 and observations from the sun-photometer located at the University of KwaZulu – Natal was used in this study. MODIS measurements were validated against the sun-photometer for

70

Durban by using regression statistical analysis and determining the R^2 correlation coefficient. R^2 is one measure of how well a model can predict the data, and falls between 0 and 1. The higher the value of R^2, the better the model is at predicting the data. A data set has n values marked y_1 to y_n (all values of y are collectively known as y_i), each value of y is associated with a predicted value represented as $\hat{y}$ and $\bar{y}$ is the mean of y. Therefore, R^2 is defined as:

$$R^2 = 1 - \frac{\sum_{i=1}^{n}(y_i - \hat{y})^2}{\sum_{i=1}^{n}(y_i - \bar{y})^2}$$

For the analysis, it was important to interpolate the AOD values from each sensor to a common wavelength. The AERONET AOD wavelength was, therefore, converted to the MODIS AOD wavelength using the power law as per Kumar, et al., (2015):

$$AOD_a = AOD_b \left(\frac{a}{b}\right)^{-AE}$$

Where a = 550 nm for MODIS, b = 500 nm for AERONET, and AE is the Ångström exponent ($\alpha_{440-870}$) (Kumar, et al., 2015).

It was important to use only days in which data existed for both instrumention in the analysis. Figure 3.2 (a) below, depicts the days in which measurements where available for the sun-photometer and the DT algorithm and (b) depicts days in which measurements where available for the sun-photometer and DB algorithm. For the DT algorithm, 109 common days existed between the sun-photometer and the Terra sensor and 108 common days existed for the sun-photometer and the Aqua sensor (Figure 3.2 b). For the DB algorithm, 89 common days existed between the sun-photometer and the Terra sensor and 80 common days existed for the sun-photometer and the Aqua sensor (Figure 3.2 b).

The monthly average AOD from MODIS's DT algorithm was compared for MODIS Terra, MODIS Aqua and a merged dataset which consisted of the average of MODIS Terra and MODIS Aqua. MODIS's DB algorithm was compared to the same parameters. This comparison was illustrated in a line graph, with the standard deviations represented by error bars. Scatterplots were also used to illustrate the slope and the intercept of the comparisons. The regression coefficient was presented in tabular format comparing the different algorithms and sensors with sun-photometer retrievals. Frequency distribution histograms of AOD was undertaken, to determine which ranges most observations fall within for the different sensors.
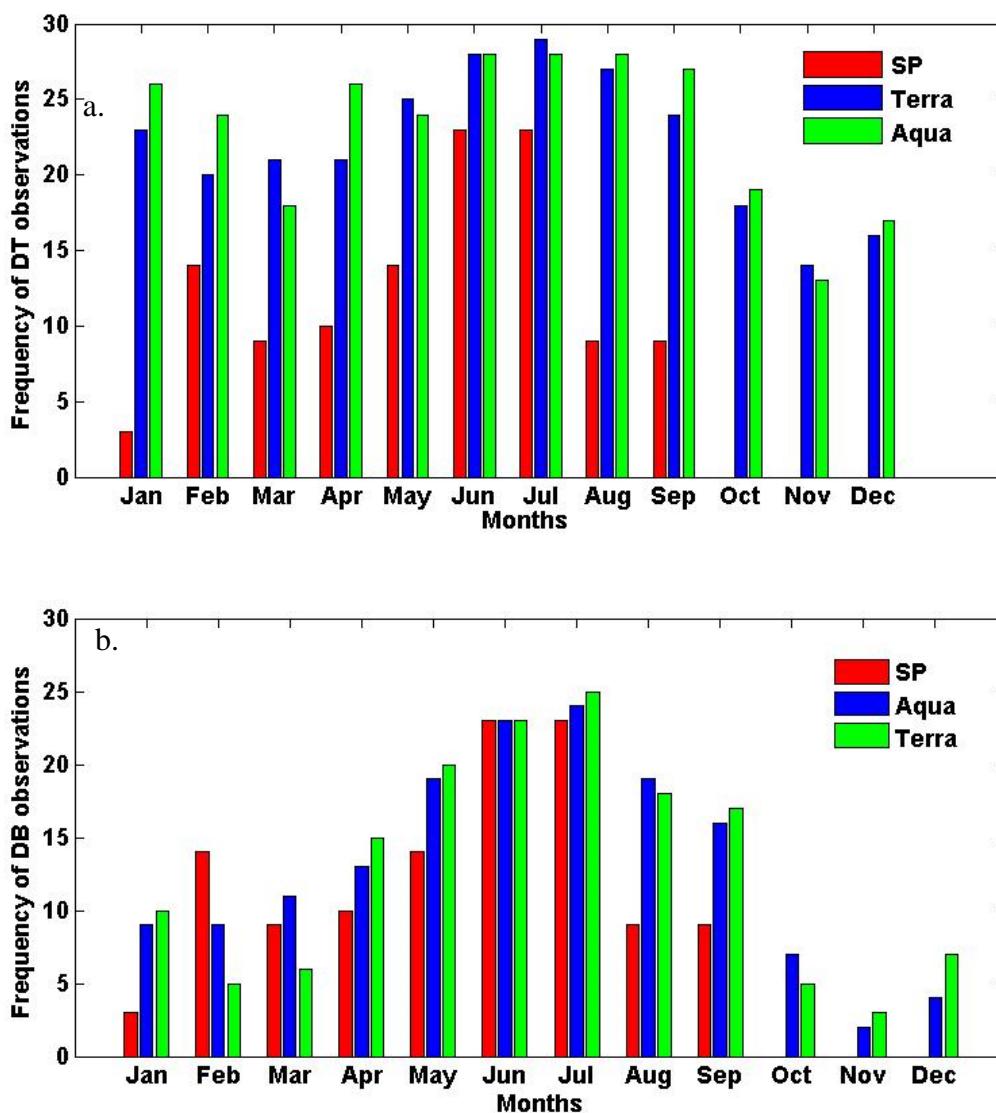
Figure 3.2 Displays the data availability for 2014 for the Sun-photometer(SP) and (a) MODIS Terra and Aqua sensors for DT algorithm and (b) MODIS Terra and Aqua sensors for DB algorithm

3.4.4 HYSPLIT Trajectories

HYSPLIT back–trajectory models were run in this study for days where sun-photometer measurements displayed high and low AOD values for the study period, for 2014. The highlighted days were the 12 August and 20 February (high AOD days) and 6 June and 3 September (low AOD days) for 2014. The trajectory analysis was performed for a time period of 7 days, ending on the aforementioned highlighted days for the back trajectory analysis. The trajectories where computed at three different levels, on the surface (0 km), 1.5 km and 3 km above sea level. The HYSPLIT trajectory model was also used to determine if air mass parcels from the Calbuco volcano in Chile which erupted on the 22, 23 and 30 April 2015 reached

72

Durban. The HYSPLIT 720 hour backward trajectory analysis was undertaken, ending on 25 May 2014, 2015 and 2016. This was done in order to determine whether air mass parcels arrive in Durban from Chile and at what height regions the air mass arrives at. This was done in order to single out whether air mass arrived from Chile to Durban from the Calbuco volcano in 2015.

3.5 Limitations and challenges of the research

The main limitation of this study was that, at the time of analysis, there was not enough data available from the sun-photometer to provide a year of analysis for comparison. Additionally, the data that were used from the Skukuza sun-photometer was not available for the same period as for the Durban sun-photometer. This impacts the results, because a climatological analysis of aerosol optical properties over Durban cannot be fulfilled. Therefore, this study will just affirm to describe observed trends in AOD. Furthermore, the results will be affected because temporal comparisons between Durban and Skukuza are hindered, due to the lack of a common time period. It was for this reason that so many years of data were used for Skukuza (from 1998 – 2011). The extensive years of data used, was so that the trends observed for Skukuza upon analysis of the data, could be seen as a proxy for the aerosol characteristics at that location. Thus allowing for the comparison between the two regions.

Another limitation of the study was that point measurements from the sun-photometer was compared with area averaged MODIS data. Daily averages from MODIS and the sun-photometerwere compared because not enough sun-photometer data were available to use only sun-photometer measurements within the satellite overpass time. This impacts the accuracy of the results because point measurements from the sun-photometer are compared with area-averaged MODIS data.

3.6 Summary

This study attempts to characterise and compare the preliminary aerosol characteristics in Durban from January to September with the aerosol characteristics from Skukuza and also means to identify the effect that meteorological trends have on aerosol loads in Durban. The study aimed to validate and compare the preliminary results from Durban with that of Skukuza. As well as to ascertain reasons for the similarities and differences in aerosol characteristics in these two regions. It also deems to compare MODIS measurements with measurements from the sun-photometer, to determine if MODIS satellite data can provide good estimations of AOD for Durban. NOAA's HYSPLIT trajectory model was also used in this study to determine the source path and trajectory of aerosol plumes on significant days for Durban. The HYSPLIT

trajectory model, together with ground based observations were used to study whether the Calbuco Volcano in Chile influenced air mass arriving in Durban. The use of ground based measurements, satellite data and air–mass models to investigate the atmosphere above Durban is anticipated to provide a robust description of aerosol properties in Durban.

CHAPTER 4

4. ANALYSIS OF THE AEROSOL OPTICAL PROPERTIES OVER DURBAN USING AERONET CIMEL SUN-PHOTOMETER WITH SOME COMPARISONS MADE WITH THE SKUKUZA SUN-PHOTOMETER

4.1 Introduction

There have been various studies around southern Africa that have made use of sun-photometers to study aerosol optical properties within the region (Adesina, et al., 2014; Adesina, et al., 2016; Adesina, et al., 2016; Adesina, et al., 2016; Kumar, et al., 2013; Kumar, et al., 2014a; Kumar, et al., 2015a; Kumar, et al., 2015b; Hersey, et al., 2015). Sun photometry was found to be an

extremely useful tool to characterise aerosol optical properties within the region, especially during the SAFARI 2000 dry field campaign (Swap, et al., 2003). It was found, in many studies that biomass burning was the major contributor to aerosol loads over the sub–continent during the austral spring (Kumar, et al., 2014b). This chapter will discuss the different studies that have utilised ground based measurements, paying particular attention to sun-photometers to study aerosol optical properties around southern Africa. It will also depict the results of comparing measurements gained from the Durban sun-photometer with the Skukuza sun-photometer. The measurements used were obtained from the CIMEL Sun-photometer (CE–318) located in Durban. In order to perform the comparative analysis, aerosol optical properties were analysed from point measurements in Durban from January 2014 to September 2014, approximating 7591 observations and for Skukuza from July 1998 to July 2011 using approximately 68000 observations.

One of the major studies that focused on southern Africa, was performed by Eck, et al., (2003) for the SAFARI 2000 dry season campaign. Much of the studies that deals with aerosol pollutants in southern Africa were undertaken during SAFARI 2000's dry season campaign. They have used sun-photometer measurements from seven AERONET sites located within the western half of Zambia to distinguish biomass burning aerosols from savanna burning aerosols. AERONET sites located in Namibia, Mozambique, Skukuza (in South Africa) and Bethlehem (in South Africa) were used in the analysis. The study found that fine mode biomass burning aerosols majorly impacted the northern part of the study region (Zambia). The southern regions i.e., South Africa and Mozambique were impacted by biomass burning to a lesser extent. South Africa and Mozambique were also affected by other aerosols which originated from fossil fuel burning, industrial activities, and Aeolian coarse mode aerosol types. Their study further supported another study conducted by Piketh, et al., (2002), which identified Aeolian dust as a major source of aerosols in South Africa outside of the biomass burning season.

Queface, et al., (2003), also conducted a study during SAFARI 2000's dry season campaign, from April to November 2000. Measurements of AOD were used from a sun-photometer located at Inhaca Island, Mozambique off the east coast of southern Africa. Comparisons were made with Mongu in Zambia and Bethlehem in South Africa. AOD values for Inhaca, showed two distinct nodes, with low values recorded during April and July and high loadings from August to November. There was a high degree of optical variability present over Inhaca Island. This variability is due to the diverse contributions of aerosols which impact the troposphere above Inhaca, such as sea–spray, wind–blown dust and the extended transport of industrial and

biomass burning emissions from southern Africa (Queface, et al., 2003). The monthly averages of AOD over Inhaca showed that high loads existed during September (0.42) and October (0.52), as well as August (0.25) and November (0.25). The high AOD values correspond to the biomass burning season in southern Africa. It was found that high AOD values also existed during the biomass burning season for Mongu and Bethlehem. The highest AOD was recorded in September for Mongu (0.89) and October for both Inhaca (0.52) and Bethlehem (0.31), thus depicting a strong north–south gradient in AOD for southern Africa, in agreement with Eck, et al., (2003).

Sun photometry was again utilised to study the physical properties of aerosols (AOD and α) during the SAFARI 2000 dry season campaign in the town of De Aar by Winkler, et al., (2008). De Aar lies in the eastern part of the Karoo in South Africa. Anthropogenic emissions in the area are quite low with minimal industries and few domestic fires causing air pollution emissions (Winkler, et al., 2008). The measurements were from 1 August 2000 to 9 February 2001, and it was found that biomass burning is the foremost source of aerosols in the region during the study period. It was found from trajectory models, that most of the biomass emissions is of African origin with a minor source of aerosols from aged smoke from fires in the Amazon basin reaching southern Africa.

A similar study, also performed for SAFARI's dry season campaign, was performed by Magi, et al., (2003). The study depicted in situ measurements of vertical profiles of aerosol light scattering, light absorption, SSA and AOD at various locations around southern Africa. The AOD was measured with a Particle and Soot Absorption Photometer (PSAP) located on board an air craft and it was compared with AOD gained from NASA's 14–channel Ames Airborne Tracking Sun-photometer (AATS–14) which was also mounted on the air craft. It was found that AOD from in–situ measurements compared very well with the sun–photometer derived AOD. The study also showed the major effects of local sources of biomass burning and of the long–range transport of biomass smoke from northern parts of southern Africa, lowering the SSA values from 0.89±0.03 before the "River of Smoke" to 0.81±0.02 after the "River of Smoke" phenomenon (Magi, et al., 2003).

Queface, et al., (2011), studied AOD at 500 nm and aerosol VSD over Mongu in Zambia (from June 1995 to June 2007) and Skukuza in South Africa (from July 1998 to June 2008). The results depicted seasonal variation in AOD, with low seasonal multi–month mean values (0.11 to 0.17) from December to May, medium values (0.20 to 0.27) between June and August, and

high to very high values (0.30 to 0.46) from September to November. The spatial distribution of aerosol loadings, agreed with earlier studies by Eck, et al., (2003) and Queface, et al., (2003) by showing that an aerosol gradient exists in southern Africa, whereby, the north has higher aerosol distributions than the south during the biomass burning season, with an opposite pattern observed during the non–biomass burning season (Queface, et al., 2011).

Tesfaye, et al., (2013), used sun-photometer, LIDAR and MISR observations of AOD to validate the Regional Climate Model (RegCM4) in South Africa, from 1998 to 2008. The model performed quite well when compared to the sun-photometer and MISR values of AOD. The magnitudes of the model simulated AODs are within the standard deviation of the sun-photometer and ±25% of MISR observations (Tesfaye, et al., 2013). Tesfaye, et al., (2014), conducted another study using the RegCM4 model to investigate biomass burning aerosols over South Africa using the twelve year runs of RegCM4 from 1 January 1997 to 31 December 2008 for the biomass burning season (July to October). The results depicted that Mpumalanga, KwaZulu–Natal and the eastern parts of Limpopo are the foremost local source areas of biomass burning aerosols in South Africa (Tesfaye, et al., 2014).

Vakkari, et al., (2013), studied submicron aerosol particle size distribution measurements in the southern African savannah within the size range of less than 100 nm. The study was undertaken at two locations in the North West province of South Africa. Measurements were obtained from Botsalano game reserve (relatively clean air), from 20 July 2006 until 5 February 2008 and from Marikana village (more polluted), from 8 February 2008 to 17 May 2010. The size distributions were measured using the ground based, differential mobility particle sizer (DMPS) with a size range 12–840 nm and a temporal resolution of 10 minutes. Carbon monoxide (CO) concentrations measured and SO_2 concentrations were measured with a Thermo 42S analyser. PM_{10} and $PM_{2.5}$ mass concentrations measured with a Tapered Element Oscillating Microbalance (TEOM). The median total concentration of aerosol particles was greater than four times higher at Marikana than at Botsalano. Seasonal variation occurs most prominently for particles greater than 100 nm. In the dry season from May to September, the particles greater than 100 nm are prevalent in both regions. During the dry season, the concentration of particles greater than 100 nm has a correlation with CO for both study sites. This was attributed to incomplete burning due to domestic heating in Marikana and due to wild fires in Botsalano (Vakkari, et al., 2013).

Mafusire, et al., (2016), studied ground based measurements of biomass burning aerosols and trace gases at Botsalano. Trajectory analysis was also undertaken to determine air mass pathways on days with high and low aerosol concentrations. Botsalano was selected because it is primarily unaffected by anthropogenic aerosol sources, therefore the aerosols represent well–mixed regional air quality. The study was conducted from 2006 to 2005. Aerosol, trace gas and meteorological variables are recorded at Botsalano using instruments kept in climate–controlled mobile measurement trailers. Aerosol number size distributions were measured in the 10 to 840 nm size range with a DMPS and individual trace gases were identified. Fire plumes were recognized as having CO above average tropospheric levels and an increased concentration of particulate matter. It was found that there were thirty six biomass burning plumes existed during the study period. Analysis of the long range transportation of aerosols revealed, most aerosols travelling easterly, then south–westerly, followed by regional recirculation and lastly, aerosols also travelled northerly. Biomass burning was recognised as the major source of Aitken mode aerosol particles in the region (Mafusire, et al., 2016).

Nyeki, et al., (2015), conducted a study on aerosol climatology in the Cape Point based on data collected from 2008 to 2013. Cape Point is one of the World Meteorological Organizations Global Atmosphere Watch (GAW) global stations, and allows for the monitoring of atmospheric parameters at a remote marine location. Ground based aerosol measurements began at the Cape Point from 2008 using a precision filter radiometer (PFR). The study used Radon (^{220}Rn) gas as a tracer of continental air mass due to values of ^{220}Rn being indicative of airmass types. Air mass classification was determined using in situ wind direction and Rn concentration and four air mass types were used to examine AOD, that being, background marine, marine, mixed, and continental. For the aerosol loads in Cape Point, average for study period was 0.059 and the median value was 0.049. There existed no extensive patterns in AOD for the study period. However peaks existed in 2009 and using back trajectory analysis it was shown to be of marine origin and in 2010 and 2011 and were shown to be of local origin. AOD from PFR analysis was compared to MISR generated AOD for continental airmasses (this was gained from determining the Rn values), using correlation regression analysis for 2008 to 2013. It was revealed that the R^2 value was 0.68 for continental air masses and 0.38 for marine air masses. For the Ångström exponent (α), values were low throughout the year, alluding to the dominance of coarse mode aerosols (Nyeki, et al., 2016).

Adesina, et al., (2014) characterised the aerosol optical properties collected from the sun-photometer located in Pretoria from January to December 2012. It was found that high AOD

values existed during February (0.36±0.19) and August (and 0.25±0.14), with lower values experienced during April and June (0.12±0.07). The α displayed maximum values during January and the lowest values during July (0.66±0.21). The α results, show that there is a greater fraction of fine mode aerosols over Pretoria during the study period. The high α noted during summer could be due to high temperatures experienced summer. The VSD in the fine–mode is higher in the summer and spring seasons, whereas in the coarse mode the VSD is higher in the winter and lower in the summer which was attributed to the hygroscopic growth of aerosol particles. The SSA ranged from 0.85 to 0.96 at 440 nm wavelength over PTR for the entire study period.

Adesina, et al., (2015), conducted another study on aerosol optical characteristics over Gorongosa, in Mozambique using a ground–based AERONET sun–sky radiometer. The study made use of data from July to December 2010 to show how aerosols evolve during the biomass burning season. The monthly mean AOD was highest in September (0.64±0.34), the α increased from July and displayed a maximum value during September (1.56±0.26), thus implying an increase in fine mode aerosols due to biomass burning. The α started to increase from October, alluding to an increase in coarse mode aerosols. The VSD showed the fine mode higher from August to October and the coarse mode higher in December. The SSA was between 0.87 and 0.94 in the wavelength region (440–670 nm) and decreased from July to October because of the relative increase of fine aerosols produced from biomass burning. The real and imaginary refractive indices also indicated the presence of mixed aerosol loads over Gorongosa (Adesina, et al., 2015).

Adesina, et al., (2016), studied trends in AOD retrieved from MODIS and MISR sensors from 2004 to 2013 over Skukuza and Richards Bay. The study was conducted using MODIS Terra, MODIS Aqua, MISR and Ozone Monitoring Instrument (OMI) data to facilitate the comparison of aerosol loads over the study sites. For Skukuza, satellite measurements were validated against AERONET sun-photometer derived measurements. Monthly and seasonal trends were also undertaken. The OMI derived Ultra–Violet Aerosol Index (UVAI) data was used to investigate the aerosol absorption property in both Skukuza and Richards Bay. The satellite validation studies, was only undertaken for Skukuza, and it was found that for MODIS Aqua and Terra sensors and for MISR, the least square fitted line was lower than AERONET, thus alluding to an underestimation of AOD by all satellites. High aerosol loads were observed from August to October. This is due to the biomass burning phenomenon that occurs in southern Africa during this time. The seasonal mean AOD was highest during spring, then

summer, followed by autumn and the lowest AOD values occurred during winter. The high AOD noted during summer was attributed to the hygroscopic growth of aerosols. The high temperature in summer aids in the development of secondary aerosol formation (Adesina, et al., 2016).

Sivakumar, et al., (2009), compared the AOD from an AERONET sun-photometer located in Johannesburg with the Council for Scientific and Industrial Research (CSIR) and the National Laser Centre's (NLC) mobile LIDAR system derived AOD and with Stratospheric Aerosol and Gas Experiment II (SAGE II) derived AOD. The days compared where the 25 February 2008 and the 10 April 2008. It was established that all measurements were in good agreement (Sivakumar, et al., 2009).

Sivakumar, et al., (2010), conducted a study over South Africa, using sun-photometer measurements from three different sites (Skukuza, Johannesburg and Bethlehem), Lidar and satellite derived aerosol extinction coefficients. It was found that the monthly average AOD displayed maximum values from October to March and minimum values from May to June for Johannesburg and Skukuza. Bethlehem displayed two maxima, during March and October and minimum values during winter. Study of the $\alpha_{440-675}$ depicted that there was a dominance of fine mode particles in Johannesburg and Bethlehem indicating aerosols of anthropogenic origin from fossil fuel burning. Coarse aerosol particles were noted for Skukuza, attributed to short and long–range transport of hygroscopic aerosols, combustion processes and their interaction with atmospheric moisture (Sivakumar, et al., 2010).

Kumar, et al., (2013), studied aerosol optical properties (AOD, $\alpha_{440-870}$, and columnar water vapour) over Skukuza using the sun-photometer from December 2005 to November 2006. The results depicted seasonal variation of AOD_{500} with low values during the autumn season (0.10 – 0.13), moderate values during summer and winter seasons (0.14 – 0.16) and high to very high values during spring (0.18 – 0.40). It was noted that the greatest contribution to tropospheric aerosols are from biomass burning and to a minor extent sea–salt, desert dust and urban industrial aerosols. The $\alpha_{440-870}$, displayed reasonably high values throughout the year suggesting a greater influence of fine mode aerosols. The mean values of CWV shows maximum values during summer and minimum values during winter, similar to rainfall pattern in the area. The strong seasonal variability in aerosol optical properties over Skukuza, was attributed to the prevailing meteorology, long–range air mass transport, and atmospheric conditions.

From the aforementioned studies, it can be ascertained that there have been various studies that have used sun photometry to study aerosol optical properties in southern Africa, especially during the austral spring. Despite the aforementioned studies, there have been no studies in Durban studying aerosol optical properties from a ground–based sun-photometer. It can also be noted that there are a vast number of studies measuring aerosol optical properties in Skukuza. This chapter presents the preliminary results from the Durban sun-photometer which was compared with the measurements from the Skukuza sun-photometer. This was done to determine the similarities and differences in aerosol optical properties in the two regions, as well as to validate the preliminary results from the Durban sun-photometer with the well–established Skukuza sun-photometer observations.

4.2 Synoptic meteorological trends in Durban

The monthly mean variations of the prevailing background meteorological conditions over Durban from 2004 to 2014 was averaged for Durban in Figures (4.1 to 4.4) and Table 4.1. The data were provided by the South African Weather Services (SAWS) from the surface of 23m above sea level. The meteorological station measures wind speed, wind direction, ambient temperature and relative humidity. The station experienced high wind speed during the months of spring and summer and low wind speed during autumn and winter, from point measurements obtained from 2004 to 2014. From Table 4.1 and Figure 4.1, it can be noted that the maximum value was recorded during October (3.56±1.92m/s). The minimum value was recorded during June (2.25±1.67 m/s).

Ambient air temperature is the lowest during the month of June (14.10±8.06°C) in winter and highest during January (24.83±2.82°C) in summer (Figure 4.3). The temperature and relative humidity display a similar relationship (Figure 4.4). The temperature is high from January to March, then displays low values from April to September, from September onwards the temperature increases. The standard deviations for temperature, was between 2 to 4 degrees for each month. High standard deviations existed for certain months, namely May, June, July and October. The high standard deviations experienced in May and October could be the result of May and October being transition months, changing from one season to the next. The month of May is the end of autumn and October is the end of spring, therefore, it could be due to the changing of the seasons. The high deviations noted in winter, could be due to the coastal low pressure system that develops during summer and winter in South Africa (Preston-Whyte & Tyson, 1988). The low pressure system causes different weather conditions on either side of

the pressure cell. Also, the South Indian High Pressure system moves over land in the winter. The differing synoptic patterns could lead to variable weather conditions thus causing the larger standard deviations noted during the winter months (Macmillan, 2014).

The relative humidity ranges from 62.66% in September to 75.51% in January (Figure 4.2). The relative humidity is high from January to April, displays lower values from May to September and displays high values from October to December. From Figures 4.1 to 4.2 and Table 4.1, the meteorological factors that govern the seasons can be observed. Durban experiences hot, humid summers. The spring months depict that Durban experiences windy conditions during spring; and during winter, temperatures are low, relative humidity is low and wind speeds are low compared to the other seasons.

At Skukuza, the climate is semi–arid subtropical, with hot rainy summers and warm dry winters. There have been continuous observation of temperature at Skukuza since 1916 and it was noted that temperature rose by approximately 0.05°C per decade. Kruger, et al., (2002), carried out a study to determine linear trends in monthly, rainfall time series from 1912 to 2001. The study also conducted long term rain fall statistics, and it was distinguished that summer experiences the highest rainfall for the area and winter is the driest season. The absolute maximum and minimum monthly rainfall suggested that rainfall in Skukuza is highly variable, thus the area is predisposed to frequent droughts and floods (Kruger, et al., 2002).

Winter (J–J–A)   **Spring (S–O–N)**
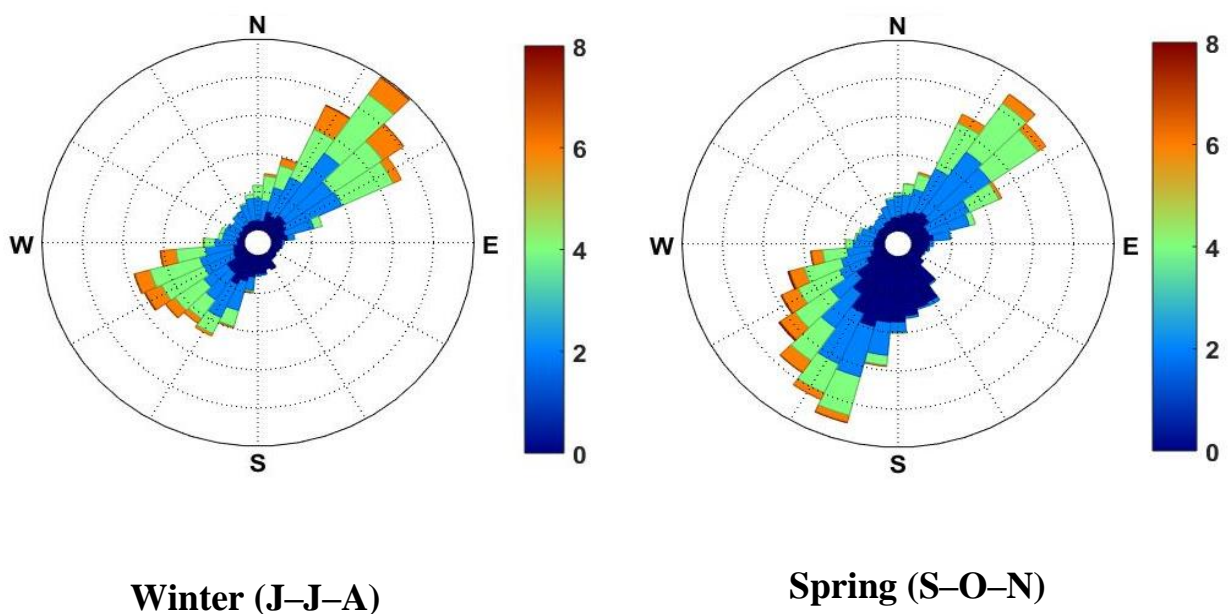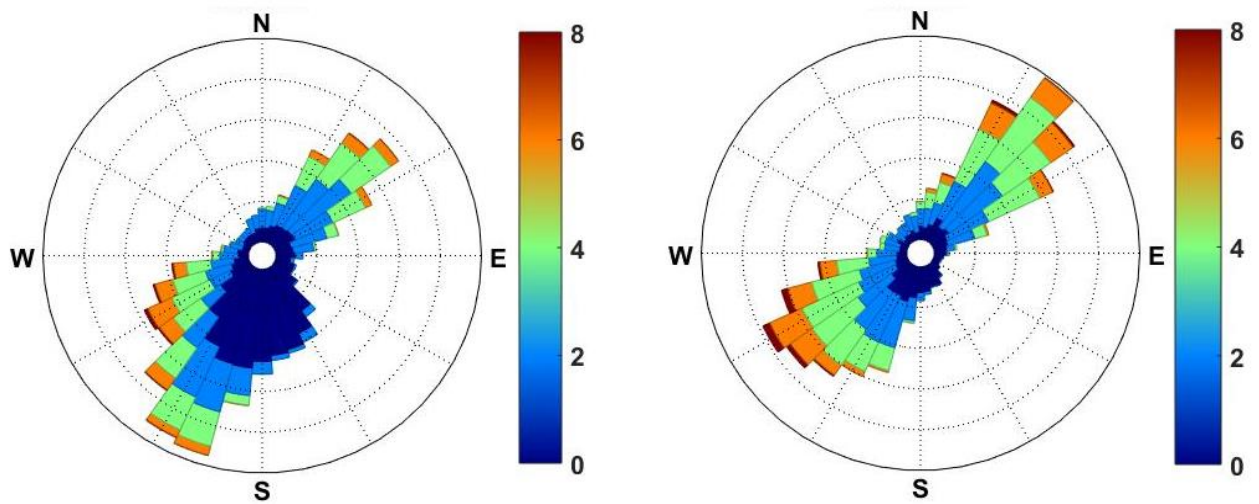
Figure 4.1 **Average speeds for Durban from 2004 to 2014 for the different seasons, depicting wind direction (°) and wind speed (m/s).**

Table 4–1 Average wind speed with standard deviations (STD), from January to December (2004 to 2015) for Durban.

Months	Wind Speed (m/s)	
	Mean	STD
January	3.40	1.75
February	3.15	1.77
March	3.12	1.86
April	2.91	1.78
May	2.44	1.72
June	2.25	1.67
July	2.47	1.80
August	3.14	2.01
September	3.40	1.99

October	3.58	1.92
November	3.56	1.86
December	3.49	1.83
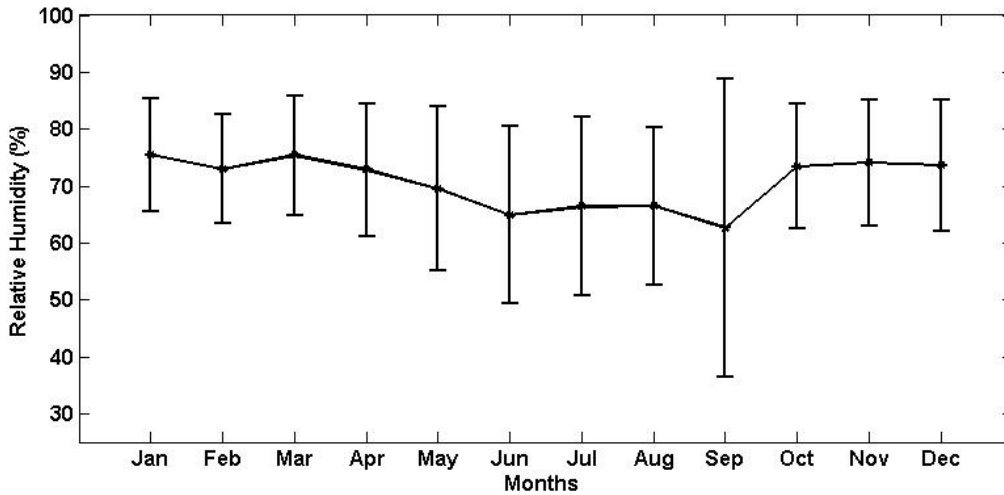
Figure 4.2 Average relative humidity (%) from January to December (2004 to 2014).
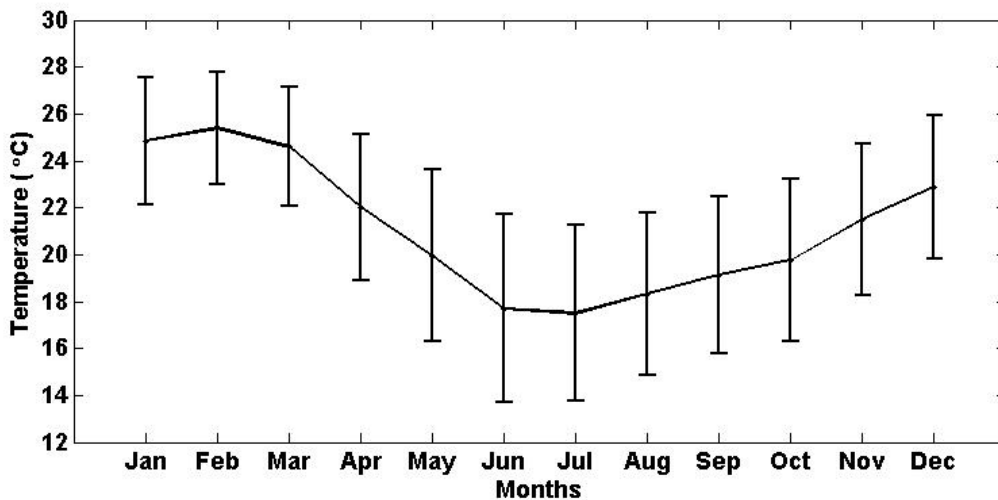
Figure 4.3 Average temperature (°C) from January to December (2004 to 2014).

4.3 Variabilities in direct aerosol optical properties for Durban and Skukuza.

Sun-photometer measurements of direct solar radiation measurements allow for the calculation of columnar AOD. The AOD can then be used to compute columnar water vapour (CWV) and to approximate the aerosol size using the Ångström Wavelength Exponent (AERONET, 2015). The following figures display the variabilities in aerosol optical properties in Durban and Skukuza. The AOD, $\alpha_{440-870}$ and CWV were averaged for Durban from January to September

2014 and for Skukuza from July 1998 to July 2011. Cloud screened and quality assured data were obtained from AERONET for the sun-photometers at each site, Skukuza and Durban. The measurements for each parameter, amounted to 7591 observations for Durban and 68000 observations for Skukuza. It was obtained from point observations, recorded approximately every five minutes, by the sun-photometers located at the respective sites. Bar graph with error bars representing the mean and standard deviations respectively, were used to display the AOD (Figure 4.4), $\alpha_{440-870}$ (Figure 4.5 – Figure 4.6) and CWV (Figure 4.7), for Durban(a) and Skukuza(b). A stacked bar graph was also used to display the frequency of $\alpha_{440-870}$ values for Durban and Skukuza. Bar graphs with error bars were chosen to represent the aforementioned aerosol optical properties because they are visual tables that allows for quick viewing of the mean and standard deviations of the dataset (Weissgerber, et al., 2015). Bar graphs are also useful to display how the aerosol optical properties change over time and gives a general picture of the monthly distribution of aerosol optical properties. The error bars are able to categorise the standard deviations to the mean and visually represent the variability of the data.

4.3.1 Aerosol Optical Depth (AOD)

Figure 4.4 below, represents the monthly average and standard deviations of AOD_{500} for Durban (Figure 4.4 a) and Skukuza (Figure 4.4 b). The AOD values for Durban, shows that all months analysed have low AOD values because the values are <0.4. The highest average AOD is recorded during winter, in the month of August 0.26±0.17. The lowest average AOD is recorded during autumn, in the month of April 0.12±0.09. The large standard deviation values indicate that AOD is highly variable. The low AOD value in April is consistent with Kumar et al. (2015a), who reported low AOD values in April in Durban, using satellite data from MODIS's Terra and Aqua sensors to measure AOD from 2003 to 2013. The mean AOD values depicted in Figure 4.4b, for Skukuza, show similar aerosol values during all months, with the exception of the months of spring (September, October and November) and August, which displays high AOD (>0.4). From previous studies, the observed increase in aerosol values during spring for Skukuza and during August for Durban is most likely due to an increase in biomass burning activities in the northern and eastern parts of South Africa. Areas of high biomass burning activity include Mpumalanga, KwaZulu–Natal and the eastern parts of southern Africa (Eck, et al., 2003; Queface, et al., 2003; Winkler, et al., 2008; Queface, et al., 2011; Tesfaye, et al., 2011; Kumar, et al., 2014a; Tesfaye, et al., 2014). During this period, biomass burning occurs in Africa at latitudes between the Kalahari Desert and the Congo basin (Winkler, et al., 2008). According to Hersey, et al., (2015), biomass burning from neighbouring

countries such as Zimbabwe and Mozambique have the greatest impact on emissions in South Africa. These neighbouring emissions tends to peak in frequency during August, September and October together with sugar cane field burning explains the higher AOD values noted during August. Although domestic burning occurs quite frequently during the winter season and is associated with high particulate concentrations in South Africa, it mainly affects particulate conditions on the ground, not stratified, vertical aerosol layers. Therefore, the early winter months for both Skukuza and Durban depict low aerosol loads (Hersey, et al., 2015). The maximum AOD noted for Durban during this study was in August, with low values experienced during the other months of the study period, the results were found to be similar to Hersey, et al., (2015), who studied AOD using MISR observations in several sites in South Africa, including Durban. However the MISR satellite values were significantly higher than the values observed for Durban during this study.

The highest emissions of biomass burning in southern Africa arises between May and September and starts in the tropics (between 0 and 20°S) thus impacting biomass burning in southern Africa (Formenti, et al., 2000; Vakkari, et al., 2013). There exists strong North – South gradients when dealing with biomass burning AOD (Eck, et al., 2003; Queface, et al., 2003; Queface, et al., 2011). Durban is placed on the eastern coast of southern Africa, therefore it is duly positioned to experience the "river of smoke" phenomenon (Swap, et al., 2003). This is a synoptic air flow that aids the transport of subtropical biomass burning aerosols over the north–eastern parts of the country. Therefore the high AOD noted for Skukuza during spring might be due to the transportation of air–mass from surrounding sub–tropical regions of southern Africa (Freiman & Piketh, 2003). Aerosol plumes from these fires are anticipated to reach the central South African plateau, through the Angolan and Namibian coastal regions whenever a sub–continental anticyclone is well advanced (Winkler, et al., 2008).

The high AOD noted during August for Durban and during spring for Skukuza, could be due to an increase in the generation of windblown dust across South Africa. This is in line with ground based data obtained from SAWS detailed in previous sections of this chapter, where wind speeds were shown to increase to maximum values from July to November. These strong convective winds could also transport dust particles from the deserts in west and North Africa and sea–salt particles caught up by strong south–easterly, southerly winds across South Africa (Piketh, et al., 2002, Hersey, et al., 2015). Therefore dust maybe a prominent source of AOD in South Africa.

Additionally, the high aerosol values observed in Durban during the winter month of August, could not only be due to biomass burning but also due to various factors, such as a combination of large–scale circulation processes, increases in temperature inversions caused by the hazy layer formation and increase in the presence of urban industrial aerosols (Kumar, et al., 2014a). Low AOD values were observed over Skukuza and Durban during the autumn season. This finding supports results from Tesfaye et al., (2011), Queface et al., (2011) and Kumar et al., (2013). The low AOD observed during summer months for Skukuza and Durban (January to February) could be due to cloud scavenging and wet removal processes, decreasing aerosol loads. The low AOD observed during June and July for Skukuza and Durban could be due to low wind speeds and low water vapour, thus the atmospheric weather conditions results in weak aerosol generation mechanisms and hinder the growth of atmospheric aerosols (Kumar, et al., 2014a). Furthermore, the wintertime low in aerosol values for both Skukuza and Durban, could be due to air–masses following the passage of cold fronts which originate over the south Atlantic or even the south Pacific oceans, thus having minimal time spent over land (Winkler, et al., 2008). The decrease in AOD noted for Durban from August to September could be due to large scale dispersion, diffusions and deposition of aerosols away from Durban (Eck, et al., 2003). When dealing with spatial distribution, the northern areas of southern Africa have greater magnitudes of biomass burning than the south due to the north–south gradient reverse in aerosol loads (i.e., greater aerosol loads experienced in the north during the biomass burning season than the south). This can be seen for Skukuza, where AOD is higher during the spring months than in Durban, probably due to Skukuza being closer to burning (Eck, et al., 2003; Queface, et al., 2003; Queface, et al., 2011; Mafusire, et al., 2016). The AOD trends noted for Skukuza and Durban are in line with those observed for southern Africa, by Piketh, et al., (1999), whereby, it can be observed that only during the biomass burning season, is biomass burning a significant contributor to aerosol loads in the region.
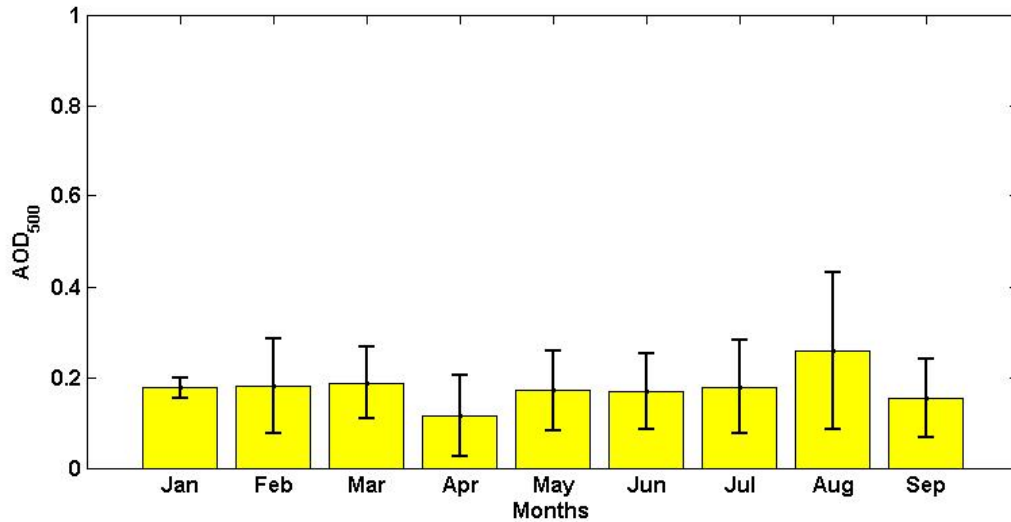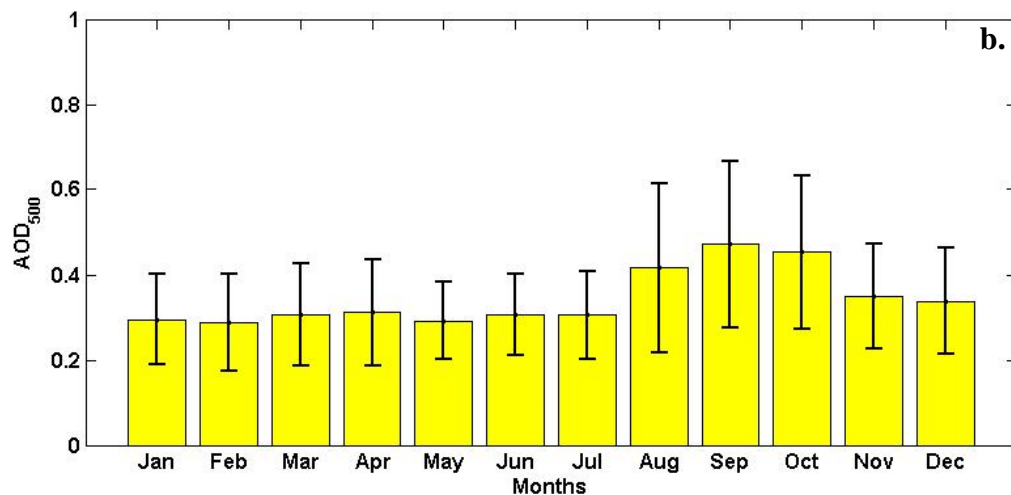
Figure 4.4 Monthly average aerosol optical depth (AOD) at 500 nm, at (a) Durban from January to September 2014 and at (b) Skukuza from July 1998 to July 2011.

4.3.2 Ångström Exponent ($\alpha_{440-870}$)

Figure 4.5 (a and b) and Figure 4.6 (a and b) depicts the Ångström Exponent ($\alpha_{440-870}$), values of $\alpha_{440-870}$ near zero relate to coarse–mode aerosols such as sea spray and desert dust, values of $\alpha_{440-870}$ greater than 1.5 corresponds to the occurrence of fine–mode particles from smoke or urban aerosols and $\alpha_{440-870}$ that is greater than 2 indicate very small particles in the Rayleigh limit. The average $\alpha_{440-870}$ for Durban during the months of January to April is less than 1 (Figure 4.5 (a), suggesting that the fine mode fraction is less than the course mode fraction during these months relating to an abundance of coarse mode aerosols in Durban. From Figure 4.6 (a), it can be seen that for Durban the coarse mode fraction dominates during January,

March and April, with most values falling between 0 and 1. This is most likely due to the presence of sea–spray aerosols (since Durban lies in a coastal region) and soil dust can become entrained within the atmosphere from the coast. Figure 4.5 (b), shows that Skukuza experienced a greater amount of fine mode aerosols than course mode aerosols for all months. These results suggest that outside of the biomass burning season, fine mode particle sources affect the atmosphere above Skukuza, probably due to fossil fuel burning from the South African Highveld (Queface, et al., 2011). Based on earlier findings by Freiman and Piketh (2002), Skukuza is located at a position whereby it can experience fossil fuel combustion plumes from the South African Highveld. Durban differs from Skukuza, in that there are more coarse mode aerosols present in Durban than what was noted for Skukuza. This was probably due to marine aerosol presence being that Durban is a coastal city (Adesina, et al., 2016).

Skukuza and Durban both experienced lower $\alpha_{440-870}$ values during the January. From Figure 4.6 (b), it can be seen that for Skukuza values within the coarse mode fraction, increase during the summer months (December, January and February) and the end of spring (November). The dominance of the coarse mode during summer was also noted by Adesina, et al., (2014) for Pretoria and Adesina, et al., (2015) for Gorongosa in Mozambique. The high temperatures experienced during January aid in the formation of coarse mode aerosols by heating the ground and lifting the loose soil particles to be later entrained by wind (Kumar, et al., 2014a). Therefore, the increase in coarse mode aerosols noticed for Skukuza and Durban, during the summer months, could also be due to the presence of sea salt mixed with some dust aerosols. It could also be due to cloud contamination caused by undetected cirrus clouds (Kumar, et al., 2013). It can be observed that during the months with higher CWV, the $\alpha_{440-870}$ implies coarser aerosol load present, this could be the result of the hygroscopic growth of aerosols in the presence of water vapour. From Figure 4.2, it can be noted that the relative humidity is also increased during the summer months, thus supporting the hygroscopic development of aerosols during this period. Furthermore, average relative humidity for all months for Durban is greater than 50%, thus, according to Kotchenruther and Hobbs (1998), humidity greater than 50% allows for the hygroscopic growth of aerosols (Kotchenruther & Hobbs, 1998).

The increased $\alpha_{440-870}$ for Durban during the winter months (Figure 4.5 (a) and Figure 4.6(a)), means that there is an increase in the fine–mode fraction of aerosols during these months, which could be due to biomass burning and urban aerosols, thus alluding to mixed aerosol presence during these months. Additionally, the higher $\alpha_{440-870}$ observed during winter in Durban could be due to the increase in biomass burning activities coupled with a decrease in rainfall during

the month of August, hindering rainout and washout processes. A decrease in rainfall also hampers the hygroscopic growth of aerosols, thereby increasing the content of aerosols in the fine mode fraction. This study contradicts other studies carried out in South Africa which expected lower $\alpha_{440-870}$ values during the dry winter seasons due to an increase in coarse mode dust particles (Hersey, et al., 2015). Similarly to Durban, from Figure 4.5 (b) it can be noted that for Skukuza, the $\alpha_{440-870}$ is below 1.5 for most months with the exception of September, suggesting an increase in fine mode particles, probably due to biomass burning aerosols in southern Africa. The higher $\alpha_{440-870}$ observed in this study for Skukuza during the spring biomass burning season positively concurs with other studies which suggest that aerosol loads in South Africa are characterised primarily Aitken mode (0.01–0.1 μm) aerosols (Eck, et al., 2003). The increase in $\alpha_{440-870}$ from May till August was also noted for Adesina, et al., (2015) for Gorongosa, this increase was also attributed to biomass burning. Queface, et al., (2003), studied three sites in southern Africa, Mongu in Zambia, Bethlehem in South Africa and Inhaca Inhaca Island in Zambia, found $\alpha_{440-870}$ to be greater during September, indicating an increase in the fine mode fraction. It was suggested, that the fine aerosols in spring could be due to biomass burning and industrial aerosol sources, whereas the fine aerosols in months outside the biomass burning season could be due to mainly urban industrial emissions. Hence, the increase in fine mode aerosols from May to July noted in Durban, could be due urban industrial emissions.

a.
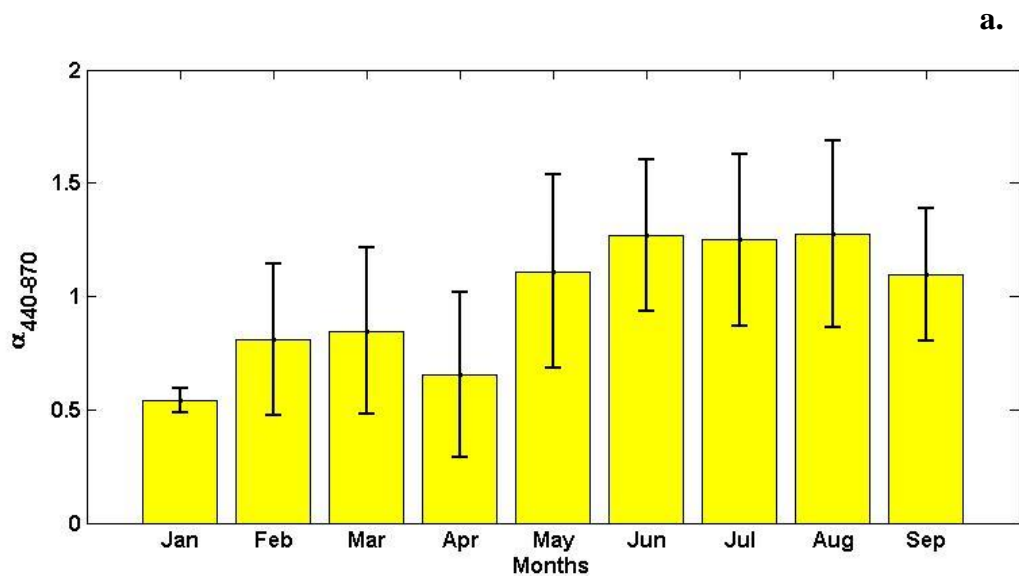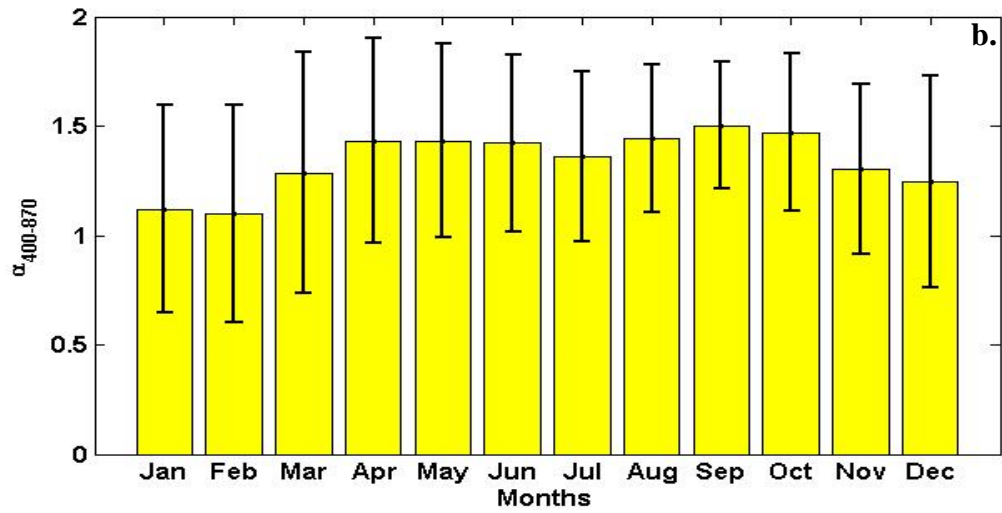
Figure 4.5 Monthly average Ångström Exponent (α440 – 870) at (a) Durban from January to September 2014 and at (b) Skukuza from July 1998 to July 2011.
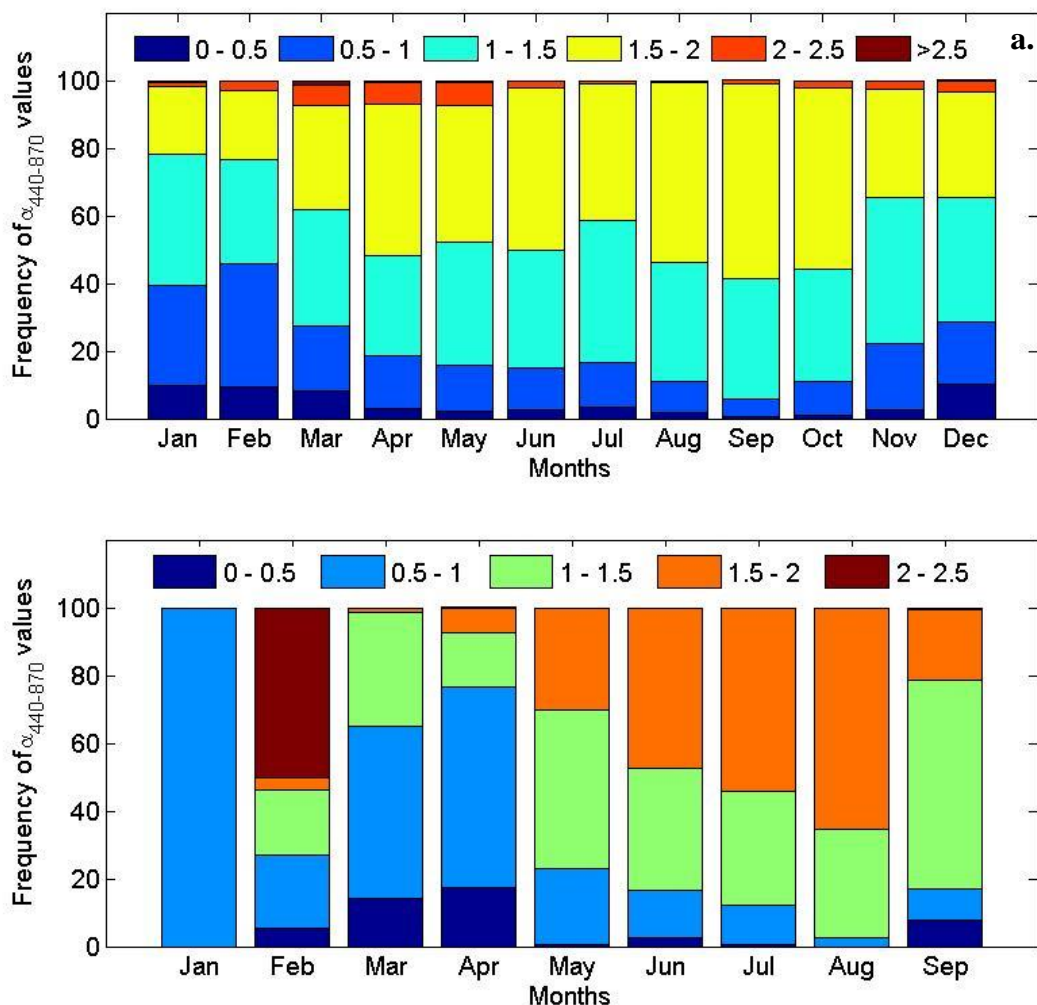
Figure 4.6 Frequency of Ångström Exponent (α440 – 870) values at (a) Durban from January to September 2014 and at (b) Skukuza from July 1998 to July 2011.

4.3.3 Columnar water vapour (CWV)

The CWV for Durban Figure 4.7 (a) and Skukuza Figure 4.7 (b) followed a similar pattern. High values were noted during January (3.60±0.22 cm), February (3.17±0.53 cm) and March (2.32±0.43 cm) for Durban and during January (3.14±0.70 cm), February (3.14±0.71 cm), March (3.18±0.64 cm) and December (3.20±0.64 cm) for Skukuza. The CWV values decreased from January to June (1.01±0.40), increased from July (1.07±0.36) to September (1.10±0.36) for Durban. For Skukuza, CWV values decreased from March to July (1.36±0.41), then increased again, from August (1.57±0.49) to December (3.20±0.64). The low correlation exhibited between CWV and AOD for Durban (0.03) and Skukuza (0.03) suggests that aerosol particles over Durban and Skukuza are, for the most part not hygroscopic in nature.
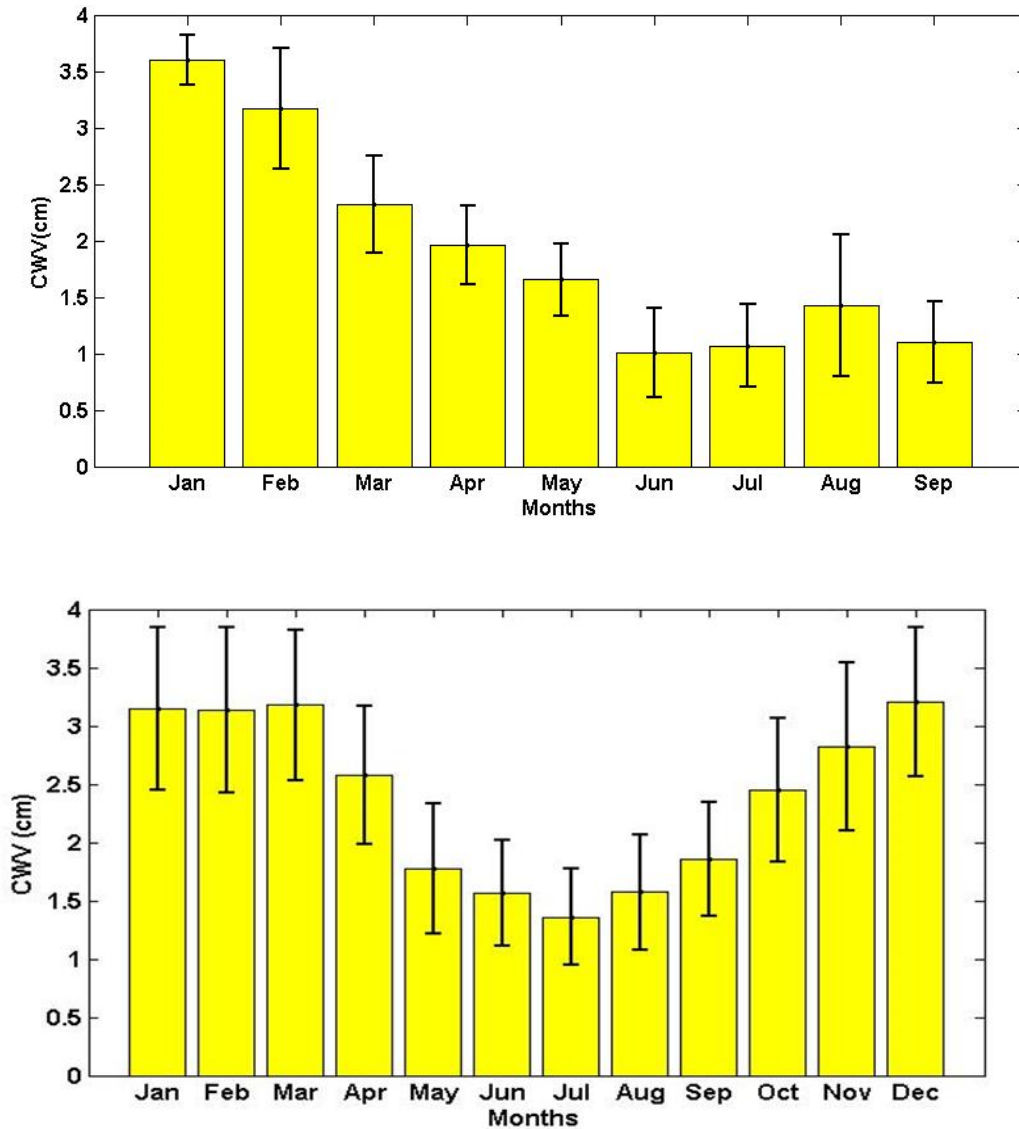
Figure 4.7 Frequency of Columnar Water Vapour (CWV) at (a) Durban from January to September 2014 and at (b) Skukuza from July 1998 to July 2011.

4.3.4 Seasonal frequency (%) distribution of AOD_{500}, CWV and $\alpha_{440-870}$ for Skukuza.

Figure 4.8 displays the percentage occurrences of AOD_{500}, CWV and $\alpha_{440-870}$ during each season for Skukuza. The seasonal frequency distribution could not be done for Durban due to the lack of data. The AOD, $\alpha_{440-870}$ and CWV were utilized from Skukuza from July 1998 to July 2011 to create the frequency distributions. The measurements for each parameter, amounted to 68000 observations for Skukuza. The seasonal frequency distribution was undertaken by determining the percentage of occurrences of the observations within each size bin. The frequency distribution was performed in order to depict whether the observations are high or low and where the observations are concentrated. It is able to show whether the data is

93

isolated mainly to one region or whether it is spread out across the entire scale. The frequency distribution illustrated how individual observations are distributed in a particular measurement scale (Manikandan, 2011).

From Figure 4.8 below, it can be noted that for Skukuza, AOD in spring has the widest probability distribution, ranging from 0.12 to 0.20, followed by winter which ranges from 0.15 to 1.00, then summer and autumn ranging from 0.10 to 0.80, and from 0.15 to 0.90 respectively. Summer, winter and spring has a modal value of 0.30, whilst autumn has a modal value of 0.25. The highest seasonal values recorded are <0.4, therefore, during most seasons >40% of observations have $AOD_{500} < 0.40$, which is favourable. Summer had the widest probability distribution for CWV, ranging from 0.80 to 5.40 cm, followed by autumn, ranging from 0.30 to 4.80 cm, than spring (0.50 to 4.50cm) and lastly winter (0.30 to 3.10cm). The modal value for summer is 3.30cm, followed by spring (2.10cm), autumn (1.90cm) and winter (1.55cm). For the $\alpha_{440-870}$, winter has the widest probability distribution with values ranging from –0.50 to 2.80, suggesting aerosols from many different sources during the winter months. Summer had the narrowest probability distribution for the $\alpha_{440-870}$ ranging from 0.50 to 2.50. With the exception of autumn, with a modal value of 1.00, summer, winter and spring have modal values of 1.50. Thus suggesting a greater abundance of coarse mode aerosols during autumn, than during the other seasons for Skukuza.
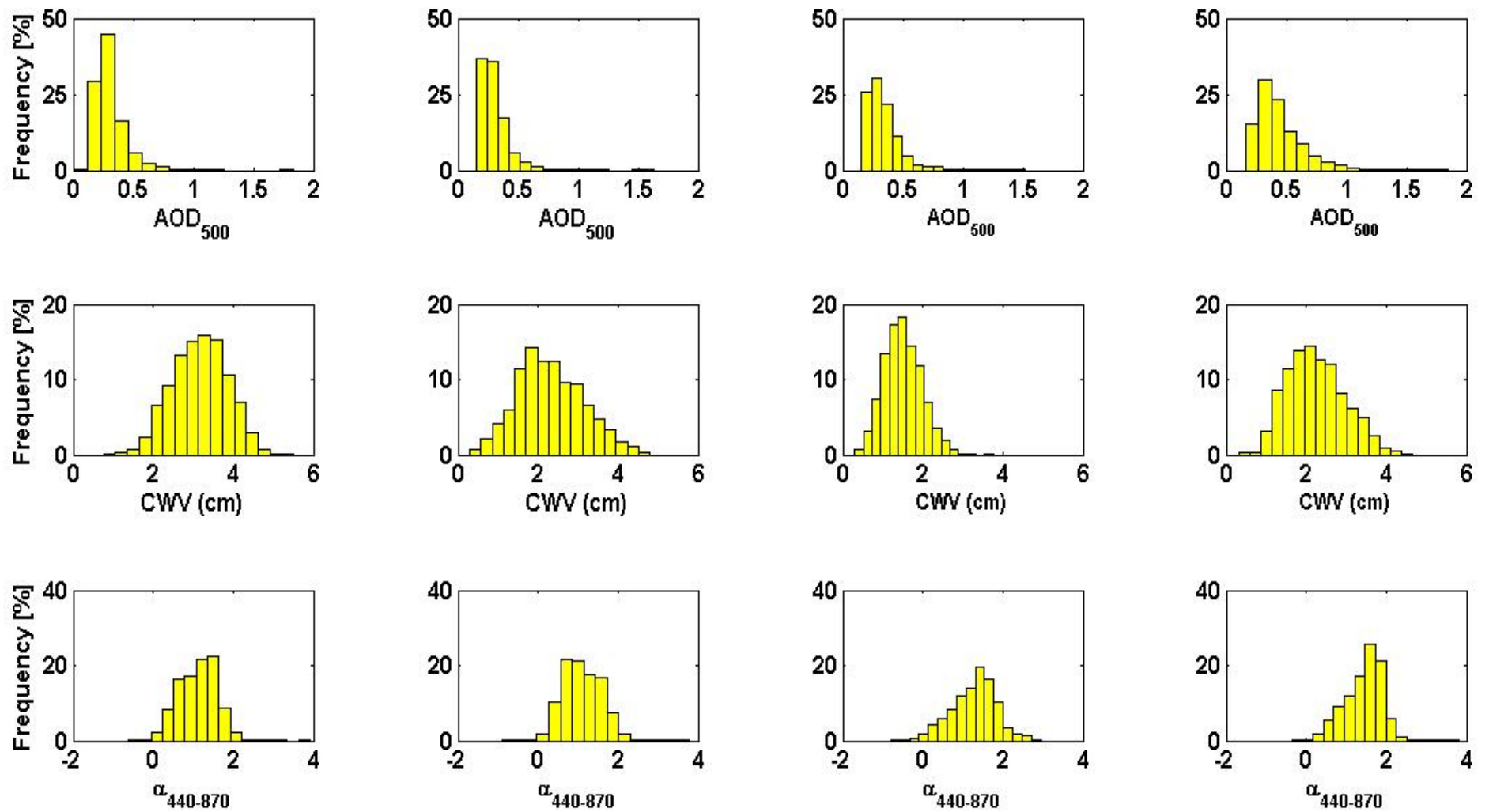
Figure 4.8 Seasonal frequency (%) distribution of AOD500, CWV and α440 − 870 from July 1998 to July 2011

4.4 HYSPLIT trajectory model

In order, to determine the origin of airmasses arriving in Durban, a 7–day back–trajectory Analysis was performed based on the NOAA HYSPLIT model using the GDAS as the meteorological input for the trajectory model. The transportation of aerosol plumes are important for understanding the radiative properties of aerosols in regions and therefore, it is important for climate change. The following section will detail the airmass transport in Durban using 7 day backward trajectories, on key aerosol loading days during the study period (January to September 2014).

Figure 4.9 (a) and (c) depict days with high AOD. It can be seen that for Figure 4.9 (c) (12 August), air mass parcels travel from surrounding arid/semi–arid regions before reaching Durban. The air mass parcels arrive from Mozambique and Botswana in the upper height region 1.5 km to 3 km, as well as northern, drier areas of South Africa (lower height regions). The high AOD values noted during August could be from biomass burning from these regions. Trajectories can also be seen to arrive from Madagascar, transporting maritime aerosols. Adesina, et al., (2014), used the HYSPLIT simulation analysis and also noted aerosols travelling from Mozambique and Madagascar to Pretoria during the biomass burning season. Furthermore, Sivakumar, et al., (2009), found air mass transport also arriving from Botswana and Mozambique to South Africa. Adesina, et al., (2015), also found air mass plumes from Madagascar impacting Gorongosa in Mozambique during the biomass burning season. For Figure 4.9 (a) (20 February), it is noted that air mass parcels from 1.5 km to 3 km travel from surrounding, north–eastern regions in South Africa, traveling a short distance, before reaching Durban. Since aerosols have short residence times, the closer they are to the source the greater the AOD noted, because the aerosols did not exit the plume as yet. Air mass parcels from the ground (0 km above sea level) travel long distances from the sea before reaching Durban. These trajectories probably contain course marine aerosols.

Figure 4.9 (b) and (d), show days in which low AOD values were noted. For Figure 4.9 (b) (5 June), air mass parcels at the surface recirculated within South Africa, and can be observed to come from north–western parts of the country, as well as from Botswana and Namibia. This could be due to the transport of soil and dust particles from these dry regions. Long range transport of air plumes can be observed to originate from Chile and Argentina in South America, travelling through pristine marine environment before eventually reaching the site

for both Figure 4.9 (b) and d (3 September). Therefore, course marine particles could dominate the atmosphere over Durban during June and September. The long range transport of air parcels across oceanic environments, results in lower AOD, due to drop out before reaching the measurement site (Adesina, et al., 2015).
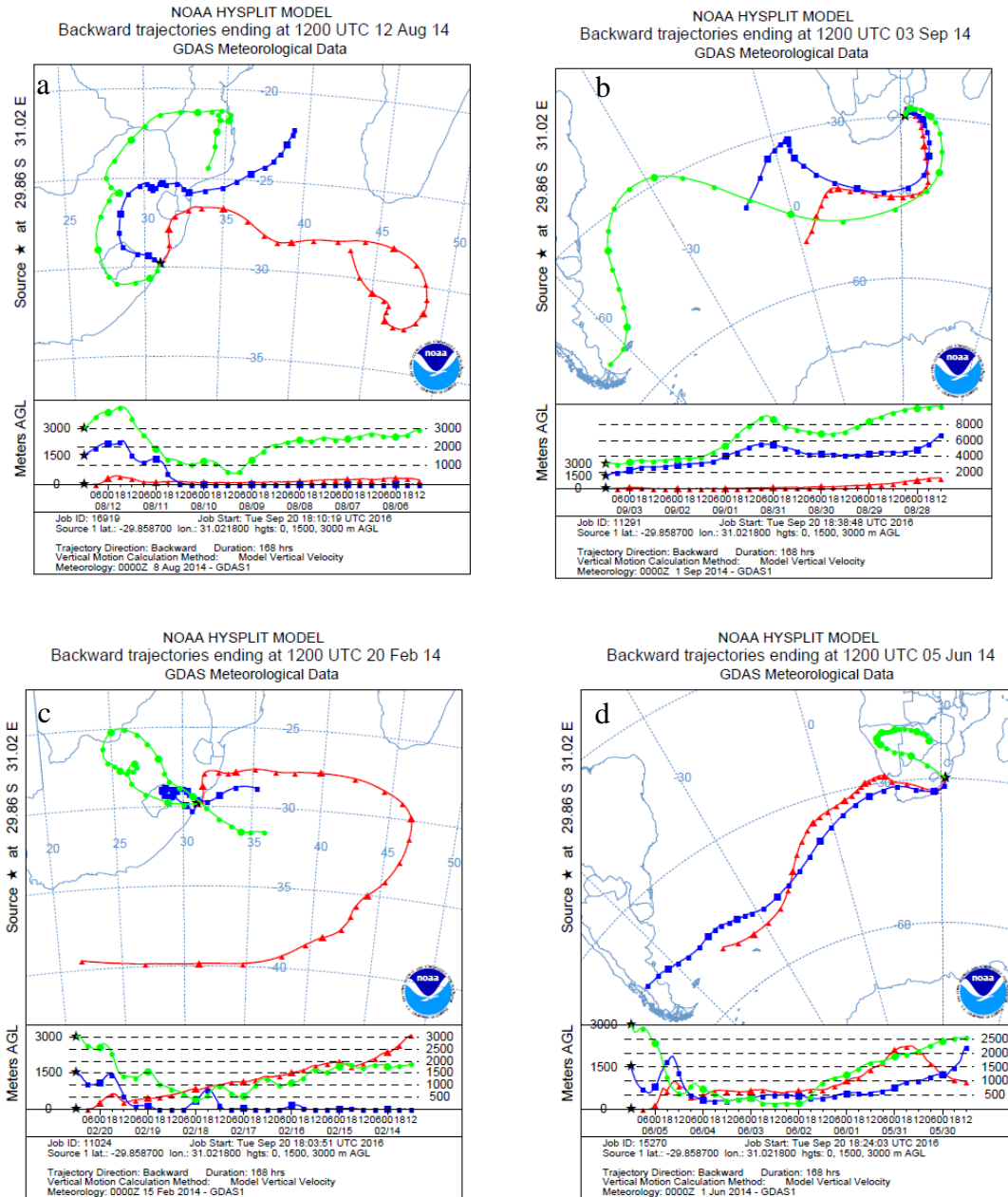
Figure 4.9 NOAA–HYSPLIT model run seven–day back trajectory analysis of airmass pathways at 0, 1.5 and 3 km altitudes on typical representative days during high AOD (a, c) and low AOD (b, d) from January to September 2014, over Durban

4.5 Variabilities in inversion algorithm aerosol optical properties for Durban and Skukuza.

The sun-photometer radiance measurements can be inverted to gain aerosol optical properties such as aerosol volume size distribution (VSD), single scattering albedo (SSA), Real (Re) and Imaginary (Im) parts of the complex refractive index and the asymmetry parameter (ASP). Sun-photometers are able to measure radiance at four or more wavelengths by using almucantar and principle plane measurements (AERONET, 2015). The almucantar scenario is used to measure radiance at azimuthal angles relative to the sun. The calculation of SSA requires the almucantar to not strictly take into account the aerosol vertical variations. The principle plane scenario measures radiance at scattering angles away from the sun. Radiance data, AOD calculations and the computation of land and water surface reflectance are inverted to estimate aerosol optical properties (AERONET, 2015). The development of inversion algorithms are focused on enhancing aerosol retrievals by including detailed statistical optimization of the impact of noise on the inversion procedure. The spectral radiances and various outlined constraints on the aerosol characteristic are considered as multi source data that are known with fixed accuracy. The algorithm allows for normal or log normal noise assumptions and the aerosols are modelled as homogenous spheres (Dubovik, et al., 2000).

4.5.1 Volume size distribution (VSD)

The aerosol VSD is important because the size of the aerosol particle impacts the climatic effects of the aerosol. In the present study, the AERONET VSDs (dV(r)/dlnr) gained from the sun-photometer are retrieved from spectral and sun radiance data using, with the following assumptions: $dV(r)/dlnr = 0.0001$, $n(\lambda i) = 1.50$, $k(\lambda i) = 0.005$, where dV/dlnr signifies aerosol volume size distribution, and $n(\lambda i)$ and $k(\lambda i)$ signify real and imaginary parts of the complex refractive index at a wavelength λi (Dubovik & King, 2000). The size distributions used by AERONET are obtained from the sun-photometer using 22 radius size bins, with sizes ranging from 0.05 to 15 μm. The VSD displays a bimodal log normal distribution due to being made up of two log–normal distributions. The equation, by Dubovik and King (2000), is given by:

$$\frac{dV(r)}{dlnr} = \sum_{i=1}^{2} \frac{C_{v,i}}{\sqrt{2\pi}\sigma_i} \exp[-\frac{(lnr - lnr_{v,i})^2}{2\sigma_i^2}]$$

Where σ_i is the standard deviation, $r_{v,i}$ is the volume median radius and $C_{v,i}$ is the volume concentration for the fine and coarse mode. The size bins were plotted against the differential equation in Figure 4.9 below to determine the size distribution. The graph underwent a log

transformation, in order to adequately display the log normal distribution. The observations from each size distribution amounted to 275 point observations from Durban and the 3621 point observations from Skukuza. The observation for each size bin was averaged for all the season for Skukuza and during autumn and winter for Durban. This was due to observations for VSD being limited to only the months of autumn and winter for Durban.
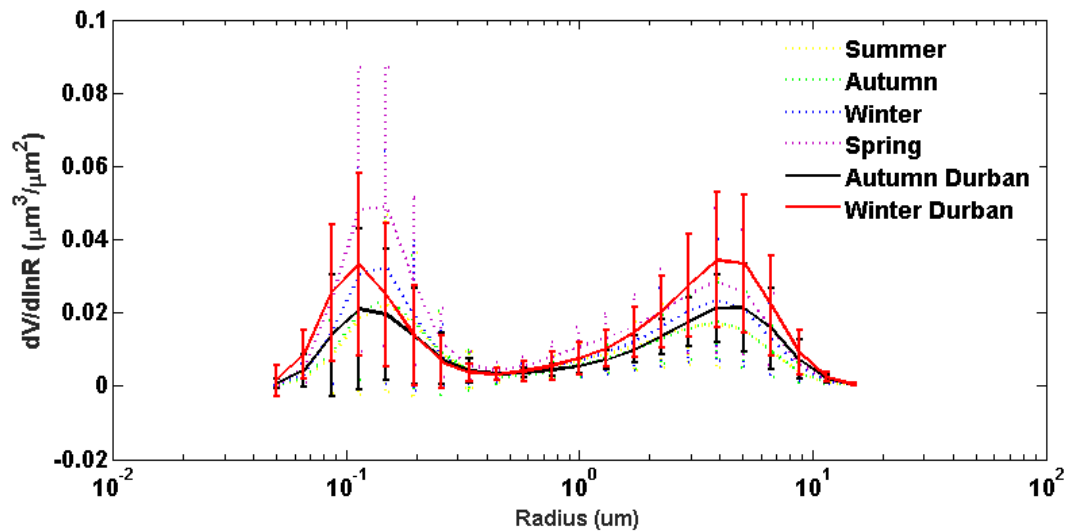
Figure 4.10 Seasonal variations with standard deviations of aerosol volume size distributions derived from sky radiance as a function of particle radiance for Durban during for autumn and winter of 2014 and for Skukuza for all the seasons (summer, autumn, winter, spring) obtained from July 1998 to July 2011.

The seasonal average volume size distribution (VSD) (dV(r)/dlnr) is depicted in Figure 4.9 for Durban, for the autumn and winter season from January to September 2014, and all seasons for Skukuza from July 1998 to July 2011. The graph shows a bimodal lognormal distribution. A radius of 0.11 μm prevails in the fine mode fraction, whereas in the course mode a radius of 4 μm prevails. From Figure 4.9 it can be observed that for Durban, the VSD for both the fine and course mode are highest during the winter months than during the autumn months. The higher values depicted during the winter season, especially the month of August is likely due to stable meteorological conditions, hindering dispersion of aerosols. For Durban, the VSDs for autumn and winter, appears to share similar peaks in both the fine and coarse modes. The coarse mode fraction aerosol loads in Durban could be due to an agglomeration of sulphur particles on the surface of dust nuclei within the aerosol plume exiting the eastern coast of Southern Africa (Piketh, et al., 1999).

For Skukuza there appears to be slightly greater VSDs in the fine mode than in the coarse mode, which suggests an increase in aerosol particles of anthropogenic origin. Furthermore, the lifetime of different particle sizes governs the development of the size distribution and as the particles move downwind, larger particles fall out more quickly hence greater VSDs are noted in the fine mode. Atmospheric aerosol loads are dominated primarily by fine mode particle size throughout the year, indicating, that the fine mode particles are not only limited to biomass burning aerosols but also due to fossil fuel combustion originated from the South African Highveld (Queface, et al., 2011). The VSDs for Skukuza in the fine mode are highest in the spring, followed by the winter autumn and summer. The higher values depicted during spring, is due to, the high amount of aerosols released due to biomass burning activities (Kumar, et al., 2013; Tesfaye, et al., 2011). The smaller distribution during autumn (for both Durban and Skukuza) and summer could be due to cloud scavenging and rain out processes and the higher distribution during winter (for both Durban and Skukuza) could be due to a lack of cloud scavenging and rainout processes, as well as aerosols generated from many different sources (Kumar, et al., 2014a). The high VSD noticed for the course mode aerosols during spring in Skukuza, could be the result of high convective activity and strong surface winds which cause a loosening of soil and dust particles causing their entrainment into the atmosphere. Also, long range transport of desert dust aerosols could also be the reason for an increase in the VSD during spring for the coarse mode fraction. The VSDs for Skukuza, are higher in the fine mode than in the coarse mode for all seasons, even outside of the biomass burning season. Besides that, the varying and diverse aerosol VSD over Skukuza, suggests that aerosol content above Skukuza is quite diverse. A reason for this is that the atmospheric circulation above the site is affected by Aeolian dust, industrial aerosols from the South African Highveld, maritime and biomass burning aerosols as well as fluctuating weather conditions (Freiman and Piketh, 2002; Queface, et al., 2011). A reason for the low VSD for Skukuza during summer could be an increase in rainfall during the summer months. Hyvarinen et al., (2011), found that during the summer monsoon rains in Gual Pahari, India, there is a decrease in the VSD of aerosols during the summer. This was attributed to rain scavenging and activation to cloud and mountain fog droplets, however the scavenging by rain is least effective for accumulation mode particles (Hyvärinen, et al., 2011).

4.5.1.1 The parameters of the size distribution

The parameters of the size distribution were retrieved from AERONET for the sun-photometer from Durban (from January to September 2014) and from Skukuza (from July 1998 to July

2011). The parameters considered are volume geometric mean radius for fine aerosols (R_f) and for coarse aerosols (R_c), the volume concentration for the fine mode fraction aerosol (V_f) and for the coarse mode fraction (V_c), the effective radius for the fine mode ($R_{eff(f)}$) and the coarse mode ($R_{eff(c)}$) and the geometric standard deviations for the fine mode (σ_f) and the coarse mode (σ_c). The observations of each parameter amounted to 275 point observations from Durban and the 3621 point observations from Skukuza. The means and standard deviations of these parameters were calculated and are shown in Table 4.2 (for the fine mode) and Table 4.3 (for the coarse mode), for both Durban and Skukuza. The parameters were tabulated, in order to display the values of the fine and coarse mode fraction in an efficient way.

Table 4.2 and Table 4.3 below, depicts the parameters of the bimodal lognormal volume size distribution, in the fine mode and course mode, respectively for Durban from March to August 2014 and for Skukuza from July 1998 to July 2011. Both tables depict the monthly mean and standard deviations of each parameter. The means and standard deviations appear quite close to each for Durban, due to a lack of data during the time period. For Durban the volume geometric mean radius for fine aerosols (R_f) ranged from 0.127±0.015 μm in June to 0.182±0.029 μm in March, whereas for Skukuza, values ranged from 0.144±0.015 in September 0.173±0.021 μm in February (Table 4.2.1). For Skukuza, for the summer and autumn months the R_f ranged from 0.144±0.015 to 0.173±0.021 μm, and for winter and spring, the radii ranged from 0.143 to 0.150 μm. For Durban, the R_f for autumn was between 0.141 to 0.182 μm and for winter it was between 0.127 to 0.148 μm. The lower values noted during winter than during autumn for the R_f for both Durban and Skukuza was also reported by Adesina et al., (2014), on their study over Pretoria. For Durban the R_c values range from 2.960±0.300 in September to 3.229±0.260 in March, whereas for Skukuza R_c values ranged from 2.454±0.319 in January to 2.865±0.332 in May. The R_c values for Durban for March to September are greater than the averages noted for Skukuza during the same months. For Durban, the volume concentration for the fine mode fraction aerosol (V_f) increased from March to August, the almost V_f doubled from July 0.034±0.023 to August 0.056±0.029 and the volume concentration for the coarse mode fraction (V_c) also increased during August (0.066±0.033), which coincided with the increase in AOD during the month of August. For Skukuza the V_f and V_c were highest from August to October and for Durban high values were noted during August, coinciding with the biomass burning season, as well as the months with the highest AOD. Eck, et al., (2003) found that for Mongu in Zambia, fine mode aerosols increased during the months of high AOD. The fine mode radius usually increases due to aging

processes such as coagulation, condensation and gas–to–particle conversion, thus resulting in fine mode particle growth as AOD increases (Eck, et al., 2003). Queface, et al., (2003), also found that the retrieved aerosol volume size distribution over Inhanca Island depicted high levels of AOD with fine particle sizes and coarse mode particles dominating when AOD is low. This contrasted with the current study, because both fine and coarse aerosols increased during August, which had high aerosol loads. This means that biomass burning is not the only contributor to aerosol loads in both regions during the biomass burning season, coarser particles could also contribute. These particles could be from windblown dust, since the biomass burning season also coincides with high wind speeds (Table 4.1) as well as due to marine aerosol species.

Table 4–2 Mean and standard deviations (given in brackets) of the monthly measurements of derived aerosol volume size distribution in the fine mode over Skukuza from July 1998 to July 2011 and over Durban from March to September 2014.

Month	Fine–mode							
	V_f		$R_{eff(f)}$		R_f		σ_f	
	Skukuza	Durban	Skukuza	Durban	Skukuza	Durban	Skukuza	Durban
January	0.017 (0.015)		0.148 (0.020)		0.160 (0.024)		0.432(0.054)	
February	0.017(0.011)		0.158(0.019)		0.173(0.021)		0.430(0.044)	
March	0.019(0.015)	0.022 (0.017)	0.148(0.025)	0.157(0.02)	0.162(0.029)	0.182(0.029)	0.420(0.053)	0.562(0.084)
April	0.023(0.018)	0.008(0.000)	0.152(0.020)	0.126(0.01)	0.167(0.023)	0.143(0.007)	0.413(0.048)	0.523(0.023)
May	0.021(0.0114)	0.027(0.021)	0.141(0.020)	0.128(0.01)	0.152(0.023)	0.141(0.015)	0.394(0.045)	0.444(0.050)
June	0.019(0.014)	0.028(0.018)	0.138(0.018)	0.115(0.01)	0.150(0.022)	0.127(0.015)	0.417(0.053)	0.462(0.071)
July	0.023(0.016)	0.034(0.023)	0.133(0.014)	0.117(0.01)	0.143(0.016)	0.128(0.009)	0.394(0.046)	0.430(0.053)
August	0.036(0.026)	0.056(0.029)	0.136(0.014)	0.136(0.02)	0.146(0.016)	0.148(0.022)	0.391(0.039)	0.412(0.036)
September	0.046(0.027)	0.019(0.00)	0.133(0.011)	0.118(0.01)	0.143(0.013)	0.130(0.013)	0.387(0.036)	0.452(0.035)
October	0.047(0.027)		0.133(0.013)		0.144(0.015)		0.399(0.051)	
November	0.025(0.017)		0.136(0.015)		0.147(0.018)		0.410(0.046)	
December	0.021(0.014)		0.142(0.016)		0.154(0.018)		0.412(0.047)	

Table 4–3 Mean and standard deviations (given in brackets) of the derived aerosol volume size distribution in the coarse mode over Skukuza from July 1998 to July 2011 and over Durban from March to September 2014

Month	Cosrse–mode							
	V_c		$R_{eff(c)}$		R_c		σ_c	
	Skukuza	Durban	Skukuza	Durban	Skukuza	Durban	Skukuza	Durban
January	0.027(0.012)		1.906(0.270)		2.454(0.319)		0.699(0.051)	
February	0.023(0.011)		2.009(0.304)		2.579(0.366)		0.691(0.050)	
March	0.025(0.010)	0.036(0.011)	2.002(0.296)	2.502(0.327)	2.565(0.336)	3.229(0.260)	0.692(0.051)	0.691(0.081)
April	0.024(0.009)	0.037(0.021)	2.107(0.302)	2.375(0.223)	2.690(0.333)	3.196(0.250)	0.684(0.053)	0.718(0.036)
May	0.029(0.014)	0.035(0.016)	2.237(0.297)	2.295(0.300)	2.865(0.332)	3.027(0.350)	0.678(0.046)	0.711(0.045)
June	0.026(0.013)	0.049(0.027)	2.146(0.315)	2.419(0.308)	2.791(0.383)	3.131(0.320)	0.700(0.041)	0.684(0.054)
July	0.034(0.017)	0.054(0.024)	2.173(0.265)	2.484(0.232)	2.815(0.311)	3.189(0.270)	0.692(0.043)	0.665(0.037)
August	0.043(0.020)	0.066(0.033)	2.180(0.301)	2.488(0.213)	2.830(0.351)	3.222(0.280)	0.700(0.049)	0.678(0.043)
September	0.048(0.022)	0.049(0.027)	2.076(0.282)	2.227(0.270)	2.746(0.341)	2.960(0.300)	0.725(0.058)	0.718(0.050)
October	0.047(0.019)		1.971(0.287)		2.581(0.351)		0.719(0.055)	
November	0.034(0.015)		1.915(0.242)		2.512(0.313)		0.721(0.045)	
December	0.033(0.015)		2.018(0.274)		2.606(0.305)		0.701(0.055)	

4.5.2 The single scattering albedo (SSA)

The SSA is given by the ratio of scattering efficiency to the total extinction efficiency. SSA depends on aerosol composition and size distribution. It is zero for pure absorbing aerosols and one for pure scattering aerosols. The SSA is measured at different wavelengths, namely, 400 nm, 675 nm, 870 nm and 1018 nm (Smirnov, et al., 2002). The observations of SSA amounted to 22 observations for Durban for the period of January to September 2014, and 556 observations for Skukuza from July 1998 to July 2011, for each of the different wavelengths. The values of SSA were averaged for each season and each wavelength for Skukuza, and for each wavelength and only winter for Durban. This was because the measurements of SSA were isolated to only the winter season for Durban. The averaged SSA and standard deviations at the different wavelengths, for the different seasons were plotted as a line graph and displayed in Figure 4.10 below.
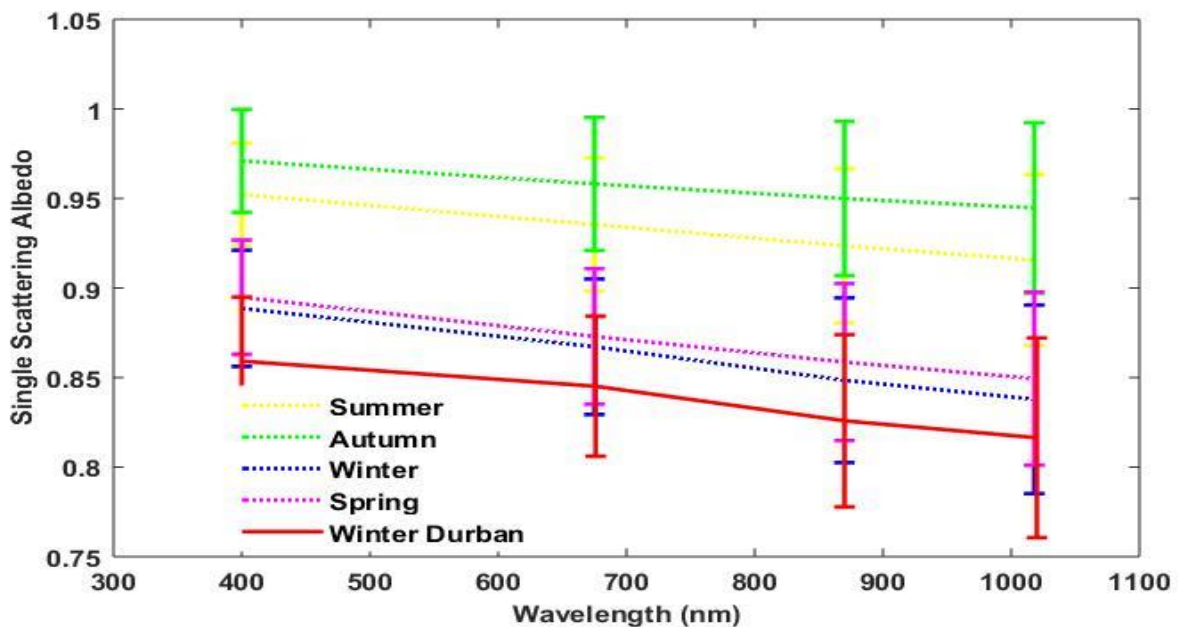
Figure 4.11 Spectral variation of single scattering albedo (SSA) for Durban for winter of 2014 and for all seasons for Skukuza from July 1998 to July 2011

From Figure 4.11, it can be noted that SSA decreases with an increase in wavelength; therefore, it has a spectral dependence. The SSA value is important because it is a measure of the degree of scattering for a particular aerosol. SSA values that are close to 1 represent aerosols that are scattering in nature. From Figure 4.10 it is observed that the mean value of SSA at 400 nm is <0.90 for winter and spring for Skukuza, whereas for summer and autumn, the values are >0.95. For Durban winter, the value is also below 0.90. This was similar to a study which was

conducted by Magi, et al., (2003) using sun photometry and a series of airborne profiles of light scattering, light absorption and SSA to determine scattering efficiency. In their study, Magi, et al., (2003) reported that during spring due to heavy smoke emissions, the mean value of SSA shifted from 0.90±0.03 before the period, to 0.83±0.02 after the period (Magi, et al., 2003). The lower SSA values noted for winter for both Durban and Skukuza could be the result of increased wood burning occurring for heating and cooking purposes due to the cold winter conditions (Hersey, et al., 2015). Winter is regarded as the onset of the biomass burning season (in August) and during spring (September) the fire season is most intensified in southern Africa. Thus causing an increase in the presence of carbonaceous absorbing type aerosols during these seasons.

The increase in wind speeds noted from July to August coupled with an increase in precipitation during September and October result in the formation of windblown dust particles which are large and highly absorbing thereby contributing to aerosol loads in Durban (Hersey, et al., 2015). Therefore, during winter, for Durban, there existed mixed aerosol loads, from dust, urban industrial activities and biomass burning processes. The SSA is shown to be greater than 0.9 for all wavelengths during autumn and summer for Skukuza. This is characteristic of scattering aerosols, which are usually anthropogenic in origin, coming from urban, industrial sources. Additionally, scattering aerosols could also come from maritime aerosols generated on the coast and transported to Skukuza by wind (Kumar, et al., 2013). There exist high humidity during the summer and autumn months, which aids with the growth of aerosols and makes it more scattering in nature, irrespective of chemical composition thus resulting in enhanced SSA during these months (Latha, et al., 2014). The high SSA values noted during summer in Skukuza could be due to an increase in industrial sulphur during summer. This occurs due to oxidation of discharged SO_2 in the moist summer atmosphere (Piketh, et al., 1999).

4.5.3 Aerosol Asymmetry Parameter (ASP)

The aerosol ASP (g) is a measure of the preferred scattering direction (forward or backward) for the light that reaches the aerosol. The value of g ranges from –1 for light that is completely back scattered to +1 for completely forward scattered light. The ASP and SSA are spectrally dependent variables (Adesina, et al., 2014). The ASP is measured at different wavelengths, 439 nm, 676 nm, 870 nm and 1020 nm. The observations of ASP amounted to 275 observations for Durban from January to September 2014, and 3621 observations for Skukuza from July 1998

to July 2011, for each of the different wavelengths. The values of ASP were averaged for each season and each wavelength for Skukuza, and for each wavelength and only winter for Durban. This was because the measurements of ASP were isolated to primarily the winter season for Durban. The averaged ASP and standard deviations at the different wavelengths, for the different seasons were plotted as a line graph and displayed in Figure 4.12 below.


Figure 4.12 Spectral variation of the Asymmetry parameter (ASP) for the winter months, for Durban from January to September 2014 and for Skukuza from July 1998 to July 2011 for all seasons

Figure 4.12, depicts the spectral variation of ASP (g) for Durban and Skukuza. For Durban, only the winter months were depicted, whereas for Skukuza seasonal trends where represented. The g values tend to decrease with an increase in wavelength, similarly to the SSA. From Figure 4.12, it can be seen that g values tend to decrease in the visible spectral region and increase gradually in the near infrared region. The value of g ranges from –1 for light that is completely back scattered to +1 for completely forward scattered light. The ASP values are wavelength dependent and the absolute value of the ASP is dependent on location or air mass type (Fiebig & Ogren, 2006). This is due to the wide range of particle sizes that are required for calculating g at a specific wavelength (λ) and it is given as a range of size parameter x =πDp/ λ. At longer wavelengths, the relevant size ranges moves to larger particle diameters, meaning, the same size distribution of particles seems to be decreasing in size, when illuminated with light of a larger wavelength. The smaller the particles appear to be, the greater the scattering maximum in the forward direction decreases in intensity and the more g decreases (Fiebig & Ogren, 2006). Therefore, the low g values reflected for winter (for Durban) and for spring (for

Skukuza) suggest a greater abundance of fine anthropogenic (absorbing) pollutants. The lower g values during spring is characteristic of biomass burning aerosol, considerably lower g values have been reported for smoke aerosol. Ross, et al., (1998), found g values of 0.54 for biomass burning in Brazil and Wong and Li (2002) found values of g to be 0.4 for boreal forest fire events (Ross, et al., 1998; Wong & Li, 2002).

Additionally, from Figure 4.12 it can be noted that the wavelength dependence decreases as the radii gets bigger, this is due to the presence of two modes in the particle size distribution. Both modes are required for calculating g and this explains the decrease in spectral dependence. From Figure 4.12, it can be observed that a higher value of g was calculated for summer and autumn (for Skukuza), this means that there is increase scattering in the forward direction resulting in dominance of course mode particles during these seasons. The dominance of course mode particles during summer and autumn, could be the result of increase in wind speeds, dislodging and entraining aerosol particles. Additionally, the slightly high g values observed during summer could be long range transport of Saharan dust aerosol. This is supported by Formenti, et al. (2000) who have reported g values (0.72 to 0.73) for Saharan dust aerosol measured during the ACE–2 program.

4.5.4 Complex index of refraction

The complex index of refraction consists of real (Re) and imaginary (Im) parts of the refractive index. The real and imaginary parts of the complex refractive index are representative of the potential of scattering and absorption of incoming solar radiation. The higher the real part values suggests a greater concentration of scattering aerosol types and the higher imaginary values suggests absorbing aerosol types. The refractive index is measured at different wavelengths, 441 nm, 675 nm, 870 nm and 1010 nm. The observations of the refractive index amounted to 22 observations for Durban from January to September 2014, and 556 observations for Skukuza from July 1998 to July 2011, for each of the different wavelengths. The values of the refractive index for the real part and imaginary part were averaged for each season and each wavelength for Skukuza, and for each wavelength and only winter for Durban. This was because the measurements of the refractive index occurred mainly during the winter season for Durban. The averaged refractive index and standard deviations at the different wavelengths, for the different seasons were plotted as a line graph and displayed in Figure 4.13 for the real part (a) and the imaginary part (b).
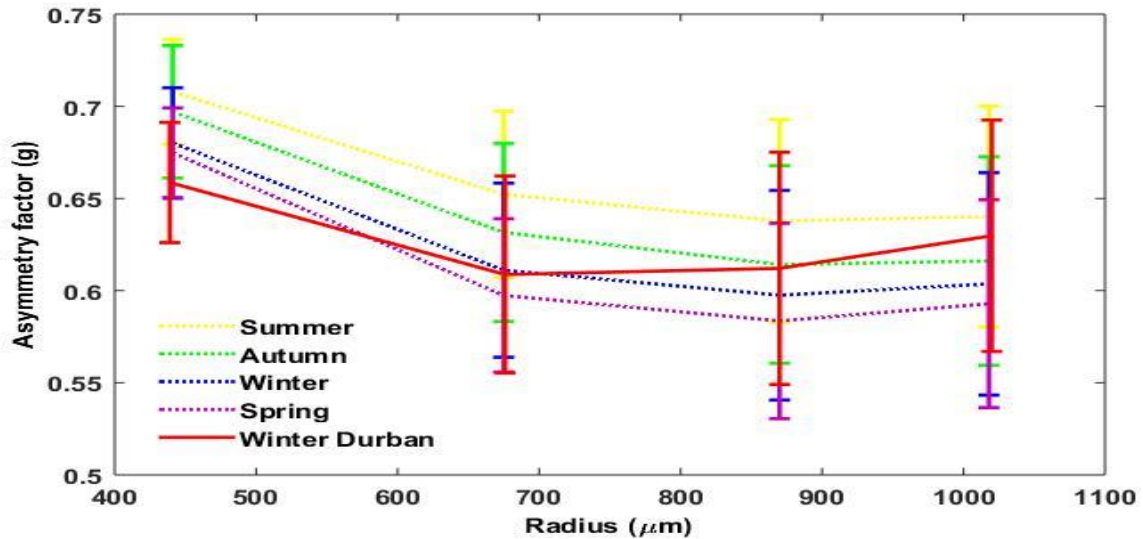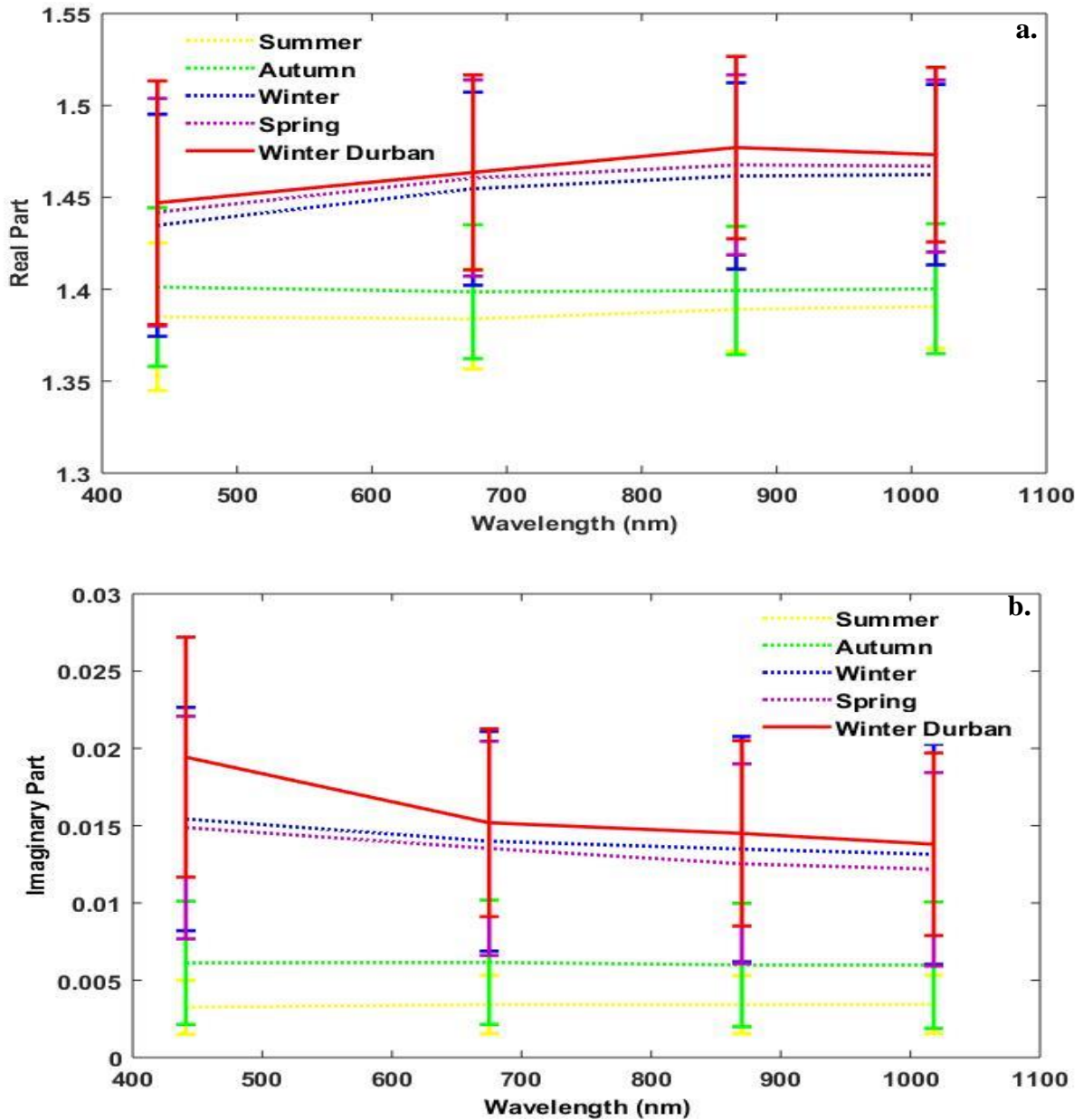
Figure 4.13 Spectral variation of the complex refractive index (a) real part and (b) imaginary part the winter months, for Durban from January to September 2014 and for Skukuza from July 1998 to July 2011 for all seasons

Following Dubovik et al., (2000), the complex index retrieval can only be obtained for aerosol optical thickness greater than 0.4 at 440 nm and has an absolute error of 0.04 for the real part and a relative uncertainty of approximately 30% for the imaginary part. Optical thickness observed over Durban (winter) and over Skukuza (during all seasons), is generally less than 0.4. The real part of derived complex refractive index generally decreased with increasing wavelength whilst the imaginary part tended to increase with increasing wavelength. These

occurrence can be explained by the physical mechanism of interaction between light and aerosols (Zhang, et al., 2013).

According to Dubovik et al., (2002), the real and imaginary part of urban aerosols has a range of values of 1.40 to 1.47 and 0.009 to 0.14, respectively and for biomass burning, the real and imaginary parts have values from 1.47 to 1.52 and 0.009 to 0.02, respectively (Dubovik, et al., 2002). For Durban during the winter season, the complex refractive index ranges from 1.45 to 1.47 and from 0.01 to 0.02, for the real and imaginary parts, respectively (see Figure 4.13). Therefore, for the real and imaginary part for Durban winter is consistent with values expected for urban industrial aerosols. The imaginary part for Durban winter is also consistent with values expected for biomass burning aerosols, thus indicative of mixed aerosol loads for Durban. During the winter for Skukuza, values range from 1.44 to 1.46 (real part) and from 0.014 to 0.015 (imaginary part) also indicative of urban aerosol presence and biomass burning aerosol loads. For Skukuza during summer, values range from 1.38 to 1.39 and around 1.4 for autumn (real) and values were around 0.003 (summer) and 0.006 (autumn) for all wavelengths. Therefore the low imaginary part values for autumn and summer and high SSA values, suggest non–absorbing aerosol types for summer and autumn in Skukuza which are consistent with urban industrial aerosols and the imaginary values are consistent with both biomass burning and urban industrial aerosols (Zhang, et al., 2013). The low imaginary type values are also associated with dust aerosol types (Wagner, et al., 2012), together with the lower $\alpha_{440–870}$ values noted for summer could attest to the presence of coarser, dust and maritime aerosol presence during summer. During summer in Skukuza, the low AOD could be the result of cloud scavenging and wet removal processes as well as low wind speed and low water vapour which cause weak generation mechanisms and a decreased chance of hygroscopic growth of aerosols, therefore explaining the low real part values for summer and autumn (Tesfaye, et al., 2011). For spring, Skukuza illustrates real values ranged from 1.46 to 1.47 and the imaginary values ranged from 0.012 to 0.014. The values are indicative of mixed aerosol loads, from both urban industrial and biomass burning type aerosols. The different seasons show different aerosol types dominating over Skukuza, which is consistent with Kumar et al., (2013) and have attributed to biomass burning and urban industrial aerosol types to be the major source of aerosols in Skukuza.

4.5.5 Aerosol Radiative Forcing

Table 4.4 depicts the monthly averages of radiative forcing (RF), forcing efficiency (FE) at the top and bottom of the atmosphere and the total aerosol radiative forcing (ARF) (bottom minus top) from July 1998 to July 2011 for Skukuza and from March to September 2014 for Durban. In order to calculate the mean and standard deviations for Durban, 275 point observations were used and for Skukuza, 3621 observations point observations were used. Due to the lack of monthly data points the standard deviations for Durban are quite large. A table was used to easily display the average radiative forcing values together with their standard deviations.

Table 4.5 depicts the SSA_{676}, ASP_{676} (g), $AE_{440-675}$ and the AOD_{675} for Durban and Skukuza for the same time period. For Durban, the radiative forcing values for the TOA for March and April are positive and therefore displays a net warming, whereas the values from May to September are negative thus indicating a net cooling effect. For Durban, the TOA (reflected to space) value ranges from -14.930 ± 9.418 W/m^2 in August to 0.904 ± 9.553 W/m^2 in March. The BOA (surface forcing) ranges from -27.178 ± 14.687 W/m^2 in April to -70.056 ± 25.282 W/m^2 in August. For Skukuza, it can be observed that the monthly mean RF for all months are negative, thus suggesting a net cooling. The TOA values for Skukuza ranged from -5.492 ± 5.001 W/m^2 in February to -15.451 ± 7.482 W/m^2 in October and the BOA values ranged from -22.398 ± 12.841 W/m^2 in January to -56.753 ± 29.554 W/m^2 in September.

The resultant atmospheric forcing (ARF) for Durban, ranged from 26.330 in April to 55.120 in August and for Skukuza the ARF ranged from 15.458 in January to 41.426 in September, thus indicating a warming effect. For Durban, the AOD was highest during the month of August (0.172 ± 0.104) and August also displayed greater surface cooling values. The SSA values in the winter months are <0.9, thus indicative of both absorbing and scattering type aerosols, however, the slight increase in SSA from July to August indicates an increase in scattering type aerosols in August. The increase in the $\alpha_{440-870}$ from June to September, indicates an increase in the amount of fine mode particles, which are characteristic of urban industrial and biomass burning aerosol types. It indicates that there is an increase in fine, industrial and biomass burning pollutants during August for Durban, probably due to the relatively stable weather conditions noted during winter.

For Skukuza, August (0.160 ± 0.118), September (0.200 ± 0.120) and October (0.190 ± 0.100) had the highest AOD values, also, the SSA values where <0.9, from July to October and the $\alpha_{440-870}$ increased from August to October thus alluding to absorbing aerosol presence. This also

corresponded to the highest ARF values, therefore, significant heating of the atmosphere occurs from August to October. The heating from August to October, is the result of the biomass burning season, increasing the amount of absorbing (heating) type aerosols in the atmosphere.

For Durban, during March and April the forcing efficiency at the bottom of the atmosphere is quite large which is common for absorbing aerosol types. The positive radiative forcing values at the TOA suggests the existence of absorbing aerosol pollutants because absorbing aerosols supplement the warming caused by greenhouse gases. Additionally, the low AOD values noted could be due to washout processes, as absorbing aerosols such as black carbon (BC) are lower during the rainfall months (Gadhavi & Jayaraman, 2010).

Furthermore, soot aerosols (BC) are produced when incomplete combustion occurs such as from diesel engines, forest fires and biomass burning. The absorption properties of soot particles are highly dependent on the combustion temperature and the other materials emitted during the combustion process (Gadhavi & Jayaraman, 2010). Therefore, although the results show that there are absorbing pollutants during March and April and during September, there exist variations within the type of absorbing pollutants that occur during these months and the spectral dependence of the aerosol absorption coefficient. Aerosols released from biomass burning have a greater likelihood to decrease the radiative forcing at the TOA, therefore, since September is the biomass burning season, it has a net cooling effect at the TOA. Absorbing pollutants that are released from fossil fuel burning have more of a warming effect, increasing radiative forcing, hence, the net warming effect observed for March and April at the TOA (Gadhavi & Jayaraman, 2010).

The forcing efficiency at the TOA for Durban ranges from -63.572 ± 6.339 W/m^2 in July to 22.284 ± 68.351 W/m^2 in March and the forcing efficiency at the BOA ranges from -388.928 ± 176.382 W/m^2 in March to -245.0454 ± 2.965 W/m^2 in July. For Skukuza the forcing efficiency at the TOA ranges from -73.669 ± 22.035 W/m^2 in May to -58.723 ± 29.045 W/m^2 February. The FE at the BOA ranges from -234.093 ± 45.643 in June to -207.30 ± 62.417 in April. For Skukuza, the higher negative values of FE were associated with the lowest AOD range (AOD for May and June 0.089 and 0.094, respectively). This is similar to Garcia, et al., (2012), where high negative FE values were observed for months with low AOD for free tropospheric aerosols. For, aerosols at the surface, the aerosols more efficient at the surface are absorbing aerosols such as biomass burning aerosols, therefore, this could be a reason for the high negative forcing efficiency noticed in Skukuza for the BOA.

At the TOA, the seasons with more absorbing aerosols show negative FE values that are not as high in value as other seasons. This is due to the higher absorption of these aerosols at the surface, which reduces the energy available to be backscattered towards the upper limit of the atmosphere and into space (Garcia , et al., 2012). Therefore, FE at the TOA for the spring months for Skukuza displays lower negative values of FE. Furthermore, in the African savannah, most of the biomass burning particles are produced by flaming combustion and 15 to 20% of the aerosol generated during the flaming combustion period is black carbon, thus reducing efficiency at the TOA and increasing it at the BOA (Garcia , et al., 2012). The high negative values of forcing efficiency at the TOA, is also indicative of scattering type aerosol (Yoon, et al., 2005). For Skukuza, the high negative FE values at the TOA, corresponded to December and January and April and May. December and January displayed the high SSA values 0.973 ± 0.02 and 0.953 ± 0.04, with relatively low $\alpha_{440-870}$ values (<1.5), therefore, indicative of coarser, scattering aerosol particles such as dust particles and marine aerosols.

Table 4–4 Comparison of monthly mean aerosol radiative forcing (ARF) at the surface (BOA) and top of the atmosphere

Month	Radiative Forcing (W/m²)				Forcing efficiency (W/m²)				ARF	
	Skukuza		Durban		Skukuza		Durban		Skukuza	Durban
	TOA	BOA	TOA	BOA	TOA	BOA	TOA	BOA	ARF	ARF
January	–6.940(65.080)	–22.398(12.841)			–69.680(27.868)	–216.833(63.309)			15.458	
February	–5.492(5.001)	–22.992(16.674)			–58.723(29.045)	–220.297(73.150)			17.500	
March	–7.709(5.300)	–24.068(12.609)	0.904(9.553)	–54.793(22.538)	–65.113(24.901)	–215.701(67.073)	22.284(68.351)	–388.928(176.382)	16.978	53.890
April	–8.545(6.110)	–24.332(14.572)	0.852(4.085)	–27.178(14.687)	–69.687(24.472)	–207.360(62.417)	6.204(50.372)	–375.285(132.400)	15.787	26.330
May	–8.148(4.530)	–25.012(13.135)	–5.377(5.809)	–40.903(19.970)	–73.669(22.035)	–214.495(52.704)	–36.060(39.754)	–303.227(103.022)	16.864	35.530
June	–7.515(4.780)	–26.617(14.120)	–8.156(4.726)	–37.775(16.527)	–65.433(19.919)	–234.093(45.643)	–58.109(23.294)	–266.862(37.815)	19.102	29.620
July	–8.556(5.226)	–31.162(17.084)	–10.308(4.771)	–41.632(21.835)	–63.991(18.595)	–233.713(47.696)	–63.572(16.339)	–245.045(42.965)	22.606	31.320
August	–12.949(6.840)	–46.761(32.920)	–14.930(9.418)	–70.056(25.282)	–66.636(18.582)	–210.289(38.309)	–46.837(29.020)	–249.327(82.643)	33.812	55.120
September	–15.327(7.040)	–56.753(29.554)	–5.902(6.110)	–33.873(15.949)	–61.845(16.210)	–218.027(35.254)	–42.078(44.130)	–290.992(122.695)	41.426	27.970
October	–15.451(7.482)	–49.467(26.013)			–66.227(17.814)	–213.011(43.602)			34.016	
November	–8.483(5.330)	–30.304(15.967)			–66.267(26.095)	–225.228(56.590)			21.821	
December	–9.203(4.910)	–26.159(11.064)			–73.194(27.015)	–207.548(62.729)			16.956	

Table 4–5 Aerosol Optical Properties

Month	SSA$_{676}$		AE$_{(440-676)}$		AOD$_{(675)}$	
	Skukuza	Durban	Skukuza	Durban	Skukuza	Durban
January	0.953(0.044)		1.046(0.451)		0.099(0.063)	
February	0.956(0.020)		1.036(0.517)		0.096(0.073)	
March	0.945(0.038)		1.180(0.531)	0.942(0.330)	0.098(0.067)	0.136(0.046)
April	0.929(0.045)		1.400(0.491)	0.805(0.390)	0.102(0.083)	0.087(0.052)
May	0.937(0.030)	0.863(0.002)	1.483(0.572)	1.307(0.332)	0.089(0.054)	0.114(0.059)
June	0.922(0.040)	0.848(0.053)	1.483(0.422)	1.359(0.363)	0.094(0.061)	0.106(0.053)
July	0.856(0.023)	0.821(0.016)	1.426(0.390)	1.437(0.330)	0.97(0.062)	0.117(0.058)
August	0.866(0.036)	0.874(0.036)	1.452(0.312)	1.518(0.159)	0.160(0.118)	0.172(0.104)
September	0.862(0.033)		1.480(0.277)	1.226(0.367)	0.200(0.120)	0.102(0.057)
October	0.885(0.039)		1.489(0.321)		0.190(0.100)	
November	0.924(0.035)		1.256(0.463)		0.135(0.081)	
December	0.973(0.021)		1.154(0.444)		0.132(0.100)	

4.6 Summary

From this chapter, it can be determined that various aerosol sources are responsible for the aerosol loads noted in Durban. The transport of biomass burning aerosols from northern parts of southern Africa affected the region during late winter, however, industrial activities, coarse mode aerosols from marine particles, dust and soot also impacted the area, especially from December to April. During spring, biomass burning aerosols impacted Skukuza, however, the high extent of fine mode aerosols present throughout the year, indicates that urban industrial emissions from the South African Highveld region can also contribute to aerosol loads in the region. The results obtained from angstrom exponents revealed that there is a greater amount of coarse aerosols in Durban than in Skukuza, this could be because Durban is a coastal area, thus being affected by marine aerosol species. Furthermore, Durban experienced higher angstrom exponent values during the winter season, indicative of fine mode aerosol particles. The higher AOD, the lower SSA (indicative of absorbing aerosol types) and the asymmetry parameter pointed to mixed aerosol loads in Durban during winter. This contradicted other studies, which attributed dust as a major contributor to aerosol loads in Durban during winter (Hersey, et al., 2015).

For Skukuza, high SSA values at the 400 nm wavelength is recorded for summer and autumn, whereas lower values are recorded for winter and spring. Low SSA values were also observed for Durban during winter, alluding to an increase presence of smoke aerosol during these months, probably the result of increased wood burning occurring for heating and cooking purposes due to the cold winter conditions and the onset of southern Africa's biomass burning. The asymmetry parameter (g) reflected low values for winter (for Durban) and for spring (for Skukuza) suggesting a greater abundance of fine anthropogenic (absorbing) pollutants during the same time period.

For Durban and Skukuza, during the winter season the values for the re and im part of the complex refractive index is consistent with values expected for urban industrial aerosols and biomass burning aerosols. For Skukuza during summer and autumn values of the re and im parts of the complex refractive index suggest non–absorbing aerosol types which are consistent with urban industrial aerosols. The low imaginary type values for summer for Skukuza are also associated with coarser, dust aerosol types (Wagner, et al., 2012). For spring, for Skukuza, the real values are indicative of mixed aerosol loads, from both urban industrial and biomass burning type aerosols. The different seasons show different aerosol types dominating for Skukuza, which is consistent with Kumar et al., (2014a), who found biomass burning and urban industrial aerosol types to be the major source of aerosols in Skukuza.

For Durban, the radiative forcing values for the TOA for March and April are positive, displaying a net warming, whereas the values from May to September are negative thus indicating a net cooling effect. For Skukuza, it can be observed that the monthly mean RF for all months are negative, thus suggesting a net cooling. For Durban, August had the highest values for AOD and also displayed higher surface cooling values. The SSA values in the winter months are <0.9, thus indicative of both absorbing and scattering type aerosols, however, there was a slight increase in SSA from July to August indicating an increase in scattering type aerosols in August. This means there is an increase in fine, industrial pollutants and biomass burning pollutants during August for Durban, probably due to the relatively stable weather conditions noted during winter. For Skukuza, August, September and October had the highest AOD values, the smaller SSA values and increased α thus alluding to absorbing aerosol presence. This also corresponded to the highest ARF implying heating from August to October, which is the result of the biomass burning season, increasing the amount of absorbing aerosols in the atmosphere. For, aerosols at the surface, the aerosols more efficient at the surface are

absorbing aerosols such as biomass burning aerosols, therefore, this could be a reason for the high forcing efficiency noticed in Skukuza for the BOA.

For Durban, during March and April the forcing efficiency at the bottom of the atmosphere is quite large which is common absorbing aerosol types. There exist variations within the type of absorbing pollutants that occur during these months and the spectral dependence of the aerosol absorption coefficient. Absorbing pollutants that are released from fossil fuel burning have a warming effect, increasing radiative forcing, hence, the net warming effect observed for March and April at the TOA. Aerosols released from biomass burning have a greater likelihood to decrease the radiative forcing at the TOA, therefore, since September is the biomass burning season, it has a net cooling effect at the TOA (Gadhavi & Jayaraman, 2010).

HYSPLIT 7 day backward trajectories were undertaken for Durban on days with high AOD and on days with low AOD. It was found that on days with high AOD, air mass arrives from Mozambique, Botswana, from northern, drier areas of South Africa and from Madagascar, transporting maritime aerosols at different altitudes. On days with low AOD, air mass at the surface is recirculated within South Africa, and also comes from Botswana and Namibia. Long range transport of air plumes can also be observed to originate from Chile and Argentina.

From this study, it can be observed that many factors influence aerosol properties in a region, namely, altitude and location, local meteorology, synoptic conditions, industry in the area and in regions close to the area as well as the energy sources that people use in that area. It is important to consider all these factors when responding to air pollution problems. A climatological study, spanning several years of sun-photometer data needs to be used in Durban, in order to make more substantial conclusions about the aerosol optical properties in the region.

CHAPTER 5

5. COMPARISON OF AEROSOL OPTICAL DEPTH ACQUIRED FROM SUN-PHOTOMETER AND MODIS SATELLITE OBSERVATIONS

5.1 Introduction

Recently, Sivakumar, et al., (2010), Queface, et al., (2011), Adesina, et al., (2015), Adesina, et al., (2016), Kumar, et al., (2015a) and Hersey, et al., (2015), used AERONET stations operational around South Africa, in Pretoria, Skukuza, Bethlehem and Johannesburg to study aerosol optical properties and compared the measurements with satellite instrumentation. There exist inconsistencies in understanding aerosol properties in many parts of the world, especially in Southern Africa due to the significant lack of ground–based monitoring stations. There are not enough monitoring stations to gauge aerosol climatology of the whole country, therefore there is a requirement for satellite comparison studies in South Africa, especially for Durban, due to the lack of continuous ground based monitoring in the city and the presence of industrial activity and agricultural activity which will potentially generate varying aerosol species. It is important to determine if satellite data can be used as a proxy for ground based measurements, to draw conclusions about the air quality and aerosol loads in a region. This section outlines a few important studies, comparing satellite and ground based measurements of AOD.

Diner, et al., (2001), performed a comparison study using Multi–angle Imaging Spectro–Radiometer (MISR) observations over land and compared it to sun-photometer derived AOD for southern Africa from 14 August to 29 September 2000. This study was performed for the SAFARI 2000 dry season campaign. AOD at 558 nm was retrieved from MISR for the locations above twelve AERONET sites located in southern Africa. The MODIS AOD was averaged for areas of southern Africa and termed "regional mean optical depth". Only observations occurring within ±30 minutes of the Terra overpass time was used. There existed a good linear correlation between MISR and AERONET retrievals. This was partly due to the steep viewing angle from MISR which highlights the smoke plumes and haze from biomass burning. Correlational statistical analysis was performed, by undertaking a simple linear correlation and fitting all the data. The linear fit generated the linear equation and yielded a slope of 1.10 and an intercept of 0.02, for all the data. A reason for this minimal bias could be because of thin cirrus clouds affecting MISR sensors (Diner, et al., 2001). Chu, et al., (2002), also studied AOD derived from MODIS measurements from the Terra sensor and compared the measurements with sun-photometer derived AOD, for over 30 AERONET sites around the

globe. The MODIS AOD retrievals were found to be similar to sun-photometer retrievals, with retrieval errors ±0.2 to ±0.05 AOD. It was found, that inland areas performed better than coastal areas due to the contamination from water (Chu, et al., 2002).

Schmid, et al., (2003), performed a study during SAFARI 2000's dry season campaign. They have used synchronized observations of aerosol layers over southern Africa. One of the comparisons was between MODIS AOD and AERONET measurements. An over–water comparison was performed, meaning, the measurements were recorded over water near Inhaca Island, of the coast of Mozambique. AOD at 1024 nm and 1064 nm from MODIS Terra sensor was compared with sun-photometer retrievals and the MODIS data were within the accepted retrieval error. An overland comparison was also done near the Kaoma AERONET site in Zambia, with the MODIS retrieval much less and the disagreement greater than the retrieval error (Schmid, et al., 2003).

An extensive study was conducted by Ichoku, et al., (2004), validating MODIS measured aerosol characteristics with AERONET sun-photometer aerosol characteristics. The study was conducted over all AERONET sites that existed during the study period, which was from August 2000 to August 2002. The MODIS data were regrouped according to AERONET sun-photometer data bins for the AOD values. For each group the MODIS data means and standard deviations were calculated for land and ocean for both Terra and Aqua sensors at 470 and 660 nm. It was found that greater than 90% of all observations have AOD values that are 0.5 or lower. It was established that over land at 470 nm, almost all MODIS means were within the accuracy limits for both Terra and Aqua. However, at 660 nm, the AOD that was greater than 0.5 for the AERONET sun-photometers and were underestimated by the Terra sensor. This underestimation was attributed to the global estimation of absorption in the initial MODIS smoke aerosol model. Other reasons for the underestimation by MODIS Terra over land may include systematic inaccuracies in the surface reflectance assumptions and other inaccurate assumptions in the aerosol models. The accuracy over the ocean was more precise, with all class means within or very close to accuracy limits. The reason for this was that the ocean algorithm has less uncertainty in surface reflectance and other assumptions. There was greater uncertainty at higher AOD, due to the uncertainty in dust aerosol retrieval because dust is non–spherical in nature (Ichoku, et al., 2004). Ichoku, et al., (2003), performed a similar study, retrieving MODIS aerosol parameters only over southern Africa and compared it to AERONET sun-photometer retrievals of AOD and found similar findings, at sites around southern Africa (Ichoku, et al., 2003).

Hao, et al., (2005), used AERONET sun-photometers from Ndola, Mongu, Mwinilunga, and Kaoma in western Zambia, to obtain AOD, as part of SAFARI 2000's dry season campaign. Measurements were compared to MODIS Terra derived AOD. The comparisons were made during the biomass burning season from 23 August to 20 September 2000. This is the biomass burning season therefore smoke aerosols dominate the region with the exception of Ndolu which contains a copper industry. This study found that MODIS AOD was significantly lower than the sun-photometer derived data. The ratio of MODIS AOD to sun-photometer derived AOD is about 0.58 at 440/470 nm and 0.57 at 670/660 nm. This means that MODIS AOD was approximately 50% lower at the wavelengths studies in regions with intense biomass burning. The differences in AOD measurements was again attributed to an error in the presumed aerosol scattering phase function or surface directional characteristics. The density of vegetation cover can also interrupt MODIS retrievals of AOD (Hao, et al., 2005).

Kumar, et al., (2015a), performed a study focusing on Durban, AOD within the 550 nm wavelength was retrieved from various satellite sensors and compared to AERONET sunphotometer measurements from 2005 to 2011. The Skukuza sun-photometer was used due to a lack of ground based measurements in Durban for the study period and due to Skukuza being located at almost the same longitude as Durban. AOD from MODIS's Terra sensor using the DT algorithm was compared with MISR satellite retrievals of AOD. Both the satellite were compared with AOD from the sun-photometer located at Skukuza. Only sun-photometer measurements that were closest to the Terra overpass time were used in the analysis. The correlation coefficient was found to be quite high between sun-photometer and MISR (0.91) and lower between the sun-photometer and MODIS Terra (0.78). The ratio of MISR AOD to the sun-photometer AOD is about 0.87 and for MODIS AOD to the sun-photometer AOD is about 0.77, therefore, the satellites greatly underestimated AOD. The factors attributed to the inaccuracies were similar to that of the previous studies i.e., improper assumptions of surface reflectance and selection of aerosol types. The correlation between land retrievals from MODIS is known to perform better than ocean retrievals as a result of to its low surface reflectivity characteristic. Adesina, et al., (2015), performed a similar study, focusing on aerosol optical properties over Gorongosa Mozambique from July to December, 2012. MODIS retrieved AOD was compared to sun-photometer derived AOD and the R^2 coefficient was determined. It was found that for MODIS DT algorithm the R^2 value was 0.80 and 0.89, for Terra and Aqua sensors, respectively.

Sun, et al., (2008), compared AOD generated from MODIS Terra sensor with sun-photometer observations over seas surrounding China, from January 2005 to May 2007. Observations were used from sun-photometers located at AERONET sites that where within a 25km radius of MODIS. The R^2 correlation coefficient was calculated and it was, 0.68, 0.65 and 0.56 for MODIS 550, 658 and 860 nm channels respectively. Using data for particular seasons only, in spring the R^2 value was much better at 0.77, 0.75 and 0.71, respectively for the different wavelengths. It was concluded that, for oceans around China, MODIS AOD measurements can attain a certain level of precision, however, validation between the two measurements were not sufficient (Sun, et al., 2008). Tripathi, et al., (2005), undertook a similar study of AOD in Kanpur, an industrial city in India, and compared MODIS Terra retrievals to sun-photometer derived AOD. The study was performed from January to December 2004 and AOD at 550 nm wavelength was studied and the R^2 coefficient was determined. The results showed that during the post–monsoon and winter seasons the R^2 (0.71) value is similar to the pre–monsoon and monsoon seasons (0.72). MODIS data were underestimated during post monsoon and winter seasons and overestimated during pre–monsoon and monsoon period (Tripathi, et al., 2005).

Adesina, et al., (2016), used MODIS's Terra satellite to determine the spatial and temporal relationship between AOD and cloud parameters over six sites in South Africa. The locations were chosen because of their contrasting features and because of the potential of the sites to experience aerosol loads from several different sources. The locations were, Pretoria, Skukuza, Durban, Bloemfontein, Cape Town and Potchefstroom. The mean AOD for the study period of 2004 to 2013, depicted Bloemfontein to have the lowest average value (0.06±0.04), moderate for Cape Town 0.08±0.02, then Potchefstroom 0.09±0.05, followed by Pretoria and Skukuza which had values of 0.11±0.05 each, and with the highest observed at Durban 0.13±0.05. The higher AOD noted over Durban, could be due to Durban being an urban, industrial and coastal region, thus having the potential to experience aerosols from various source regions. All locations, with the exception of Pretoria, have the highest seasonal AOD observed during spring, followed by summer. For Pretoria, the AOD, was highest during spring and summer, this could be due to Pretoria being an urban region, experiencing dust storms during summer and local vehicle emissions. Also, due to the high temperature and relative humidity in summer, the hygroscopic growth of aerosols is supported. In terms of the mean $\alpha_{440–870}$, Durban and Skukuza had the highest values, followed by Pretoria and Cape Town, then Bloemfontein and Potchefstroom. The low $\alpha_{440–870}$ for Bloemfontein and Potchefstroom is due to being regions with less vegetation therefore dust might be more of an impact to aerosol

loads. For the entire study period, Durban and Skukuza have $\alpha_{440-870} > 1.0$, Cape Town has $\alpha_{440-870} > 1.0$ in all the months except, in January. Bloemfontein, Potchefstroom and Pretoria have AE<1.0 for most of the year except, for a few months. The $\alpha_{440-870}$ has higher values for coastal sites than inland sites. Skukuza has a close proximity to the biomass burning activities in Mozambique, hence the high $\alpha_{440-870}$ values were noted (Adesina, et al., 2016).

Kumar, et al., (2014b), studied the spatial and temporal distributions of aerosol optical properties in Pretoria, Bloemfontein and Cape Town, from December 2003 to November 2013. The three sites were chosen, due to the unique aerosol regimes which affect each region. Pretoria is affected by anthropogenic, industrial activities and mineral dust aerosol species, Bloemfontein is located in central South Africa and is directly influenced by smoke aerosols produced by biomass burning and Cape Town is usually characterised by low aerosol loads. MODIS satellite data, from the Terra sensor, was used to gain the AOD, $\alpha_{440-870}$ and fine mode fraction (FMF) for the ten year study period. It was found that South Africa displays moderate to high AOD for Gauteng (Pretoria), Mpumalanga, Limpopo and the upper part of KwaZulu–Natal. High AOD was noted for North–West Province due in part to dust from the Kalahari and low AOD was observed in the central and southern parts of South Africa, that is, Free State (Bloemfontein), upper part of Northern Cape, Eastern Cape and Western Cape (Cape Town). AOD was found to be very low in the lower regions of Northern Cape. The $\alpha_{440-870}$ values indicated the existence of fine particles in KwaZulu–Natal, Western Cape and Free State Provinces. This was attributed to local anthropogenic and urban/industrial activities. The FMF results found very small FMF values in the western parts of South Africa, moderate values in the central part of South Africa and the contribution of fine and coarse particles to aerosol loads was almost even with higher values in the north and northwest parts. There existed an aerosol gradient in the country, with higher AOD values noted for north of the country and lower values noted over the south of the country. From the trend analysis conducted there has been a decrease in AOD noticed over all three sites. The seasonal trends depicted that for the three sites, average AOD values were higher during spring (September) and summer (January/February) seasons, whereas the lower values were found in the late autumn/early winter periods (June) (Kumar, et al., 2014b).

From the aforementioned studies, it is clear that the validity of MODIS satellite data depends upon various factors, one of which, is the location. Different locations have different values of accuracy, depending on the climate and the type of aerosols present in that region. This chapter will compare AOD derived from MODIS dark target (DT) and deep blue (DB) retrieval

algorithms for both the Aqua and Terra sensors and Terra and Aqua merged (the average of Terra and Aqua) with the Durban sun-photometerderived AOD from January to September 2014, using correlation statistical analysis.

5.2 Comparison of MODIS data and AERONET retrievals from the Durban sun-photometer

.

In this study, statistical analysis was performed for MODIS derived AOD and sun-photometer derived AOD for Durban. Only days in which data existed for both instrumention were included in the analysis. For MODIS's DT algorithm, 109 common days existed between the sun-photometer and the Terra sensor and 108 common days existed between the sun-photometer and the Aqua sensor. For the DB algorithm, 89 common days existed between the sun-photometer and the Terra sensor and 80 common days existed between the sun-photometer and the Aqua sensor. The daily average AOD at 550 nm retrieved from the different algorithms and sensors were compared with sun-photometer derived AOD at 550 nm. The AOD from the sun-photometer at 500 nm was extrapolated, using the power law, to determine the AOD at 550 nm, in order to compare with MODIS observations. For the comparison of sun-photometer derived AOD to MODIS Terra, MODIS Aqua and a merged dataset (the average of MODIS Aqua and Terra), for both algortithms (DT and DB), the regression coefficient was determined and is presented in the Table 5.1 below. Scatterplots were also used to illustrate the parameters of the regression analysis, i.e., the R^2 correlation coefficient, the root mean square error (RMSE), the slope and the intercept of the comparisons. This was presented in Figure 5.1 for the DT algorithm and Figure 5.2 for the DB algorithm.

From Figure 5.1, it can be noted that for Durban, DB has a higher R^2 (0.70) for the Terra sensor than DT (0.60), however, DT performed better for the Aqua sensor with a higher R^2 (0.78) than the value for DB ($R^2 = 0.68$). The Terra and Aqua sensors correlated better using the DT algorithm ($R^2 = 0.66$) than the DB algorithm ($R^2 = 0.56$). Due to the varying correlations, aqua and terra values were averaged and the merged dataset was used for the different algorithms. DB performed better with a higher R^2 (0.79) value than DT (0.74). The RMSE for all algorithms ranges from 0.05 to 0.09, however, it is lowest between the Aqua sensor and the Durban sun-photometer for the DT algorithm and between the Aqua and Terra sensor for the DB algorithm. Here, the non–zero intercepts are quite low, perhaps due to the low AOD values noted for Durban which displayed a mean of <0.4 for the study period (Figure 4.5 (a) above). This could be due to sensor calibration error or an unsuitable assumption about the ground surface

reflection (Ichoku, et al., 2003; Ichoku, et al., 2004; Tripathi, et al., 2005; Sayer, et al., 2014; Kumar, et al., 2015a). From the slopes, it can be observed that both algorithms were lower than unity suggesting an underestimation of AOD by MODIS with regards to AOD retrieved from the Durban sun-photometer (Tripathi, et al., 2005). A slope that is different from unity, point towards inconsistencies between the aerosol microphysical and optical properties used in the retrieval algorithm. For example, thin cirrus clouds can affect MODIS data collection, but might not be in the field of view of the sun-photometer (Diner, et al., 2001). Also, the assumption for MODIS aerosol retrieval is that up–welling reflectance measured at the top of the atmosphere is calculated by summing the surface and atmospheric components in the solar wavelength range. The atmospheric components of the refelctance includes parameters relating to molecular scattering, clouds and aerosols. MODIS aerosol retrieval algorithms screen cloud pixels so that aerosol properties can be determined in clear skies. There are complex procedures involved in removing the surface contribution and retrieving aerosol optical characteristics over land and ocean. Therefore, assumptions are made of ground surface reflectance and inaccuracies in these assumptions can decrease the accuracy in measurements. During southern Africa's biomass burning season, MODIS algorithms tend to make inaccurate assumptions of ground surface reflectance by over–estimating SSA parameters (Abel, et al., 2005). This leads to an underestimation of AOD. Another reason for the disagreements was provided by Chu, et al., (2002), who found that, MODIS performed better for inland areas than coastal areas due to the contamination from water. This is because surface inhomogeneity caused by sub–pixel water contamination affects AOD retrieved from MODIS satellites.

Table 5.1 R^2 value obtained by linear and 2nd degree interpolation for the different retrieval algorithms on common days from January to December 2014.

Algorithm	Sun-photometer vs. Terra		Sun-photometer vs. Aqua		Terra vs. Aqua		Terra and Aqua vs. Sun-photometer	
	R^2(1st degr. interpolation)	R^2(2nd degr. interpolation)	R^2(1st degr. interpolation)	R^2(2nd degr. interpolation)	R^2(1st degr. interpolation)	R^2(2nd degr. interpolation)	R^2(1st degr. interpolation)	R^2(2nd degr. interpolation)
Deep Blue	0.70	0.70	0.68	0.68	0.55	0.56	0.79	0.79
Dark Target	0.60	0.61	0.78	0.78	0.65	0.65	0.74	0.74
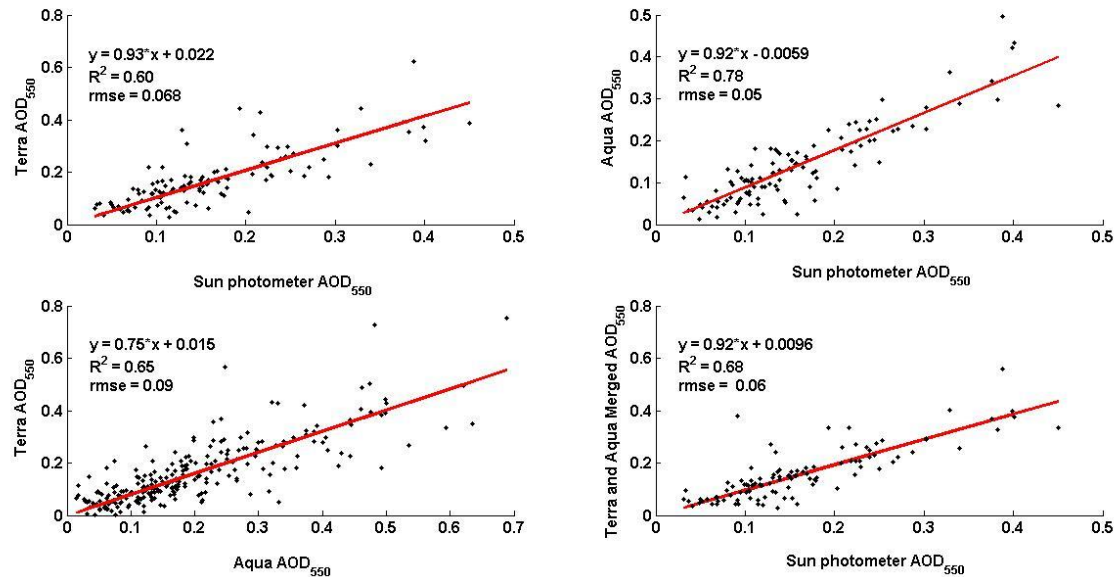
Figure 5.1 Scatter plots between (a) AERONET retrievals from the Durban sun-photometer and MODIS Terra (b) AERONET retrievals from the Durban sun-photometer and MODIS Aqua (c) MODIS Terra and Aqua and (d) MODIS Terra/Aqua merged and AERONET retrievals from the

Durban sun-photometer for AOD at 550 nm over Durban during the study period, using the dark target algorithm. The red line indicates the linear regression fitted line to the data. The regression parameters obtained from the fitting namely, the linear equation, the R square (R^2) and the root mean square error (rmse) are also shown.
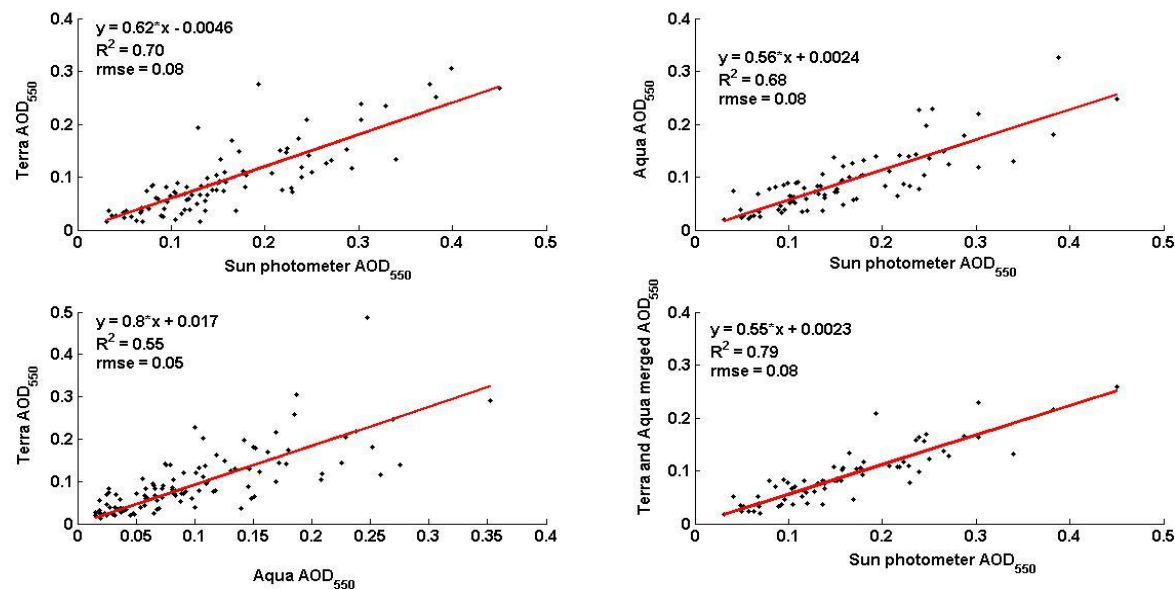
Figure 5.2 Scatter plots between (a) AERONET retrievals from the Durban sun-photometer and MODIS Terra (b) AERONET retrievals from the Durban sun-photometer and MODIS Aqua (c) MODIS Terra and Aqua and (d) MODIS Terra/Aqua merged and AERONET retrievals from the Durban sun-photometer for AOD at 550 nm over Durban during the study period, using the deep blue algorithm. The red line indicates the linear regression fitted line to the data. The regression parameters obtained from the fitting namely, the linear equation, the R square (R^2) and the root mean square error (rmse) are also shown.

5.3 *Monthly mean comparison between different MODIS retrieval algorithms and AERONET retrievals from the Durban sun-photometer .*

The monthly means and the standard deviations of MODIS derived AOD and sun-photometer derived AOD were compared Durban, for January to September 2014. Days in which AOD observations existed for both the MODIS sensors and the sun-photometer were included in the analysis. For MODIS's DT algorithm, 109 daily observations existed for the Terra sensor and 108 daily observations existed for the Aqua sensor. For the DB algorithm, 89 daily observations existed for the Terra sensor and 80 daily observations existed for the Aqua sensor. These observations were divided into the respective months and the means and standard deviations were calculated, for all the sensors and for both algorithms and compared to AOD derived from the sun-photometer. The AOD data used was averaged from sun-photometer derived AOD, MODIS Terra, MODIS Aqua and an averaged dataset of MODIS Aqua and Terra combined AOD and displayed in a line graph for the DT algorithm (Figure 5.3). The same parameters were calculated for the DB algorithm and compared with sun-photometer means and displayed in Figure 5.4. Monthly means from MODIS Terra and MODIS Aqua and the merged dataset (the average of MODIS Terra and Aqua), were individually correlated against sun-photometer monthly means of AOD, for both the DT and DB algorithm. This was done by computing the regression coefficient for all the months and it is presented in the Table 5.2 for the DT algorithm and Table 5.3 for the DB algorithm, below.
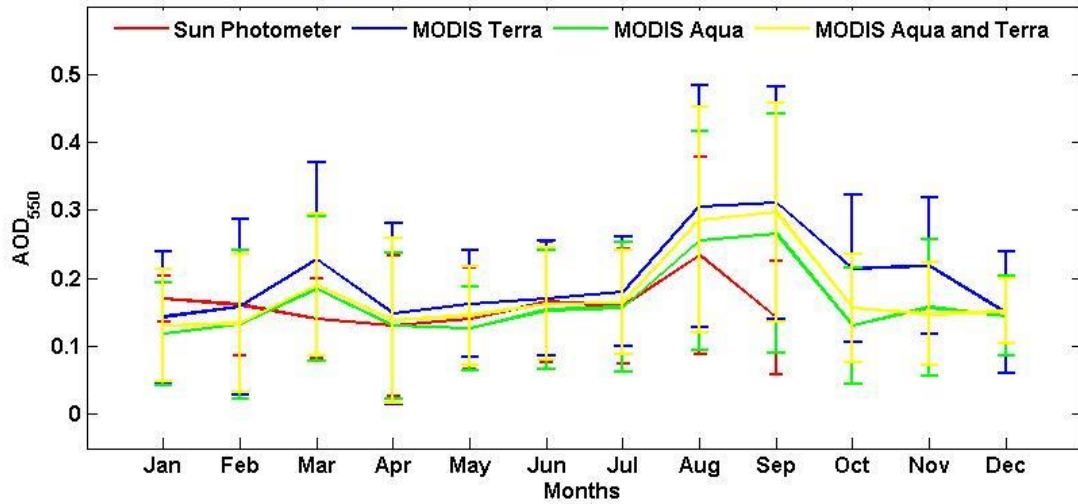
Figure 5.3 Monthly averaged AOD at 550 nm wavelength over Durban during the year 2014 retrieved from MODIS (DT) and AERONET retrievals from the Durban sun-photometer. The error bars represent the standard deviation of AOD for that month
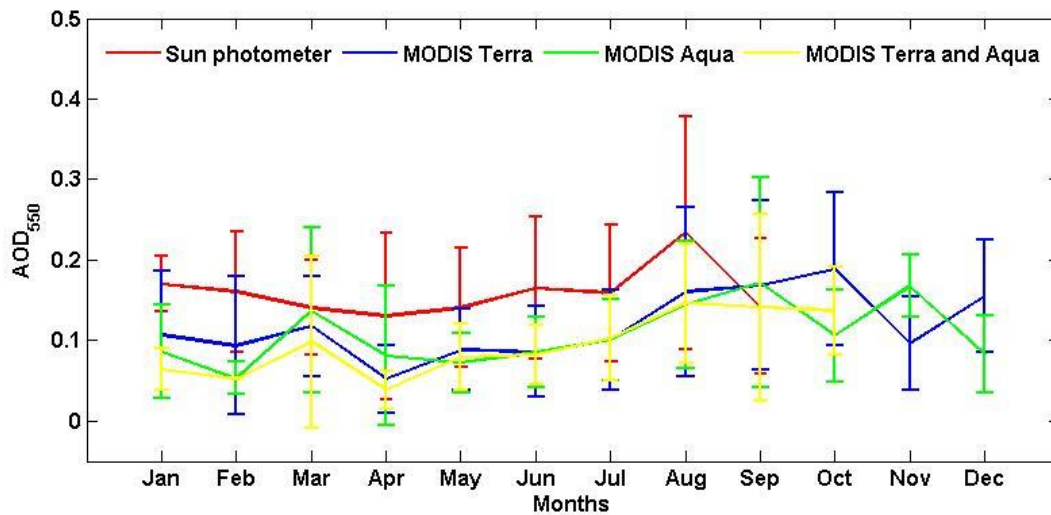
Figure 5.4 Monthly averaged AOD at 550 nm wavelength over Durban during the year 2014 retrieved from MODIS (DB) and AERONET retrievals from the Durban sun-photometer. The error bars represent the standard deviation of AOD for that month

Figure 5.3 and 5.4, depicts the monthly averaged AOD values at 550 nm obtained from MODIS Aqua and Terra sensors and from the Durban sun-photometer from January to December 2014 (for MODIS sensors) and from January to September 2014 (for the Durban sun-photometer), using the DT and DB algorithm respectively. From Figure 5.3 for the DT algorithm, it can be ascertained that MODIS Aqua and Terra merged derived AOD closer to values from the Durban sun-photometer than MODIS Terra and MODIS Aqua. For the DB algorithm, MODIS Aqua AOD appears closer to the sun-photometer derived AOD values. The MODIS sensors,

for both algorithms (DT and DB), depict a rise in AOD from February to March, whereas AOD values from the Durban sun-photometer depicts a drop in AOD values during this time. AOD values dropped from March to April, for both the Durban sun-photometer and MODIS sensors. From April to July, both the sun-photometer derived AOD and MODIS derived AOD remained at low values and quite constant (<0.2). For all instruments and sensors, and for both algorithms, AOD increased from July to August. AOD then decreased drastically for sun-photometer derived values from August to September. AOD was still high for both the MODIS sensors and algorithms from August to September and then decreased from September to October. AOD derived from the MODIS sensors from October to December remained relatively low. Figure 5.3 (DT algorithm) displays some seasonal variation, with maximum values depicted during August (sun-photometer) and during October for most MODIS sensors and algorithms. For DT algorithm AOD means greater than 0.2 occurred for Aqua (March and August), Aqua and Terra merged (March and August) and sun-photometer derived AOD (August) and AOD mean was greater than 0.3 for Terra during August. From Figure 5.4 (DB algorithm), MODIS derived AOD is <0.2 and is always less than sun-photometer derived AOD, for all sensors. This means that the DB algorithm underestimated AOD during all months studied. For MODIS DT algorithm, from February of 2014, MODIS derived AOD was greater than AOD from the Durban sun-photometer, thus suggesting an overestimation of AOD by the DT algorithm. This supports the aforementioned studies (Ichoku, et al., 2003; Ichoku, et al., 2004; Tripathi, et al., 2005; Sayer, et al., 2014; Kumar, et al., 2015b). It is in line with findings from Sayer, et al., (2014) a study who validated MODIS Aqua sensor DB and DT algorithms using 111 AERONET sites, suggesting that while one algorithm does perform better than the other on occasion, performance of retrieval algorithms are region specific and complicated (Sayer , et al., 2014).

Aerosol layers were studied as part of the SAFARI program using different instrumentation. Airborne measurements were performed using the Ames Airborne Tracking 14–channel Sun-photometer, ground based AERONET sun-photometers, ground based lidars and spaceborne sensors (Total Ozone Mapper (TOMS), MODIS, MISR and ATSR–2). The comparison between AOD from MODIS and sun-photometers generated mixed results, over water, there was good agreement whereas over land MODIS significantly underestimated AOD over Zambia (Swap, et al., 2003; Schmid, et al., 2003). This can also be noted in this study, whereby MODIS main land retrieval algorithm (DT) underestimated AOD for Durban.

Table 5.2 (DT) and 5.3 (DB) depicts the correlation coefficients obtained from the linear regression and second degree linear regression. The R^2 values for the 2nd degree interpolation are found to be better than from the linear interpolation. From Table 5.2 (DT), the low R^2 values noted in January could be due to the lack of common sensor days during January. It can be noted that R^2 values are higher during the winter months, for AOD from the sun-photometer and Aqua, for the sun-photometer and Terra and Aqua merged and for Aqua and Terra. High correlations also exist between sun-photometer and Terra and sun-photometer and Aqua, sun-photometer and Terra and Aqua merged during April and September, which correspond to the months with the lowest AOD measurements from the sun-photometer (Table 5.2 DT). Moderate correlations exist between sun-photometerand Terra, sun-photometer and Aqua, sun-photometer and Terra and Aqua merged and Terra and Aqua during August, which corresponds to higher AOD values. This suggests that during months with low AOD, the DT retrieval algorithm performs better. This was similar to Ichoku, et al., (2004), who found that during months of high AOD MODIS tended to underestimate AOD. Such underestimation was assumed to be the result of the global estimation of absorption in the initial MODIS smoke aerosol model. March and July exhibit very low correlations between MODIS sensors and sun-photometer derived AOD.

Table 5.3 (DB) algorithm, exhibits missing data during certain months due to a lack of common days during these months. It can be observed that high correlations existed during August and February between sun-photometer and Terra, sun-photometer and Aqua and sun-photometer and Terra and Aqua merged. For the DB algorithm, Terra and Aqua sensors only correlated well during February and March, displaying moderate correlation throughout the rest of the study period. For April, May, June and September, moderate correlations exist between sun-photometer and Terra and sun-photometer and Aqua. Similar to the DT algorithm, very low correlations exist in March and July between MODIS sensors and sun-photometer derived AOD for the DB algorithm.

The low correlation observed between MODIS Terra and sun-photometer in Table 5.1 above, using DT and DB ($R^2 = 0.60$ and $R^2 = 0.70$, respectively), was also noted for Durban by Kumar et al., (2015a), who studied AOD for the period from 2005 to 2011, using sun-photometer observations from Skukuza to validate results. The non–unitary nature of the slopes for both Terra and Aqua (0.96 and 0.92 respectively) highlights the underestimation of AOD. This trend was also noticed by Kumar, et al., (2015b) and with earlier studies conducted by Chu, (2002) and Diner, et al., (2001) for South Africa, with a limited dataset from July to September, 2000.

The non–zero slope intercepts observed (Figure 5.1 and 5.2) could be the result of the biasing of the algorithm to low AOD values, which can be the reason MODIS DB retrieval algorithm underestimates AOD. Factors responsible for these inaccuracies and inconsistencies in AOD, could be incorrect assumptions of surface reflectance (Ichoku, et al., 2003; Ichoku, et al., 2004; Tripathi, et al., 2005; Sayer, et al., 2014; Kumar, et al., 2015a; Schmid, et al., 2003; Swap, et al., 2003). Inaccuracies could also be the result of single point measurements from sun-photometer versus 10km area avergaed MODIS retrievals (Sayer, et al., 2014).

From the previous mentioned studies, it can be noted that various researchers have been performing intercomparisons between retrievals from AERONET sun-photometers and MODIS for several years. Sun, et al., 2008, showed a moderate correlation between MODIS Terra and AERONET over seas around China ($R^2 = 0.68$), however, better results were noted during certain seasons such as spring and ($R^2 = 0.77$). This is consistent with the results presented in this study, where a moderate seasonal correlations can be observed when using both retrieval algorithms (DT and DB). Tripathi, et al., (2005) also displayed good seasonal correlations during winter and post monsoon seasons, where there was no dust–loading ($R^2 = 0.72$). More, et al., (2013) also noticed strong correlations on the seasonal scale between MODIS and AERONET AOD over Pune, India with seasonal R^2 values ranging from 0.62 to 0.93 (More, et al., 2013). Similar to results in this study, reasonable correlations between MODIS, MISR and AERONET derived AOD ($R^2 = 0.71, 0.67, 0.61$) were found over Karachi, Lahore, Jaipur, and Kanpur, respectively (Bibi, et al., 2015). Reasonable correlations were also noted for MODIS and AERONET derived AOD in southern Africa (Chu, et al., 2002; Ichoku, et al., 2003; Ichoku, et al., 2004; Hao, et al., 2005; Kumar, et al., 2015a; Adesina, et al., 2015).

Table 5–1 R^2 value obtained by linear (1st degree) and 2nd degree interpolation from January to September, 2014 for MODIS DT retrieval algorithm.

	Sun-photometer vs. Terra		Sun-photometer vs. Aqua		Sun-photometer vs. Terra and Aqua		Terra vs. Aqua	
	R^2 (1st degr. interpolation)	R^2 (2nd degr. interpolation)	R^2 (1st degr. interpolation)	R^2 (2nd degr. interpolation)	R^2 (1st degr. interpolation)	R^2 (2nd degr. interpolation)	R^2 (1st degr. interpolation)	R^2 (2nd degr. interpolation)
Jan	–0.48	0.96	–0.99	0.82	–0.63	0.94	0.49	0.53
Feb	0.54	0.56	0.66	0.76	0.69	0.74	0.64	0.65
Mar	0.33	0.33	0.55	0.58	0.49	0.50	0.57	0.60
Apr	0.93	0.98	0.90	0.93	0.93	0.96	0.85	0.85
May	0.38	0.43	0.88	0.89	0.74	0.74	0.74	0.76
Jun	0.82	0.86	0.93	0.93	0.94	0.95	0.75	0.75
Jul	0.38	0.49	0.78	0.80	0.63	0.71	0.60	0.61
Aug	0.65	0.73	0.78	0.81	0.76	0.81	0.78	0.78
Sep	0.95	0.97	0.89	0.89	0.96	0.98	0.40	0.43
Oct							0.31	0.32
Nov							0.40	0.46
Dec							–1.65	0.06

Table 5–2 R2 value obtained by linear (1st degree) and 2nd degree interpolation from January to September, 2014 for MODIS DB retrieval algorithm

	Sun-photometer vs. Terra		Sun-photometer vs. Aqua		Sun-photometer vs. Terra and Aqua		Sun-photometer vs. Aqua	
	R^2 (1st degr. interpolation)	R^2(2nd degr. interpolation)	R^2(1st degr. interpolation)	R^2(2nd degr. interpolation)	R^2(1st degr. interpolation)	R^2(2nd degr. interpolation)	R^2(1st degr. interpolation)	R^2(2nd degr. interpolation)
Jan			0.74	0.99			–0.55	0.05
Feb	0.83	0.90	0.99	0.99			0.99	0.95
Mar	0.19	0.33	0.77	0.98			0.98	0.99
Apr	0.78	0.79	0.95	0.98			–0.13	0.22
May	0.60	0.60	0.66	0.66	0.81	0.83	0.54	0.60
Jun	0.67	0.67	0.64	0.64	0.67	0.68	0.15	0.30
Jul	0.47	0.49	0.48	0.56	0.55	0.59	0.34	0.50
Aug	0.93	0.93	0.96	0.96	0.98	0.98	0.63	0.66
Sep	0.83	0.91	0.52	0.57	0.89	0.92	0.48	0.48
Oct							0.49	0.65
Nov								
Dec								

5.4 Frequency distribution of AOD for MODIS retrieval algorithms and AERONET retrievals from the Durban sun-photometer .

The histogram of the frequency range of AOD values is displayed in Figure 5.5 and 5.6 below, for MODIS DT and DB algorithms in order to characterise the retrievals from all data points. The histograms correspond to each other for the range of AOD values. For the DT algorithm, the majority of AOD values for the Durban sun-photometer, MODIS Terra and MODIS Terra and Aqua merged range from 0.1 to 0.2 and range from 0 to 0.1 for MODIS Aqua. For the DB algorithm, the majority of values for MODIS Terra, MODIS Aqua, and Terra and Aqua merged ranges from 0 to 0.1. Additionally, there are no AOD values that are greater than 0.4 (Figure 5.6), thus highlighting MODIS DB's underestimation of AOD when compared to MODIS DT and AERONET derived AOD from the Durban sun-photometer.
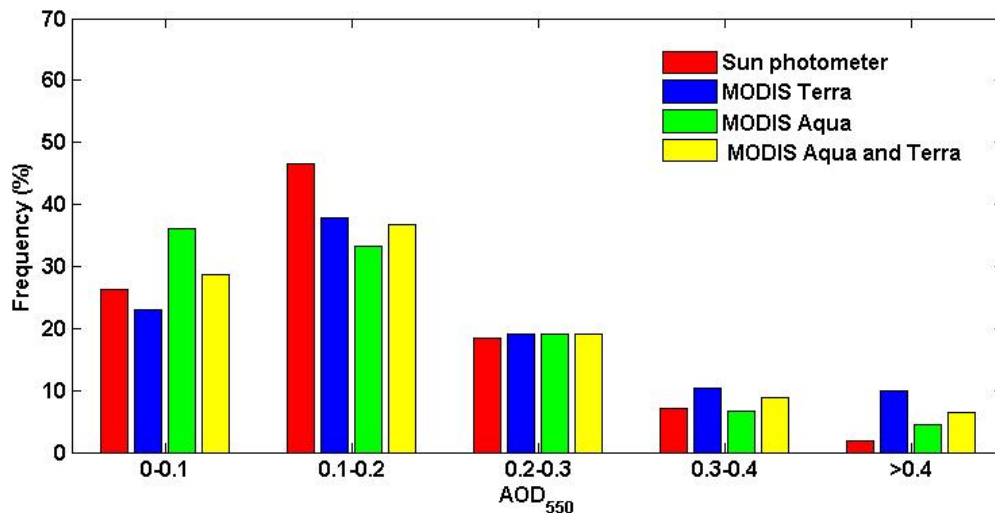

Figure 5.5 Frequency distribution of AOD derived from sun-photometer and MODIS (DT) from January to September 2014.
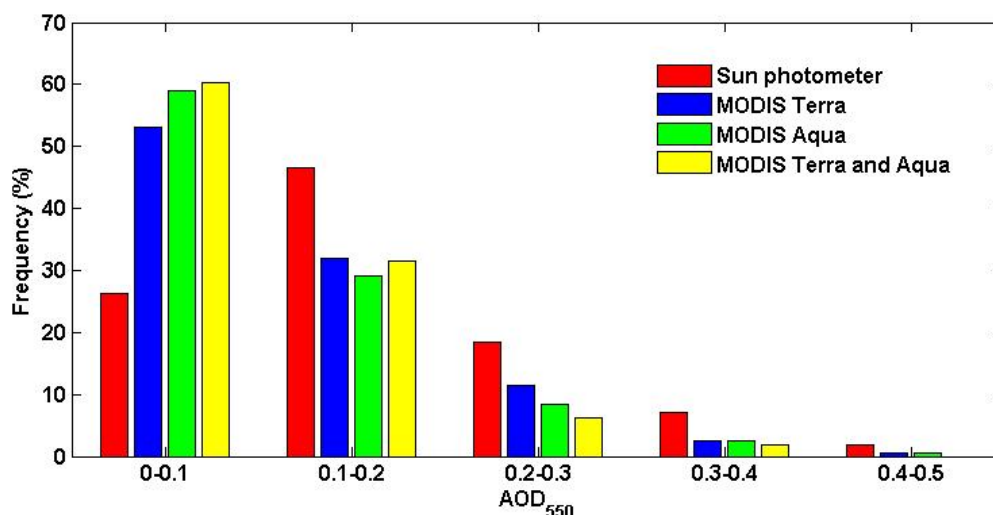
Figure 5.6 Frequency distribution of AOD derived from sun-photometer and MODIS (DB) from January to September 2014.

5.5 Summary

For Durban, it can be observed that MODIS can act as a proxy for ground based measurements of AOD. However due to, sensor calibration errors or an unsuitable assumption about the ground surface reflection, inconsistencies between the aerosol microphysical and optical properties used in the retrieval algorithm. This underestimation was also indicated to be the result of the global estimation of absorption in the initial MODIS smoke aerosol model. Also, where one algorithm does perform better than the other on occasion, performance of retrieval algorithms are region specific and complicated. It was found that MODIS performed better during certain months such as during April, June, August and September for the DT and DB algorithms. Therefore, it can be ascertained that AOD can be used as a subtle proxy for ground based measurements in the region. However, time of year needs to be taken into consideration. Further studies need to be done, using a larger dataset in order to make more robust conclusions for Durban. Also, it is important for comparisons to be made during the MODIS overpass time, this was not able to be done in this study due to a lack of match–up days.

From this study, as well as previous studies mentioned which compare AOD from AERONET sun-photometers with MODIS satellite data it can be noted that MODIS is able to reasonably act as a proxy for ground based measurements. However, the validity and accuracy of the results depends also on the location and time of year. There are many other elements that should be considered when using different sensor sources such as retrieval algorithms, consistency, revisit times, instrument calibration, cloud screening, data availability, algorithm assumptions

135

regardig aerosol micrphysical properties and surface boundary environments (Kahn, et al., 2009).

CHAPTER 6

6. A CASE STUDY ON AIR MASS TRANSPORT FROM THE CALBUCO VOLCANO IN CHILE TO DURBAN

6.1 Introduction

Volcanoes are a major natural source of pollutants in the atmosphere both during and between eruptions. Volcanic emissions have aided atmospheric evolution throughout earth's history. It is valuable to imperatively understand the chemistry of natural tropospheric emissions in order to investigate and understand the impacts of their interactions with anthropogenic pollutants. It was found that without major volcanic eruptions, emissions from volcanoes regularly affect stratospheric aerosol levels (Chin, et al., 2002). Due to the high altitude of emissions, the ratio of volcanic SO_2 to anthropogenic SO_2 is approximately 2:1 (Chin, et al., 2014). Air pollution studies in Mexico City have shown how anthropogenic SO_2 emission mitigation strategies may have been affected by the adsorption of volcanic SO_2 from the Popocatépetl volcano (Stremme, et al., 2011). Adsorption is a process that occurs when a gas or liquid solute accumulates on the surface of a solid or a liquid (adsorbent), forming a molecular substance. The adsorption of SO_2 from the Popocatépetl volcano onto existing particulates resulted in an increase in the concentration of sulphates produced (Stremme, et al., 2011).

Volcanic eruptions cause distress to the communities which live near the eruption site. This is because ash is entrained upwards within the eruption column, eventually, falling out of suspension and affecting the communities below the eruption site. This affects public health, by damaging infrastructure, disrupting aviation and causing economic fallout. Communities that are near sources of volcanic ash, can potentially experience anxiety about the health ramifications of inhaling ash, the negative impacts on pets and the possible damage to property. Volcanic activity thus leads to socio–economic disturbances such as evacuation, school closure and business closure. It is useful to gain the air mass trajectory of volcanic plumes, to determine which regions might be affected by the aerosol loads (Jenkins, et al., 2015).

Eruptions of the El Chichón volcano in Mexico in 1982 emphasized the radiative and chemical importance of stratospheric aerosols associated with large explosive volcanoes. Furthermore, samples of volcanically produced aerosols resulted from Kasatochi (Alaska), Sarychev (Russia) and also during the Eyjafjallaj¨okull (Iceland) eruptions from 2008 to 2010 (Anderson, et al., 2013). Aerosols from the Eyjafjallaj¨okull volcanic clouds had high concentrations of sulphur and carbon elements, thus also indicating aerosols of crustal origin. Volcanic aerosol

was also discovered in stratospheric samples collected after the Sarychev and Kasatochi eruptions (Anderson, et al., 2013).

Kilauea is one of the three active volcanoes on the Island of Hawaii. It erupted in 1983 and has since become one of the most active volcanoes on earth. Kilauea is responsible for releasing 300 metric tons of SO_2 per day and as much as 30,000 tons of SO_2 per day during vigorous eruptive activity (Tam, et al., 2016). Volcanic gases, including SO_2, react with each other and oxygen, water vapour and dust to produce fine respirable particles which can potentially impact pulmonary function. A study by Tam, et al., (2016) reported that, chronic exposure to volcanic activity from the Kilauea volcano, is associated with increase cough (Tam, et al., 2016).

The HYSPLIT model has also been utilized to determine air mass trajectories leaving the site of volcanic eruptions. Jamieson, et al., (2015), used the HYSPLIT Volcanic Ash model to determine whether ash cloud trajectories for volcanic eruptions reached the Actun Tunichil Muknal cave site in Belize. Aerosol data was also studied to determine if volcanic ash reached the site. The HYSPLIT model was able to determine the trajectory of volcanic plumes from 6 volcanoes around South America (Jamieson, et al., 2015). The HYSPLIT model was also used to study the 2008 Kasatochi volcanic eruption. The accuracy of HYSPLIT model trajectories is dependent on the initialization parameters. Satellite observations from passive infrared sensors are used both to produce the initialization parameters and for verification purposes. It was found that the HYSPLIT trajectory model was able adept at predicting the height and thickness of ash clouds and was also able to resolve many thin ash layers. The HYSPLIT forecast of vertical height prediction agreed with Cloud–Aerosol Lidar with Orthogonal Polarization (CALIOP) data (Crawford, et al., 2016).

This study will focus on the Calbuco volcano (see Figure 6.1), to determine, if volcanic ash from the eruption reached Durban. Calbuco is a 2015 m, active, truncated–cone composite, glacier capped, stratospheric volcano located in the Los Lagos region of the Southern Andes of Chile (41°20′S, 72°37′W) (Dussaillant, et al., 2016; Romero, et al., 2016). It was built during the last ~300 thousand years (Romero, et al., 2016). Calbuco has a history of large scale volcanic eruptions, in 1893– 95, 1906–7, 1911–12, 1917, 1932, 1945, 1961 and 1972 (Dussaillant, et al., 2016). The most recent eruption of the Calbuco volcano, occurred on 22 April 2015 at 18:04h LT. This was a major 90 minute eruption of a greyish column of ash that rose up approximately 15km above the crater. It drifted towards the north and north east (Reckziegel, et al., 2016). It and was followed by smaller eruptions on 23 April 2015 at 01:00h

LT and 30 April 2015 at 13:10h LT. The second eruption obtained a column height exceeding 15km from the crater and the direction of the plume was similar to the prior eruption. The third eruption, occurring on 30 April 2015, produced an ash column of up to 4 km above the crater and moved southeast (Reckziegel, et al., 2016). Due to the volcanic activity, villages north of the volcano, were affected by structural damage and livestock were harmed. It also causes water body contamination and disrupts air transport activities. Also, due to ash cloud dispersion, various airports in Chile cancelled flights. The eruptive process of the Chile volcano resulted in flight cancellations, respiratory problems for human and animals due to re–suspended material (Reckziegel, et al., 2016). The eruptions resulted in the evacuation of approximately 6500 people who lived 20km around the eruption site (Dussaillant, et al., 2016). The Calbuco eruption releases silicic andesite lavas, domes, block–and–ash blasts and cold and hot lahars. Calbuco is regarded as one of the most hazardous volcanoes in the Chilean Andes (Segura, et al., 2015)

This study used HYSPLIT backward trajectory analysis, aerosol optical properties derived from the sun-photometer, Lidar data and satellite imagery, to investigate if air mass parcels from the Calbuco volcano in Chile, reached Durban.

Figure 6.1 Depicts the location of the Calbuco volcano in Chile, image obtained from Google Earth.

6.2 Using HYSPLIT Trajectories to determine air mass transport of volcanic aerosols

The HYSPLIT trajectory model has provided useful information regarding the source, path and extent of pollutant emissions regionally and globally. The transportation of aerosol plumes are important for understanding the radiative properties of aerosols in regions and therefore, it is important for climate change. The distance between Durban and Los Lagos, is 8986.66 km. It takes several days for airmasses to form, and they usually form when there is high air pressure. Airmasses travelling from the Calbuco volcano, travels through marine environments and are modified significantly before reaching Durban. The time that it takes for an air mass to reach Durban, depends on meteorological conditions, such as wind speed and directions and relative humidity (Beddows, et al., 2014). Figure 6.2 and Figure 6.3 below depicts the HYSPLIT trajectory model of air mass plumes reaching Durban at the end of May, for 2014, 2015 and 2016 in different height regions. Different height regions were chosen in order to determine at what altitudes the air masses were formed at and at what part of the atmosphere the arriving plumes are located. Figure 6.2 depicts air masses at height regions from 3 km to 9 km. From Figure 6.2 it can be noted that air mass plumes, for all years are travelling from Chile in the height regions of 6 km to 9 km. This trend of air masses arriving from Chile to Durban was also noted at 3 km to 3.5 km height regions for 2014.

Figure 6.3 below depicts the HYSPLIT trajectory model for air masses reaching Durban at the end of May, for 2014, 2015 and 2016 at height regions from 10 km to 20 km. From Figure 6.3 below, it can be noted that for 2014, 2015 and 2016 air masses arrive from Chile to Durban, however they are formed in different height regions for the different years. It can be observed from Figure 6.3 that only during 2015 was air mass travelling within the height region of 20km from Chile to Durban. This could potentially be due to the volcanic activity in Calbuco, releasing aerosols directly into the stratosphere. These stratospheric aerosols can exist within the stratosphere and are transported via stratospheric winds. Stratospheric aerosols can remain in the atmosphere for longer periods (several years) than tropospheric aerosols which are only present for a few days (Junge, et al., 1961). These stratospheric aerosols then travel from Chile to South Africa and thus influence the aerosols present in these regions. Therefore it can be observed that aerosol plumes from the Calbuco volcano influences aerosol particles in Durban. From Figure 6.2 and 6.3 for May 2015, it can be seen that aerosols also originated from continental air masses as well as from marine air masses, pointing to a diversity of aerosol sources for the region. The aerosols that reach Durban, are greatly modified due to dynamic processes such as changes in aerosol size distribution. This occurs primarily due to

condensation, coagulation and gas to particle conversion. Aerosols can also modify due to the hygroscopic growth of particles in the presence of increasing relative humidity and aerosol cloud interactions (Eck, et al., 1999).

Figure 6.2 NOAA–HYSPLIT model run 720–hour backward trajectory analysis of airmass pathways at 3 km, 6 km and 9 km altitudes on 20 May, 2014, 2015 and 2016.
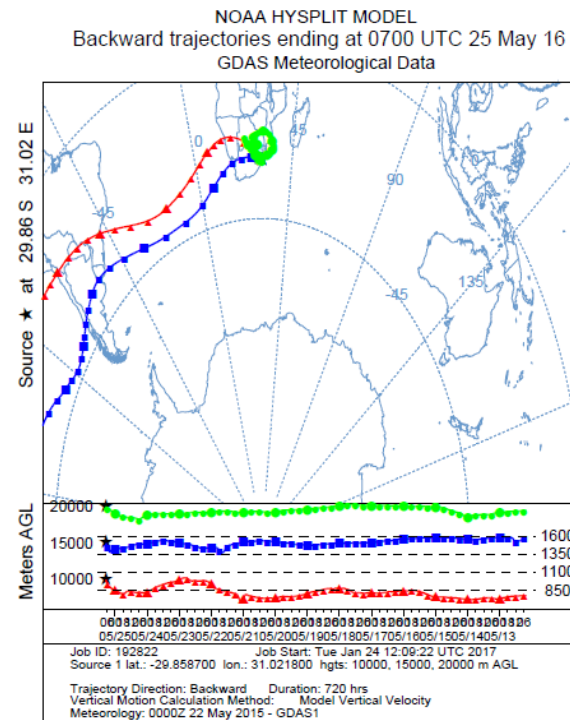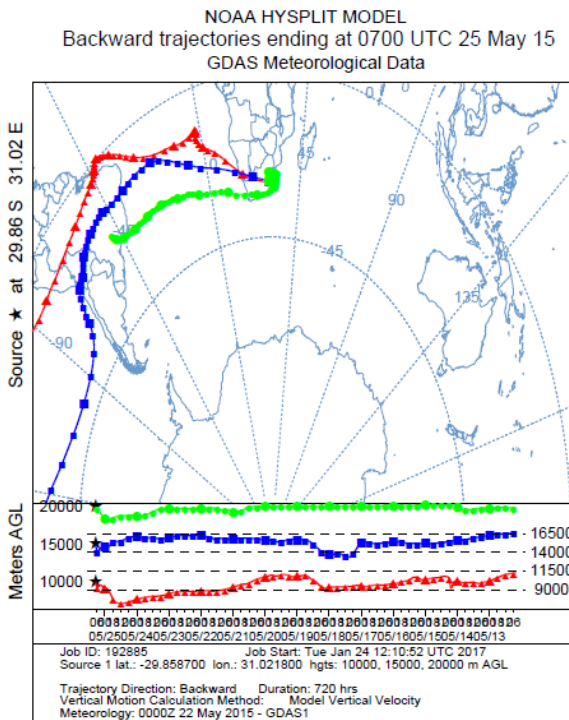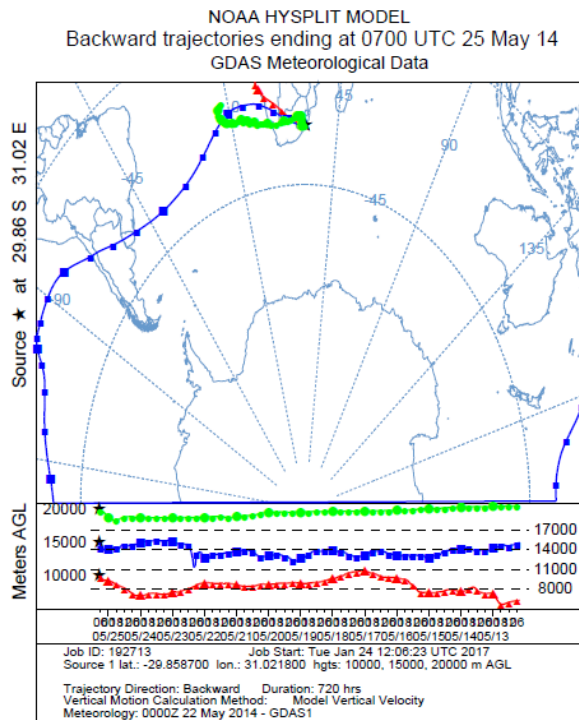
Figure 6.3 NOAA–HYSPLIT model run 720–hour backward trajectory analysis of airmass pathways at 10 km, 15 km and 20 km altitudes on 20 May, 2014, 2015 and 2016.

6.3 Using the AOD and Ångström Exponent (α) detected from the sun-photometer to determine atmospheric properties in Durban, from 1 April to 3 June for 2014, 2015 and 2016

Figure 6.4 and 6.5 below, depict the daily average AOD and α, respectively, from 1 April to 3 June for 2014, 2015 and 2016. The values were obtained from the Durban sun-photometer from AERONET, Level 2 cloud screened data. The values of AOD were obtained from the different wavelengths, namely, 1640 nm, 1020 nm, 870 nm, 675 nm, 500 nm, 440 nm, 380 nm and 340 nm. From Figure 6.4 below, it can be noted that greater AOD was observed for the smaller wavelengths. For 2014, the AOD displayed high values for the 22 April, 8 May and the 23 and 26 May. For 2014, from the 20 to the 25 May, the AOD fluctuated, with certain days displaying high AOD and other days depicting low AOD. For 2015, days with high AOD, was the 20, 24 and 25 May. For, 2015, from 20 to 25 May, it can be observed that high AOD was noted, and it was quite consistent. This consistency, could be due to a constant phenomenon, such as the entrainment of aerosols from the Calbuco volcano reaching Durban's atmosphere. For 2016, high aerosol values existed on the 18 and 26 May and from 20 to 25 May, the AOD showed fluctuations. The years 2014 and 2015, showed fluctuating AOD values towards the end of May, however, for 2015, the AOD remained constant until to the end of May. This could be due to aerosols from the Calbuco volcano reaching Durban.

Figure 6.5 below, depicts the Angstrom exponent, α, from 1 April to 3 June, for 2014, 2015 and 2016. From Figure 6.5 it can be observed that α values fluctuated from 1 April to 3 June for all years studied. For 2014, high α, existed on 22 April and 8 May, this coincided with days of high AOD. For 2015, high α, was depicted on the 20, 24 and 25 May, coinciding with days of high AOD. For 2016, high α, was also observed on days where the AOD was high, i.e., 19 and 27 May. The trend of higher AOD and higher α, deals with an increase of aerosols of fine origin into Durban. This could be due to urban industrial activities releasing fine aerosol particles into the Durban region.

The high α values, noted for 2015 at the end of May, suggests to the inclusion of aerosols that have originated from fine particles, such as from fine volcanic ash and industrial activities. From Figure 6.6, an increase in aerosol particles of fine mode origin can be noted for Durban for the month of May 2015. Additionally, from the HYSPLIT backward trajectory analysis of air mass plumes in Durban, it can be noted that air masses from the lower height regions circulate from inner parts of southern Africa, such as Pretoria, Botswana and Namibia to Durban. The HYSPLIT back trajectory, shows that in the upper troposphere, lower

stratospheric regions, air masses arrive from Chile, travelling through pristine marine environments to Durban. This would explain the presence of mixed aerosol loads in 2015, noted by the values of α.
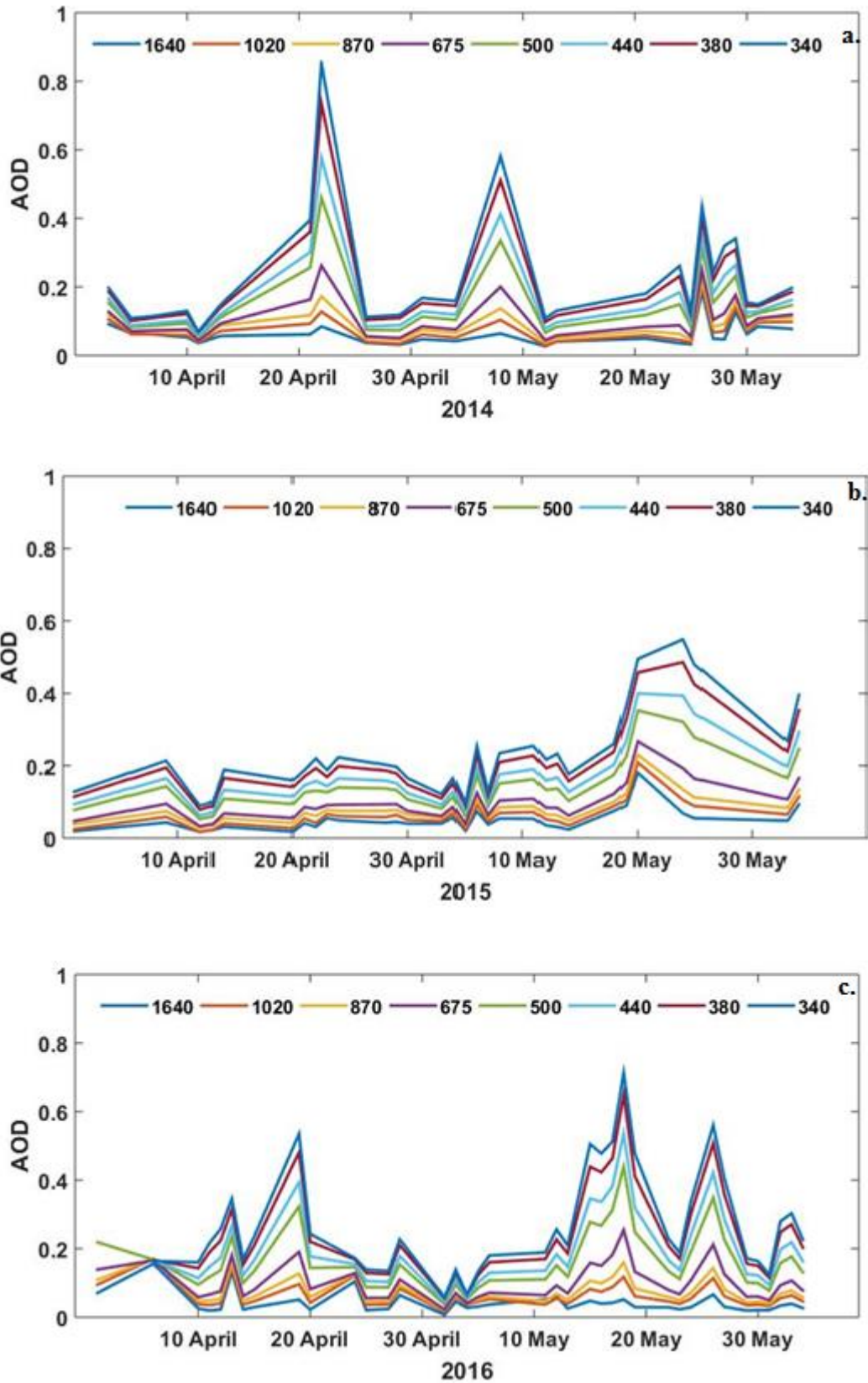
Figure 6.4 AOD from daily averages from the Durban sun-photometer from 1 April to 3 June for 2014 (a), 2015(b) and 2016(c).
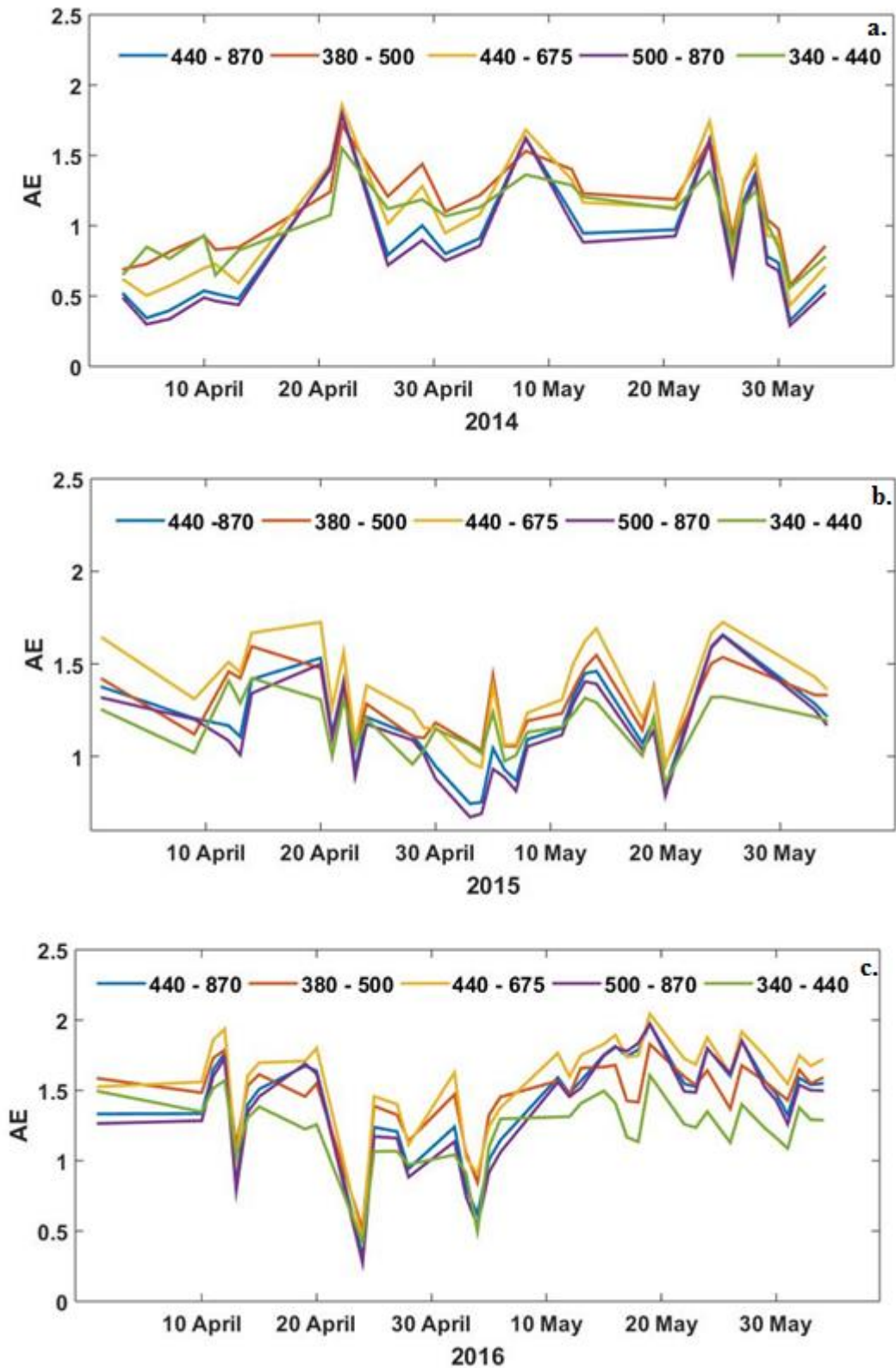
Figure 6.5 Angstrom Exponent from daily averages from the Durban sun-photometer from 1 April to 3 June for 2014 (a), 2015(b) and 2016(c).
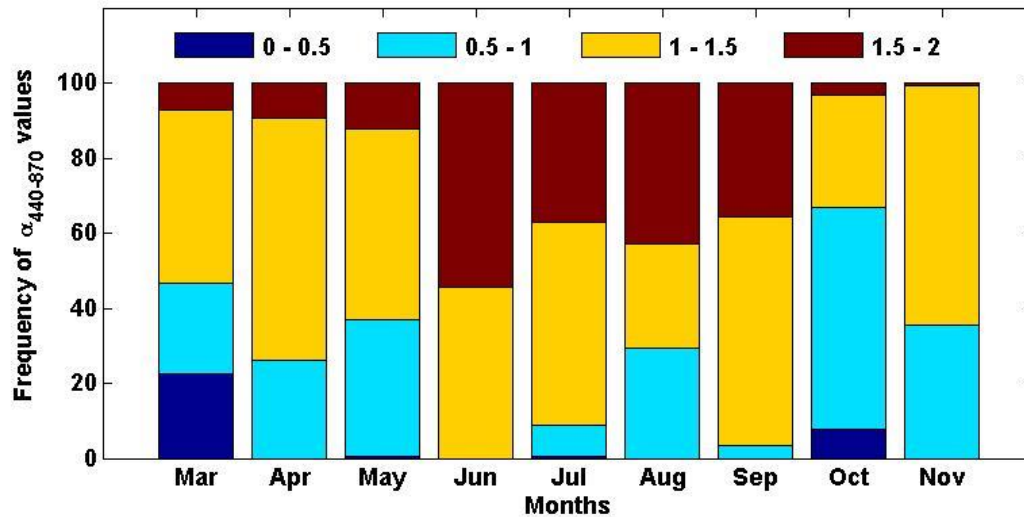
Figure 6.6 Frequency of Ångström Exponent (α440–870) values at Durban, from March to November 2015.

6.4 Using UKZN–Scanning portable 2D Lidar data to determine atmospheric properties above Durban on 14 May 2015

Atmospheric laser remote sensing uses Light Detection and Ranging (Lidar) instruments to investigate the atmosphere at altitudes of up to 120 km. The Lidar is based on the application of sensors that are modified on the basis of lasers. The development of matured pulsed laser sources has allowed range resolved measurement of atmospheric gases as well as meteorological parameters by using a short laser light pulse which is transmitted to the atmosphere in one or more wavelengths. The atmospheric volume being analysed by the laser, backscatters the laser radiation and a receiving telescope is then used to collect the backscattered portion of the laser light which occurs through elastic and inelastic processes (Moorgawa, et al., 2007). This section will make use of Lidar measurements, to study the atmosphere of altitudes of up to 5 km, for the 14 May 2015. This study will make use of Raymetric's scanning 2D portable Lidar, which is located at the University of KwaZulu–Natal's Westville campus. It consists of a transmitter with three sub–units, a laser, a beam expander with a beam trap and a beam splitter containing two highly reflective mirrors. The laser source used is a water cooled pulsed Neodymium – Yttrium Aluminium Garnet (Nd:YAG) laser which transmits short pulses at 1064 nm. The pulse repetition rate is generally 20Hz. The pulse duration is of the order of 6 – 9ns. Through the Second Harmonic Generation (SHG) 532 nm is produced and through the Third Harmonic Generation (THG) 355 nm is produced. This specific laser transmits 355 nm and rejects the rest. Therefore, the laser is

148

factory set for maximum energy output at its THG frequency (355). The laser consists of two major components: the optical head and the Power Supply Unit (PSU). They are connected together by power signal cables and water hoses for cooling the head. The receiving system consists of two sub–units, a receiving telescope and a Wavelength Separation Unit (WSU). The telescope has to amplify the weak returning signal by collecting as much light as possible. It uses a 200mm diameter Cassegrain telescope (Sivakumar, et al., 2015). More information on the laser specifications can be gained from Sivakumar, et al., (2015).

Figure 6.7, depicts a height time colour graph of the Lidar signal for 14 May 2015. This study made use of HYSPLIT 720–hour back trajectory analysis ending on 14 May 2015 at 15:00 UTC. The Lidar profile is able to depict atmospheric masses and through HYSPLIT trajectory analysis, it was possible to determine the location of air mass sources. This was done in order to determine if air mass observed by the Lidar, was sourced from the Calbuco volcano in Chile.
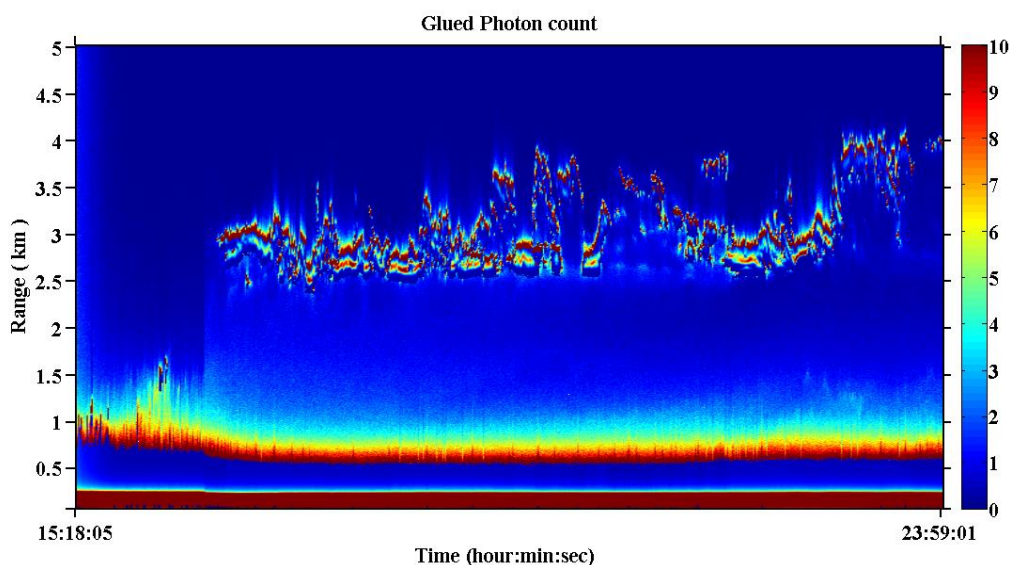
Figure 6.7 Height–time colour profile of UKZN portable LIDAR backscatter signal returns in Durban on 14 May 2015, from 15h18 to 23h59

The glued photon count refers to the merged analog and photon count signals after appropriately scaling the signal. The glued data tends to increase the detection range (Sivakumar, et al., 2009). The red colouring depicts a strong backscatter signal from the Lidar. From the analysis of the backscatter it can be noted that there was a presence of a cloud at an altitude of approximately 2 km, from 15:18 to 23:59. The cloud displayed a thickness of around 2km. Back trajectory analysis was performed using the HYSPLIT model for a period of approximately 720 hours before the 14 of May, the day of the Lidar measurement. Figure 6.8 describes the 720 hour, back trajectory analysis at height levels of 3 km, 6 km and 9 km (Figure

149

6.8a) and at height levels of 10 km, 15 km and 20 km (Figure 6.8b), ending on 14 May 2015. Lidar measurements on the same day, during 15:18 to 23:59 depicts cloud presence from 2 km to 4 km and a boundary layer at approximately 1 km. Figure 6.8a, shows that there is airmass transport from the Calbuco volcano site, at around 3 km to 4 km. This means that it is likely that the air mass noted by the Lidar, arrived from the Calbuco volcano. Air mass also arrives from northern parts of South America, within the height regions of 2 km to 9 km. In the upper height regions, air mass transport from 4.5 km to 15km originated from South America and air mass within the altitude of 20 km circulated from within South Africa. Figure 6.9 shows clouds travelling in a south westerly direction to South Africa. During winter seasons, prevailing winds, known as "westerlies" influence the weather in the southern and south–eastern coastal areas of southern Africa. When the Atlantic high pressure system moves more eastwards and remains strong, gale force winds can spread to the KwaZulu–Natal coast and towards the Mozambique Channel (Kruger, et al., 2010). This could be the reason why HYSPLIT trajectory analysis (Figure 6.2 and 6.3) observed that air mass travelled in a south–westerly direction from Chile to Durban for 2014, 2015 and 2016, at the end of May (the beginning of the winter season). These synoptic regimes, such as the presence of westerlies, supports the satellite image of cloud cover over South Africa (Figure 6.9), obtained from Eumetsat satellite imagery on 15 May 2015. The image depicts clouds travelling from a south–west direction. Therefore, the presence of westerlies and the satellite image supports the presence of aerosols from the Calbuco volcano in Chile, arriving in Durban.
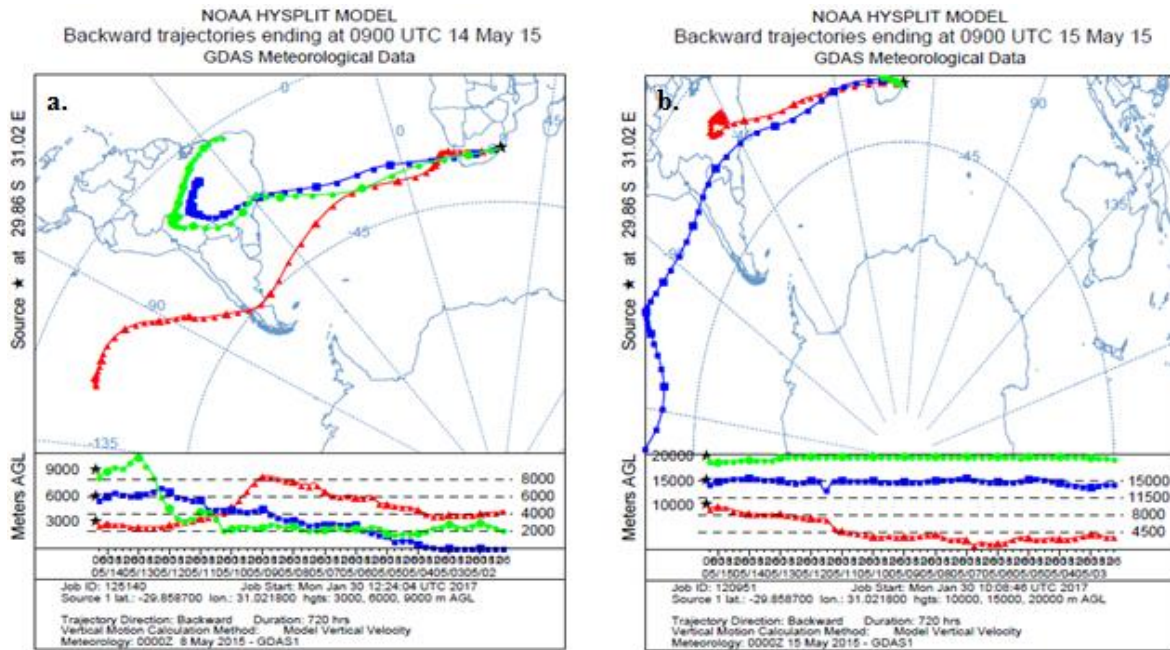
Figure 6.8 NOAA–HYSPLIT model run 720–hour backward trajectory analysis of airmass pathways at (a) 3 km, 6 km and 9 km and at (b) 10 km, 15 km and 20 km altitudes on 14 May 2015
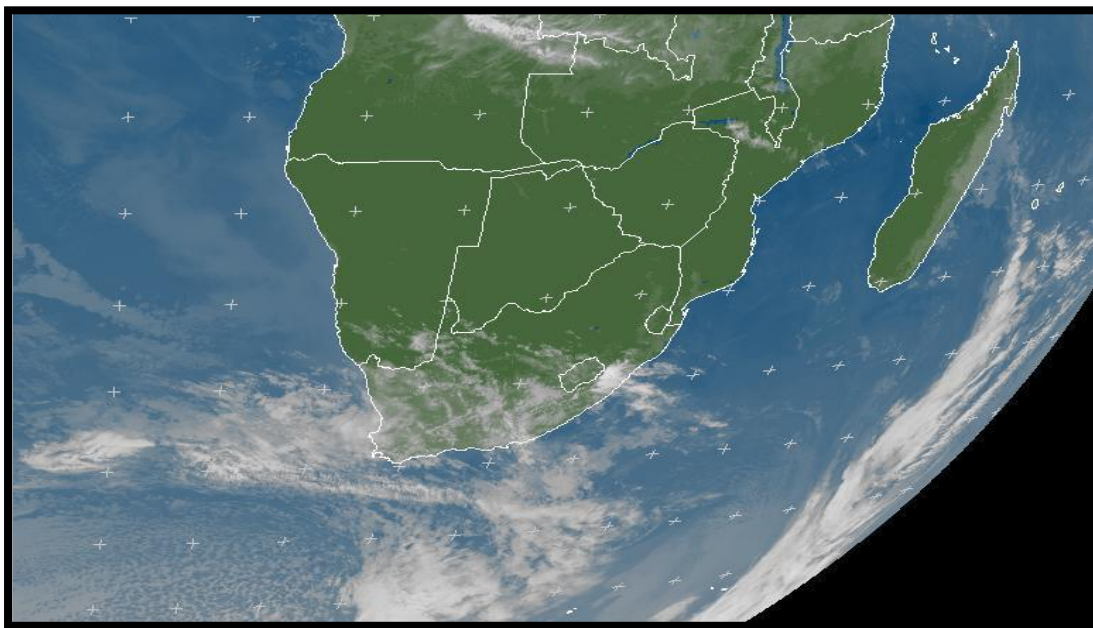
Figure 6.9 Cloud distributions in the troposphere derived from Eumetsat satellite imagery for 15 May 2015 obtained from (http://www.eumetsat.int/)

6.5 Summary

The 720 hour–backward trajectory of aerosols entering Durban was studied for 25 May 2014, 2015 and 2016, in order to determine if air masses from Chile arrives in Durban. It was noted

151

that during all years, air masses from Chile reached Durban, at various altitudes. However, it was found that only during 2015, was air masses arriving from South America, within the 20 km altitude. This lead to the assumption, that stratospheric aerosols from the Calbuco volcano, travelled to Durban. Furthermore, a reason for the aerosols arriving from Chile, is due to prevailing south–westerly winds influencing coastal regions in Southern Africa. Daily average AOD and α, values were ascertained from the sun-photometer, from 1 April to 3 June 2014, 2015 and 2016. This was done in order to determine if aerosol properties in Durban differed during 2015 than during other years. It was found that contrary to other years, AOD in Durban was constant towards the end of May. This constant was attributed to an independent factor, that being, aerosols released from the Calbuco volcano in Chile arriving in Durban towards the end of May 2015. The study also made use of Lidar observations coupled with the backward trajectory analysis allowing for the identification of the source of aerosol emissions and clouds. The meteosat image also enabled the identification of the direction air mass occurring in Durban. It was found that the clouds noted in the Lidar profile occurred around 2 km to 4 km. Additionally, the backward trajectory analysis depicted air mass travelling from the Chile volcano at the same altitude. The Eumetsat satellite image also showed clouds travelling to Durban from a south–westerly direction. This allows us to infer that the Calbuco volcano in Chile did affect aerosol loads in Durban.

CHAPTER 7

7. CONCLUSION

There has been a rise in aerosol research around the world, however, Africa is yet to catch up with the northern hemisphere with regards to aerosol research. The purpose of this study was to provide robust insight into aerosol optical properties in the Durban region, using different remote sensing instrumentation, namely the sun-photometer located at the University of KwaZulu-Natal and MODIS satellite sensors. This study analysed the preliminary results from the Durban sun-photometer to generate trends in aerosol optical properties in Durban and compared the results with the well-established sun-photometer located in Skukuza. The study also compared the AOD obtained from the Durban sun-photometer with AOD obtained from MODIS satellite data (both Aqua and Terra) using both DB and DT retrieval algorithms to determine if MODIS data can be used to analyse AOD in Durban. The study also included a case study, whereby, the sun-photometer was used to investigate if aerosols from the Calbuco Volcano in Chile arrived in Durban.

It was determined that several sources were attributed to the aerosol loads in Durban. One of the major influences on aerosol loads is the transport of biomass burning aerosols from northern parts of southern Africa. Other aerosol sources that affected the Durban region are fine mode aerosols from industrial activities and coarse mode aerosols from marine particles, dust and soot. Analysis of the trends in the α depicted smaller values for Durban, thus indicative of coarser particles in Durban than Skukuza, attributed to sea salt particles. For the trends in SSA it was found that there were low SSA values during winter due to an increase in wood burning and the onset of southern Africa's biomass burning season. From analysis of the SSA at Skukuza it was found that there are more scattering type aerosols during autumn and summer and less scattering during winter and spring. The decrease in scattering could be due to an increase in absorbing type aerosols from biomass burning. Analysis of the asymmetry parameter (g), depicted low values for the winter months in Durban and the spring months in Skukuza – suggesting an increase in fine mode absorbing type pollutants.

Analysis of the complex index of refraction for Durban, during winter, found that the real (re) part ranges from 1.45 to 1.47 and the imaginary (im) part ranges from 0.01 to 0.02. During winter for Skukuza, values range from 1.44 to 1.46 (re) and from 0.014 to 0.015 (im). Analysis of the values suggest it was consistent with urban industrial aerosol and biomass burning aerosols for Durban and Skukuza during winter. For Skukuza during summer, values range

from 1.38 to 1.39 (re) and 0.003 (im), for autumn values were around 1.4 (re) and around 0.006 (im). The low imaginary part values suggests aerosols that are of urban industrial origin, as well as coarse, scattering type aerosols from dust (Wagner, et al., 2012). The re and im values observed for Skukuza during spring were in line with mixed aerosol loads such as biomass burning and urban industrial (Dubovik & King, 2000).

The radiative forcing values depicted for Durban, indicated positive values for March and April thus suggesting a net warming effect and negative values from May to September, thus indicative of a net cooling effect. For Skukuza, from January to December, the monthly mean RF was negative, suggesting a net cooling effect. The net cooling effect noted for Durban during August, is probably due to an increase in scattering type aerosols, reflecting radiation away from the surface. The increase in pollutants during August could be due to the stable weather conditions noted for August, increasing the presence of key scattering type aerosols from urban industrial emissions. For Skukuza, the months with the highest average AOD, namely, August, September and October also experienced the highest ARF and lowest SSA, probably due to absorbing aerosols released from biomass burning emissions. In terms of forcing efficiency, for Durban during March and April the forcing efficiency at the bottom of the atmosphere is positive which is common for absorbing aerosol types. However, different types of absorbing aerosols creates warming of different magnitudes. Therefore, aerosols released from biomass burning decrease the radiative forcing at the TOA, and, since September is the biomass burning season, it has a net cooling effect at the TOA. Absorbing pollutants released from fossil fuel burning have a warming effect, increasing radiative forcing, hence, the net warming effect observed for March and April at the TOA for Durban.

For Skukuza, certain high mean values of forcing efficiency at the BOA were associated with the months with the lowest AOD, namely, May and June. This could be because the aerosols more efficient at the surface are absorbing aerosol types associated with biomass burning. At the TOA it is observed that the more absorbing type aerosols present, depict lower FE values. This is because the higher absorption of these aerosol types, decreases the energy available to be backscattered towards the upper limit of the atmosphere and into space, thus maintaining a higher percentage of solar energy in the atmosphere.

This study also utilised 7-day backward trajectories for Durban, on the days with high AOD and on the days with low AOD during the study period, in order to determine what influences aerosol loads arriving in Durban. On days with high AOD, namely 12 August 2014 and 20

February 2014, air mass arrived from Mozambique, Botswana, from northern, drier areas of South Africa and from Madagascar. On days with low AOD, namely 5 June 2014 and 3 September 2014, air mass at the surface is recirculated within South Africa, and origin from Botswana and Namibia through long-range transport of maritime aerosols, occurring at different altitudes. Long range transport of air plumes can also be observed to originate from Chile and Argentina.

Comparison of sun-photometer derived AOD with MODIS Terra, MODIS Aqua and a merged dataset (the average of MODIS Aqua and Terra), for both algortithms (DT and DB) was undertaken in order to determine if MODIS satellite retrievals can be used as a subtle proxy for ground based measurements. DB had an R^2 of 0.70 and DT had an R^2 of 0.60 for the Terra sensor. DT had an R^2 of 0.78 and DB had an R^2 of 0.68 for the Aqua sensor. For the aqua and terra merged dataset DB performed better with a higher R^2 of 0.79 than DT with a R^2 of 0.74. From the correlations it was noted that MODIS can act as a subtle proxy for sun-photometer measurements of AOD in Durban because modertae to good correlations were observed. However, MODIS show an underestimate AOD and this was attributed to sensor calibration errors, an unsuitable assumption about the ground surface reflection, and inconsistencies between the aerosol microphysical and optical properties used in the retrieval algorithm. Also, algorithm performance tends to be dependent on season and regions.

The last objective of the study was to determine if the Durban sun-photometer could pick up aerosols reaching Durban as a result of the Calbuco volcanic eruption in Chile in late April 2015. It was found from performing HYSPLIT 720 hour–backward trajectory analysis that at the end of May 2015, air masses in the upper stratospheric region of 20 km arrived from Chile to Durban. Further analysis of meteosat imagery of southern Africa, depicted clouds travelling to Durban from a south–westerly direction from Chile. This is probably due to prevailing south–westerlies wind which impact coastal regions in southern Africa. Daily average AOD and α, values were analysed from the Durban sun–photometer, from 1 April to 3 June 2014, 2015 and 2016. It was found that AOD in Durban was constant towards the end of May 2015 and this was attributed to an independent factor, namely, aerosols released from the Calbuco volcano in Chile. The study also made use of Lidar observations coupled and backward trajectory analysis and it was found that the clouds noted in the Lidar profile occurred around 2 km to 4 km. The backward trajectory analysis also depicted air mass travelling from the Chile at the same altitude. Therefore, it was ascertained that aerosols from the Calbuco Volcano arrived in Durban at the end of May 2015.

This study used various instruments to determine aerosol optical properties for the region of Durban, the results provided a robust insight into the aerosol properties related to Durban. The study achieved the objective of understanding aerosol properties in Durban. It was determined that there are many factors influencing aerosol properties in the region, such as synoptic climatology, industrial pollutants, seasonality, distance to the sea and altitude. Another objective was to compare aerosol optical properties in Durban with that of Skukuza. The results showed that there were many similarities in the aerosols that affect both regions, such as the influence of biomass burning during certain seasons. However, Skukuza appeared to be affected more by industrial pollutants than Durban, due to the Highveld being in close proximity to Skukuza. Durban, being a coastal region was affected more by marine aerosol species than Skukuza. The study also identified the sources if pollutants entering Durban using the HYSPLIT trajectory model. The study also proposed to compare AOD obtained from the Durban sun-photometer with satellite based measurements and it was found that the, similar to previous studies, MODIS compared well with sun-photometer derived AOD. However, the accuracy of the result is dependent on the location, sky-conditions, time of year and satellite sensor characteristics. Moreover, the study, further investigated the atmosphere above Durban and found that air mass plumes from the Calbuco volcanic eruption in Chile, impacted Durban due to prevailing south–westerlies transporting air mass plumes to Durban.

Further studies need to focus on long term climatological data, spanning several years of sun-photometer data for Durban. This will be made to provide a robust picture of aerosol properties in Durban. Also, comparisons between MODIS and sun-photometer derived AOD needs to continuously be performed to ensure that MODIS is predicting AOD adequately in the Durban region.

References

Abel, S. J., Highwood, E. J., Haywood, J. M. & Stringer, M. A., 2005. The direct radiative effect of biomass burning aerosols over southern Africa. *Atmospheric Chemistry and Physics,* Volume 5, pp. 1999 - 2018.

Adesina, A. J., Kumar, K. R., Sivakumar, V. & Griffith, D., 2014. Direct radiative forcing of urban aerosols over Pretoria (25.75° S, 28.28° E) using AERONET Sunphotometer data: First scientific results and environmental impact. *Journal of Environmental Sciences,* 26(12), pp. 2459 - 2474.

Adesina, J. A., Kumar, K. A. & Sivakumar, V., 2016. Aerosol-Cloud-Precipitation Interactions over Major Cities in South Africa: Impact on Regional Environment and Climate Change. *Aerosol and Air Quality Research,* 16(10), pp. 195 - 211.

Adesina, J. A., Kumar, K. A., Sivakumar, V. & Piketh, S. J., 2016. Intercomparison and assessment of long-term (2004 - 2013) multiple satellite aerosol products over two contrasting sites in South Africa. *Journal of Atmospheric and Solar-Terrestrial Physics,* 148(10), pp. 82 - 95.

Adesina, J. A., Kumar, K. R. & Sivakumar, V., 2015. Variability in aerosol optical properties and radiative forcing over Gorongosa (18.97 - 34.35 degrees) in Mozambique. *Meteorology and Atmospheric Physics,* 2(2), pp. 217 - 228.

Adler, G. et al., 2011. Chemical, physical, and optical evolution of biomass burning aerosols: a case study. *Atmospheric Chemistry and Physics,* 11(18), pp. 1491-1503.

AERONET, 2015. *AERONET.* [Online] Available at: aeronet.gsfc.nasa.gov/ [Accessed 29 June 2015].

Anderson, S. M. et al., 2013. Composition and evolution of volcanic aerosol from eruptions of Kasatochi, Sarychev and Eyjafjallaj¨okull in 2008–2010 based on CARIBIC observations. *Atmospheric Chemistry and Physics,* 13(4), pp. 1781 - 1796.

Andreae , M. O. & Crutzen, P. J., 1997. Atmospheric aerosols: Biogeochemical sources and role in atmospheric chemistry. *Science,* pp. 1052 - 1058.

Ångström, A., 1964. The parameters of atmospheric turbidity. *Tellus,* 16(1), pp. 64 - 75.

Bauer, S. E. et al., 2007. Nitrate aerosols today and in 2030: a global simulation including aerosols and tropospheric ozone. *Atmospheric Chemistry and Physics,* 7(19), pp. 5043 - 5059.

Baumgardner, D. et al., 2011. Airborne instruments to measure atmospheric aerosol properties, clouds and radiation: A cook's tour of mature and emerging climatology. *Atmospheric Research,* Volume 102, pp. 10 - 29.

Beddows, D. C. et al., 2014. Variations in tropospheric submicron particle size distributions across the European continent 2008 - 2009. *Atmospheric Chemistry and Physics,* 14(8), pp. 4327 - 4348.

Ben-Ami, Y. et al., 2010. Transport of North African dust from the Bodélé depression to the Amazon Basin: a case study. *Atmospheric, Chemistry and Physics,* 10(10), pp. 7533 - 7544.

Bencherif, H. et al., 2000. First validation of stratospheric temperature profiles obtained by a Rayleigh LIDAR over Durban, South Africa. *South African Journal of Science ,* Volume 96, pp. 487 - 492.

Bencherif, H. et al., 2003. LIDAR observations of lower stratospheric aerosols over South Africa linked to large scale transport across the southern subtropical barrier. *Journal of Atmospheric and Solar-Terrestrial Physics,* 65(6), pp. 707 - 715.

Berne, B. J. & Pecora, R., 2000. *Dynamic light scattering: with applications to chemistry, biology and physics.* s.l.:Courier Corporation.

Bibi, H. et al., 2015. Intercomparison of MODIS, MISR, OMI, and CALIPSO aerosol optical depth retrievals for four locations on the Indo-Gangetic plain and validation against AERONET data. *Atmospheric Environment ,* Volume 111, pp. 113 - 126.

Boucher, O., 2015. *Physical,. Chemical and Optical Properties of aerosols.* Netherlands: Springer .

Boucher, O. et al., 2007. Clouds and Aerosols. In: T. F. Stocker , et al. eds. *Climate Change 2013: The Physical Science Basis. Contribution to Working Group I to the Fifth Assessment Report of the Intergovernmental Panel on Climate Change.* Cambridge: Cambridge University Press, pp. 571 - 657.

Bruhl, C., Lelieveld, J., Crutzen, P. J. & Tost, H., 2012. The role of carbonyl as a source of stratospheric sulphate aerosol and its impact on climate. *Atmospheric Chemistry and Physics,* 12(3), pp. 1239 - 1253.

Calvo, A. I. et al., 2013. Research on aerosol sources and chemical composition: Past, current and emerging issues. *Atmospheric Research,* 1(28), pp. 120 - 121 .

Cheng, C. S. et al., 2007. A synoptic climatological approach to assess climatic impact on air quality in south-central Canada. Part I: historical analysis.. *Water, Air, and Soil Pollution,* 182(1 - 4), pp. 131 - 148.

Chin, M. et al., 2014. *NASA Technical Reports Server (NTRS).* [Online] Available at: http://ntrs.nasa.gov/search.jsp?R=20150000360 [Accessed 14 12 2016].

Chin, M., Diehl, T., Bian, H. & Kucsera, T., 2016. Aerosols in the Atmosphere: Souces, Transport, and Multi-decadal Trends. In: D. G. Steyn & N. Chaumerliac, eds. *Air Pollution Modeling and its Application XXIV.* Switzerland: Springer International Publishing, pp. 3 - 10.

Chin, M. et al., 2002. Tropospheric Aerosol Optical Thickness from the GOCART model and Comparisons with Sun photometer Measurements. *American Meteorological Society,* Volume 59, pp. 461 - 482.

Chu, D. A. et al., 2002. Validation of MODIS aerosol optical depth retrieval over land. *Geophysical Research Letters ,* Volume 29, pp. 1612 - 1617.

Cook, J. & Highwood, E. J., 2004. Climate response to tropospheric absorbing aerosols in an intermediate general-circulation model. *Quarterly Journal of the Royal Meteorological Society,* 130(569), pp. 175 - 191.

Crawford, A. M., Stunder, B. J., Ngan, F. & Pavolonis, M. J., 2016. Initializing HYSPLIT with satellite observations of volcanic ash: A case study of the 2008 Kasatochi eruption. *Journal of Geophysical Research: Atmospheres,* 121(10), pp. 786 - 803.

Creamean, J. M. et al., 2013. Dust and biological aerosols from the Sahara and Asia influnce precipitation in the western US. *science,* 339(6127), pp. 1572 - 1578.

Dall'Osto, M. et al., 2012. Nitrogenated and aliphatic organic vapors as possible drivers for marine secondary organic aerosol growth. *Journal of Geophysical Research,* pp. 1 - 10.

DEA, 2013. *2013 State of Air in South Africa Report – Summary,* South Africa: Department of Environmental Affairs.

Deboudt, K. et al., 2010. Mixing state of aerosols and direct observation of carbonaceous and marine coatings on African dust by individual particle analsis. *Journal of Geophysical Research,* Volume 115, pp. 1 - 14.

Després, V. R. et al., 2012. Primary biological aerosol particles in the atmosphere: a review. *Tellus B ,* 22(64), pp. 1 - 58.

Deutscher Wetterdienst , 2010. *DWD.* [Online] Available at: http://www.dwd.de/ [Accessed 12 11 2016].

Diab, R. D. & Motha, A., 2007. An analysis of key institutional factors influencing air quality in South Durban using the DPSIR framework. *South African Geographical Journal ,* 89(1), pp. 22 - 33.

Diab, R. D., Rahman, M. Z., Moorgawa, A. & Freiman, M. T., 2003. First measurements of tropospheric aerosol profiles above Durban using a LIDAR. *South African Journal of Science,* Volume 99, pp. 168 - 172.

Diner, D. J. et al., 2001. MISR aerosol optical depth retrievals over southern Africa during the SAFARI-2000 dry season campaign. *Geophysical Research Letters,* Volume 28, pp. 3127 - 3130.

Draxler, R. R. & Hess, G. D., 1998. An overview of the HYSPLIT_4 modelling system for trajectories, dispersion and deposition.. *Australian Meteorological Magazine ,* 47(4), pp. 295 - 308.

Draxler, R. R. & Rolph, G. D., 2003. *HYSPLIT Model Access via NOAA ARL Website.* [Online] Available at: (http://www.arl.noaa,gov/ready/hysplit4.html) [Accessed 20 July 2016].

Dubovik, O. et al., 2002. Variability of absorption and optical properties of key aerosol types observed in worldwide locations. *Journal of the atmospheric sciences,* 59(3), pp. 590 - 608.

Dubovik, O. & King, M. D., 2000. A flexible inversion algorithm for retrieval of aerosol optical properties from Sun and sky radiance measurements. *Journal of Geophysical Research: Atmospheres (1984 - 2012),* 105(D16), pp. 20673 - 20696.

Dubovik, O. et al., 2000. Accuracy assessments of aerosol optical properties retrieved from Aerosol Robotic Network(AERONET) Sun and sky radiance measurements. *Journal of Geophysical Research,* 105(D8), pp. 9791 - 9806.

Dussaillant, A. et al., 2016. Causes, Dynamics, Impacts of Lahar Mass Flows due to the April 2015 Eruption of Calbuco Volcani Chile. *Geophysical Research Abstract,* 18(3), p. 14924.

Du, Y., Ulbay, F. T. & Dobson, M. C., 2000. Sensitivity to soil moisture bt active and passive microwave sensors. *Geoscience and Remote Sensing, IEEE Transactions ,* 38(1), pp. 105 - 114.

Eck, T. F. et al., 1999. Wavelength dependence of the optical depth of biomass burning, urban, and desert dust aerosols. *Journal of Geophysical Research,* 104(D24), pp. 333 - 349.

Eck, T. F. et al., 2013. A seasonal trend of single scattering albedo in southern African biomass-burning particles: Implications for satellite prodicts and estimates of emissions for the worlds largest biomass-burning source. *Journal of Geophysical Research: Atmospheres,* 118(10), pp. 6414-6432.

Eck, T. F. et al., 2003. Variability of biomass burning aerosol optical characteristics in southern Africa during the SAFARI 2000 dry season campaign and a comparison of single scattering albedo estimates from radiometric measurements. *Journal of Geophysical Research,* 108(D13), pp. 13 - 21.

Eichelberger, S., McCaa, J., Nijssen, B. & Wood, A., 2008. *Climate Change Effects on Wind Speed,* s.l.: Zackin Publications Inc.

Escudero, M. et al., 2006. Determination of the contribution of northern Africa dust source areasto PM10 concentrations over the central Iberian Peninsula using the Hybrid Single-Particle Lagrangian Integrated Trajectory model. *Journal of Geophysical Research,* Volume 111, pp. 1 - 15.

eThekwini Municipality, 2006. *eThekwini Air Quality Monitoring Network, Annual Report,* Durban: Pollution Control Support Section.

Fernández, C., Garcia, S., Picaud, S. & Devel, M., 2015. Calculations of the mass absorption cross sections for carbonaceous nanoparticles modelling soot. *Journal of Quantitative Spectroscopy and Radiative Transfer,* Volume 164, pp. 69 - 81.

Fiebig, M. & Ogren, J. A., 2006. Retrieval and climatology of the aerosol asymmetry parameter in the NOAA aerosol monitoring network. *Journal of Geophysical Research: Atmospheres ,* 111(D21), pp. 1984 - 2012.

Formenti, P., Andreae, M. O. & Lelieveld, J., 2000. Measurements of aerosol optical depth above 3570 m asl in the North Atlantic free troposphere: results from ACE-2.. *Tellus B,* 52(2), pp. 678 - 693.

Freiman, M. T. & Piketh, S. J., 2002. Air transport into and out of the Industrial Highveld Region of South Africa. *Journal of Applied Meteorology,* 42(7), pp. 994 - 1002.

Freiman, M. T. & Piketh, S. J., 2003. Air transport into and out of the industrial Highveld region of South Africa. *Journal of applied Meteorology,* 42(7), pp. 994 - 1002.

Gadhavi, H. & Jayaraman, A., 2010. Absorbing aerosols: contribution of biomass burning and implications for radiative forcing. *Annales Geophysicae,* Volume 28, pp. 103 - 111.

Garcia , O. E. et al., 2012. Shortwave radiative forcing and efficiency of key aerosol types using AERONET data. *Atmospheric Chemistry and Physics ,* Volume 12, pp. 5129 - 5145.

Gillette, D. A. & Goodwin , P. A., 1974. microscale transport of sand sized soil aggregates eroded by wind. *Journal of Geophysical Research,* Volume 79, pp. 4080 - 4084.

Ginoux, P. et al., 2001. Sources and distributions of dust aerosols simulated with the GOCART model. *Journal of Geophysical Research,* 106(17), pp. 255 - 273.

Goudie, A. S. & Viles, H. A., 2013. *The earth transformed: an introduction to human impacts on the environment.* 5 ed. Oxford: John Wiley and Sons.

Greenberg, J. P. et al., 2003. Eddy flux and leaf-level measurements of biogenic VOC emissions from mopane woodland of Botswana. *Journal of Geophysical Research Letters,* 108(D13), p. 8468.

Guastella, L. & Knusden, S., 2007. *South Durban Multi-point Plan - Case Study.* Durban, Department of Environmental Affairs and Tourism.

Hallquist, M. et al., 2009. The formation, properties and impact of secondary organic aerosol: current and emerging issues. *Atmospheric Chemistry and Physics,* 9(14), pp. 5155 - 5236.

Halthore, R. N., Eck, T. F., Holben, B. N. & Markham, B. L., 1997. Sun photometric measurements of atmospheric water vapor column abundance in the 940-nm band. *Journal of Geophysical Research- All Series,* Volume 102, pp. 4343 - 4352.

Hand, V. L. et al., 2010. Evidence of internal mixing of African dust and biomass burning particles by individual particle analysis using electron beam techniques. *Journal of Geophysical Research,* 115(10), pp. 1 - 11.

Hao, W. M. et al., 2005. Comparison of aerosol optical thickness measurements by MODIS, AERONET sun photometers, and Forest Service handheld sun photometers in southern Africa during the SAFARI 2000 campaign. *International Journal of Remote Sensing,* 26(19), pp. 4169 - 4183.

Haywood, J. & Boucher, O., 2000. Estimates of the direct and indirect radiative forcing due to tropospheric aerosols: A review. *Reviews of Geophysics,* 38(4), pp. 513 - 543.

Heintzenberg, J., 2003. Physics and Chemistry of Aerosols. *Elsevier Science,* pp. 34 - 40.

Hersey, S. P. et al., 2015. An overview of regional and local characteristics of aerosols in South Africa using satellite, ground, and modeling data. *Atmospheric Chemistry and Physics,* 15(10), pp. 4259 - 4278.

Hinds, W. C., 2012. *Aerosol technology: properties, behaviour, and measurement of airborne particles.* 2 ed. New York: John Wiley and Sons.

Holben, B. N. et al., 2001. An emerging ground-based aerosol climatology: Aerosol Optical Depth from AERONET. *Journal of Geophysical Research,* 106(D11), pp. 12.067 - 12.097.

Houghton, J. et al., 2001. *IPCC 2001: Climate Change 2001. The Climate Change Contribution of Working Group I to the Third Assessment Report of the Intergovernmental Panel on Climate Change,* s.l.: IPCC.

Hsu, C. N., Tsay, S. C., King, D. M. & Herman, J. R., 2004. Aerosol properties over bright-reflecting source regions. *IEE Transactions on Geoscience and Remote Sensing ,* Volume 2, pp. 557 - 569.

Hyvärinen, A. P. et al., 2011. Effect of the summer monsoon on aerosols at two measurement stations in Northern India–Part 2: Physical and optical properties. *Atmospheric Chemistry and Physics,* 11(16), pp. 8283-8294.

Ichoku, C., Kaufman, Y. J., Remer, L. A. & Levy, R., 2004. Global aerosol remote sensing from MODIS. *Advances in Space Research,* Volume 34, pp. 820 - 827.

Ichoku, I. et al., 2003. MODIS observation of aerosols and estimation of aerosol radiative forcing over southern Africa during SAFARI 2000. *Journal of Geophysical Research,* 108(D13), pp. 1 - 13.

IRIN, 2014. *Environment and Disasters.* [Online] Available at: http://www.irinnews.org/ [Accessed 13 11 2016].

Jamieson, R. A., Baldini, J. U., Frappiera, A. B. & Muller, W., 2015. Volcanic ash fall events identified using principal component analysis of a high-resolution speleothem trace element dataset. *Earth and Planetary Science Letters,* Volume 426, pp. 36 - 45.

Jenkins, S. F. et al., 2015. Volcanic ash fall hazard and risk. In: S. C. Loughlin, et al. eds. *Global Volcan Hazards and Risks.* United Kingdom: Cambridge University Press, p. 173.

Jeong, M. J., Chu, D. A. & Tsay, S. C., 2005. Quality abd comparability analyses of global aerosol products derived from the advanced very high resolution radiometer and Moderate Resolution Imaging Spectroradiometer. *Journal of Geophysical Research,* 110(D10), pp. 1984 - 2012.

Junge, C. E., Chagnon, C. W. & Manson, J. E., 1961. Stratospheric Aerosols. *Journal of Meteorology,* Volume 18, pp. 81 - 108.

Kahn, R. A. et al., 2009. MISR Aerosol Product Attributes and Statistical Comparisons With MODIS. *IEEE Transactions on Geoscience and Remote Sensing ,* 47(12), pp. 4095 - 4114.

Kang, H. et al., 2013. Analysis of a long-lasting haze episode in Nanjing, China. *Atmospheric Research,* 28(120), pp. 78 - 87.

Kanike, R. K. & Sivakumar, V., 2015. *Remote Sensing of Aerosols using Sunphotometer: Optical Properties, Aerosol Types and Sources.* Germany: LAMBERT Academic Publishing.

Kaufman, Y. J., Tanre, D. & Boucher, O., 2002. A satellite view of aerosols in the climate system. *Nature,* 419(6903), pp. 215 - 223.

Kaufman, Y. J. et al., 1997. Passive remote sensing of tropospheric aerosol and atmospheric correction for the aerosol effect. *Journal of Geophysical Research: Atmospheres,* 102(D14), pp. 16815 - 16830.

Koch, D. & Del Genio, A. D., 2010. Black carbon semi-direct effects on cloud cover: review and synthesis. *Atmospheric Chemistry and Physics,* 10(16), pp. 7685 - 7696.

Kok, J. F., Parteli, E. J., Michaels, T. I. & Karam, D. B., 2012. The physics of wind-blown sand and dust. *Reports on Progress in Physics,* 75(10), p. 106901.

Koppmann, R. et al., 1996. Airborne measurements of organic trace gases from savanna fires in southern Africa during SAFARI-92. *Biomass Burning and Global Change,* Volume 1, pp. 303 - 319.

Kotchenruther, R. A. & Hobbs, P. V., 1998. Humdification factors of aerosols from biomass burning in Brazil. *Journal of Geophysical Research Letters,* 103(32), pp. 81 - 89.

Krintz, I. A. et al., 2014. *A study of Aerosol Optical and Chemical Properties from the Perspectives of Source Region, Local, and Synoptic Meteorology During Summer 2013 at Southeast US Regionally Representative Site,* United States: American Geophysical Union.

Kruger, A. C., Goliger, A. M., Retief, J. V. & Sekele, S., 2010. Strong wind climatic zones in South Africa. *Wind and Structures,* 13(1), pp. 1 - 19.

Kruger, A. C., Makamo, L. B. & Shongwe, S., 2002. An analysis of Skukuza climate data. *Koedoe,* 45(1), pp. 1 - 7 .

Kulmala, M. et al., 2001. On the formation, growth and composition of nucleation mode particles. *Tellus,* pp. 479 - 490 .

Kumar, K. R. et al., 2013. Inferring Wavelength Dependence of Angstrom Exponent over a subtropical Station in South Africa Using AERONET data: Influence of Meteorology, Long range Transport and Curvature Effect. *Science of the Total Environment,* Volume 461 - 462, pp. 397 - 408.

Kumar, K. R. et al., 2014b. Long-term (2003-2013) climatological trends and variations in aerosol optical parameters retrieved from MODIS over three stations in South Africa. *Atmospheric Environment,* Volume 95, pp. 400 - 408.

Kumar, K. R. et al., 2014a. Identification and classification of different aerosol types over a subtropical rural site in Mpumalanga, South Africa: seasonal variations as retrieved from AERONET Sunphotometer. *Aerosol and Air Quality Research,* 14(1), pp. 108 - 123.

Kumar, K. R. et al., 2015a. Aerosol climatology and discrimination of aerosol types retrieved from MODIS, MISR and OMI over Durban (29.88° S, 31.02° E) South Africa.. *Atmospheric Environment,* Volume 117, pp. 9 - 18.

Kumar, M. et al., 2015b. Wintertime characteristics of aerosols at middle Indo-Gangetic Plain: Impacts of regional meteorology and long range transport. *Atmospheric Environment,* 104(31), pp. 162 - 175.

Laakso, L. et al., 2012. South African EUCAARI measurement: seasonaly variation of trace gases and aerosol optical properties. *Atmospheric Chemistry and Physics,* 12(110), pp. 1847 - 1864.

Latha, R. et al., 2014. Aerosol Optical Properties and Composition over a Table Top Complex Mining Area in a Monsoon Through Region. *Aerosol and Air Quality Research,* Volume 14, pp. 806 - 817.

Lee, K. H., Li, Z., Kim, Y. J. & Kokhanovsky, A., 2009. *Atmospheric aerosol monitoring from satellite observations: a history of three decades.* Netherlands : Springer .

Lee, K. H., Li, Z., Kim, Y. J. & Kokhanovsky, A., 2009. Atmospheric Aerosol Monitoring from Satellite Observations: A History of three decades. In: Y. J. Kim, ed. *Atmospheric and biological monitoring.* Netherlands: Springer, pp. 13 - 38.

Lee-Tayler, J. et al., 2015. Multiday production of condensing organic aerosol mass in urban and forest outflow.. *Atmospheric Chemistry and Physics ,* Volume 15, pp. 595 - 615.

Lehola, P., 2012. *Census 2011 Municipal Report KwaZulu-Natal.* [Online] Available at: http://www.statssa.gov.za/census/census_2011/census_products/KZN_Municipal_Report.pdf [Accessed 22 03 2017].

Li, Z. et al., 2011. Long-term impacts of aerosols on the vertical development of clouds and precipitation. *Nature Geoscience,* 4(12), pp. 1 - 7.

Lloret, J. & Valiela, I., 2016. Unprecedented decrease in deposition of nitrogen oxides over North America: the realtive effects of emission controls and prevailing air-mass trajectories. *Biogeochemistry,* 129(1), pp. 165-180.

Long, C. M., Nascarella, M. A. & Valberg, P. A., 2013. Carbon black vs. black carbon and other airborne materials containing elemental carbon: Physical and chemical distinctions. *Environmental Pollution,* 181(9), pp. 271 - 286.

Lushnikov, A. A., 2010. Introduction to aerosols. In: *Aerosols: Science and Technology.* Germany: Wiley - VCH, p. 492.

Macmillan, 2014. *Subtropical anticyclones and associated weather conditions.* [Online] Available at: http://learn.mindset.co.za/sites/default/files/resourcelib/emshare-show-note-asset/LXL_Gr12Geography_03_Subtropical
[Accessed 12 12 2015].

Mafusire, G. et al., 2016. Submicrometer aerosols and excess CO as tracers for biomass burning air mass transport over southern Africa. *Journal of Geophysical Research: Atmospheres,* 121(10), pp. 262 - 282.

Magi, B., Hobbs, P. V., Schmid, B. & Redemann, J., 2003. Vertical profiles of light scattering, light absorption and single scattering albedo during the dry, biomass burning season in southern Africa and comparisons of in situ measurements of aerosol optical depths. *Journal of Geophysical Research,* 108(D13).

Manikandan, S., 2011. Frequency Distrubution. *Journal of Pharmacology and Pharmacotherapeutics,* 2(1), pp. 54 - 56.

McMurry, P. H., 1999. A review of atmospheric aerosol measurements. *Atmospheric Environment,* 34(2000), pp. 1959 - 1999 .

Meskhidze, N. et al., 2011. Global distribution and climate forcing of marine organic aerosols: 1. Model improvements and evaluation. *Atmospheric Chemistry and Physics,* 11(11), pp. 11689 - 11705.

Montilla, E. et al., 2011. Absorption, scattering and single scatterin albedo of aerosols obtained from in situ measurements in the subarctic coastal region of Norway. *Atmospheric Chemistry and Physics,* Volume 11, pp. 2161 - 2182.

Moorgawa, A. et al., 2007. The Durban atmospheric LIDAR. *Optics and Laser Technology,* Volume 39, pp. 306 - 312.

More, S. et al., 2013. Comparison of aerosol products retrieved from AERONET, MICROTOPS and MODIS over a tropical urban city, Pune, India. *Aerosol and Air Quality Research,* 13(1), pp. 107 - 121 .

Naidu, S., Hounsome, R. & Iyer, K., 2006. *Climate Future For Durban: Revised Report,* Durban: CSIR Environmenttek.

NASA, 2015. *NASA Simulation Indicates Ancient Flood Volcanoes Could Have Altered Climate.* [Online]
Available at: https://www.nasa.gov/content/goddard/nasa-simulation-indicates-ancient-flood-volcanoes-could-have-altered-climate
[Accessed 3 11 2016].

Nyeki, S. et al., 2016. The GAW-PFR aerosol optical depth network: The 2008-2013 time series at Cape Point Station, South Africa. *Journal of Geophysical Research: Atmospheres,* 120(11), pp. 1 - 15.

Oanh, N., 2012. *Integrated Air Quality Management: Asian Case Studies.* Boca Raton: CRC Press.

Ogren, J. A. et al., 2006. *New Insights into Aerosol Asymmetry Parameter.* Albuquerque, Sixteenth ARM Team Meeting Proceedings .

Ogunjobi, K. O., He, Z. & Simmer, C., 2008. Spectral aerosol optical properties from AERONET Sun-photometric measurements over West Africa. *Atmospheric Research,* Volume 88, pp. 89 - 107.

Palmer, P. I., 2008. Quantifying sources and sinks of trace gases using space-bourne measurements: current and future science. *Philosophical Transactions of the Royal Society: Mathematical, Physical and Engineering Sciences,* 366(1885), pp. 4509 - 4528.

Patterson, E. M., Gilletter, D. A. & Stocktom, B. H., 1977. Complex Index of Refraction Between 300 and 700 nm for Saharan Aerosols. *Journal of Geophysical Research,* 82(21), pp. 3153 - 3160.

Petrenko, M. et al., 2012. The use of satellite measured aerosol optical depth to contrain biomass burning emissions source strength in the global model GOCART. *Journal of Geophysical Research: Atmospheres,* 117(D18), pp. 1 - 26.

Petzold, A. et al., 2013. Recommendations for reporting "black carbon"measurements. *Atmospheric Chemistry and Physics,* 13(11), pp. 8365-8379.

Piketh, S. J., Annegarn, H. J. & Tyson, P. D., 1999. Lower tropospheric aerosol loadings over South Africa: The relative contribution of aeolian dust, industrial emissions, and biomass burning. *Journal of Geophysical Research,* 104(D1), pp. 1597 - 1607.

Piketh, S. J. et al., 2002. Chemical evidence of long-range atmospheric transport over southern Africa. *Journal of Geophysical Research,* 107(D24), pp. 1 - 13.

Pöschl, U., 2005. Atmospheric aerosols: composition, transformation, climate and health effects. *Angewandte Chemie International Edition,* pp. 7520 - 7540.

Prather, K. A. et al., 2013. Bringing the ocean into the laboratory to probe the chemical complexity of sea spray aerosol. *Proceedings of the National Academy of Sciences of the United States of America,* 110(19), pp. 7550-7555.

Preston-Whyte, R. A. & Tyson, P. D., 1988. *The Atmosphere and Weather of Southern Africa.* Cape Town: Oxford University Press.

Queface, A. J. et al., 2003. Retrieval of aerosol optical thickness and size distribution from the CIMEL Sun photometer over Inhaca Island, Mozambique. *Journal of Geophysical Research ,* 108(D13), pp. 1 - 9.

Queface, A. J. et al., 2011. Climatology of aerosol optical properties in Southern Africa. *Atmospheric Environment,* 45(17), pp. 2910 - 2921.

Rainwater, M. & Gregory, L., 2005. *Cimel sunphotometer (CSPHOT) handbook. ARM TR-056.* [Online] Available at: http://www. arm.gov/instruments [Accessed 14 June 2015].

Ramachandran, S. & Kedia, S., 2013. Aerosol Optical Properties over South Asia from Ground-Based Observations and Remote Sensing: A Review. *Climate,* pp. 84 - 119 .

Ramanathan, V. C., Crutzen, P. J. & Kiehl, J., 2001. Aerosols, climate, and the hydrological cycle. *Science ,* pp. 2119 - 2124.

Ramanathan, V. & Feng, Y., 2009. Air pollution, greenhouse gases and climate change: Global and regional perspectives. *Atmospheric Environment ,* 43(1), pp. 37 - 50.

Ramaswamy, v. et al., 2001. *Intergovernmental Panel on Climate Change (IPCC): Radiative Forcing of Climate Change,* Richland : Pacific Northest National Laboratory (PNNL).

Ramsay, L. F. & Naidoo, R., 2012. Carbon footprints, industrial transparency and community engagement in a South Durban neighbourhood. *South African Geographical Journal,* 2012(2), pp. 174-190.

Reckziegel, F. et al., 2016. Forecasting volcanic ash dispersal and coeval resuspension during the April May 2015 Calbuco eruption. *Journal of Volcanology and Geothermal Research,* 321(7), pp. 44 - 57.

Redmond, H. & Thompson, J. E., 2011. Evaluation of a quantitative structure-property relationship (QSPR) for predicting mid-visible refractive index of secondary organic aerosols (SOA). *Physical Chemistry Chemical Physics,* 13(15), pp. 6872-6882..

Remer, L. A. et al., 2005. The MODIS Aerosol Algorithm, Products and validation. *Journal of atmospheric sciences,* 62(4), pp. 947 - 973.

Roberts, D., 2008. Thinking globally, acting locally, institutionalizing climate change at the local government level in Durban, South Africa. *Environment and Urbanization,* 20(2), pp. 521 - 537.

Roberts, D., 2010. Prioritizing climate change adaptation and local level resilience in Durban, South Africa. *Environment and Urbanization,* 22(2), pp. 397 - 413.

Romero, J. E. et al., 2016. Eruption dynamics of the 22 - 23 April 2015 Calbuco Volcano (Southern Chile): Analyses of tephra fall deposits. *Journal of Volcanology and Geothermal Research,* Volume 317, pp. 15 - 29.

Rosenfield, D. et al., 2008. Flood or Drought: How Do Aerosols Affect Precipitation?. *Science,* Volume 321, pp. 1309 - 1313.

Ross, J. L., Hobbs, P. V. & Holben, B. N., 1998. Radiative characteristics of regional hazes dominated by smoke from biomass burning in Brazil: Closure tests and direct radiative forcing. *Journal of Geophysical Research,* 103(D24), pp. 31925-31941.

Safarik, D., Ursini, S. & Wood, A., 2016. Megacities: Setting the Scene. *CTBUH Journal,* Volume 4.

Sahu, L. K., 2012. Volatile organic compounds and their measurements in the troposphere. *Current Science (Bangalore),* 102(12), pp. 1645-1649.

Sakaeda, N., Wood, R. & Rasch, J., 2011. Direct and semi-direct aerosol effects of southern African biomass burning aerosol. *Journal of Geophysical Research: Atmospheres,* 116(D12), pp. 1 - 19.

Sayer , A. M. et al., 2014. MODIS Collection 6 aerosol products: Comparison between Aqua's e-Deep Blue, Dark Target and "merged"data sets and usage recommendations. *Journal of Geophysical Research: Atmospheres,* Volume 13, pp. 965 - 989.

Schmid, B. et al., 2003. Coordinated airborne, spaceborne, and ground-based measurements of massive thick aerosol layers during the dry season in southern Africa.. *Journal of Geophysical Research Letters: Atmospheres,* 108(D13).

Schuster, G. L., Dubovik, O. & Holben, B. N., 2006. Angstrom Exponent and bimodal aerosol size distributions. *Journal of Geophysical Research,* 111(D7), pp. 1984 - 2012.

Scott, G. & Diab, R. D., 2000. Forecasting Air Pollution Potential: A Synoptic Climatological Approach. *Journal of Air and Waste Management Association,* 40(10), pp. 1831 - 1842.

Segura, A. et al., 2015. *Fallout deposits of the 22-23 April 2015 eruption of Calbuco volcano, Southern Andes.* Chile, Congreso Geogogico Chileno.

Seinfeld, J. H. & Pandis, S. N., 2012. *Atmospheric chemistry and physics from air pollution to climate change.* New Jersey: John Wiley & Sons.

Sellers, C., 1994. Environmental History Review: Indusrial Hygeine, Professional Collaboration and the Modern Sciences of Pollution. *Forest History Society,* pp. 55 - 83.

Shao, S., Huang, Y. & Rao, R., 2012. A Method Analyzing Aerosol Particle Shape and Scattering Based on Imaging. In: H. Abdul-Razzak, ed. *Atmospheric Aerosols - Regional Characteristics - Chemistry and Physics.* s.l.:InTech.

Shrey, K. et al., 2011. Air pollutants: The key stages in the pathway towards the development of cardiovascular disorders. *Environmental Toxicology and Pharmacology,* Volume 31, pp. 1 - 9 .

Sivakumar, V. E. et al., 2010. Aerosol Measurement over South Africa using satellite, sun photometer and Lidar. *Advanced Geoscience,* Volume 16, pp. 253 - 262.

Sivakumar, V. et al., 2015. *A new 2-D Scan portable Durban Lidar for atmospheric studies - System description and first scientifc result.* Durban, SASAS.

Sivakumar, V. et al., 2009. CSIR South Africa mobile LIDAR—First scientific results: comparison with satellite, sunphotometer and model simulations. *South African Journal of Science,* 105(11-12), pp. 449 - 455.

Smirnov, A. et al., 2002. Atmospheric aerosol optical properties in the Persian Gulf. *Journal of the atmospheric sciences ,* 59(3), pp. 620 - 634 .

Smirnov, A. et al., 2000. Cloud-screening and quality control algorithms for the AERONET database. *Remote Sensing of Environment ,* 73(3), pp. 337 - 349.

Solomon, S. D. Q. M. M. Z. C. M. M. K. A. M. a. H. M., 2007. *IPCC, 2007: Climate Change 2007: The Physical Science Basis. Contribution of Working Group I to the Fourth Assessment Report of the Intergovernmental Panel on Climate Change.* 4 ed. Cambridge and New York: Cambridge University Press.

South Africa , 2009. *National Environmental Management: Air Quality Act 2004 (Act No. 39 of 2004), National Ambient Air Quality Standards.,* South Africa: Government Gaazette.

Specialists, New Jersey Allergy and Asthma, 2016. *Guidelines for Pollen Allergy Sufferers.* [Online]
Available at: http://www.njallergydoctors.com/guidelines_for_pollen_allergies [Accessed 2 11 4].

Srimuruganandam, B. & Nagendra, S. M., 2011. Chemical characterization of PM 10 and PM 2.5 mass concentrations emitted by heterogeneous traffic. *Science of the Total Environment,* 409(17), pp. 3144-3157.

Stier, P., Seinfeld, J. H., Kinne, S. & Boucher, O., 2007. Aerosol absorption and radiative forcing. *Atmospheric Chemistry and Physics ,* Volume 7, pp. 5237 - 5261.

Stocker, T. F. et al., 2013. *IPCC, 2013: Climate Change 2013: The Physical Science Basis. Contribution of Working Group I to the Fifth Assessment Report of the Intergovernmental.* United Kingdom and New York: Cambridge University Press.

Stremme, W., Ortega, I., Siebe, C. & Grutter, M., 2011. Gas composition of f Popocatépetl Volcano between 2007 and 2008: FTIR spectroscopic measurments of an explosive event and during quiescent degassing. *Earth and Planetary Science Letters,* 301(3), pp. 502 - 510.

Sun, L., Li, X. & Guo, M., 2008. Validation of MODIS aerosol optical thickness product distributed by NSMC over seas around China and its adjacent area. *The International Archives of the Photogrammery, Remote Sensing and Spatial Information Sciences ,* 34(1), pp. 95 - 98.

Swap, R. J. et al., 2003. Africa burning: A thematic analysis of the Southern African Regional Science Initiative (SAFARI 2000). *Journal of Geophysical Research,* Volume 108, pp. 1 - 15.

Takemura, T. et al., 2002. Single-Scatterinf Albedo and Radiative Forcing of Various Aerosol Species with a GLobal Three-Dimensional Model. *Journal of Climate,* 15(4), pp. 333 - 352.

Tam, E. et al., 2016. Volcanic air pollution over the Island of Hawii: Emissions, dispersal, and composition. Associaton with respiratory symptoms and lung function in Hawaii Island school children.. *Environment International,* 92(93), pp. 543-552.

Terblanche, D. E. et al., 2000. The Aerosol Recirculation and Rainfall Experiment (ARREX): an initial study on aerosol-cloud. *South African Journal of Science,* Volume 96, pp. 15 - 20.

Tesfaye, M., Botai, J., Sivakumar, V. & Mengistu, T., 2013. Evaluation of Regional Climatic Model Simulated Aerosol Optical Properties over South Africa Using Ground-Based and Satellite Observations. *Internationally Scholarly Notices ,* pp. 1 - 17.

Tesfaye, M., Botai, J., Sivakumar, V. & Tsidu, G. M., 2014. Simulation of biomass burning aerosols mass distributions and their indirect and semi-direct effects over South Africa using a regional climate model. *Meteorology and Atmospheric Physics,* 125(7), pp. 177 - 195.

Tesfaye, M., Sivakumar, V., Botai, J. & Mengistu, T., 2011. Aerosol climatology over South Africa based on 10 years of Multiangle Imaging Specctroradiometer (MISR) data. *Journal of Geophysical Research,* Volume 116, pp. 1 - 17.

Thambiran, T. & Diab, R., 2010. A review of scientific linkages and interactions between climate change and air quality, with implications of air quality management in South Africa. *South African Journal of Science,* 106(3/4), pp. 1 - 8.

Thambiran, T. & Diab, R. D., 2011. The case for integrated air quality and climate change policies. *Environmental Science and Policy,* 14(8), pp. 1008 - 1017.

Tiitta, P. et al., 2014. Chemical composition, main sources and temporal variability of PM1 aerosols in southern African grassland. *Journal of Atmospheric Chemisty and Physics,* Volume 14, pp. 1909 - 1927.

Tripathi, S. N. et al., 2005. Comparison of MODIS and AERONET derives aerosol optical depth over the Ganga Basin, India. *Annales of Geophysicae,* 23(4), pp. 1093 - 1101.

USGS, 2016. *Volcanic gases can be harmful to health, vegetation and infrastructure..* [Online] Available at: http://volcanoes.usgs.gov/vhp/gas.html [Accessed 24 11 2016].

Vakkari, V. et al., 2013. Long-term observations of aerosol size distributions in semi-clean and polluted savannah in South Africa. *Atmospheric Chemistry and Physics,* 13(6), pp. 1751 - 1770.

Vakkari, V. et al., 2011. New particle formation events in semi-clean South African savannah. *Journal of atmospheric, chemisrty and physics ,* Volume 11, pp. 3333 - 3346.

van Donkelaar, A. et al., 2015. *Global estimates of ambient fine particulate matter concentrations from satellite-based aerosol optical depth: development and application.* Vancouver: University of British Columbia.

Vernier, J. P. et al., 2011. Major influence of tropical volcanic eruptions on the stratospheric aerosol layer during the last decade. *Geophysical Research Letters,* 38(L12807), pp. 1 - 8.

Vinoj, V. et al., 2014. Short term modulation of Indian summer monsoon rainfall by West Asian dust. *Nature Geoscience,* 7(10), pp. 308 - 313.

Wagner, R. et al., 2012. Complex refractive indices of Saharan dust samples at visible and near UV wavelengths: a labratory study. *Atmospheric Chemistry and Physics,* Volume 12, pp. 2491 - 2512.

Watson , R. T., Rodhe, H., Oeschger, H. & Siegenthaler, U., 1990. Greenhouse gases and aerosols. In: *Climate change: the IPCC scientific assessment 1.* s.l.:Intergovernmental Panel on Climate Change (IPCC), p. 17.

Weissgerber, T. L., Milic, N. M., Winham, S. J. & Garovic, V. D., 2015. Beyond Bar and Line Graphs: Time for a New Data Presentation Paradigm. *PLoS,* 13(4), p. e1002128.

Whelan, M. E., Min, D. & Rhew, R. C., 2013. Salt marsh vegtation as carbonyl sulfide (COS) source to the atmosphere. *Atmosphere Environment,* 73(31), pp. 131-137.

WHO, 2016. *Ambient (outdoor) air quality and health.* [Online] Available at: http://www.who.int/mediacentre/factsheets/fs313/en/ [Accessed 10 11 2016].

Winker, D. M. et al., 2013. The global 3D distribution of tropospheric aerosols characterised by CALIOP. *Atmospheric Chemisrty and Physics,* 13(6), pp. 3345 - 3361.

Winkler, H. et al., 2008. Evidence for large-scale transport of biomass burning aerosols from sunphotometry at a remote Soth African site. *Atmospheric Environment,* Volume 42, pp. 5569-5578.

Wong, J. & Li, Z., 2002. Retrieval of optical depth for heavy smoke aerosol plumes: Uncertainties and sensitivities to optical properties. *Journal of Atmospheric Science,* Volume 59, pp. 250 - 261.

Xie, Y. et al., 2011. Validation of MODIS aerosol optical depth product over China using CARSNET measurements. *Atmospheric Environment ,* Volume 45, pp. 5970 - 5978.

Yoo, J. M. et al., 2014. New indices for wet scavenging of air pollutants (O3, CO, NO2, SO2 and PM10) by summertime rain. *Atmospheric Environment,* Volume 82, pp. 226 - 237.

Yoon, S. C. et al., 2005. Estimation of the radiative forcing by key aerosol typesin worldwide locations using a column model and AERONET data. *Atmospheric Environment,* Volume 39, pp. 6620 - 6630.

Zeleza, P. T., 2002. The Politics of Historical and Social Science Research in Africa. *Journal of Southern African Studies,* 28(1), pp. 9 - 23.

Zhang, J. & XingMing, L., 2012. Vertical distribution of sand-dust aerosols and the relationships with atmospheric environment. *Journal of Arid Land,* 4(4), pp. 357 - 368.

Zhang, X., Huang, Y., Rao, R. & Wang, Z., 2013. Retrieval of effective complex refractive index for intensive measurements of characteristics of ambient aerosols in the boundary layer. *The Optical Society of America ,* 21(15), pp. 17849 - 17862.

Zheng, X. Y., Fu, Y. F., Yang, Y. J. & Liu, G. S., 2015. Impacts of atmospheric circulations on aerosol distributions in autumn over eastern China: observational evidences.. *Atmospheric Chemistry and Physics Discussions,* 15(3), pp. 3285 - 3325.

Zhu, T. et al., 2012. *Impacts of Megacities on Air Pollution and Climate,* Geneva: WMO.

Zunckel, M. et al., 2004. Surface ozone over southern Africa: synthesis of monitoring results during the Cross border Air Pollution Impact Assessment project.. *Atmospheric Environment,* 38(36), pp. 6139-6147.